Structural and functional effects on large artery stiffness: an in-vivo experimental investigation.

Author:
Butlin, Mark

Publication Date:
2007

DOI:
https://doi.org/10.26190/unsworks/17464

Structural and functional effects on large artery stiffness: an *in-vivo* experimental investigation

A thesis of The Graduate School of Biomedical Engineering of The University of New South Wales submitted in fulfilment of the requirements for the degree of Doctor of Philosophy.

Mark Butlin

Graduate School of Biomedical Engineering
The University of New South Wales

November 2007

Supervisors

Professor Albert Avolio
Graduate School of Biomedical Engineering
The University of New South Wales

Doctor Ian Wilkinson
Clinical Pharmacology Unit
University of Cambridge

Structural and functional effects on large artery stiffness: an *in-vivo* experimental investigation

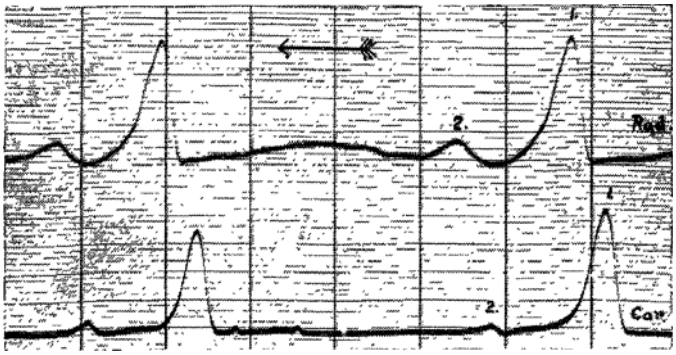

We have had occasion to make a considerable number of observations on the velocity of transmission of the pulse-wave, both in health and in disease. Since the technique is simple, and the records yield very accurate measurements, it seems likely that the method employed will not only be of service in the investigation of problems of purely scientific interest, but may also have a practical application in the field of clinical medicine.

J. Crighton Bramwell & A.V. Hill*, Lancet, 1922.

* The Nobel Prize in Physiology or Medicine 1922.

Originality statement

'I hereby declare that this submission is my own work and to the best of my knowledge it contains no materials previously published or written by another person, or substantial proportions of material which have been accepted for the award of any other degree or diploma at UNSW or any other educational institution, except where due acknowledgement is made in the thesis. Any contribution made to the research by others, with whom I have worked at UNSW or elsewhere, is explicitly acknowledged in the thesis. I also declare that the intellectual content of this thesis is the product of my own work, except to the extent that assistance from others in the project's design and conception or in style, presentation and linguistic expression is acknowledged.'

Mark Butlin
28th November 2007

Acknowledgements

I would like to acknowledge and thank the following people for their contribution to the work contained in this thesis. In alphabetical order, by first name:

Professor Albert Avolio.[1] His supervision and facilitation of this research has been invaluable. I would like to especially thank him for his support, guidance, and interest not just in the work here presented, but also in the development of my further research career. Albert's never ending, infectious enthusiasm and his philosophical outlook on all matters has been integral in the completion of the work contained within this thesis. I would also like to thank Albert for teaching me how to use a pair of scissors.

Dr Carmel McEniery.[2] The ovine model work was facilitated by Carmel in the opening stages of my research. Her hard working attitude helped see the project completed in spite of much comedic distraction.

Daniel Chan.[1] Daniel assisted in the *ex-vivo* tensile testing of aortic sections in the study of rat aortic calcification.

Eddie Davidson.[2] Eddie's initial work helped commence the study assessing the viability of using reactive hyperaemia as a tool for determining arterial structural stiffness. His contribution and humour in this project was much appreciated, least of which was his invention of the oxymoron that was the study's working namesake.

Dr Greg Jones.[3] His previous knowledge of the Brown Norway model of genetic predisposition to aortic elastic lesions permitted the study of pulse wave velocity in relation to such lesions. His generosity is much appreciated in welcoming a week of experimental work at his facilities in the Otago Medical School Vascular Research Clinic, the University of Otago, Dunedin, New Zealand.

Dr Ian Wilkinson.[2] I would like to thank Ian not just for his role as co-supervisor and the ideas he put forward for my projects within that role, but also for his well thought out critical appraisal and discussion of the work contained within this thesis. Also must be acknowledged is the use of his facilities at the Clinical Pharmacology Unit, Addenbrooke's Hospital, Cambridge, UK, where he invited me upon several visits over the duration of this

research work, his hospitality only surpassed by his drive for productivity, both of which have been a pleasure. Thanks are also given for his words of wisdom, including the advice in my first year to "just finish the PhD so you can do some real work".

Professor John Cockcroft.[4] John has been the motivating force behind the pilot study of the vasodilatory effect of nebivolol in humans. He was also the largest source of the aforementioned welcomed comedic distraction in the work in the ovine model.

Kaisa Mäki-Petäjä.[2] Kaisa kindly availed herself for the study measuring structural stiffness with the use of reactive hyperaemia. Of greater benefit still was the many and varied discussions we have had on all things haemodynamic. For this I thank her.

Dr Nigel Jepson.[5] Thank you to Nigel for facilitating access to the patient base at the Eastern Heart Clinic for the study of the vasoactive properties of nebivolol.

Sharon Wallace.[2] Sharon's professional and highly skilled abilities in experimental measurements were of great use in her work in the study measuring structural stiffness with the use of reactive hyperaemia. The time she has contributed to this project, aside from her own thesis work, is greatly appreciated.

Dr Trudie Binder.[6] Thanks must go to Trudie for allowing us to use her study animals in work to quantify the effect of adjuvant induced inflammation on aortic stiffness in rats.

Veronica Tatarinoff.[1] In the absence of Vicki's help, early starts, and surgical skills, the ovine studies would not have reached success. Also, her help in the housing of rats, facilitating of extended experimental periods in the animal house, and understanding in trying circumstances have assisted infinitely in achieving, if not always the desired aim, an appropriate outcome.

Dr Wilmer Nichols.[7] Discussions at conferences and his prompt e-mail replies to questions in the study of arterial stiffness during reactive hyperaemia have always been useful and enlightening.

An Australian Research Council Postgraduate Award (Industry) funded the research contained in this thesis, the industry sponsor being Glaxo Smith Kline (ARC Linkage Grant LP0349227).

[1] Graduate School of Biomedical Engineering, University of New South Wales, Sydney, Australia.
[2] Clinical Pharmacology Unit, University of Cambridge, Addenbrookes Hospital, England.
[3] Department of Surgery, Dunedin Medical School, University of Otago, Dunedin, New Zealand.
[4] Department of Cardiology, University of Wales College of Medicine, Cardiff, Wales.
[5] Eastern Heart Clinic, Sydney, Australia.
[6] School of Medical Sciences, University of New South Wales, Sydney, Australia.
[7] Department of Cardiovascular Medicine, University of Florida, Gainesville, USA.

Publications

Some of the concepts and figures presented in this work have appeared previously in the following publications and presentations:

Articles

1. Schmitt M, Avolio A, Qasem A, McEniery CM, Butlin M, Wilkinson IB, Cockcroft JR. Basal NO locally modulates human iliac artery function in vivo. *Hypertension*. 2005;46(1):227-31.

Invited presentations

2. Assessment of arterial structural stiffness by ischaemia-induced reactive hyperaemia in the human arm. Invited talk. Clinical Pharmacology Unit, School of Clinical Medicine, University of Cambridge, UK. September 2006.

3. Assessment of arterial stiffness – theory and experimental applications. Invited talk. Vascular Research Group, Dunedin School of Medicine, University of Otago, Dunedin, New Zealand. July 2005.

Conference presentations

4. Butlin M, Jones GT, Wilkinson IB, Avolio AP. Spontaneous lesions in the internal elastic lamina of the aorta are not associated with aortic stiffness in the rat. 17th Scientific Meeting of the European Society of Hypertension, Milan, June 15-19, 2007.

5. Butlin M, Davidson E, Wallace S, Mäki-Petäjä K, McEniery C, Avolio AP, Wilkinson IB. Use of ischaemia-induced reactive hyperaemia to quantify arterial structural stiffness. National Heart Foundation, Sydney, 23-25th March 2006.

6. Butlin M, Avolio AP, Binder W, Wilkinson IB. Acute Inflammation causes reduced aortic stiffness in rats. National Heart Foundation Conference, Sydney, 23-25th March 2006.

7. Butlin M, Avolio AP, Davidson EH, Wallace SM, Mäki-Petäjä K, McEniery C, Wilkinson IB. Assessment of arterial structural stiffness by ischaemia-induced reactive hyperaemia in the human forearm. 16th Scientific Meeting of the European Society of Hypertension, Madrid Spain, 12-15th Junes 2006.

8. Butlin M, Avolio AP, Kong L, Binder W, Wilkinson IB. Effect of experimental inflammation on rat aortic pulse wave velocity. Artery 5, Paris France, 30th September-1st October 2005.

9. Butlin M, Avolio AP, Kong L, Binder W, Wilkinson IB. Effect of Experimental Inflammation on Rat Aortic Pulse Wave Velocity. 15th European Meeting on Hypertension, Milan Italy, 17th-21st June 2005.

Abstract

Large artery stiffness is predictive of adverse cardiovascular events and all cause mortality. Artery structure and function are determinants of artery stiffness. This thesis presents a series of *in-vivo* experimental studies of effect of structural and functional changes on large artery stiffness. Improved analysis methods were developed for measurement of arterial stiffness indexes, Pulse Wave Velocity (PWV) and pressure wave reflection. These were applied in studies of acute inflammation, active and passive changes in systemic pressures, aortic elastic laminae defects, and aortic calcification in rats using a novel, high fidelity, dual pressure sensing technique of measuring aortic rat PWV. Findings indicated that acute inflammation does not increase large artery stiffness, and that localised effects altering arterial structure do not manifest in *in-vivo* changes in large artery stiffness. The functional component of stiffness was investigated using graded systemic infusion of vasoconstrictor agents (angiotensin-II, noradrenaline, and Endothelin-1 (ET-1)) in the *in-vivo* ovine iliac artery. There was a markedly greater dose dependency of pressure independent change in PWV (angiotensin-II) compared to direct endothelial effects (ET-1), although blocking of ET-1 receptors produced marked changes in iliac blood flow. A similar experiment in the human iliac artery found that the β-antagonist and nitric oxide (NO) donor,

nebivolol, potentially causes a decrease in regional functional stiffness. An additional study in human subjects directly measured the decrease in forearm arterial stiffness during reactive hyperaemia following different periods of ischaemia. The findings precluded the use of this method in measuring brachial artery structural stiffness with maximal smooth muscle relaxation. Increasing periods of ischaemia had a bi-phasic relationship with changes in arterial stiffness, the first phase linked to endogenous nitric oxide release. This finding is of importance in the clinical quantification of endothelial dysfunction. These findings in basic research of arterial haemodynamics provide new quantitative contributions to the *in-vivo* experimental investigation of the aetiology of large artery stiffness related to structure and function of endothelial and medial wall properties. This can lead to potential clinical applications and techniques for assessment of cardiovascular risk.

Contents

List of Figures

List of Tables

CHAPTER 1

Introduction

Cardiovascular disease has a large and increasing cost in human and economic terms. Worldwide, 3.8 million men and 3.4 million women die from coronary heart disease annually. An additional 2.5 million men and 3 million women die from stroke (Mackay and Mensah, 2004). Cardiovascular disease accounts for 30% of global deaths and kills more people than any other single cause. In 2005, 17.5 million people died due to cardiovascular disease. This is predicted to reach nearly 20 million deaths annually by 2015 (World Health Organisation, 2007). In 1994, the direct cost to the Australian health system was $7.6 billion, conservative estimates placed indirect costs at an additional $6.6 billion – a combined total of 1.7% of gross domestic product. This is predicted to rise to an annual cost of $11.5 billion by 2011 (Access Economics Pty Limited, 2005b).

Large artery stiffness is predictive of both adverse cardiovascular events, and of all-cause mortality, in a range of sub-populations and disease types. Blacher et al. (1999a) demonstrated in a study of 710 hypertensive subjects that higher cardiovascular risk was associated with increased pulse wave ve-

locity, a measure of arterial stiffness. A similar study (Laurent et al., 2001a) reiterated the same trends in a group of 1,980 hypertensive patients, with arterial stiffness being associated with both cardiovascular and all-cause mortality. The study of end-stage renal disease patients confirmed that arterial stiffness as measured by pulse wave velocity (Blacher et al., 1999b) and by aortic pressure augmentation index (London et al., 2001) was associated with cardiovascular events and outcomes. A correlation between arterial stiffness and cardiovascular mortality was also apparent in diabetes sufferers (Cruickshank et al., 2002). More generally, in the elderly population, aged 70 to 100 years, Meaume et al. (2001) proved arterial stiffness as a predictor of all-cause and cardiovascular death.

The importance of arterial stiffness is not limited to specific sub-populations or disease groups. The Rotterdam study (Mattace-Raso et al., 2006) of 2,835 subjects showed that, in apparently healthy people, arterial stiffness remains an independent predictor of coronary heart disease and stroke. Increased arterial stiffness is specifically a risk factor of cardiovascular conditions and of cardiovascular diseases (Arnett et al., 1994) including: hypertension (Avolio et al., 1985; Laurent and Boutouyrie, 2007; Simon et al., 1985); atherosclerosis (Herrington et al., 2004; van Popele et al., 2001); coronary heart disease (Boutouyrie et al., 2002); and stroke (Laurent et al., 2003). Collectively, the evidence supports the use of arterial stiffness as a diagnostic tool in the clinical setting (Laurent et al., 2006; Mackenzie et al., 2002; Nichols, 2005; O'Rourke et al., 2002). The clinical importance arterial stiffness in treatment and prevention of cardiovascular disease was highlighted by the inclusion of Pulse Wave Velocity (PWV) measurement, an index of arterial stiffness, in the European Society of Hypertension guideline for the treatment of hypertension (Mancia et al., 2007).

Increased stiffness, or decreased elasticity, in the large arteries, as is observed specifically in older individuals (Avolio et al., 1983; McEniery et al., 2005), decreases the capacitive effect of those arteries. This directly increases the aortic central and pulse pressures. Increased central and pulse pressure subsequently increases left ventricular load, left ventricular mass, and cardiovascular events (Mitchell and Pfeffer, 1999). Stiffer vessels also give rise to greater pressure wave reflection, which has an additive effect to systolic pressure. Again, the increased pressure increases left ventricular load and subsequent cardiovascular risk.

It follows that knowledge of the aetiology of large artery stiffness will enable a better understanding of treatment and prevention of cardiovascular diseases. Diagnosis of alterations in arterial properties may help identify patients at risk of cardiovascular complications and allow early prevention and intervention in the progress of the disease.

Changes in structural components of the artery wall, such as elastin and collagen, provide long-term regulation of arterial stiffness. Short-term regulation of arterial stiffness and differential loading of the arterial structural components is provided by functional changes in smooth muscle tone. This thesis concerns a series of experiments concerning the relative changes in large artery stiffness under conditions invoking either structural or functional changes in arterial stiffness. The methods developed, and the studies conducted, concern *in-vivo* measures of arterial stiffness. *In-vivo*, as opposed to *ex-vivo*, measurement of arterial stiffness permits the physiological impact of arterial structural and functional changes to be ascertained in the intact circulation.

A new, adaptable set of pressure analysis tools were developed for the purposes of pulse-by-pulse pressure wave analysis and PWV calculation for

in-vivo measurement of arterial stiffness. The summary of these tools in Chapter 3 includes an outline of a novel method of measuring foot-to-foot pressure wave transit time and PWV across a variety of waveform shapes encountered at various vascular sites in both humans and animals. In addition, decomposition of the pressure waveform into the incident and reflected components is addressed, with two new parameters for measurement of wave reflection intensity proposed.

In all studies presented in this thesis, PWV was measured using simultaneous dual pressure sensing techniques. Of note is the method used in the study of aortic PWV in the rat using a high fidelity, dual pressure sensing, 2.5F catheter (Millar SPC-721). The catheter, with two pressure sensors a fixed distance (50 mm) apart, permitted high fidelity, highly accurate measurement of PWV. The fixed distance between the sensors mounted on the rigid catheter completely eliminated any error due to distance measurement. This is a crucial point in these types of experiments in rats as the distances between measuring sites are small, and so small errors in distance measurement (of the order of 1 mm) can produce substantial errors in PWV calculation. This method was explored in a concept study of aortic stiffness during experimental inflammation in rats with Adjuvant-Induced Arthritis (AIA) (Chapter 4). The method was extended to investigate PWV over a full range of physiological pressures in the rat by pharmacological control of systemic blood pressure (Chapter 5). The active, pharmacological change in blood pressure was compared to a passive acute hypotensive mechanism in terms of the effect on aortic stiffness.

Using the novel method of high fidelity PWV measurement in the rat aorta and pharmacological alteration of blood pressure, the effect of two models of structural change in the rat aorta were investigated across a full

physiological blood pressure range. The effect of aortic lesions in the internal elastic laminae was studied in the Brown Norway (BN) strain of rat, genetically predisposed to such lesions (Chapter 6). The study is the first to address the effect of genetically acquired lesion defects on aortic stiffness. Aortic structural changes were also induced in the rat by treatment with hypervitaminosis D_3 and nicotine (VDN) (Chapter 7). In addition to *in-vivo* measures of arterial stiffness, *ex-vivo* testing of aortic sections was used to give indication of changes in structural stiffness and compared to the *in-vivo* measures of combined structural and functional aortic stiffness. The effect of the calcifying VDN treatment was investigated with respect to the duration of treatment, the first study to address the effect of time on this established model of rat aortic calcification.

Functional changes in large artery stiffness in the intact ovine iliac artery were studied with respect to three vasoconstrictor agents with different modes of action, namely, angiotensin-II, noradrenaline, and Endothelin-1 (ET-1) (Chapter 8). The study addressed both flow and PWV changes in the iliac artery in response to the vasoconstrictor agents with difference in response were noted.

The method of analysing functional and structural changes in large arteries was also applied to an invasive study in humans. The acute effect of nebivolol, an adrenergic β-antagonist and nitric oxide (NO) donor, on large artery stiffness was conducted in a localised, invasive technique (Chapter 9). The pilot study is the first to investigate whether the conclusions drawn from the previous work of McEniery et al. (2004) in an ovine hind-limb preparation, that nebivolol decreases large artery stiffness by a NO dependent mechanism, has the potential to be transferred to human large arteries.

Structural and functional components of stiffness were also investigated

by non-invasive means in humans. The viability of the use of non-invasive PWV measurement during a hyperaemic response to forearm ischaemia to assess the structural stiffness of the human brachial artery was investigated (Chapter 10). Arterial stiffness has not previously been directly measured during increasing time periods of ischaemia. Regression modelling of the change in functional stiffness with increasing periods of ischaemia resulted in a greater understanding of the mechanisms underlying vascular relaxation during the hyperaemic response and potentially assists in the standardisation of Flow-Mediated Dilatation (FMD) measurement techniques for the quantification of endothelial dysfunction.

This *in-vivo* experimental investigation of large artery stiffness under conditions of structural and functional changes has produced novel quantitative findings in basic research on arterial haemodynamics leading to a greater understanding of the physiological significance of large artery stiffness in cardiovascular health.

CHAPTER 2

Background

Arteries, once viewed as passive conduits for blood transport, are now considered a dynamic and responsive organ system with a role in regulating blood flow, blood pressure, and cardiovascular function through changes in capacitance and resistance (Nichols and O'Rourke, 1998). The aorta and large arteries are capacitive, storing approximately 50% of the stroke volume during the systolic contraction of the heart (Belz, 1995). The elastic recoil of the large arteries during diastole generates blood flow continuously throughout the cardiac cycle. Reverend Stephen Hales (1677-1761) proposed the analogy of *windkessel* water pumps (Figure 2.1), used in fire fighting during his time, that converted a pulsatile pumping of water to a continuous flow of water at the fire hose end (Greenwald, 2002). Increases in arterial stiffness limits the ability of an artery to expand and contract and convert pulsatile blood ejection from the heart into a continuous blood flow to the body organ systems and peripheral microvascular beds. Increased arterial stiffness also increases the pressure on the left ventricular cavity, and thus increases the mechanical load on the heart muscle (Nitta et al., 2004; O'Rourke, 1982;

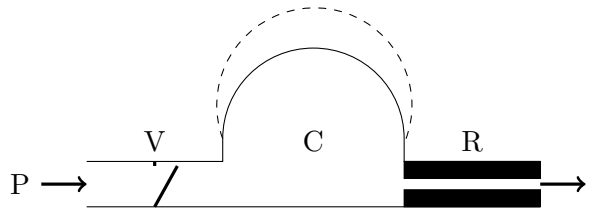

Figure 2.1: The *windkessel* model of arterial blood flow. The supply of fluid is pumped by a pulsatile pump (P) through the valve (V) into a capacitive storage tank (C) that is able to elastically extend to accommodate additional volume (dashed line). The *windkessel* effect of the capacitive tank leads to a constant fluid flow at the resistive outlet (R), in spite of a pulsatile flow input. This is analogous to the arterial system, with the pulsatile pump being the left ventricle, the valve the aortic valve of the heart, the capacitive tank the large arteries, and the outlet the smaller, resistive arteries. (Adapted from Milnor, 1982)

O'Rourke and Mancia, 1999).

The capacitance and resistance of arteries is a result of the geometry of the vascular tree, and the proportion and action of the constituents of the vessel wall. Approximately 70% of the arterial wall is water, with the other components being elastin, collagen, smooth muscle cells, adipose tissue, and various proteins (Apter et al., 1966; Milnor, 1982). The mechanical properties of the vessels are largely derived from the quantity of elastin, collagen and smooth muscle, the structure of these components within the vessel wall, and the support of the surrounding body tissue.

The arterial wall is divided into three circumferential regions: the tunica intima; the tunica media; and the tunica adventitia (Milnor, 1982). The lumen of the vessel is the conduit for blood transport and is lined by the tunica intima or endothelium, comprised of a monolayer of squamous epithelial cells (Ferro, 2003). The endothelium lines the luminal surface of the tunica media, a layer of interconnected elastin and collagen fibres and smooth muscle cells. The outermost layer, the tunica adventitia, is comprised primarily of a network of elastin and collagen fibres that provide mechanical support and serve as connective tissue to the surrounding anatomy. The surrounding

anatomy and this connective tissue cannot be ignored in the study of arterial dynamics, as it provides further circumferential load bearing capabilities and tethers the artery in the longitudinal direction.

The majority of the circumferential stiffness of the artery is derived from a structural network of elastin and collagen fibres in the tunica media and adventitia. Elastin and collagen are extracellular matrix fibrous proteins with widely differing mechanical properties that constitute half to two thirds of the dry weight of artery walls (Milnor, 1982). The structural morphology and quantity of collagen and elastin give the arterial wall it's inherent stiffness properties, influencing the stress seen within the vessel wall (Avolio et al., 1998). A greater extent of the load at low transmural pressures is borne by the internal elastic lamina of the vessel wall. With increasing transmural pressures, stiffer collagen fibres take up a greater extent of the load (Dobrin, 1978).

Smooth muscle cells in the arterial wall are in bundles in the order of 100μm in diameter (Milnor, 1982) and are an active, functional component of arterial vessels. Smooth muscle contracts and relaxes, changing the lumen diameter and directly affecting arterial stiffness through its own stiffness, and indirectly altering stiffness by differentially loading elastin and collagen fibres in the arterial wall (Gow, 1972).

The proportion of the major load bearing components, elastin, collagen and smooth muscle, vary throughout the arterial network of the body. Arteries more proximal to the heart have a lower smooth muscle content than those more distal, whilst elastin has an inverse relationship with distance from the heart. This is true more locally within the length of the aorta itself, with elastin content decreasing and smooth muscle content increasing from ascending, to thoracic, to abdominal aortic section (Apter et al., 1966).

The structure of components within the vessel wall also changes throughout the arterial tree. Smooth muscle alignment approximates a helical arrangement in the large arteries of the body, such as the aorta, but towards the smaller arteries, alignment adopt a more circumferential nature (Milnor, 1982). Smooth muscle also contributes to wall viscoelasticity (Nichols and O'Rourke, 1998) and has recently been shown to possess possible 'smart' material properties in the regulation of vascular wall behaviour (Armentano et al., 2006). Arteries more proximal to the heart have a lower inherent stiffness than those more distal due to the proportion and structure of load bearing components (Latham et al., 1985; McDonald, 1968). These large arteries have a capacitive role in the pulsatile circulatory system, dampening the impulse of the stroke volume (Belz, 1995) and accommodating wave reflection in the role of continuously supplying blood to body systems whilst optimally limiting the pressure load on the heart muscle.

2.1 Arterial stiffness and the elastic modulus

The material properties of arteries define how they respond in the physiological system. The relationship between the pressure applied to an artery and the resulting stretch of the artery wall has been a matter of great theoretical and practical study. Stiffness is a fundamental material property and is a function of the stress applied to the material and the resulting strain that the material experiences. Stress is the force applied to a material per unit area (Equation 2.1). A stress applied to a material causes the material to deform, the extent of deformation defined as strain. Strain is a non-dimensional ratio of the change in material dimensions to an applied stress over the original dimensions of the material (Equation 2.2). Stress and strain are defined in six directions: the orthogonal directions x, y and

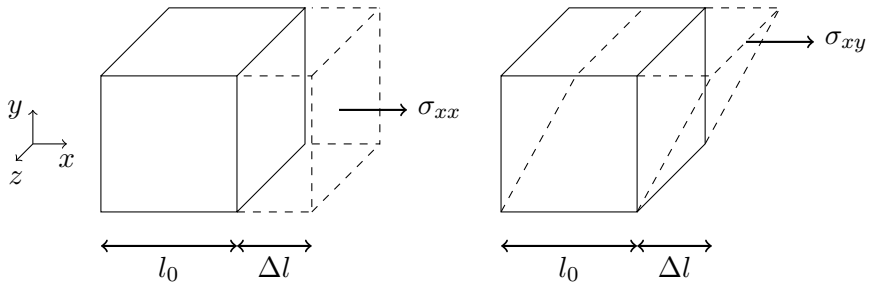

Figure 2.2: Representation of tensional stress (σ_{xx}) and shear stress (σ_{xy}) in a unit cube, the subsequent strain being equal to the ratio of the change in length (Δl) to the original length (l_0).

z; and the shear directions xy, yz and zx (Figure 2.2).

$$\sigma = \frac{F}{A} \tag{2.1}$$

$$\varepsilon = \frac{\Delta l}{l_0} \tag{2.2}$$

The elastic modulus, or stiffness, of a material is defined as the tendency of the material to deform (strain) under an applied load (stress). The elastic modulus can be expressed in four different ways, depending on the direction of the applied force. Young's modulus (E) is the deformation along a single axis under a situation of uni-axial applied pressure. The bulk modulus (K) measures the deformation in volume under a uniform load applied to that volume. The shear modulus (μ) is the deformation in shape under two opposing forces. The longitudinal loading modulus (λ) is the longitudinal strain under an applied transverse stress. The various terms of modulus, detailed in Table 2.1, are interrelated by Poisson's ratio (ν), the elongation along one axis under a tensile strain over the reduction in dimension on the other two axes (Equation 2.3). The arterial wall has an average Poisson's ratio of 0.5, approximating that of water (Dobrin, 1978; Nichols and

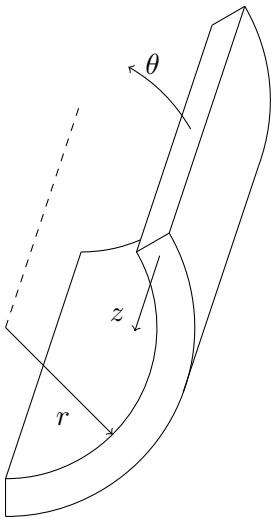

Figure 2.3: The orthotropic nature of arteries, showing circumferential (θ), longitudinal (z), and radial (r) directions within the arterial wall. (Adapted from Dobrin, 1978)

O'Rourke, 1998). That is, the material is essentially incompressible, and an applied load causes no change in volume. However, Poisson's ratio varies with the axis of stress due to the anisotropy of the vessel wall (Milnor, 1982).

$$\nu_{xy} = \frac{\varepsilon_{xx}}{\varepsilon_{yy}} \tag{2.3}$$

Arteries are usually treated as an orthotropic material, having different material properties symmetrical about each of three perpendicular planes: longitudinal; radial; and circumferential (Figure 2.3). The anisotropy of arterial vessels was elegantly presented by Patel et al. (1969) in data obtained from investigation of the dog thoracic aorta (Figure 2.4). Patel et al. showed a near two fold difference between radial and longitudinal elastic modulus, with circumferential modulus falling between the two.

In addition to the assumptions of incompressibility and orthotropic nature, a further assumption of homogeneity is used in many calculations of mechanical properties of arteries. The assumption of homogeneity holds

Table 2.1: Elastic moduli that describe material properties. All have the units of load (Newtons per unit area, mmHg, or equivalent) and all can be expressed in terms of Young's Modulus (E) and Poisson's ratio (ν). For completeness, Poisson's ratio is defined at the bottom of the table. (Adapted from Milnor, 1982)

Modulus	Ratio	Definition	In terms of E & ν
Young's modulus	$\frac{tensile\ stress}{tensile\ strain}$	$E = \frac{\sigma_{xx}}{\varepsilon_{xx}}$	$2\mu\,(1+\nu)$
Shear modulus	$\frac{shear\ stress}{shear\ strain}$	$\mu_{xy} = \frac{\sigma_{xy}}{\varepsilon_{xy}}$	$\frac{E}{2\,(1+\nu)}$
Bulk modulus	$\frac{compressive\ stress}{volumetric\ strain}$	$K = \frac{P \cdot V_o}{\Delta V}$	$\frac{E}{3\,(1-2\nu)}$
Longitudinal modulus	$\frac{transverse\ stress}{longitudinal\ strain}$	$\lambda = \frac{\sigma_{yy}}{\varepsilon_{xx}}$	$\frac{E \cdot \nu}{(1+\nu)\,(1-2\nu)}$
Poisson's ratio	$\frac{transverse\ strain}{longitudinal\ strain}$	$\nu_{xy} = -\frac{\varepsilon_{yy}}{\varepsilon_{xx}}$	$\frac{E-2\mu}{2\mu}$

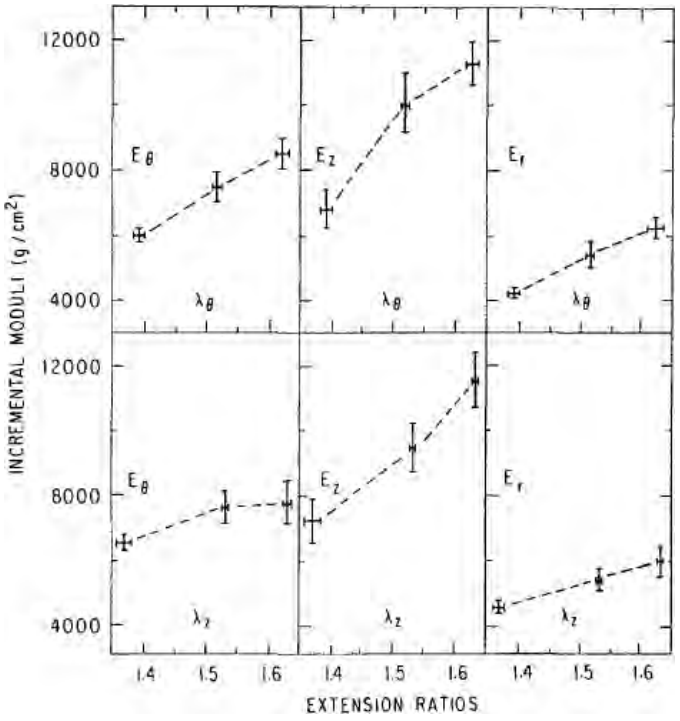

Figure 2.4: Anisotropy of arterial vessels demonstrated in the thoracic aorta of live dogs. The elastic modulus (E) measured orthotropically plotted against extension ratio (λ) in the circumferential (θ) and longitudinal (z) direction. Note that $E_z > E_\theta > E_r$, indicating anisotropy, and that modulus increases with extension. (Reproduced from Patel et al., 1969)

true for most applications of theoretical and practical study in localised longitudinal sections and in the circumferential direction. However, the assumption does not hold true in the radial plane due to the laminar nature of the arterial wall. Due to the mutli-layered, in-homogeneous nature of the artery wall, the elastic modulus of the artery is non-linear across a range of working pressures (Langewouters et al., 1984). That is, the arterial wall does not obey Hooke's Law of a perfectly elastic material. The modulus of the arterial wall increases with increasing applied stress and resulting strain (Figure 2.4), giving a curvilinear stress-strain relationship (Figure 2.5). In terms of observed physiology, the higher the working blood pressure, the smaller the change in circumference for a given change in pressure. The adjustment of the elastic modulus with applied stress ensures the integrity of the arterial wall in the range of physiological pressures.

For a curvilinear relationship between stress and strain as observed in arterial wall tissue (Krafka Jr, 1938), Young's modulus for a given pressure is defined as the slope of the tangent to the curve at that point. The incremental elastic modulus (E_{inc}) is a measure of the slope at any given point of the stress-strain curve and is calculated by dividing the small change in stress ($\Delta\sigma$) about that point by the change in strain ($\Delta\varepsilon$) that results (Equation 2.4).

$$E_{inc} = \frac{\Delta\sigma}{\Delta\varepsilon} \tag{2.4}$$

2.2 Impedance in arteries

Impedance in the arterial system refers to the pressure per unit flow that opposes the motion of blood (Milnor, 1982; Nichols and O'Rourke, 1998). It

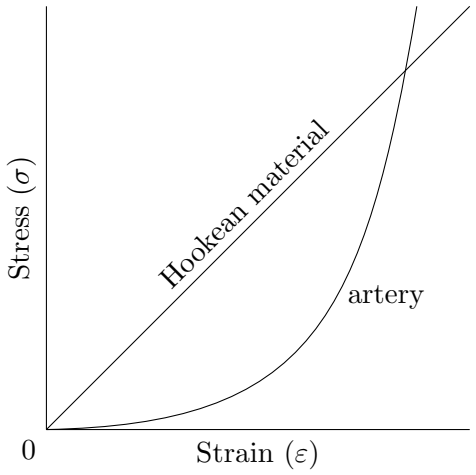

Figure 2.5: A stress strain curve for a purely elastic (Hookean) material and for an arterial segment. The arterial segment shows an increasing elastic modulus with increasing applied stress.

is a term derived from the study of electricity and is analogous to electrical impedance insofar as transmural pressure is analogous to voltage, blood flow analogous to current, and the pulsatile characteristic of arterial dynamics similar to the oscillation of an alternating current. Due to the complexities introduced by wave reflection and changes in arterial wall geometry and structure, four different terms of impedance have been developed to describe the opposition to the flow of blood. These terms are longitudinal, characteristic, input, and terminal impedance. The concept of impedance is relevant when expressed as a function of frequency (ω). Thus impedance is a complex quantity usually described in terms of modulus and phase as a function of frequency. As impedance is affected by arterial properties, stiffness of the arterial wall is a significant determinant of vascular impedance and a major factor determining oscillatory flow in large arteries (Milnor, 1982; Nichols and O'Rourke, 1998).

2.2.1 Longitudinal impedance

Longitudinal impedance (Z_L) is the ratio of the pressure gradient ($-dP/dx$) in a section of vessel to the rate of flow (Q) in that same section (Equation 2.5). It is a parameter particular to the local segment of artery being studied and does not depend on the dynamics of the arterial bed distal to that site (Nichols and O'Rourke, 1998).

$$Z_L(\omega) = \frac{-dP(\omega)/dx}{Q(\omega)} \tag{2.5}$$

2.2.2 Input impedance

The input impedance (Z_{in}) is the ratio of measured pressure (P_m) to measured flow (Q_m) (Equation 2.6). It is a condition at a localised site, is regarded as the input for the vascular tree distal of that point, and is a property reliant on both the properties of the distal arterial tree and of the site itself (Milnor, 1982).

$$Z_{in}(\omega) = \frac{P_m(\omega)}{Q_m(\omega)} \tag{2.6}$$

2.2.3 Characteristic impedance

Characteristic impedance (Z_c) is the input impedance of a section of vessel with an infinite downstream continuation of the segment of vessel. That is, characteristic impedance is the input impedance in conditions causing zero wave reflection. This is expressed mathematically as the ratio of the incident pressure wave (P_i) to the incident flow wave (Q_i), or equally the negative of the ratio of the reflected pressure (P_r) and flow (Q_r) waveform (Equation 2.7).

$$Z_c(\omega) = \frac{P_i(\omega)}{Q_i(\omega)} = \frac{-P_r(\omega)}{Q_r(\omega)} \tag{2.7}$$

True characteristic impedance cannot readily be calculated in the arterial system as wave reflections are always present. However, various methods have been devised for estimating the characteristic impedance in circumstances where the effect of wave reflection is minimal (Nichols and O'Rourke, 1998). O'Rourke and Taylor (1966) assumed a maximally dilated arterial bed had near zero wave reflection and therefore the ratio of measured pressure and measured flow was indicative of characteristic impedance. A second method analyses pressure and flow in the Fourier domain within frequencies where the effect of wave reflection is assumed to be minimal (O'Rourke, 1982). In the time domain, the region of late diastole and early systole is also assumed to be largely free from the influence of wave reflection. Dujardin et al. (1982) used this property to estimate characteristic impedance from the pressure and flow values during the initial systolic upstroke of the arterial pulse using the slope of phase plots of pressure and flow.

2.2.4 Terminal impedance

Terminal impedance, also known as peripheral resistance, is the input impedance in the hypothetical situation where the artery of interest is terminated immediately downstream of the site being measured. This approximates the situation of arteries terminating in arterioles of high resistance (Nichols and O'Rourke, 1998). Terminal impedance is expressed as the ratio of mean pressure ($\bar{P}$) to mean flow ($\bar{Q}$) (Equation 2.8).

$$Z_T = \frac{\bar{P}}{\bar{Q}} \tag{2.8}$$

Terminal impedance of tubular models can be expressed as a complex quantity incorporating a real term associated with resistance to steady state flow and an imaginary term associated with compliance of the peripheral vascular bed and blood inertia. Resistance (R) to steady-state flow depends on vessel calibre (r) and blood viscosity (η) and is a ratio of the pressure gradient ($P_1 - P_2$) and the flow (Q) through the arterial segment of length l (Equation 2.9–2.10). Vascular resistance is a major determinant of peripheral wave reflection.

$$R = \frac{P_1 - P_2}{Q} \tag{2.9}$$

$$= \frac{8\eta l}{\pi r^4} \tag{2.10}$$

2.3 *In-vivo* measurement of arterial stiffness

Due to the complexities in accurately measuring the stiffness of arteries, both *in-vivo* and *ex-vivo*, there have been many different indexes developed that proportionally relate experimental measurements to arterial wall stiffness. An extensive, though not exhaustive list of these indexes is tabulated for reference in Appendix A. Many measures of arterial stiffness have been made *ex-vivo* through either static or dynamic mechanical testing of arterial samples (Lillie and Gosline, 2006; Xie et al., 1995) or through *ex-vivo* inflation of arterial segments (Bergel, 1961a,b; Cox, 1978; Langewouters et al., 1984, 1985). Whilst *ex-vivo* work has applications furthering the understanding of the mechanics of the artery wall material, *in-vivo* analysis is required to fully understand arterial response in the physiological setting. Additionally, *in-vivo* methods are paramount in longitudinal studies of arterial proper-

ties, and in the study of acute arterial changes in human physiology. It is for these reasons that *in-vivo* experimental measurements of arterial stiffness are the main parameters of interest in the study of large arteries within this thesis.

In-vivo measurement of pressure-diameter relationships using external calipers (Gow, 1966) or intraluminal sensors (Stefanadis et al., 2000) have provided significant data on static and dynamic properties as well as data on wall viscoelasticity (Gow, 1972). These techniques are useful in providing quantitative data. However, they are quite complex. The work within this thesis extends these *in-vivo* investigations by the association of Pulse Wave Velocity (PWV) and arterial stiffness, a method which can readily be used in both experimental and clinical settings.

2.3.1 Pulse wave reflection

The incident, or forward going pressure wave is reflected from sites of impedance mismatch, such as arterial branching, changes in arterial diameter, and changes in vessel wall material stiffness. The magnitude of the reflected waveform is therefore dependent upon the geometry and the stiffness of the arterial tree distal to the site being measured. To resolve the incident (i) and reflected (r) waves from the measured (m) waveforms, both a measured pressure and flow waveform at the same site are required and must be decomposed into their frequency components (Nichols and O'Rourke, 1998; Westerhof et al., 1972). The measured waveform is the sum of the incident and reflected waveforms (Equation 2.11–2.12).

$$P_m = P_i + P_r \tag{2.11}$$

$$Q_m = Q_i + Q_r \tag{2.12}$$

The definition of characteristic impedance (Equation 2.7) can be substituted into Equation 2.11 to give Equation 2.13.

$$P_i = P_m + Z_c Q_r \tag{2.13}$$

Conversely, substituting Equation 2.12 into the equation for characteristic impedance (Equation 2.7) gives Equation 2.15.

$$P_i = Z_c \left(Q_m - Q_r\right) \tag{2.14}$$

$$Z_c Q_r = Z_c Q_m - P_i \tag{2.15}$$

Combining Equation 2.15 and Equation 2.13, the incident pressure wave can be expressed in terms of the measured pressure wave and the characteristic impedance (Equation 2.16). By repeating the method for reflected pressure, and incident and reflected flow, all incident and reflected waves can be expressed in terms of the characteristic impedance of the vessel, and the measured flow and pressure at that point (Equation 2.16–2.19).

$$P_i = \frac{P_m + Z_c Q_m}{2} \tag{2.16}$$

$$P_r = \frac{P_m - Z_c Q_m}{2} \tag{2.17}$$

$$Q_i = \frac{Q_m + P_m/Z_c}{2} \tag{2.18}$$

$$Q_r = \frac{Q_m - P_m/Z_c}{2} \tag{2.19}$$

With an estimate of characteristic impedance by one of several methods (Dujardin et al., 1982; O'Rourke and Taylor, 1966; O'Rourke, 1982), the incident and reflected waves can be directly calculated from the Fourier transforms of measured pressure and flow, the magnitude of the reflected wave compared to the incident wave giving indication of the distal geometry and arterial stiffness.

Often pressure but not flow is measured at a single site. Westerhof et al. (2006) developed a method of resolving the incident and reflected waveforms without a measured flow wave by approximating flow as a triangular waveform, peaking at either 30% of the ejection duration, or at the point of pressure wave inflection. In the study cited, aortic reflected and incident pressure waveforms calculated from the approximated flow wave did not differ significantly from values calculated from measured flow, suggesting that estimation of the flow pulse as a triangular wave is accurate for the purposes of calculating the incident and reflected pressure wave (Figure 2.6). Westerhof et al. (2006) also suggested two parameters for the measurement of the intensity of the reflected wave peak, indicative of arterial stiffness in the bed downstream from the site of measurement. These two parameters were the reflection magnitude of the pulse pressures (RM_{PP}) and reflection index of the pulse pressures (RI_{PP}) and are ratios of the pulse pressures of the

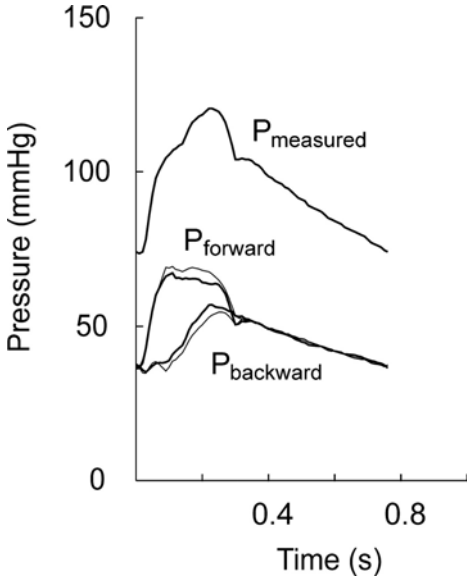

Figure 2.6: An example of a human aortic pressure wave decomposed into the incident and reflected components using measured flow (bold lines) and an estimated triangular flow (thin lines). A high correlation exists between the two methods. (Reproduced from Westerhof et al., 2006)

reflected (PP_r) and incident (PP_i) waves (Equation 2.20–2.21). The concept of flow wave estimation and pressure wave decomposition has been extended to a method of determining PWV using non-invasive measurement of a single peripheral pulse (Qasem and Avolio, 2007).

$$RM_{PP} = \frac{PP_r}{PP_i} \tag{2.20}$$

$$RI_{PP} = \frac{PP_r}{PP_r + PP_i} \tag{2.21}$$

An alternative to the widely accepted theory of wave transmission and reflection (Milnor, 1982; Nichols and O'Rourke, 1998) was been proposed by Wang et al. (2003) and Davies et al. (2007). This theory was based primarily on the *windkessel* principle (Figure 2.1) in which potential energy is stored in an aortic reservoir. Aortic pressure (P_{Ao}) is viewed as the summation

of the *windkessel* pressure (P_{Wk}) and the pressure due to wave motion, or "excess pressure" (P_{Ex}) where *windkessel* pressure is a function of time, and excess pressure a function of time and distance (Equation 2.22; Wang et al., 2003).

$$P_{Ao}(x,t) = P_{Wk}(t) + P_{Ex}(x,t) \tag{2.22}$$

Wang et al. (2003) found in a study of aortic pressure and flow in dogs that the excess pressure waveform was similar in shape to that of the aortic flow and the ratio of these two components was equal to the characteristic impedance of the vessel. If this alternate theory were to be adopted, wave reflection would no longer be viewed as a relevant phenomenon and arterial stiffness could be estimated by measuring characteristic impedance by resolving the aortic flow and excess pressure waves.

2.3.2 Pulse wave velocity, a biomarker of arterial stiffness

The study of the basic scientific principles of the velocity of the pulse wave through the arterial tree dates back to 1808 with the work of Thomas Young (Young, 1809). The relationship between PWV and arterial wall stiffness can be calculated from first principles using Newton's equation, $F = ma$. Using some simplifying assumptions, the following procedure can be applied to derive the Moens-Korteweg equation (Equation 2.35), an equation that directly relates PWV and artery wall stiffness (Milnor, 1982).

Examining an infinitesimally small segment of artery, the decrease in force within that segment is equal to the change in the pressure imposed on the area of that segment (Equation 2.23). Assuming the change in area of the vessel segment is small to the point of insignificance, the derivative of area can be substituted (Equation 2.24).

$$-\frac{\Delta F}{\Delta x} = \frac{\Delta(AP)}{dx} \tag{2.23}$$

$$\approx \frac{\pi r_i^2 dP}{\Delta x} \tag{2.24}$$

The force imposed by the fluid upon the segment is the product of the mass of fluid within the segment ($\rho\pi r_i^2 \Delta x$), and the acceleration of the fluid (dv/dt). Substituting this into Equation 2.24 and rearranging gives an equation for fluid motion in the vessel for the limiting case of $\Delta x \rightarrow dx \rightarrow 0$ (Equation 2.25).

$$-\frac{dP}{dx} = \rho\frac{dv}{dt} \tag{2.25}$$

The decrease in flow across the arterial segment can be expressed in terms of the change in volume in that segment (Equation 2.26). Alternatively, the decrease in flow can be expressed in terms of the product of the velocity of the fluid and the cross sectional area of the vessel, simplified again by the assumption that change in area is insignificant (Equation 2.27). Equating Equation 2.26 and Equation 2.27 gives the time dependent change in the internal radius of the vessel (Equation 2.28).

$$-\frac{dQ}{dx} = \frac{dV/dt}{dx} = \frac{2\pi r_i dr_i}{dt} \tag{2.26}$$

$$-\frac{dQ}{dx} = -\frac{d\,(vA)}{dx} = -\frac{\pi r_i^2 dv}{dx} \tag{2.27}$$

$$-\frac{dr_i}{dt} = \frac{r_i dv}{2dx} \tag{2.28}$$

Taking the definition of incremental elastic modulus (Equation 2.4), a substitution for stress and strain can be made (Equation 2.30). Under the assumption of a thin walled tube where changes in thickness are zero, stress is the force per unit area, or $r_i P/h$ (Peterson et al., 1960), the incremental change in stress subsequently being $r_i dP/h$, and the strain the change in radial dimension, dr_i/r_i.

$$E_{inc} = \frac{\Delta\sigma}{\Delta\varepsilon} \tag{2.29}$$

$$\approx \frac{r_i dP}{h} \cdot \frac{r_i}{dr_i} \tag{2.30}$$

The value of dr_i from Equation 2.28 substituted into Equation 2.30, gives Equation 2.31.

$$-\frac{dP}{dt} = \frac{E_{inc} h}{2r_i} \cdot \frac{dv}{dx} \tag{2.31}$$

Differentiating the equation for fluid motion (Equation 2.25), and differentiating Equation 2.31 gives Equation 2.32 and Equation 2.33 respectively. Equation 2.33 assumes that the term $dv(dr^{-1})dxdt$ is insignificant. Equation 2.32 and Equation 2.33 can then be equated for the common term $d^2v/dxdt$ to give Equation 2.34.

$$-\frac{d^2P}{dx^2} = \rho\frac{d^2v}{dxdt} \tag{2.32}$$

$$-\frac{d^2P}{dt^2} \approx \frac{E_{inc} h}{2r_i} \cdot \frac{d^2v}{dxdt} \tag{2.33}$$

$$\frac{d^2P}{dt^2} \cdot \frac{2r_i}{E_{inc} h} = \frac{d^2P}{\rho dx^2} \tag{2.34}$$

The term dx/dt, the PWV, is contained within Equation 2.34. Rearranging gives Equation 2.35, the Moens-Korteweg equation.

$$PWV = \sqrt{\frac{E_{inc} \cdot h}{2r\rho}} \tag{2.35}$$

The Moens-Korteweg equation states that PWV is proportional to the square root of the incremental elastic modulus of the vessel wall given constant ratio of wall thickness (h) to vessel radius (r) (Milnor, 1982; Nichols and O'Rourke, 1998) under the assumptions used to derive the equation, these assumptions being:

(i) there is no, or insignificant, change in vessel area,

(ii) there is no, or insignificant, change in wall thickness,

(iii) that $dv(dr^{-1})dxdt$ is small to the point of insignificance.

Measuring PWV

PWV by definition is the distance traveled (Δx) by the wave divided by the time (Δt) for the wave to travel that distance (Equation 2.36).

$$PWV = \frac{\Delta x}{\Delta t} \tag{2.36}$$

This holds true for a system with zero wave reflections. The transmission of the arterial pressure pulse does not give the true PWV as it is a sum of vectors of the incident and reflected waves. Therefore, appropriate pressure and flow measurements must be made to estimate the characteristic impedance and to calculate the incident, or the reflected pressure wave at two separate locations a known distance apart (Equation 2.16–2.19).

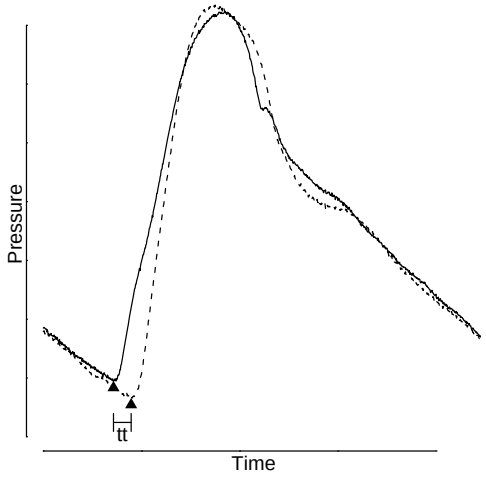

Figure 2.7: Measurement of PWV by the foot-to-foot method. The transit time (tt) of the pressure waveform between two sites a known distance apart is measured at the foot of the waveform, where wave reflection is absent, or minimal.

An alternate method of measuring PWV utilises the feature of the arterial waveform that during late diastole and early systole, there is no, or minimal, interference of the incident pressure wave by the reflected pressure wave (Bramwell and Hill, 1922b). With this assumption, PWV can be measured between two sites a known distance apart using the pressure 'foot' of the waveform to calculate the transit time (Figure 2.7). Exactly locating the pressure waveform foot can be subjective and less than accurate (Milnor, 1982). Chapter 3 addresses this issue with the development of a high fidelity, user independent method of finding the pressure waveform foot and calculating PWV. The advantage of foot-to-foot PWV measurement is the simplicity of measurement, requiring only two pressure wave forms recorded with invasive catheters, or mechanical tonometers applied non-invasively to the pulse across the skin, where the site of the two measurements are a known distance apart.

Bramwell and Hill (1922a) cited the Moens-Kortweg equation and proposed a series of substitutions relevant to observable haemodynamic mea-

sures. Quoting directly these substitutions were:

> *A small rise δp in pressure may be shown to cause a small increase, $\delta y = y^2 \delta p/Ec$, in the radius y of the artery, or a small increase, $\delta V = 2\pi y^3 \delta p/Ec$, in its own volume V per unit length. Hence $2y/Ec = dV/V dp$*

where c represents the wall thickness (defined here as h) and y the vessel radius (defined here as r). Substituting these observations into the Moens-Korteweg equation (Equation 2.35) gives the Bramwell-Hill equation with wave speed in terms of $dV/V dP$ (Equation 2.37; Bramwell and Hill, 1922b). This provides an alternate method of measuring PWV, where pressure can be measured, and flow and arterial dimension measured through techniques such as A or M-mode ultrasound or Doppler measurement of flow.

$$PWV = \sqrt{\frac{dP \cdot V}{\rho \cdot dV}} \tag{2.37}$$

A similarity between the Moens-Kortweg equation and Newton's equation for the wave speed (c_o) in a material (Equation 2.38) is evident, and both the Moens-Kortweg and Bramwell-Hill equations can be derived from Newton's equation for wave speed using the substitution of the equation of the bulk modulus in terms of volumetric strain (Equation 2.39).

$$c_0 = \sqrt{\frac{B}{\rho}} \tag{2.38}$$

$$B = -\frac{PV_0}{\Delta V} \tag{2.39}$$

The Waterhammer equation (Murgo et al., 1980; O'Rourke, 1982) gives an another alternate expression of PWV (Equation 2.41). The equation directly relates characteristic impedance (Z_c) to PWV through the ratio of

pressure (P) and linear flow velocity (v) in the absence of wave reflection. Subsequently, an estimate of characteristic impedance through pressure and flow measurement provides a measure of PWV, which is proportional to arterial stiffness.

$$PWV = P_i / (v_i \cdot \rho) \tag{2.40}$$

$$= Z_c / \rho \tag{2.41}$$

Throughout this thesis, the main value used as a measure of arterial stiffness is PWV. PWV was chosen as a marker of arterial stiffness due to the ease of measurement in intact animals and human subjects, the reproducibility of the stiffness parameter (Wilkinson et al., 1998a), the strong correlation between PWV and cardiovascular events and all-cause mortality (Blacher et al., 1999a,b; Cruickshank et al., 2002; Laurent et al., 2001a), the acceptance of PWV as a measure of arterial stiffness (Nichols, 2005; Wilkinson et al., 1998b), and the recent acceptance by the European Society of Hypertension that PWV measurement is integral to the diagnosis and treatment of hypertension (Mancia et al., 2007). The PWV measurement method used in all experimental work was the pressure wave foot-to-foot method. This method was chosen due to the ease of measurement and the ability to access arterial segments in the live animal without disturbing the physiology of the segment by the introduction of a dual pressure sensing catheter. Such methods allow the study of the artery in the natural state.

2.3.3 Pressure-strain elastic modulus

The pressure-strain elastic modulus, or Peterson's modulus, (E_p) is defined as the change in pressure multiplied by the inverse of strain (Equation 2.42). The subscript, p, refers to the relation of the elastic modulus to pressure, as opposed to tension (Peterson et al., 1960). Bergel (1961a,b) derived Equation 2.43 for the incremental modulus in a thick walled tube. The definition of Peterson's modulus can be substituted into Equation 2.43 to define the relation between Peterson's modulus and the incremental modulus (Equation 2.45; Gow and Taylor, 1968). Substituting the Bramwell-Hill equation (Equation 2.37) into the volumetric definition of the pressure-strain elastic modulus (Equation 2.42) defines the pressure-strain modulus in terms of PWV, the relationship shown in Equation 2.46 (Farrar et al., 1978).

$$E_p = \frac{\Delta P \cdot r_o}{\Delta r_o} = \frac{2\Delta P \cdot V}{\Delta V} \tag{2.42}$$

$$E_{inc} = \frac{2r_i^2 r_o \left(1-\nu^2\right) \Delta P}{\left(r_o^2 - r_i^2\right) \Delta r_o} \tag{2.43}$$

$$= \frac{2r_i^2 \left(1-\nu^2\right) \cdot E_p}{r_o^2 - r_i^2} \tag{2.44}$$

$$= \frac{2\left(1-\nu^2\right)\left(1-\frac{h}{r_o}\right)^2 E_p}{1-\left(1-\frac{h}{r_o}\right)^2} \tag{2.45}$$

$$E_p = 2\rho PWV^2 \tag{2.46}$$

A measure of transmural pressure and arterial radius gives the parameters required to calculate Peterson's modulus, an indicator of the incremental

elastic modulus, assuming the change in wall thickness (h) and vessel radius (r) is insignificant. This assumption is generally true, but the assumption does not hold true for comparisons between disease groups (de Groot et al., 2004) and across longitudinal studies (de Groot et al., 2005).

The inverse of Peterson's modulus gives an inverse parameter of arterial stiffness, defined as distensibility by O'Rourke et al. (2002) and compliance by Gosling and Budge (2003) (Equation 2.47).

$$\frac{1}{E_p} = \frac{\Delta r}{\Delta P \cdot r} \tag{2.47}$$

2.3.4 Augmentation Index (AIx)

The reflection of the forward going pressure wave by elastic non-uniformity and partial barriers such as branching and narrowing of arteries creates a backward travelling wave. This backward travelling wave sums with the forward travelling wave to form the augmented or measured waveform. Augmentation index is a measure of the degree to which the peak of a measured pressure wave is over and above the peak of the incident pressure wave due to the addition of the reflected pressure wave (Figure 2.8). Augmentation index is dependent on the timing and magnitude of the reflected waveform and is a measure of the compliance and structure of vessels distal to the site of measurement.

Two methods of calculating augmentation index exist (Equation 2.48–2.49), each giving rise to a different value of the index. The more prevalent augmentation index quoted in current literature is the definition provided in Equation 2.49, where P_s is the systolic pressure, P_d the diastolic pressure, and P_i the inflection point in the pressure waveform. The inflection point can be located by the time of peak of a simultaneously recorded blood flow,

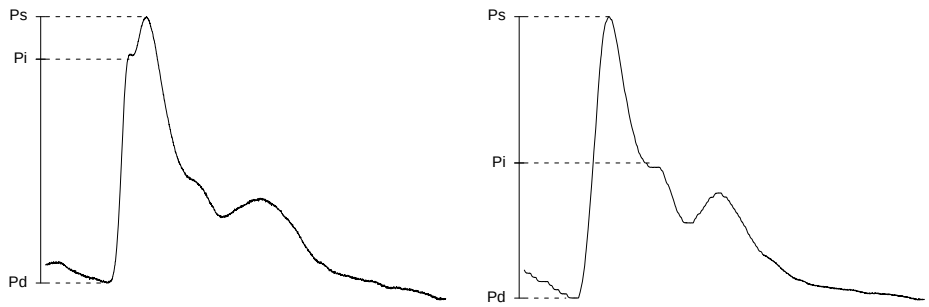

(a) **(b)**

Figure 2.8: Positive and negative augmentation index and the location of the inflection point in radial artery waveforms. P_s is the systolic pressure, P_d the diastolic pressure, and P_i the inflection point in the pressure waveform. If the inflection point occurs before the systolic peak, the AIx is positive (a). If the inflection point occurs after the systolic peak, the AIx is negative (b).

which coincides with the first positive to negative zero crossing of the fourth derivative of pressure (Nichols and O'Rourke, 1998).

$$AIx = \frac{P_i - P_d}{P_s - P_i} \tag{2.48}$$

$$AIx = \frac{P_s - P_i}{P_s - P_d} \tag{2.49}$$

Augmentation index is dependent on the transit time of the reflected wave and the time of arrival of the reflected wave during the pressure pulse. Therefore, augmentation index is sensitive to heart rate. A slower heart rate will cause the reflected wave peak to occur relatively earlier in systole, which will increase the augmentation index. Conversely, a faster heart rate is associated with the the reflected wave arriving relatively later in systole, or during diastole, causing a decrease in the augmentation index.

The importance of the distinction between PWV and augmentation index was highlighted in the recent Anglo-Cardiff Collaborative Trial (ACCT) (McEniery et al., 2005). The study showed that whilst both PWV and aug-

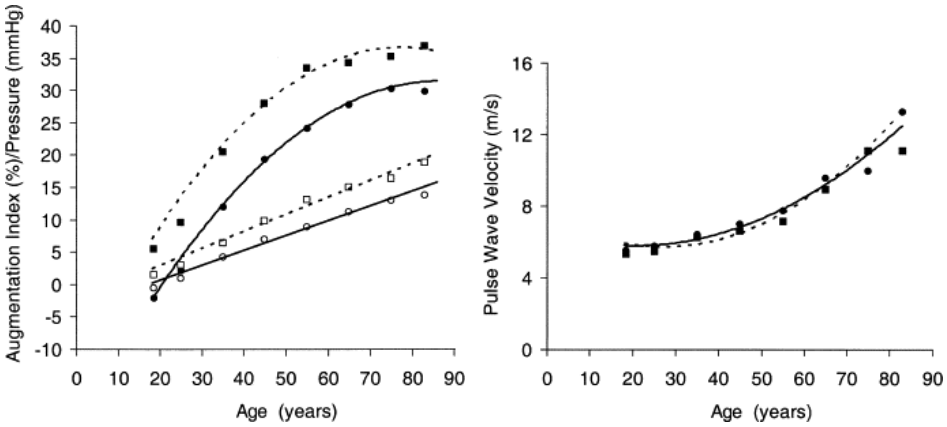

Figure 2.9: Age related changes for males (●) and females (■) in AIx and PWV. Augmentation pressure is also plotted for males (○) and females (□). AIx increases substantially more than PWV in youth, whilst PWV is the dominant changing factor in older years. (Reproduced from McEniery et al., 2005)

mentation index increased with age, age related changes in augmentation index were more prominent in younger subjects, and changes in PWV were much more pronounced in older subjects (Figure 2.9). The different changes in the two stiffness parameters with age highlights the fact that whilst PWV and augmentation index are both measures of arterial stiffness, the two parameters are measures of different elements of the arterial system. Generally, PWV is a characteristic of the local segment of artery being studied, and augmentation index is a measure dependent upon both the local segment and the vascular tree beyond that segment.

2.4 Functional control of large arteries

The artery wall is a composite material of load bearing structural components elastin and collagen, and an additional functional, dynamic component, smooth muscle. Both structural and functional components contribute to arterial stiffness and the subsequent load on the heart (Figure 2.10; Greenwald, 2002, 2007). Functional change in arteries refers to the dynamic alter-

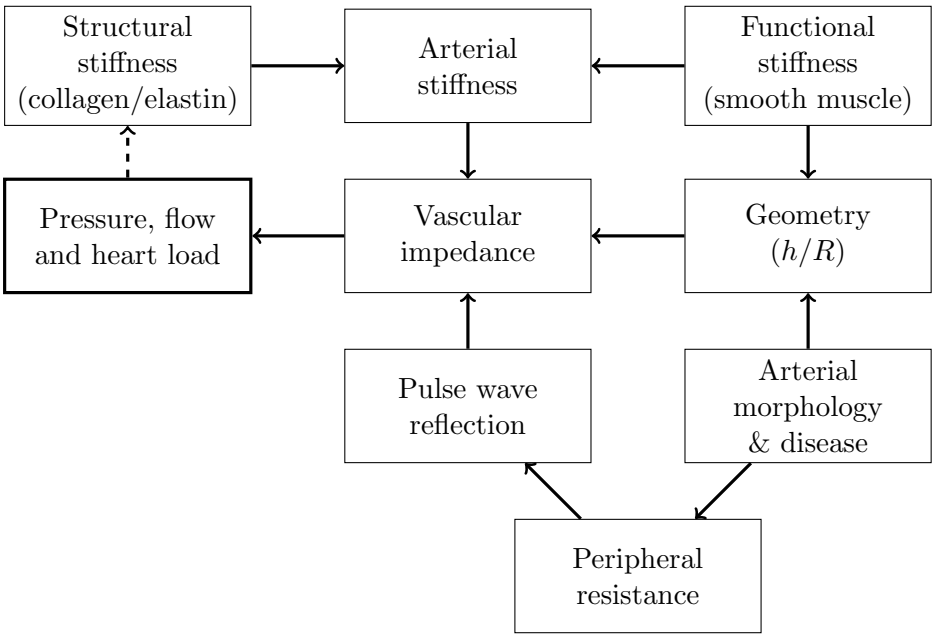

Figure 2.10: Block diagram showing the contribution of structural and functional stiffness, arterial geometry, and pulse wave reflection on impedance and arterial pressure and heart load. Arterial pressure has a medium to long term feedback mechanism on arterial structure (dashed line). (Concept from Greenwald, 2002, 2007).

ation of stiffness through changes in smooth muscle tone. Changes in smooth muscle tone are affected through chemical signalling pathways initiated either endogenously, or exogenously. There are a vast array of endogenous and exogenous vasoactive drugs. The following is a discussion of the vasoactive substances that are of direct concern within the work presnted in this thesis.

2.4.1 Endothelium derived nitric oxide

The role of the endothelium in the relaxation of arterial vessels was first proposed by Furchgott and Zawadzki (1980). Furchgott and Zawadzki showed that denuded arterial vessels exhibited little or no relaxation in response to acetylcholine *in-vitro*. However, carefully extracted segments with the endothelial lining intact did show a dilatory response to acetylcholine. The conclusion drawn was that the endothelium has a role in the relaxation of

arterial vessels and is not simply a passive component providing an inert interface between blood and tissue. It was proposed that the endothelium secretes a substance, or substances, in response to the presence of acetylcholine, that permits the relaxation of the smooth muscle fibres in the arterial wall.

The term endothelial derived relaxing factor (EDRF) first appeared in 1984 in a review of endothelium dependent relaxation studies performed up to that point, including the response to acetylcholine, bradykinin, histamine, thrombin, serotonin, and noradrenaline (Furchgott et al., 1984). It was not until 1987 that Palmer et al. proposed that EDRF was nitric oxide (NO), based upon evidence showing that the relaxation shown by vessels in response to EDRF and NO were identical and indistinguishable (Figure 2.11a; Palmer et al., 1987). Palmer et al. (1988a), in *ex-vivo* study of porcine endothelial cells and the effect of relaxation on rabbit aortic strips, found that L-arginine was the precursor in the formation of endogenous NO (Figure 2.11b; Palmer et al., 1988a).

An intermediate step between the generation of NO from L-arginine is the formation of nitric oxide synthase (NOS) . There are three types of NOS, defined by the location at which they are generated: Type I NOS is generated in epithelial and neural cells; type II in macrophages; and type III in endothelial and myocardial cells and in platelets (Gamboa et al., 2007). Two further sub-classifications of NOS have been made, namely inducible nitric oxide synthase (iNOS), mostly of the category of type II NOS, and a form produced specifically by vascular endothelial cells, endothelial derived nitric oxide synthase (eNOS). The role of eNOS in human vascular tone was studied by Vallance et al. (1989). N^G-monomethyl-L-arginine (L-NMMA), an L-arginine analogue that inhibits the formation of endothelial derived NO

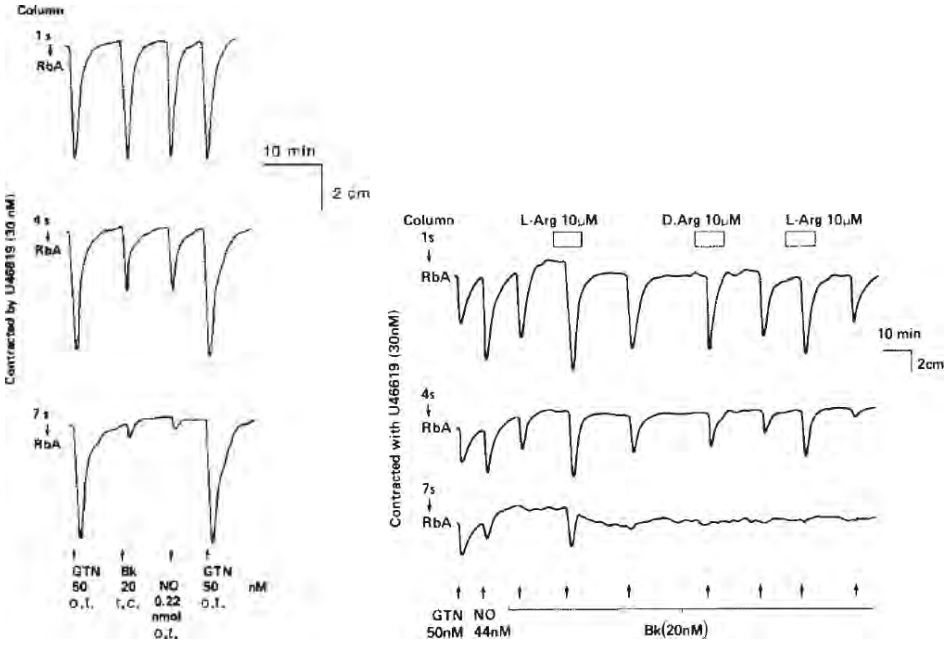

Figure 2.11: Revealing the source of EDRF. In the studies of Palmer et. al. on the contraction of rabbit aortic strips (RbA), 2.11a endogenous NO was shown to be indistinguishable from the EDRF effect of bradykinin (Bk). GTN was used to standardise the test. 2.11b In tests of similar method, L-arginine (L-Arg) but not D-arginine (D-Arg) was shown to have an additive effect to that of NO release through bradykinin. (Reproduced from Palmer et al., 1988a, 1987)

(Palmer et al., 1988b), infused in the brachial artery of healthy subjects caused a reduction in forearm blood flow, indicating vascular constriction (Vallance et al., 1989). The study also demonstrated that L-NMMA reduced the dilatory response of infused acetylcholine, which promotes endothelial derived NO , but not that of GTN, an exogenous NO source, indicating that eNOS is involved in the maintenance of basal vascular tone. Wilkinson et al. (2002b), with systemic infusion of L-NMMA in healthy individuals, showed an increase in aortic augmentation index, demonstrating that endothelial derived NO also regulates stiffness in large arteries. Arterial stiffness was also measured directly by local PWV, and local infusion of L-NMMA, acetylcholine, and GTN in the ovine iliac artery demonstrated the direct effect of endothelial derived NO on large artery stiffness (Wilkinson et al., 2002c). Schmitt et al. (2005) later repeated the experiment in the human iliac artery and found the results consistent with previous observations in the animal model. The production of endogenous NO has potential blood pressure regulation effects significant enough to play a role in hypertension (Haynes et al., 1993).

Vascular smooth muscle relaxation induced by NO occurs through the generation of cyclic guanosine monophosphate (cGMP), derived from guanosine triphosphate (GTP), which in turn is activated by the NO product guanylate cyclase (Figure 2.12; Vane et al., 1990). Endothelium derived NO also has a role in preventing blood coagulation by inhibiting platelet aggregation and cell adhesion (Ferro, 2003; Moncada et al., 1991) and plays a role in vascular remodelling by inhibiting the proliferation of smooth muscle cells (Moncada et al., 1991).

Endogenous NO is stimulated by shear stress on endothelial cells and a basal release of endothelium derived NO is responsible for maintenance of vascular smooth muscle relaxation (Haynes et al., 1993; Kinlay et al., 2001;

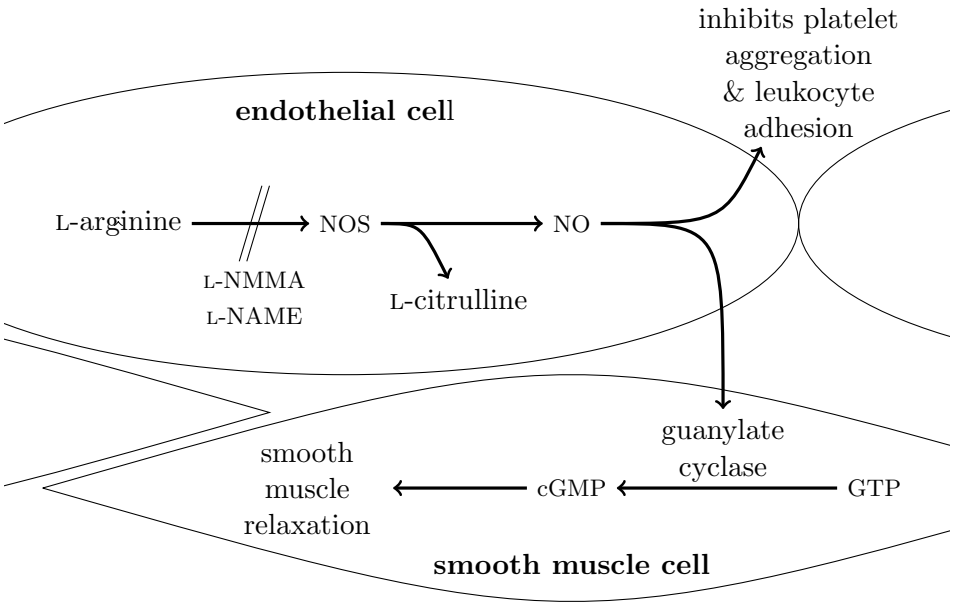

Figure 2.12: The L-arginine–nitric oxide (NO) pathway inducing smooth muscle relaxation. L-arginine is oxidised via nitric oxide synthase (NOS) to form NO. NO in the smooth muscle cell stimulates guanylate cyclase, which converts guanosine triphosphate (GTP) to cyclic guanosine monophosphate (cGMP), which in turn causes smooth muscle relaxation. NO is also involved in the inhibition of platelet aggregation and leukocyte adhesion. The conversion of L-arginine to NO is prevented by analogues of L-arginine, such as N^G-monomethyl-L-arginine (L-NMMA) and N^ω-nitro-L-arginine methyl ester (L-NAME). (Adapted from Vane et al., 1990)

Vallance et al., 1989). An exogenous source of NO is sodium nitroprusside (SNP). SNP releases NO directly, though the mechanism of release is not fully understood (Brunton, 2006). NO derived from SNP acts on vascular smooth muscle in the same manner as endothelial derived NO, through activation of cGMP. It is fast acting, with an onset within 30 seconds and has a maximal hypotensive effect in humans in less than 2 minutes of continuous intravenous infusion (Brunton, 2006).

Prostacyclin is another factor derived from the endothelium that induces vascular smooth muscle relaxation. Prostacyclin is synthesised from phospholipase A_2 in a pathway involving arachidonic acid, cyclooxygenase, and prostaglandin in endothelial cells (Vane et al., 1990). Prostacyclin has antithrombotic properties and causes smooth muscle relaxation, however, it is NO, not prostacyclin, that is primarily associated with vasodilation due to increased shear stress on the endothelium (Joannides et al., 1995).

2.4.2 Vasoconstrictors

A select number of vasoconstrictors are of direct concern in the work presented in this thesis. These substances include the vasoconstrictors phenylephrine, noradrenalin, angiotensin-II, and Endothelin-1 (ET-1). The work contained in Chapter 8 investigates the role of a selection of these vasoconstrictors in the alteration of functional large artery stiffness.

Phenylephrine

Phenylephrine is an adrenergic α_1-receptor agonist causing vasoconstriction in the peripheral vasculature when introduced intravenously (Brunton, 2006). Phenylephrine is also a cardiotonic agent, associated with activation of α_1-adrenergic receptors and upregulation of cyclic adenosine

monophosphate (cAMP) (Tahiliani et al., 1982).

Noradrenaline

Noradrenaline, the precursor of adrenaline, is a vasoconstrictor produced by the adrenal medulla, synthesised from the amino acid tyrosine, and is released by the central nervous system and peripheral sympathetic nerves (Brunton, 2006). Noradrenaline is an α_1- and α_2-adrenoreceptor antagonist (Bevan et al., 1988) causing smooth muscle contraction associated with adenosine triphosphate (ATP) sensitive K^+ channels and membrane depolarisation (Tan et al., 2007).

Angiotensin-II

Angiotensin-II is the active form of the decapeptide angiotensin, synthesised from angiotensin-I in the presence of renin and Angiotensin-Converting Enzyme (ACE) (Equation 2.50; Brunton, 2006). Both renin and angiotensin are found in the circulatory system, renin originating in the kidneys and ACE found in plasma and on the vascular lumen surface that is the endothelial cells. Angiotensin has both a chronic, and an acute vasopressor action. Angiotensin-II rapidly increases peripheral resistance and systemic pressure by increasing smooth muscle tension in arterioles, by increasing noradrenaline concentration at sympathetic nerve synapses thereby increasing sympathetic stimulated vasoconstriction, and increases vessel response to circulating noradrenalin (Brunton, 2006; Zimmerman et al., 1984). Chronic increases in blood pressure by angiotensin-II are effected by alteration to Na^+ reabsorption in the kidneys, and by stimulating aldosterone expression from the adrenal cortex, which increases Na^+ reabsorption and K^+ excretion (Brunton, 2006; Zimmerman et al., 1984).

$$\text{Angiotensinogen} \xrightarrow{\text{Renin}} \text{Angiotensin}-\text{I} \xrightarrow{\text{ACE}} \text{Angiotensin}-\text{II} \qquad (2.50)$$

Endothelin-1 (ET-1)

Endothelin-1 (ET-1) is is a 21-amino acid peptide produced at various sites throughout the body including in the central nervous system and in endothelial and smooth muscle cells of blood vessels (Vane et al., 1990). As such, it is an endothelial derived contracting factor. It is derived from pro-ET-1 in the presence of endothelin converting enzyme (ECE), which is found in endothelial cells (Ferro, 2003). Vascular ET-1 release is stimulated by a number of factors, including agiotensin-II, thrombin, cytokines, and shearing forces on the vascular wall, whilst inhibited by NO, prostacyclin, and Atrial Natriuretic Peptide (ANP) (Ferro, 2003). The vasoconstrictive properties of ET-1 were first demonstrated by Yanagisawa et al. (1988), who showed that the action of ET-1 is extremely potent and prolonged. Endogenous ET-1 has been shown to increase vascular tone in the peripheral vasculature in humans (Haynes and Webb, 1994) and in the large arteries in sheep (McEniery et al., 2003). The action of ET-1 on arterial smooth muscle is predominantly associated with activation of the Endothelin-A (ET_A) receptor, as demonstrated by co-infusion of the selective ET_A receptor antagonist, BQ-123 (Spieker et al., 2003; Spratt et al., 2001). This was confirmed for endogenous vascular ET-1 in the work of Halcox et al. (2007) by contrasting the effects of the selective ET_A receptor antagonist, BQ-123, with the effects of the ET_A and ET_B receptor antagonist, BQ-788.

2.4.3 Inflammation and the effect on arterial stiffness

Systemic inflammation has been identified as central to atherosclerotic processes (Libby, 2002; Libby et al., 2002) and is considered a risk factor for cardiovascular disease (Ridker et al., 1997, 2000; Willerson and Ridker, 2004). In various sub-populations, inflammatory markers such as c-reactive protein (CRP) have shown a high correlation to arterial stiffness indexes such as augmentation index (Kampus et al., 2004, 2007, 2006) and both aortic and brachial PWV (Mattace-Raso et al., 2004; Yasmin et al., 2004), as well as being associated with increased pulse pressures (Abramson et al., 2002). Yki-Jarvinen et al. (2003) suggest a role of endothelial dysfunction associated with inflammation, showing correlation between increased levels of inflammation and reduced endogenous NO associated with iNOS activity. The role of inflammation in arterial stiffness, including investigation of the role of vasoactive substances associated with inflammation and the impact on functional arterial stiffness, is the subject of ongoing research. Chapter 4 in this thesis addresses an experimental model of acute inflammation in rats, providing new findings in this current area of research.

2.5 Structural changes in large arteries

Functional changes in arterial distensibility concern short acting, reversible alterations in arterial smooth muscle tension. Over longer periods of time, spanning months or years, the artery undergoes changes in the structural arrangement and quantities of smooth muscle, collagen and elastin, altering vessel wall stiffness, vessel wall thickness, and luminal diameter (Mulvany, 1993). This arterial remodelling is in response to chronic applied forces such as pulse pressures (Laurent et al., 2001b) and endothelial shear stress

(Gambillara et al., 2005; Stone et al., 2007). Arterial remodelling can also be induced by genetic predisposition to changes in elastin and collagen networks, and by environmental factors such as diet (Avolio, 1995; Avolio et al., 1985). This thesis investigates two specific structural changes in large artery composition, namely calcification of arterial vessels (Chapter 7), and the development of lesions in the internal elastic laminae of the abdominal aorta (Chapter 6).

CHAPTER 3

Continuous pressure wave analysis and measurement of pulse wave velocity

Conventional use of the arterial pulse is essentially related to measurement of heart rate, systolic and diastolic pressure, and other secondary associations such as changes in blood oxygen saturation using finger photoplethysmography (Mackenzie et al., 2005; Middleton and Henry, 2000). However, long before the quantification of levels of blood pressure (Riva-Rocci, 1896), the morphology of the the pressure pulse wave obtained from a peripheral location was used to describe various pathological conditions (Mahomed, 1872). Is is now generally accepted that the pressure pulse wave carries significant information that may be used in interventional and longitudinal studies in both human and animal subjects (Lacolley et al., 2006; O'Rourke, 2006). This information includes simple markers such as the systolic, diastolic and mean pressures, time intervals and waveform features such as the Augmentation Index (AIx). If two pressure waveforms are recorded simultaneously at a known distance apart, a measurement of Pulse Wave Velocity (PWV) can be made, an indicator of the stiffness of arterial vessels. The addition of

flow wave data allows calculation of impedance values, power calculations, and the resolving of incident and reflected wave components (Chapter 2). A suite of adaptable analysis tools were developed in the Octave programming language (Eaton, 2002) for the beat-to-beat measurement of pressure waveform characteristics and PWV from haemodynamic data acquired in experimental animals and humans both invasively and non-invasively, the results of which are presented throughout this thesis. Commercial software is available to perform some of these operations. ADInstruments Powerlab Chart software (ADInstruments, 2007) is able to dynamically analyse signal peaks, however mathematical computation is limited and the accuracy in finding poorly defined peaks is inadequate. AtCor Medical provide SphygmoCor software (Atcor Medical, 2007), designed for analysis of non-invasive pressure waveform data with the ability to analyse any human pressure waveform when provided with that data. However, variability of waveform input, for example from different animal species with differing heart rates or variable interference from respiratory pressure fluctuations, limits the use of this software. The commercial software lacks the flexibility for detailed experimental analysis and the need to perform more complex or novel analysis methods is not met.

The basis of the developed tools was the ability to analyse each individual pulse and output this pulse-by-pulse analysis for statistical analysis, allowing the interrelationship between multiple haemodynamic variables with respect to time to be ascertained (Figure 3.1). Within the experimental work described in this thesis, analysis was confined to the interrelationship of pressure and arterial stiffness on a pulse-by-pulse basis. Ongoing work applies these analysis tools to inspect the dynamic response of mean and pulse pressures, arterial stiffness, heart rate and heart rate variability to various

haemodynamic interventions, including acute pharmacological changes in systemic pressure.

The analysis tools were designed to be devoid of operator qualitative input. Therefore, the process was user independent and so blinding to experimental data was not required. Automation of the analysis process also permitted analysis of large amounts of data. Where traditionally an average PWV measurement was taken over 10 to 30 representative waveforms (Niederhoffer et al., 1997b), the automation of the process permitted analysis of large segments of data, from minutes to hours in length. The following is a brief description of the methods used to analyse the pressure waveform and to calculate PWV on a pulse-by-pulse basis. The algorithms outlined are those settled upon as the most reliable and accurate after an exhaustive analysis, and have been used to arrive at the results presented throughout this thesis.

3.1 Segmenting of the pressure waveform

All recorded signals were divided into individual periods or pulses bounded by the peak of the QRS complex in the electrocardiogram (ECG) waveform. The recorded ECG was down-sampled to 200Hz for large animals (sheep) and humans and 1kHz for small animals (rats). The lower sampling rate filtered out high frequency noise and minimised processing time without losing signal features. To counteract baseline fluctuation or drift, analysis was conducted on the first derivative of the ECG waveform. The steep slope of the QRS complex is associated with a peak in the first derivative of ECG that is easily detectable.

To extend the flexibility of the analysis package, a method of segmenting the pressure waveform in the absence of an ECG signal was developed. This

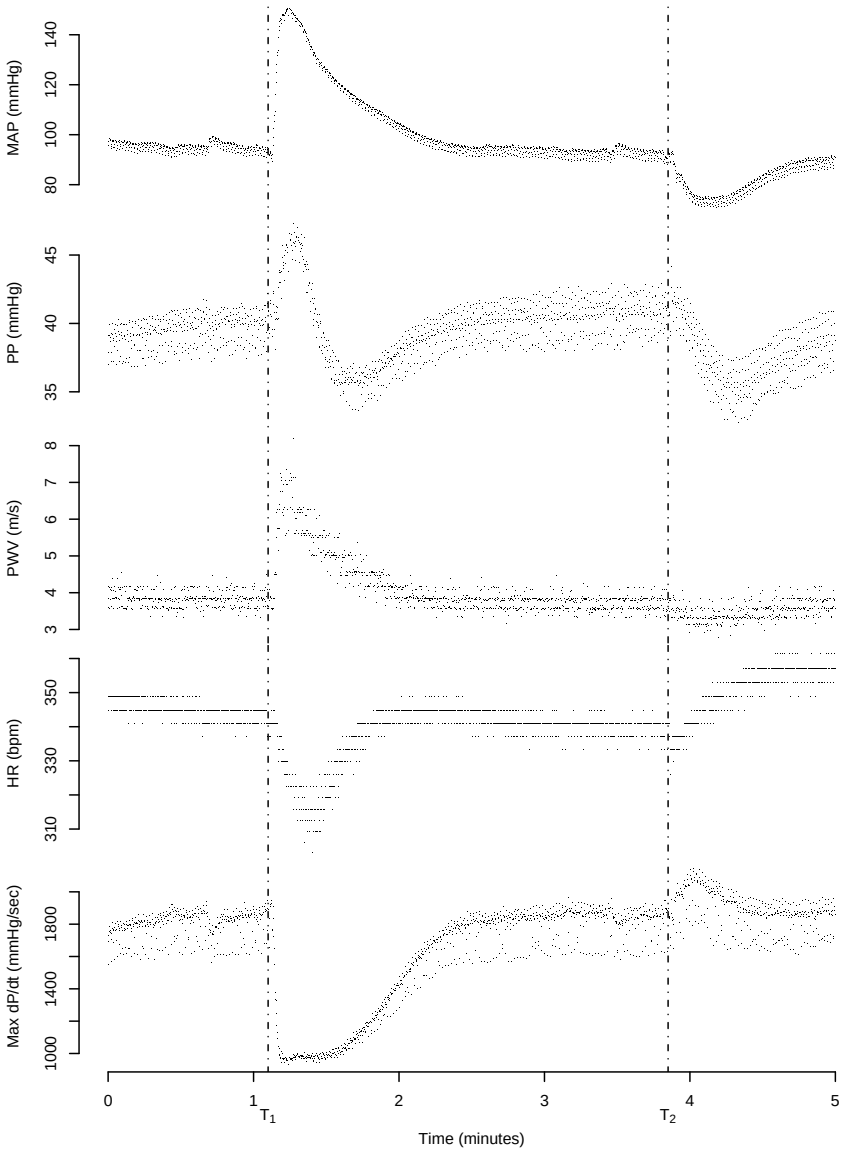

Figure 3.1: An example of the pulse-by-pulse analysis across time recorded in a rat during venous bolus dose of phenylephrine at time T_1 and sodium nitroprusside (SNP) at time T_2. Haemodynamic variables plotted are the MAP, PP, PWV, HR and an experimental variable, the maximum rate of pressure change, dP/dt. Each dot represents a single pressure pulse. Variability in MAP is due to respiratory changes in intrathoracic pressure. The pulse-by-pulse nature of analysis addresses this variability. The effect of pharmacologically induced changes in mean pressure can be seen simultaneously on all variables. Of note is the vagal reflex response to an increase in MAP, with a decrease in HR and also in maximum of dP/dt, indicating a decrease in cardiac contractility. The inverse is true when pressure is pharmacologically reduced.

method was utilised where the ECG signal was absent or excessively noisy. The first derivative of the pressure waveform was used, and the peak of the first derivative detected using the same algorithm applied to the ECG signal, previously described. The peak of the first derivative of pressure falls during the systolic upstroke. To segment the pressure wave during late diastole, the midpoint between peaks of the first derivative of pressure was calculated, and the pressure wave segmented using those points.

Where the ECG signal was analysed, the period of the segmented waveform defined the R to R interval, which was made available in the output with potential for calculation of heart rate variability indexes. For segmenting of the waveform by both ECG and directly by the pressure waveform, the inverse of the period was output as a measure of heart rate.

Using the segmented pressure waveforms, simple haemodynamic markers were calculated for each individual pulse. The simplest of these included the diastolic pressure (minimum point), systolic pressure (maximum point) and mean pulse pressure (mean for the individual pressure pulse).

3.2 Pulse wave velocity measurement

The PWV algorithm was designed with robustness and accuracy in mind across a range of different pressure waveform shapes, across different animal species (Figure 3.2). The algorithms were designed to calculate PWV using two simultaneously recorded pressure waveforms a known distance apart, or two non-simultaneous recordings of pressure superimposed by gating to a recorded ECG signal. A high sampling rate was used to increase the sensitivity of the PWV measurement. A sampling rate of 10 kHz was chosen, which gives a sensitivity of ±0.05 milliseconds for any individual detected point, equivalent to ±0.001 $m \cdot s^{-1}$ for a PWV of 10 $m \cdot s^{-1}$, that is, a resolution of

0.1%. For data recorded at sampling rates lower than 10 kHz, the data was re-sampled using a summation of sinc functions across a Blackman window of the data.

A number of techniques were trialled in finding an algorithm to accurately calculate the transit time of the pulse wave and the PWV robustly across a variety of waveform shapes. The final techniques used were those that detected the diastolic foot of the pressure wave (Chapter 2), assuming this region free from the effect of wave reflection (Bramwell and Hill, 1922b).

3.2.1 Foot detection by the absolute minimum

The simplest method to locate the pressure waveform foot is to find the minimum point of the waveform. Whilst this is accurate in some cases (Figure 3.3a), it can be erroneous in cases where the foot of the pressure wave is elongated (Figure 3.3e), or where the minimum point is not associated with the pressure waveform foot (Figure 3.3c). In the analysis conducted within this thesis, PWV in the rat was measured by foot-to-foot transit time defined by the pressure waveform feet located by the minimum point of the pressure waveform as the waveform foot was consistently acute and defined at the minimum point.

3.2.2 Foot detection by a single line of fit during early systole

An alternative method locates the pressure waveform foot at the intersection of linear regression during late diastole and early systole (Mitchell et al., 1997). Whilst the method is accurate in isolated cases, in situations where a large degree of diastolic variation is present the algorithm produces pulse-to-pulse results of high variability. A new method of pressure foot location has been developed that relies solely on the early segment of the systolic up-

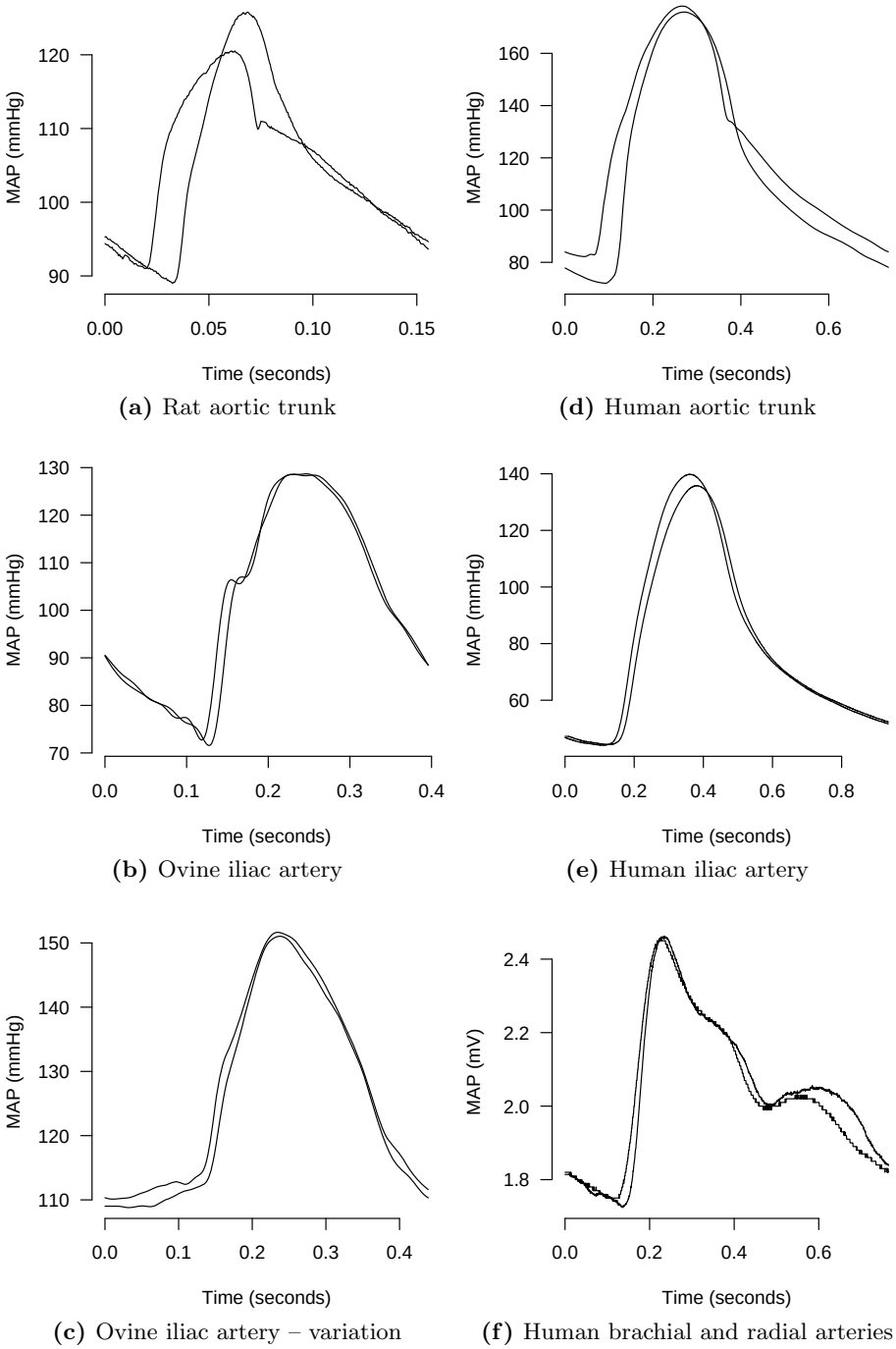

(a) Rat aortic trunk

(d) Human aortic trunk

(b) Ovine iliac artery

(e) Human iliac artery

(c) Ovine iliac artery – variation

(f) Human brachial and radial arteries

Figure 3.2: Examples of differing pressure waveform shapes in different animal species at different vascular sites. (a) Typical waveforms from the thoracic and abdominal rat aorta recorded invasively with a dual pressure sensing catheter. (b) The pulse of the iliac artery in the sheep, also taken invasively with a dual pressure sensing catheter. (c) One of many variations on the sheep iliac pulse, showing that variance from one individual to the next, and within the individual, can cause large changes in the shape of the pressure waveform foot. (d) Invasively taken dual pressure recording in the human aorta. (e) An example of a waveform recorded invasively in the human iliac artery. (f) A non-invasive, uncalibrated pressure waveform at the brachial and radial sites in a human subject.

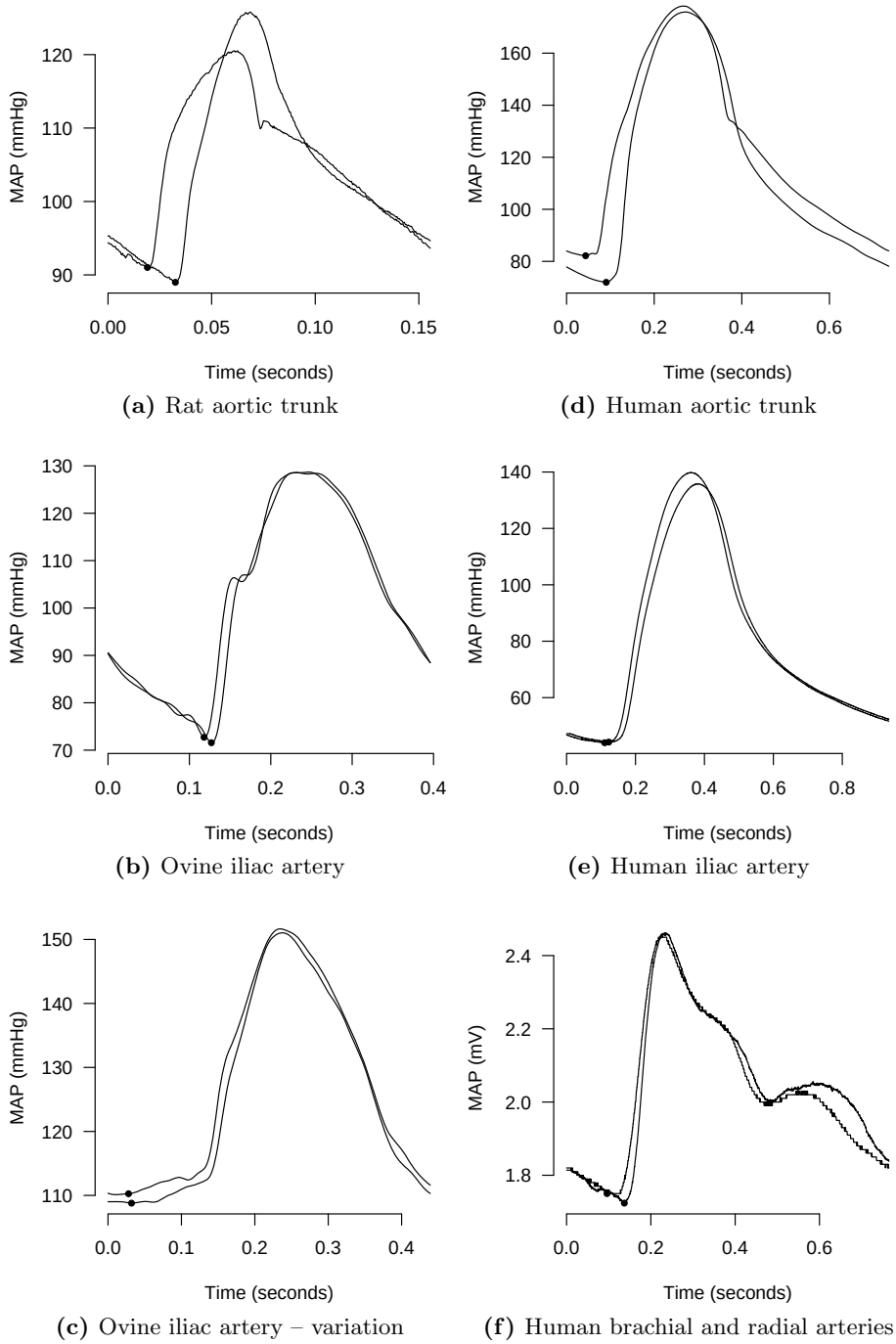

(a) Rat aortic trunk

(d) Human aortic trunk

(b) Ovine iliac artery

(e) Human iliac artery

(c) Ovine iliac artery – variation

(f) Human brachial and radial arteries

Figure 3.3: Transit time measured by a foot-to-foot method, using the minimum point to locate the pressure wave foot (●). This simple method locates the pressure waveform foot in most cases. However, it is an unsuitable method for certain pressure waveform variations, such as where end diastole plateaus at the minimum point (e). There are also certain variations where a clear minimum point is not associated with the start of systole (c).

stroke of the pressure waveform. The early systolic upstroke is not subject to the variability of late diastole, and is assumed to be free from augmentation by the reflected pressure wave (Bramwell and Hill, 1922b). A linear regression was fitted to the early component of the systolic upstroke, between an adjusted point related to the maximum of second derivative, and the point at one third of the pressure waveform height. The maximum of the second derivative itself is associated with the pressure waveform foot, thus the line of regression passes close to the pressure waveform foot. The deviation of the regression line from the pressure waveform was calculated and the point where the regression line deviated from the pressure waveform by 10% of the pulse pressure height was defined as the pressure waveform foot (Figure 3.4).

The method of locating the pressure waveform foot by linear regression solely during early systole provided accurate results for various arterial pressure waveforms recorded in rats, sheep, and humans, including waveforms where both the minimum point and the intersection of regression lines during late diastole and early systole failed (Figure 3.5). The novel method of pressure foot location by the deviation of linear regression during early systole from the pressure waveform has been used throughout the analysis in this thesis for all pressure waveforms recorded in sheep and in humans. The method produced reliable results of lower variation than other foot finding methods and has the advantage that diastolic variation does not affect the location of the pressure waveform foot.

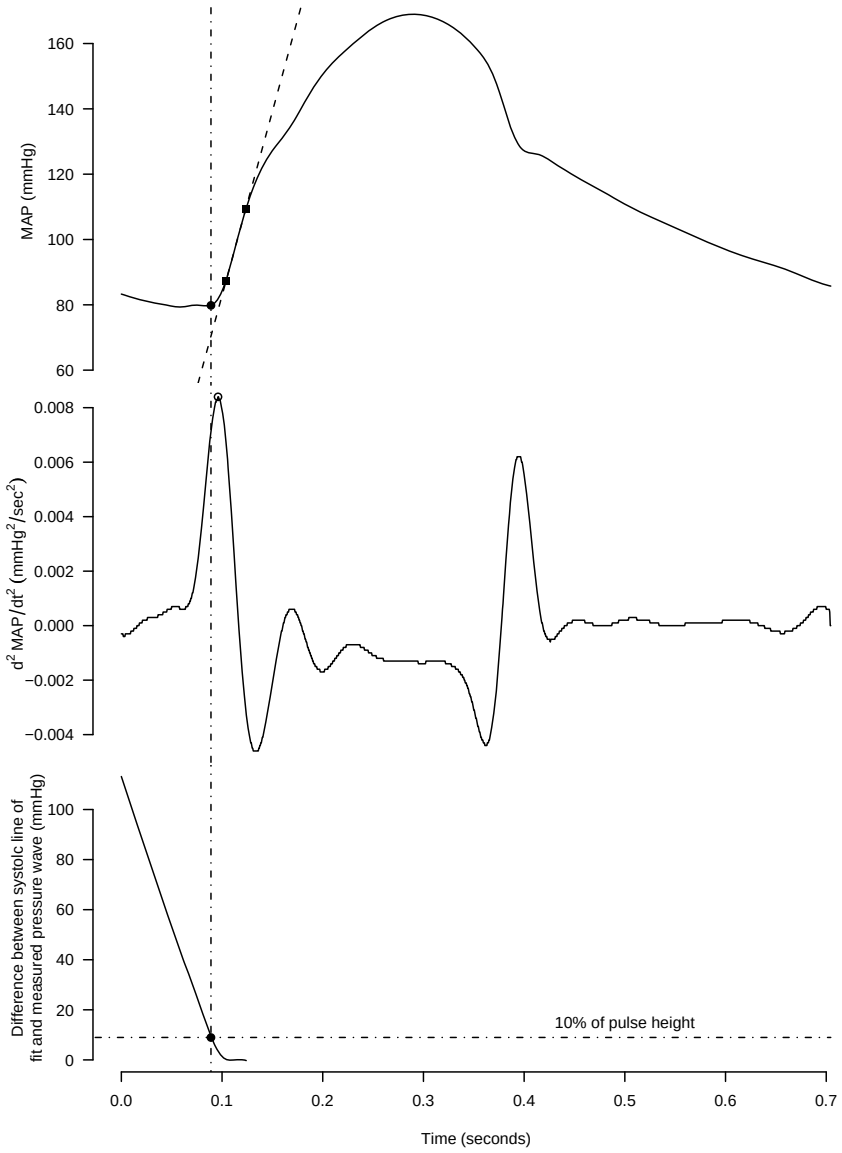

Figure 3.4: A novel method of reliably finding the pressure waveform foot in a variety of waveform shapes. A line is fitted to the early systolic upstroke, the area of linear regression defined by an adjusted point relating to the peak of the second derivative (○) and a point at one third of the pressure pulse height (■). The difference between the linear regression and the pressure wave is calculated, and the point where the difference is equal to 10% of the pressure pulse height defined as the pressure waveform foot (●). The dependence on the systolic upstroke alone means the method is robust even in situations where late diastole is subject to wave reflection perturbations. The example waveform shown is an invasively recorded aortic pressure waveform from an elderly male.

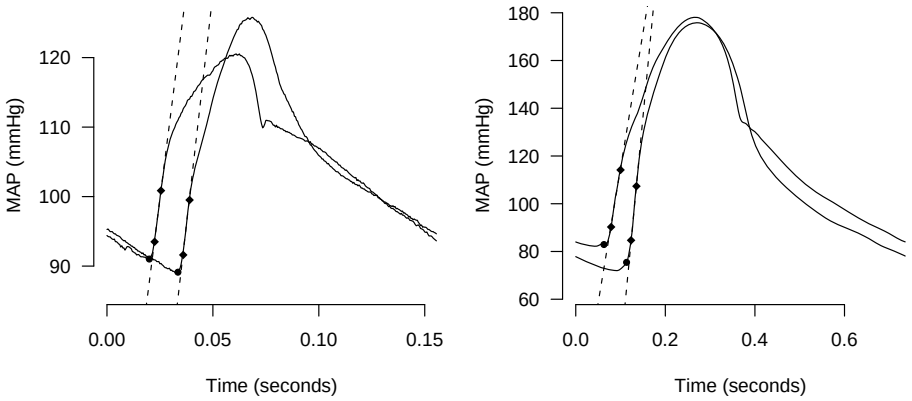

(a) Rat aortic trunk

(d) Human aortic trunk

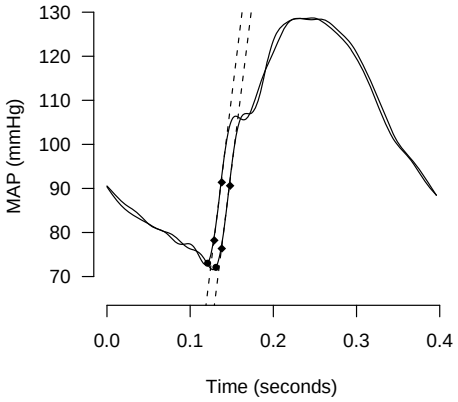

(b) Ovine iliac artery

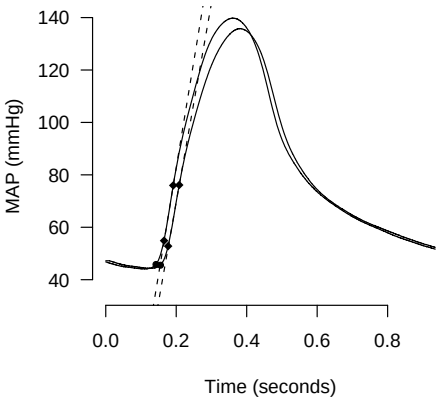

(e) Human iliac artery

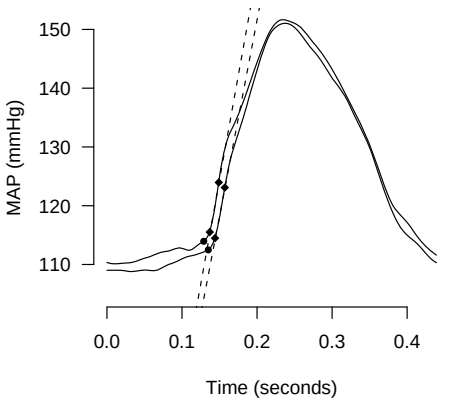

(c) Ovine iliac artery – variation

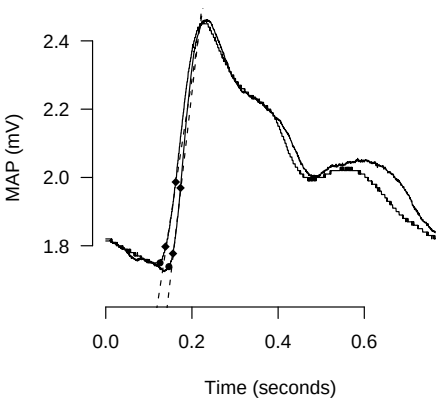

(f) Human brachial and radial arteries

Figure 3.5: Location of the pressure waveform foot by linear regression during early systole. The region of linear regression is indicated by the ◆ points and the foot by the ● points. The method is robust in accurately defining the pressure foot, including in more complex waveforms such as where the beginning of systole is not associated with the minimum point (c) and where the pressure waveform foot plateaus at the minimum point (e). As the method does not depend on the diastolic portion of the waveform, variation during diastole does not affect the accuracy of the algorithm (a), (b).

3.3 Calculation of the incident and reflected pressure wave

A method of calculating the incident and reflected pressure wave from measured pressure and flow waves was developed using established Fourier decomposition methods (Nichols and O'Rourke, 1998). The principle of pulse-by-pulse analysis was maintained, as opposed to wave averaging, such that parameters for each individual pulse could be calculated and output for statistical analysis. Both pressure and flow wave were decomposed into their Fourier series, and input impedance calculated as the ratio of the modulus of the pressure and flow Fourier transforms (Figure 3.6). The characteristic impedance was estimated from the average of the 4th to 7th harmonic of the calculated input impedance (Westerhof et al., 2006) and the incident and reflected pressure and flow waves calculated from Equation 2.16–2.19.

Throughout the work presented in this thesis, flow was not measured simultaneously at the same site as that where pressure was recorded. Consequently, the pressure waveform could not be decomposed into the incident and reflected components using measured pressure and flow. A method of estimating flow from the pressure pulse, outlined in Chapter 2, was proposed by Westerhof et al. (2006). The estimated flow wave was defined as zero outside of the ejection duration, maximal at 30% of the ejection duration, and linear between those points. The resulting triangular flow wave does not have to be calibrated for calculation of the incident and reflected waveform shape. The algorithm for decomposing pressure into the incident and reflected components was extended to include a triangular estimate of the flow wave where a measured flow wave was not present. The foot of the pressure wave was located and defined as the commencement of the flow upstroke. The end of the down-stroke of the flow waveform was located at

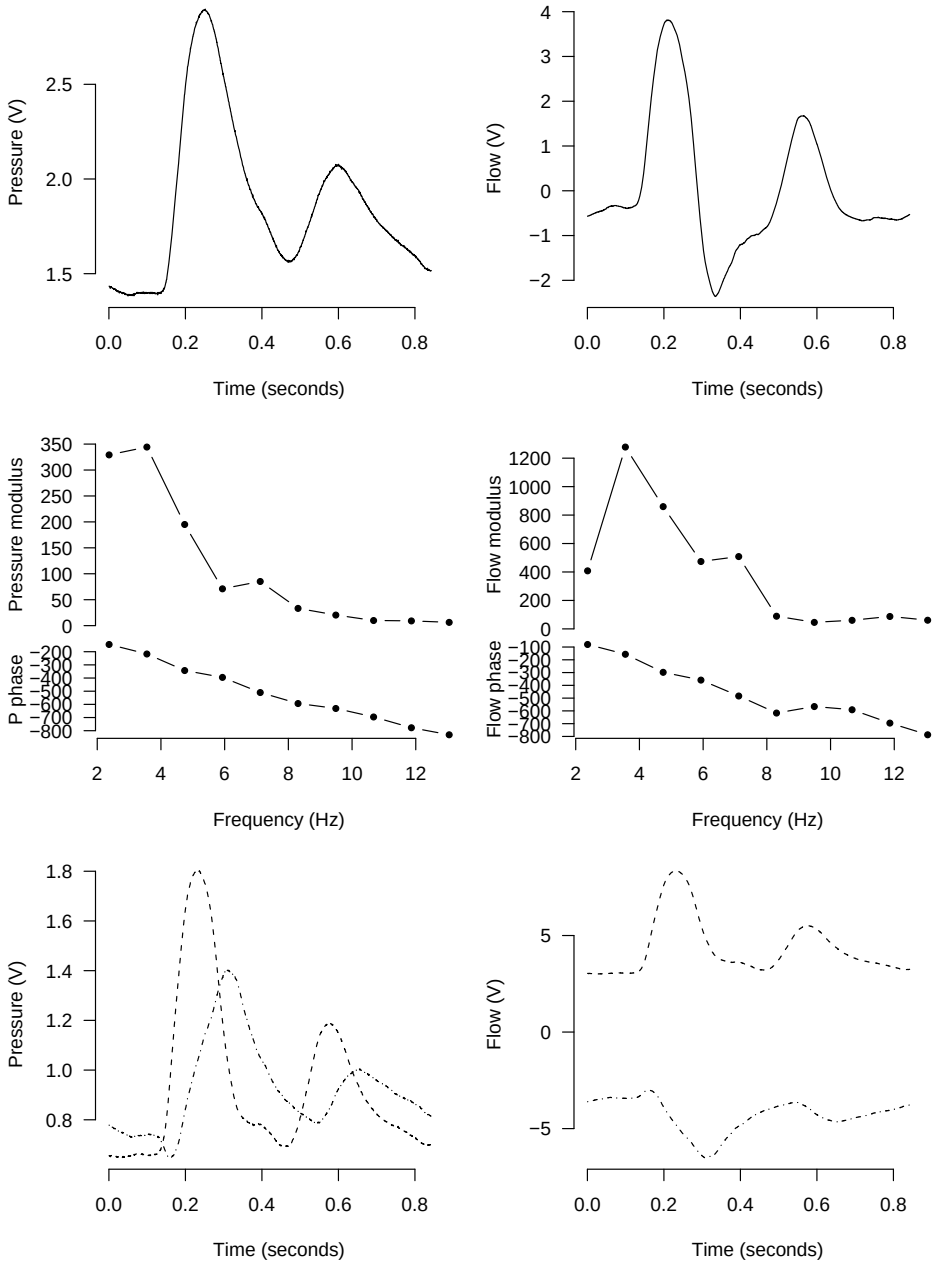

Figure 3.6: An example of a single pulse of pressure and flow measured uncalibrated, simultaneously, and non-invasively with pressure tonometry and flow Doppler techniques in the brachial artery of a 27 year old, healthy male (solid lines). The waveforms, expressed in arbitrary units, were expressed as Fourier transforms (●), and decomposed into the incident (dashed) and reflected (dot-dashed) waveforms using the characteristic impedance estimated from the 4th to 7th harmonics of the input impedance, calculated from the Fourier transforms of pressure and flow.

the incisura of the aortic waveform, associated with aortic valve closure; or the dichrotic notch in more distal arteries, which is not necessarily associated with the closing of the aortic valve, but generally occurs at the same time as the end of systole (Nichols, 2006). Flow peak was located at 30% of the ejection duration, and Fourier analysis and pressure wave decomposition carried out upon the estimated flow, and measured pressure waves (Figure 3.7). Westerhof et al. (2006) showed that a 10% deviation of flow peak location from 30% of ejection duration resulted in a small error (5%) in reflection indices. Thus in this thesis a 30% of ejection period was defined as the flow peak and reflection waves and indices calculated from that estimated flow wave.

Parameters were calculated on each individual pulse for the incident and reflected pressure waves and output for statistical analysis. These parameters included, in addition to the wave reflection parameters outlined in Chapter 2 (Equation 2.20–2.21), novel measures of the proportionality of the root mean square (RMS) value of the reflected pressure wave (Equation 3.1–3.2).

$$RM_{rms} = \frac{(P_r)_{rms}}{(P_i)_{rms}} \tag{3.1}$$

$$RI_{rms} = \frac{(P_r)_{rms}}{(P_r)_{rms} + (P_i)_{rms}} \tag{3.2}$$

The reflection magnitude of the RMS values (RM_{rms}) and reflection index of the RMS values (RI_{rms}) relate the average magnitude of the whole reflected waveform to the incident waveform. This is an extension of the reflection magnitude of the pulse pressures (RM_{PP}) and reflection index of the pulse pressures (RI_{PP}) proposed by Westerhof et al. (2006) that concern the peak

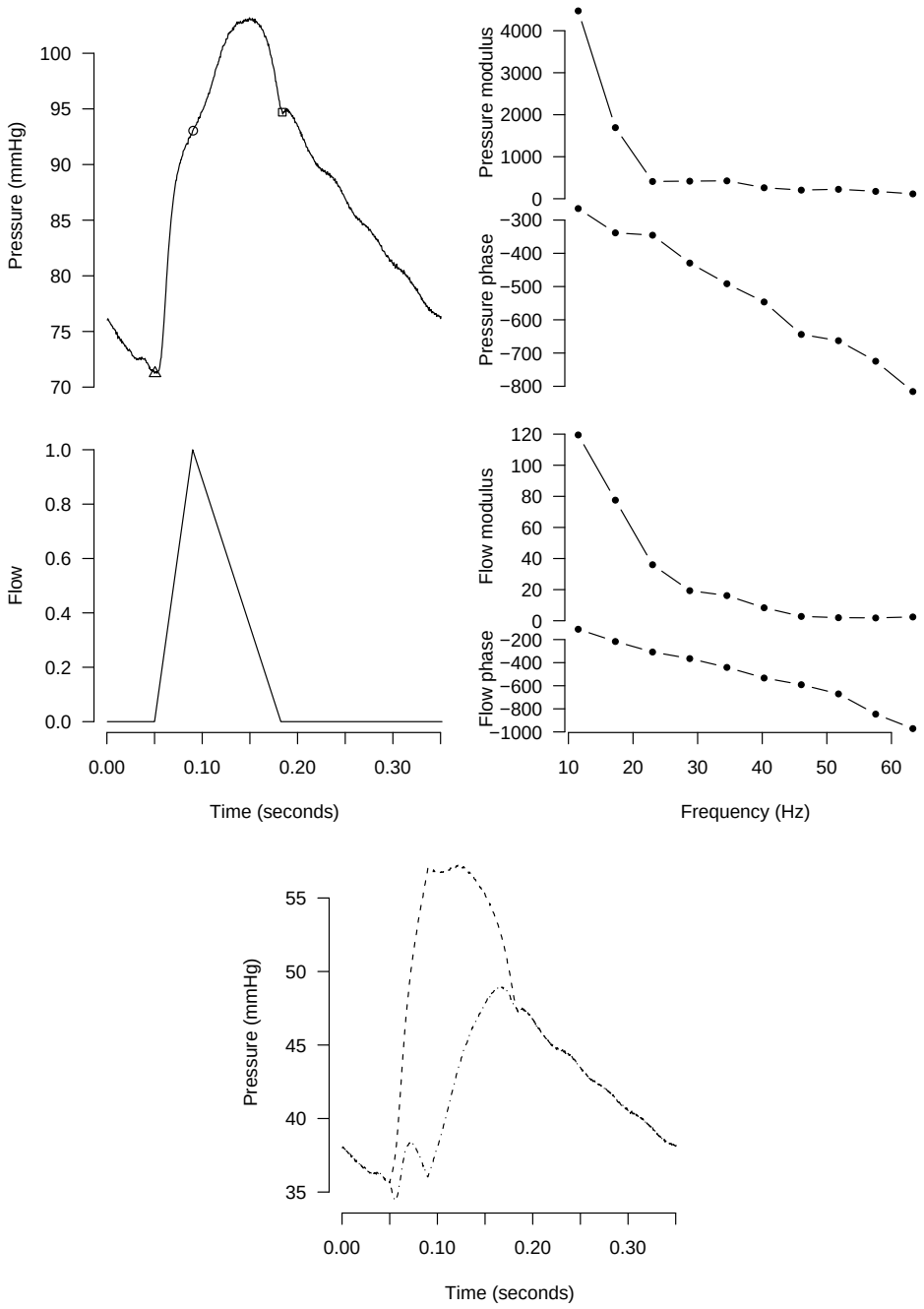

Figure 3.7: Decomposition of a rat aortic pressure wave into the incident and reflected components using triangular flow wave estimation. The uncalibrated triangular flow wave was fitted to the diastolic (△), dichrotic (□) and 30% ejection duration (○) time points of the pressure wave. Fourier analysis and characteristic impedance estimation was carried out as previously described, and the incident (dashed line) and reflected (dot-dashed line) calculated.

parameters of the reflected and incident waveforms. The RM_{PP} and RI_{PP} are representative of the impact of the reflected wave peak on pressure wave augmentation. The RM_{rms} and RI_{rms} are representative of the contribution of the reflected pressure wave to the measured mean arterial pressure.

CHAPTER 4

The effect of acute experimental inflammation on rat aortic stiffness: a proof of concept study

Atherosclerosis is viewed as an inflammatory condition (Libby, 2002; Libby et al., 2002). Chronic rheumatoid arthritis (Klocke et al., 2003) and Antineutrophilic Cytoplasmic Antibody (ANCA) associated vasculitis (Hurlimann et al., 2002; Mäki-Petäjä et al., 2006) are associated with increased arterial stiffness, a risk factor for atherosclerosis. Stiffness itself is associated with levels of inflammation in healthy individuals (Tomiyama et al., 2004; Yasmin et al., 2004). This study investigates the effect of acute arthritic inflammation on arterial stiffness of the descending aorta in rats. An arthritic model of inflammation, established by Stoerk et al. (1954), was chosen over other models of inflammation due to the high economic and social cost of arthritis (Access Economics Pty Limited, 2005a; Grimm, 2005), and subsequent interest in combating this degenerative disease. The experiment was also designed as a proof of concept of the novel method of using a 2.5F, high fidelity, dual pressure sensing catheter in the rat aorta for highly accurate

measurement of aortic Pulse Wave Velocity (PWV).

4.1 Methods

4.1.1 Experimental animals

Male, Dark Agouti (DA) rats (Animal Resource Centre, Perth) were used due to their previously shown high inflammatory susceptibility to Freund's complete adjuvant (FCA) (Binder et al., 2000). FCA induces joint inflammation in rats similar in symptoms to rheumatoid arthritis (Joe and Wilder, 1999). Rats of 7 weeks of age were kept in groups of 10 in a temperature controlled environment (22 $\pm$ 1 ℃), with 12 hours light each day. Rats were fed standard rat chow and water *ad libitum*. The Animal Care and Ethics Committee of the University of New South Wales approved all husbandry and experimental procedures.

4.1.2 Adjuvant-Induced Arthritis (AIA) and treatment

Six groups of rats were established. Arthritic inflammation was induced in five groups by injecting rats of seven weeks of age with 100μl of FCA (10mg/ml heat killed and dried Mycobacterium butyricum in paraffin oil and mannide mono-oleate; Difco Laboratories, Detroit, MI), intradermally in the base of the tail whilst under anaesthetic (ketamine, 50 mg/kg and xylazine, 5 mg/kg). The efficacy of the induced arthritis was confirmed through observation of reduced limb mobility and joint swelling. AIA in rats is a chronic inflammatory disease (Billiau and Matthys, 2001) associated with upregulation of inflammatory markers tumour necrosis factor-α (TNF-α), interleukin-1 (IL-1) and interleukin-6 (IL-6) (Joe and Wilder, 1999).

The bisphosphonate, zoledronic acid, an osteoclast bone resorption inhibitor (Food and Drug Administration, 2003), was chosen as the drug treat-

Table 4.1: The experimental protocol of the inflammatory model. Treatment groups, treatment methods and sample size of each group are tabulated.

Group	Induced arthritis	Treatment	Sample size
A	No	none	10
B	Yes	saline injection every 3rd day	5
C	Yes	zoledronic acid once on day 12	5
D	Yes	zoledronic acid once on day 0	7
E	Yes	zoledronic acid every 3rd day from day 12	7
F	Yes	zoledronic acid every 3rd day from day 0	5

ment due to its possible benefit in the treatment of arthritis in maintaining joint integrity (Sims et al., 2004). Four groups of inflamed rats were subjected to graded injections of zoledronic acid (3 mg/kg Zometa s.c) over 19 days. The fifth group was used as a treatment control, injected with equal volume of saline. A sixth group of non-inflamed, untreated rats were used as a control for the inflammation model. The six groups were established as per the sample sizes outlined in Table 4.1.

4.1.3 Measurement of aortic stiffness

Haemodynamic measurements were made in the anaesthetised rat 19 days following FCA or control treatment. Anaesthesia was induced with 5% isofluorane in 0.5 lpm oxygen, and maintained at 2% isofluorane in 0.5 lpm oxygen.

PWV was measured with a 2.5F catheter containing two high fidelity pressure sensors set 5cm apart (Millar SPC-721). The catheter was introduced into the descending aorta via the femoral artery in anaesthetised (isofluorane) rats (Figure 4.1). The catheter position was confirmed directly upon completion of the experiment. Heart Rate (HR) was calculated from a three lead, type II, electrocardiogram (ECG) signal. Data was recorded at 1kHz on a Biopac MP100 data acquisition unit with associated Acquire Knowledge

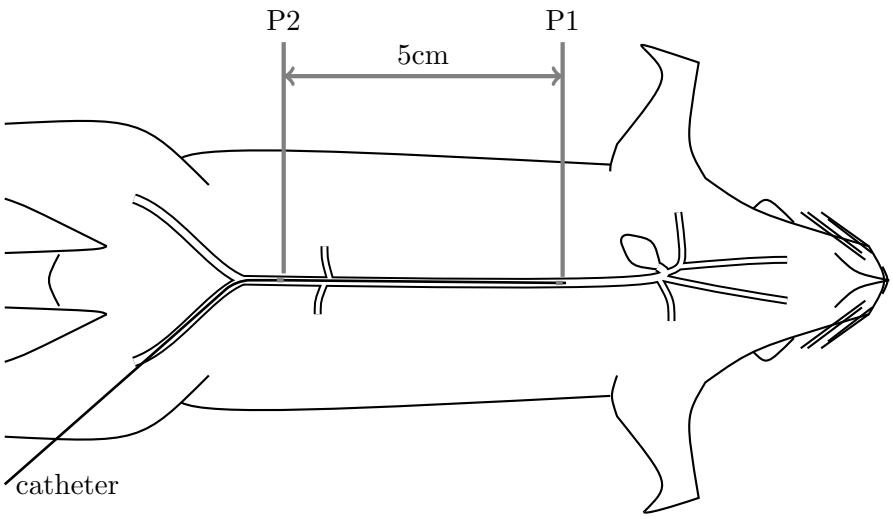

Figure 4.1: A diagrammatic representation of the placement of the dual pressure sensing catheter in the aorta, introduced via the left femoral artery in the rat. P1 and P2 are the proximal and distal pressure pressure transducers respectively. Both transducers lie in the descending aorta.

software. Aortic blood pressure, PWV and HR were calculated using custom designed software as detailed in Chapter 3.

4.1.4 Data analysis

Statistical analysis was conducted using the statistical package, R, by one way Analysis of Variance (ANOVA) with post-hoc Bonferroni test with significance taken for $P<0.1$. Results are expressed as mean $\pm$ standard deviation.

4.2 Results

4.2.1 Proof of concept of procedure

The dual pressure sensing catheter was introduced into the aorta via the femoral artery under stereomicroscope (Figure 4.2). It was reliably positioned in the descending aorta, confirmed directly upon completion of each set of measurements. Clear pressure waveforms were received in the pres-

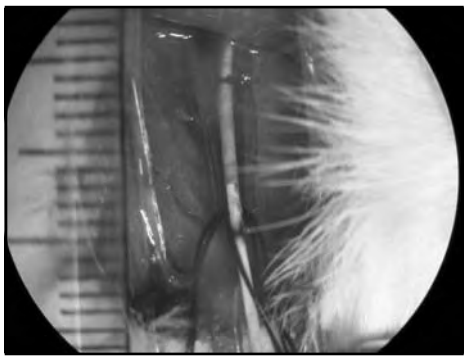

Figure 4.2: Image under stereomicroscope of the femoral access site showing the introduction of the dual pressure sensing catheter in the femoral artery of the rat for access to the descending aorta. Graduations on the left are in millimetres.

sure transducers positioned in the thoracic and abdominal aorta (Figure 4.3). The waveforms were of the expected shape and pressure range. An acute pressure waveform foot in both thoracic and abdominal signals combined with a high sampling rate of recording and a precisely known distance between pressure sensors permitted high fidelity calculation of aortic PWV. Calculated PWV values (3.44 ± 0.40 m·s^{-1} for all rats in the experiment) were of the order previously quoted in literature (Fitch et al., 2001). Beat to beat variation in measured PWV was small. For example, a randomly selected segment of data recorded over three respiratory cycles containing seventeen pulses had a relative standard deviation (RSD) of 5%, the RSD being the ratio of standard deviation to the mean value.

A linear relationship between PWV and Mean Arterial Pressure (MAP) was observed in the pressure range recorded (Figure 4.4). The reliance of PWV upon MAP shows the sensitivity of the PWV measurement technique to alterations in arterial stiffness. This was confirmed in experimental data in which PWV was measured with direct MAP intervention in the rat as presented in Chapter 5.

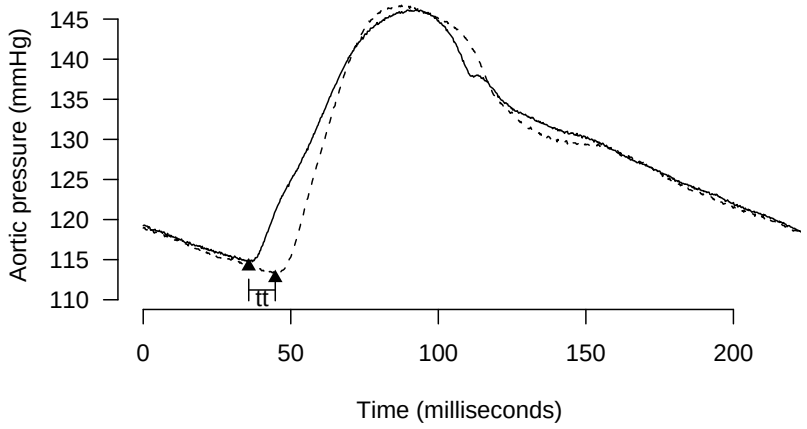

Figure 4.3: An example of the recorded thoracic (solid) and abdominal (dashed) aortic pressure waveforms recorded with the 2.5F, dual pressure sensing catheter in the rat. Both waveforms show an expected shape and are within the expected pressure range, supporting that the catheter accurately relays the haemodynamic parameters of the aorta. The incisura in the thoracic waveform is evident and the expected pulse pressure amplification from thoracic to abdominal waveform is also present. The pressure waveform feet are acute and are located at the minimum point of the pressure waveforms (▲), permitting accurate calculation of the transit time (tt). As the exact distance between the sensors (50mm) is known, a highly accurate measurement of PWV results.

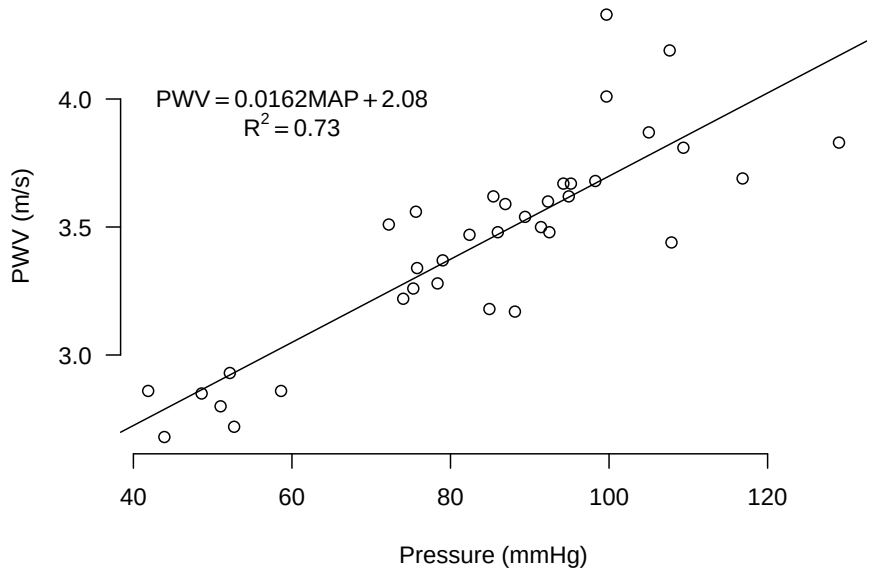

Figure 4.4: The PWV – MAP relationship across all rats in the study of experimental inflammation. Across the pressure range observed there is a linear relationship between PWV and MAP.

4.2.2 Haemodynamic changes in the presence of AIA

A statistical difference in pulse pressure (PP) was observed between groups A and B (48±10 mmHg and 35±9 mmHg respectively, $p<0.1$), and A and E (48±10 mmHg and 35±3 mmHg, $p<0.1$). There was no statistical difference in MAP between groups and there was no change in HR between the groups. Results for MAP, PP and HR are summarised in Table 4.2.

There was no statistically significant difference in PWV between groups. To compare PWV in a pressure independent manner, PWV was corrected for changes in pressure (Appendix B). There was also no statistical difference in PWV once corrected for changes in MAP (Figure 4.5).

Table 4.2: Statistical summary of mass, aortic length, heart rate, aortic pulse pressure, and MAP in the study of acute experimental inflammation, expressed as mean ± standard deviation. A statistical difference was observed in pulse pressure only between groups A and B, and groups A and E.

Group	Mass (g)	Aortic length (mm)	MAP (mmHg)	PP (mmHg)	HR (bpm)
A	197±13	87±5	98±23	48±10	393±28
B	181±14	87±3	68±24	35±9*	365±68
C	200±32	87±3	82±22	40±7	402±15
D	192±13	85±2	78±14	39±4	392±34
E	203±18	90±2	89±11	35±3*	395±38
F	193±17	89±4	78±23	40±9	401±32

* $p<0.1$ compared to group A by one-way ANOVA with Bonferroni correction.

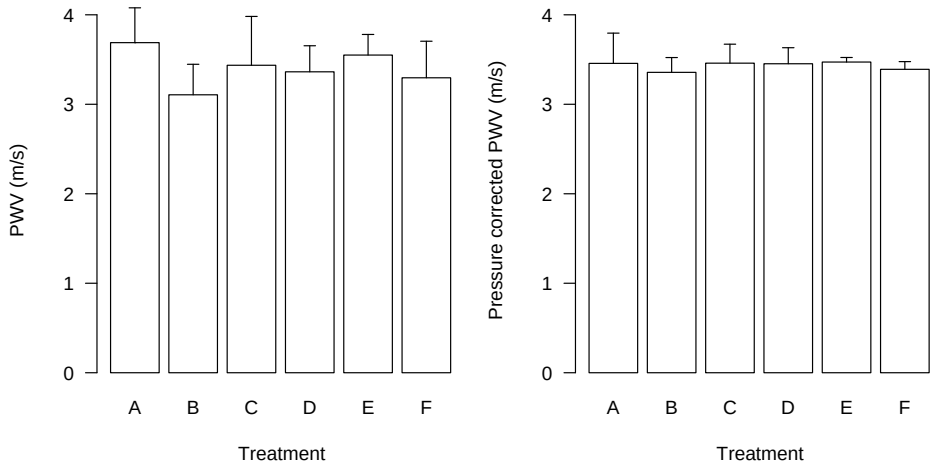

Figure 4.5: PWV and PWV corrected for changes in MAP for control (A), AIA (B), and zoledronic acid treatment (C–F) groups. Results expressed as mean ± standard deviation. There was no statistical difference between groups in either PWV or PWV corrected for changes in MAP.

4.3 Discussion

The 2.5F, high fidelity, dual pressure transducer catheter successfully recorded both the thoracic and abdominal aortic pressure waveform. The MAP – PWV relationship validates the dual pressure sensor method of measuring PWV in the rat aorta.

The results show that AIA does not cause a change in pressure independent aortic stiffness. Whilst inflammation markers such as c-reactive protein (CRP) levels in healthy human subjects correlate with arterial stiffness and PWV (Tomiyama et al., 2004; Yasmin et al., 2004), and rheumatoid arthritis itself is associated with arterial stiffness (Mäki-Petäjä et al., 2006), no relationship was observed between aortic stiffness and inflammatory disease, AIA, in the rat model.

Whilst AIA is effectively treated by most rheumatoid arthritis therapies, the model of inflammation is more akin to widespread inflammatory conditions like spondyloarthritis, or specifically, Reiter's syndrome (Joe and Wilder, 1999). Inflammation is systemic in nature and affects not only the joints, but also the skin, eyes, gastrointestinal tract and genitourinary tract (Joe and Wilder, 1999). It is assumed that inflammatory cytokines would be prevalent in the circulatory system. However, this could be considered a limitation of this study that no measurement of inflammation, such as high sensitive CRP assay, was taken.

The phase of inflammation potentially contributes to the vasoactive response. The expression of inducible nitric oxide synthase (iNOS) derived from converted arginine is characteristic of the acute inflammation pathway (Satriano, 2004). Increased iNOS expression increases nitric oxide (NO) levels, NO being a potent vasodilator (Schmitt et al., 2005; Wilkinson et al., 2002c). Increased iNOS expression has been observed previously in models of acute

inflammation in rats, including acute neuroinflammation (Ambrosini et al., 2005) and acute pulmonary inflammation in response to introduced asbestos fibres (Dörger et al., 2002). Conversely, chronic inflammation is associated with increased arterial stiffness in humans (Arroyo-Espliguero et al., 2003; Booth et al., 2004; Klocke et al., 2003; Mäki-Petäjä et al., 2006). The phase of inflammation at the 19 day end-point of the AIA study is important in interpreting the arterial stiffness observations. Jacobson et al. (1999) measured circulating levels of fibrinogen and neutrophils in Lewis rats with AIA. Fibrinogen peaked five days after injection, then decreased in levels before peaking again from 7 to 15 days following injection. Circulating neutrophils also peaked during the acute phase of inflammation, peaking after 2 days. Between 5 and 20 days following adjuvant injection, neutrophil levels were 400% above baseline.

Extending these results to the current study, the time point at which PWV was measured (19 days) would be during the peak of circulating neutrophil population, but during falling levels fibrinogen. This is suggestive of a chronic inflammatory phase, where iNOS levels would not be mediating arterial stiffness, and an increase in large artery stiffness, consistent with results in the human population, would be expected. The absence of such an increase in stiffness in the current study could be ascribed to the time period of the study. Using the cytokine measurements of Jacobson et al. (1999), chronic inflammatory conditions were present for approximately 12 to 14 days. Such a time period may not have been sufficient to observe changes in large artery stiffness. Alternatively, the thoracic–abdominal region of aorta studied may be resistant to inflammation induced changes in stiffness. Further conclusions may be drawn in a longer term study of AIA in rats, measuring PWV and different end points. However, there are limitations on

any long term study utilising AIA in rats due to ethical considerations associated with the debilitating nature of the inflammatory model, especially in the pain and loss of function in supporting limbs and the spine.

Zoledronic acid, the arthritic treatment, protects against bone erosion by inhibiting osteoclast activity and helps maintain joint integrity. However, zoledronic acid increases the severity of arthritis and increases synovitis (Sims et al., 2004) and may have a pro-inflammatory role. Whilst the effect of zoledronic acid on large artery stiffness in arthritic inflammation would be of interest, a direct anti-inflammatory treatment might lead to greater understanding of the effect of AIA on arterial stiffness.

The inflammation model utilised in this study had a short inflammatory duration (19 days). Without quantifying inflammatory levels over the time course of the experiment, it is difficult to ascertain whether the inflammatory model can be considered acute or chronic. AIA over 19 days does not causes a pressure independent change in aortic stiffness in the rat. Whilst inflammation markers such as CRP levels in healthy subjects, and rheumatoid arthritis correlate with arterial stiffness and PWV, the contradictory finding in this study may be due to the phase of the inflammatory model at which PWV was measured or the short time span of the inflammatory condition. Further work is required to quantify inflammatory markers such as CRP to gauge the extent of inflammation in the circulatory system and resolve whether there is any correlation between the severity of inflammation and PWV. Such a study would ideally take samples at various time points in the progression of AIA to ascertain the inflammatory profile and any associated changes in large arterial stiffness.

In conclusion, this study confirms the validity of the dual pressure sens-

ing catheter technique in measuring aortic PWV rats. The results of these experiments concerning acute experimental inflammation may constitute potentially new findings with regards to the relation between functional arterial stiffness and inflammatory phase and the role of iNOS within such a framework. Further studies will either provide confirmation of this mechanism,or confirmation of the possible limitations of the study.

CHAPTER 5

Effects of active and passive changes in pressure on aortic pulse wave velocity through alteration of venous return and pharmacological reduction of peripheral resistance

Arterial Pulse Wave Velocity (PWV) is a complex function of arterial wall structure, functional vasomotor tone and transmural pressure (Benetos et al., 1992; Levy et al., 1989). Therefore, the value of PWV varies with both the location and arterial pressure at which it is measured. Manipulation of arterial pressure in the rat for comparative study of arterial stiffness has previously been conducted by Fitch et al. (2001) through venous infusion of phenylephrine. Phenylephrine increases blood pressure directly by increasing cardiac contractility, thereby increasing cardiac output, and also by vasoconstriction of the peripheral vasculature (Chapter 2; Brunton, 2006; Tahiliani et al., 1982). The present study investigates the effect on aortic stiffness of a pharmacological method of lowering blood pressure and compares this to a reduced cardiac output model of suppressed mean arterial pressure induced by reduced venous return. The pharmacological method used to reduce mean pressure was the venous infusion of the exogenous ni-

tric oxide (NO) donor, sodium nitroprusside (SNP) (Chapter 2). To ensure that the volume rate of venous infusion *per se* did not alter venous return and mean pressure, systemic haemodynamic parameters and aortic stiffness were measured during an equivalent rate of venous saline infusion and any changes from baseline values noted.

An additional study was undertaken to measure pressure-static changes in arterial stiffness. Arterial stiffness is known to increase along the length of the aorta (Nichols and O'Rourke, 1998). Using the dual pressure sensing catheter technique, PWV was measured from thoracic to abdominal aorta with the aim of profiling stiffness in the length of the aorta in the rat to confirm, *in-vivo*, increasing arterial stiffness along the aortic trunk.

5.1 Methods

5.1.1 Experimental animals

Male Lewis rats (n=10, Animal Resource Centre, Perth) of 14 weeks of age were kept in a temperature controlled environment (22 ± 1 ℃), with 12 hours light each day. Rats were fed standard rat chow and water *ad libitum*. The Animal Care and Ethics Committee of the University of New South Wales approved all husbandry and experimental procedures.

On the day of the experiment, animal anaesthesia was induced with 5% isofluorane in 0.5 lpm oxygen, and maintained at 2% isofluorane in 0.5 lpm oxygen.

5.1.2 Haemodynamic measurements

A 2.5F catheter containing two high fidelity pressure sensors set 5cm apart (Millar SPC-721) was introduced via the femoral artery into the descending aorta (Figure 4.1; Figure 4.2). Heart rate and pulse gating was calculated

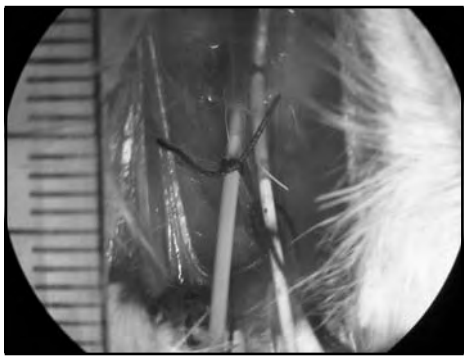

Figure 5.1: Image under stereomicroscope showing the placement of the catheter (right) and canular (left) in the femoral artery and vein respectively. Graduations on the left are in millimetres.

from a three lead, type II electrocardiogram (ECG) recording. Data was sampled at 2kHz using a Powerlab 8/30 data acquisition unit and associated Chart 5 software (ADInstruments). PWV and other haemodynamic calculations were performed offline using custom designed software, as previously described (Chapter 3).

5.1.3 Pressure-dynamic aortic stiffness changes

The dual pressure sensing catheter was positioned in the descending aorta and pressure allowed to stabilise. The left external iliac vein was exposed and occluded until mean pressure at the catheter tip reduced to approximately 60 mmHg. The occlusion was then released, and pressure allowed to return to baseline values.

The left femoral vein was canulated (Figure 5.1) and SNP (10 μg/ml, David Bull Laboratories, Australia) was infused at a rate of 1ml/min for a 1 minute duration with data recording made during and following the venous infusion across the induced change in arterial blood pressure.

To ascertain whether venous infusion at a rate of 1ml/min significantly inflated venous return and impacted on cardiac output and mean pressure,

saline was infused through the canulated left femoral vein for 1 minute at a rate of 1 ml/min with data acquired before and during infusion.

5.1.4 Pressure-static aortic stiffness changes

Pressure waveform at the catheter tip, most proximal to the heart, was recorded as the catheter was introduced from the femoral artery. The catheter was advanced until the pressure waveform recorded at the catheter tip changed from one typical of the aortic arch to a waveform typical of the branches off the aortic arch (Figure 5.2). The catheter was then withdrawn 1cm and pressures from the dual pressure sensors recorded for 30 seconds. The catheter was then withdrawn a further centimetre, and another 30 second recording made. Recordings of 30 second length were made every centimetre in the descending aorta until the pressure in the second, distal, sensor was positioned in the iliac artery, evident by a suppressed pressure waveform (Figure 5.2). The procedure was then repeated in reverse from iliac artery to aortic arch. The position of the catheter in the aortic arch was confirmed directly upon completion of the experiment. Thoracic and abdominal aortic length dimension were measured *in-situ* with wetted string.

5.1.5 Data analysis

Data recorded across mean arterial pressure changes induced by SNP and venous occlusions were divided into 5 mmHg segments. Statistical difference between SNP infusion and venous occlusion induced pressure changes were calculated by Student's paired t-tests within each 5 mmHg pressure range. Changes across pressure ranges in each the SNP infusion and the reduction of venous occlusion were assessed by one-way Analysis of Variance (ANOVA) with post-hoc Tukeys Honest Significant Difference (HSD) method with a

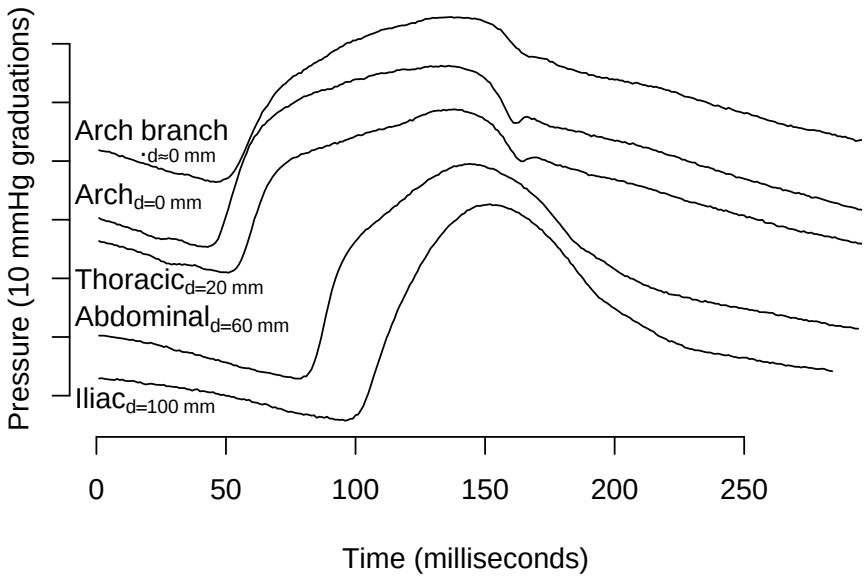

Figure 5.2: Representative waveforms in a branch off the aortic arch, the aortic arch itself, the thoracic and abdominal aorta, and the iliac artery recorded by the dual pressure sensing catheter introduced via the femoral artery in the rat. The waveform shape changes with position of the catheter in the aortic trunk. Note especially the presence and shape of the dichrotic notch. The waveforms have been gated by the R-peak of the ECG waveform. Distances (d) from the aortic arch (d=0) are as marked.

family-wise confidence level of 95%. Differences between baseline and venous infusion of saline at 1 ml/min were also detected by Student's paired t-tests. Alterations across the stiffness profile of the rat aorta were detected by Student's paired t-tests compared to the abdominal value of aortic stiffness. All values are expressed as means and standard error of mean, unless specified otherwise.

5.2 Results

The 10 Lewis rats of 14 weeks of age had a weight of 279±20 g, nose to rump length of 251±4 mm, and Body Mass Index (BMI) of 6.0±0.4 $kg{\cdot}m^{-2}$ (mean±standard deviation).

5.2.1 Pressure-dynamic aortic stiffness changes

Resting mean aortic pressure under anaesthesia in the group of rats studied was between 90 and 110 mmHg. Both venous occlusion and SNP infusion reduced mean pressure to 60 mmHg, except in one case for venous occlusion and two cases with SNP infusion, where mean pressure was reduce to 65 mmHg. Heart rate did not change across the range in pressure following either reduced venous return (p=0.83) or venous SNP infusion (p=0.99). There was a significant difference across pressure ranges for pulse pressure induced by both reduced venous return and by SNP infusion (Table 5.1; Appendix C: Figure C.1 and Figure C.3 respectively). Aortic PWV differed across multiple pressure ranges induced both by reduced venous return and venous SNP infusion (Table 5.1; Appendix C: Figure C.2 and C.4 respectively).

There was no difference in pulse pressure between the two methods of lowering mean pressure, reduced venous return and venous SNP infusion, and heart rate differed only at mean pressures less than 75 mmHg (Table 5.1).

Table 5.1: Results for the reduction of mean pressure by pharmacological means (SNP), and by reduction in venous return, across pressure ranges. ANOVA p-values are quoted for differences across pressure ranges for individual haemodynamic variables, with post-hoc Tukey's HSD plots included in Appendix C (Figure C.1-C.4). Superscripts denote significant differences between SNP infusion and reduced venous return within each pressure range.

	Reduced venous return			SNP		
MAP range (mmHg)	HR (bpm)	PP (mmHg)	PWV ($m \cdot s^{-1}$)	HR (bpm)	PP (mmHg)	PWV ($m \cdot s^{-1}$)
60—65	355±18	31.5±1.2	3.25±0.05	418±21†	30.9±1.7	3.20±0.10
65—70	366±16	29.6±1.2	3.20±0.09	419±19†	29.9±1.3	3.26±0.05
70—75	370±16	28.5±1.0	3.27±0.06	419±20*	28.5±1.3	3.28±0.05
75—80	373±16	26.7±1.0	3.34±0.07	418±20	27.0±1.3	3.35±0.06
80—85	376±16	25.5±0.9	3.42±0.07	418±20	26.1±1.4	3.44±0.05
85—90	379±16	24.6±0.8	3.54±0.07	421±20	25.4±1.5	3.55±0.05
90—95	384±16	24.7±0.8	3.62±0.07	426±22	24.3±1.7	3.69±0.06
95—100	388±17	25.0±0.8	3.71±0.07	431±22	23.7±1.9	3.81±0.07
100—105	395±18	25.2±0.7	3.83±0.11	425±19	24.8±1.9	3.92±0.09
105—110	401±28	26.6±1.1	4.01±0.15	440±11	24.5±1.6	4.15±0.11
ANOVA (p-value)	0.83	<0.001	<0.001	0.99	<0.05	<0.001

* $p<0.1$, $^{\dagger}p<0.05$, compared to reduction in venous return value by Student's paired t-test

Table 5.2: Results for the infusion of saline at 1ml/min via the femoral vein. There were no significant changes in HR, MAP, PP, or aortic PWV.

	Baseline	Saline infusion	p-value*
HR (bpm)	414.2±5.7	414.4±5.4	0.995
MAP (mmHg)	96.5±2.5	96.5±2.4	0.997
PP (mmHg)	30.0±0.9	30.4±0.9	0.916
PWV ($m \cdot s^{-1}$)	3.92±0.06	3.91±0.05	0.973

* p-values by Student's paired t-test

Figure 5.3, plotting PWV against mean pressure ranges, shows that PWV did not differ at any level of measured Mean Arterial Pressure (MAP) between the two methods of lowering blood pressure.

Infusion of saline at 1 ml/min via the femoral venous route for a 1 minute duration did not affect venous return of a magnitude suitable to change any of the haemodynamic parameters measured. Heart rate, mean aortic pressure, pulse pressure and PWV remained the same before and during saline infusion (Table 5.2).

5.2.2 Pressure-static aortic stiffness changes

The mean aortic length was 93±4 mm, the thoracic aorta comprising 47% of this (44±2 mm) and the abdominal aorta the remaining 53% (50±2 mm, mean±standard deviation). These dimensions are represented in the scaled diagram, Figure 5.4, with an example catheter position marked. Representative pressure waveforms recorded at each of the locations along the aortic trunk is printed in Figure 5.5.

Heart rate and MAP was consistent across all measurements (Table 5.3). Pulse pressure also increased with distance from the aortic arch, with a significant difference existing between the catheter tip being 20 and 40 mm from the aortic arch (29.7±0.1 and 32.4±0.1 mmHg respectively, $p<0.1$, Table 5.3). PWV was corrected for changes in MAP to ensure independence

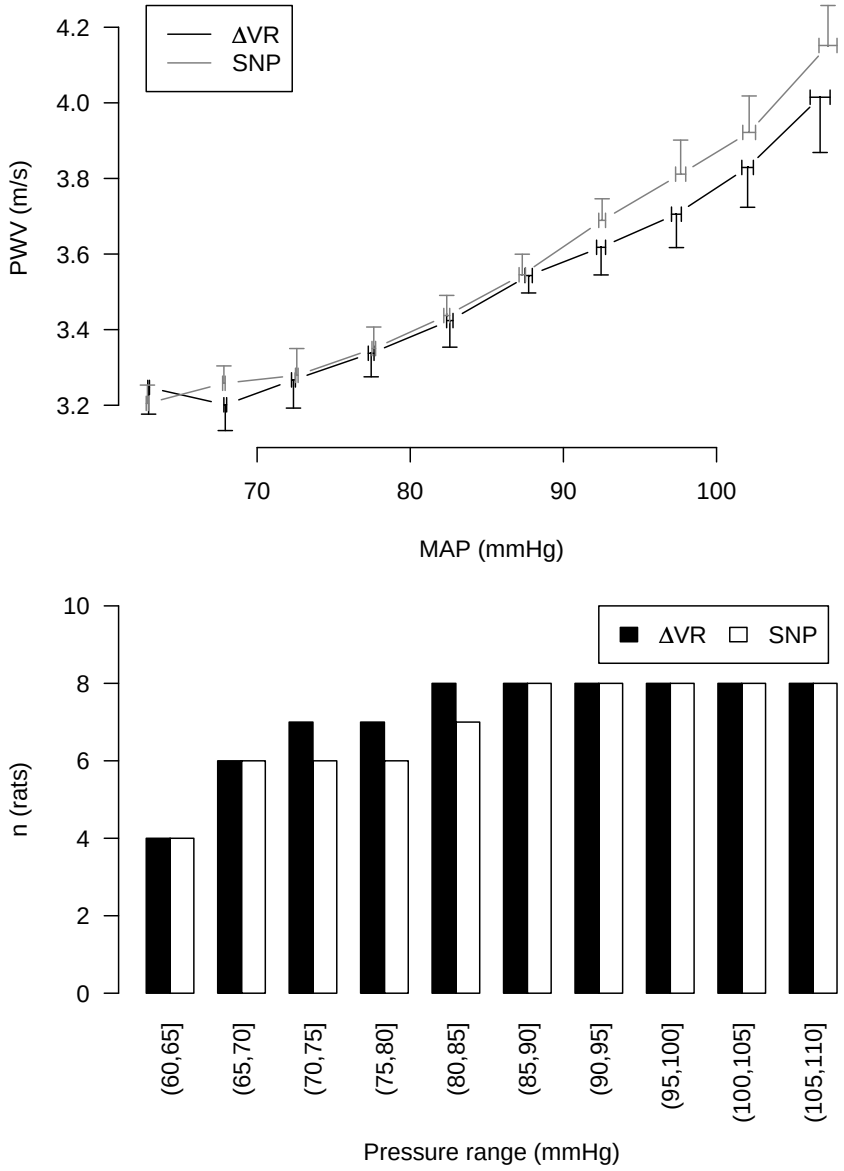

Figure 5.3: A plot of PWV measured across pressure ranges for both SNP infusion and reduced venous return. PWV changed significantly with pressure change induced by both reduced venous return and SNP infusion (not marked, see Figure C.2 and Figure C.4 respectively). No statistical difference between the two methods of altering pressure exists in any pressure range measured.

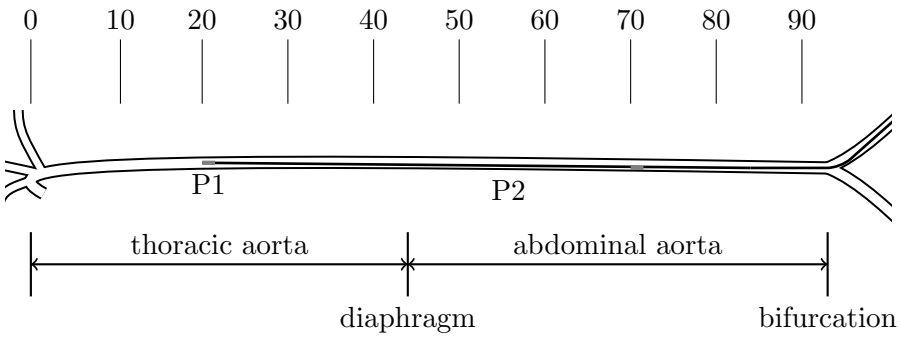

Figure 5.4: Diagrammatic representation of the rat aorta with length scaled to the average *in-vivo* dimensions observed in the current study. Labelled dimensions from the tip of the aortic arch are in millimetres. The catheter is drawn in a position with the catheter tip 20mm from the tip of the aortic arch. P1 and P2 are the proximal and distal pressure sensors respectively.

Table 5.3: Mean heart rate, MAP, pulse pressure and PWV for the measurements taken at the positions 10, 20, 30, and 40 mm from the aortic arch.

Distance (mm)	Heart rate (bpm)	MAP (mmHg)	PP (mmHg)	PWV_{MAP} ($m \cdot s^{-1}$)
10	379±1	90.1±0.3	30.3±0.2	3.65±0.01*
20	381±1	90.1±0.3	29.7±0.1*	3.67±0.01*
30	383±1	90.8±0.3	30.8±0.1	3.72±0.01*
40	383±1	91.3±0.3	32.4±0.1	3.76±0.01

* $p<0.05$ compared to the 40 mm position.

from pressure induced changes in arterial stiffness. Pressure corrected PWV increased with distance from the aortic arch, with a significant difference existing between catheter positioned with the tip 40 mm from the aortic arch, and the positions 10, 20, and 30 mm from the aortic arch (Table 5.3, Figure 5.6). A linear regression was fitted to the individual results for pressure corrected PWV (Figure 5.6). The linear regression suitably described the mean values, and predicts a 0.04 $m \cdot s^{-1}$ increase in PWV for every 10 mm increment from along the descending aorta, with a PWV intercept of 3.59 $m \cdot s^{-1}$at the aortic arch.

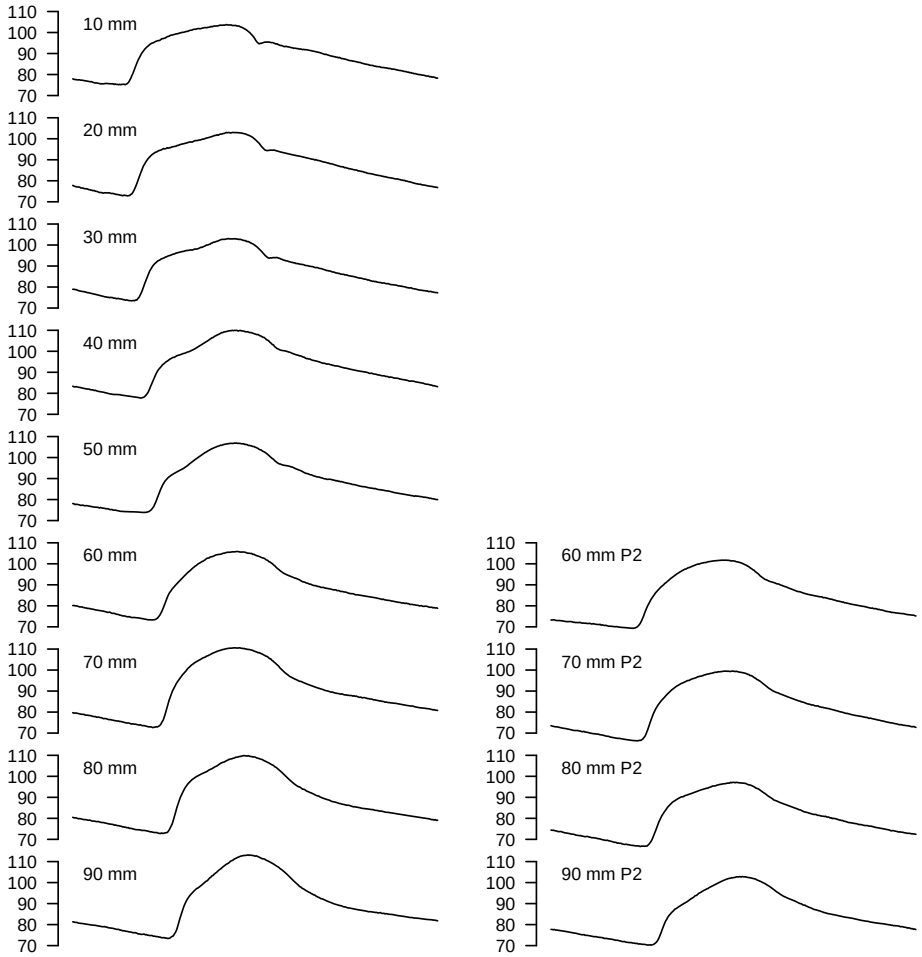

Figure 5.5: The change in pressure waveform shape along the length of the aorta with distance from the aortic arch as marked. The ordinate is labelled in mmHg. 'P2' denotes pressure waveforms measured with the second of the two pressure transducers, all other waveforms being those detected by the pressure transducer at the catheter tip. The similarity in waveform shape recorded by the first and second pressure transducers at locations 60 to 90 mm from the aortic arch indicate minimal interference of the catheter in the lumenal space with the natural travel of the pressure waveform.

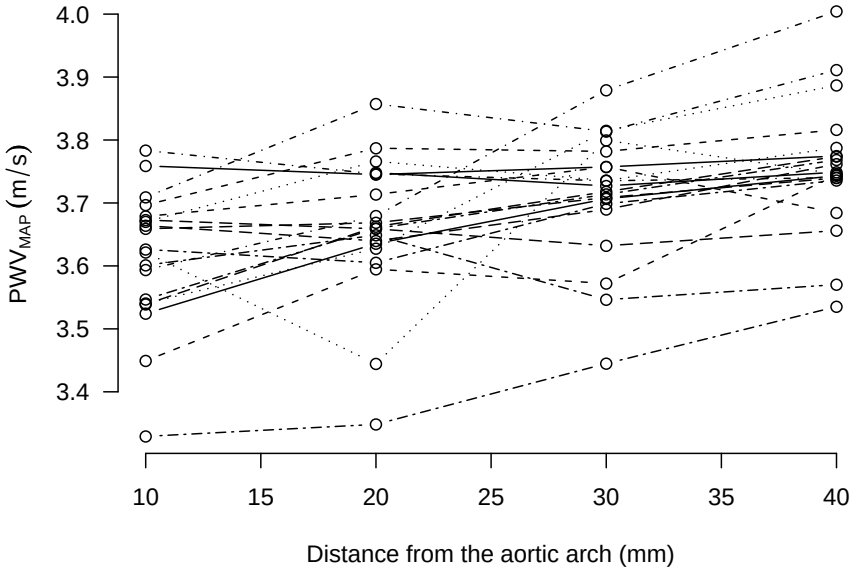

(a)

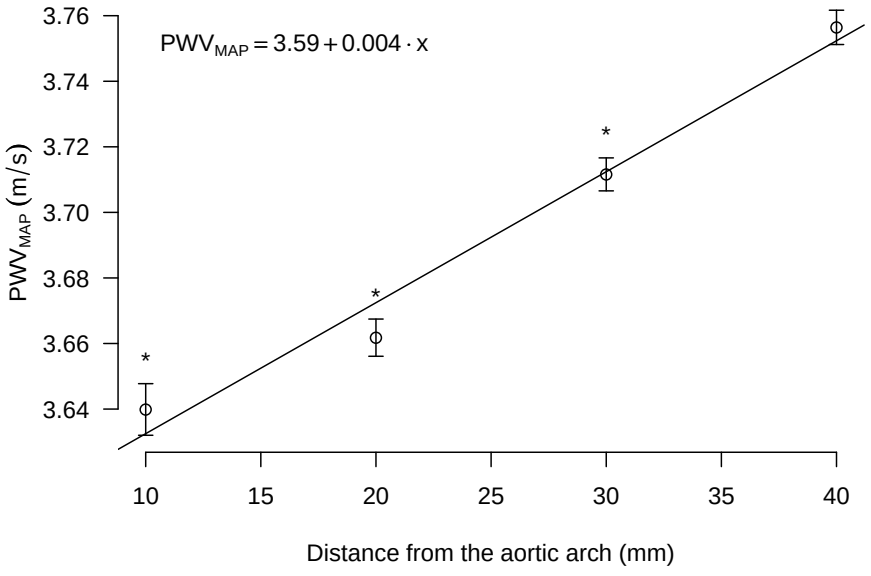

(b)

Figure 5.6: Pressure corrected PWV (PWV_{MAP}) in the aortic trunk with the distal tip of the catheter 10, 20, 30, and 40 mm distal of the aortic arch showing (a) individual results and (b) mean values with a linear regression that was fitted to the individual data in (a). Pressure corrected PWV were significantly different between the thoracic (10 and 20 mm) and abdominal (40mm) positions (* $p<0.5$ compared to 40 mm position). Individual data points and standard error of means at each distance point are plotted. The linear regression, fitted to the individual data, is defined where x is the distance from the aortic arch in millimetres.

5.3 Discussion

Changes in PWV were detected using the dual pressure transducer catheter technique for both active and passive interventions to change mean arterial pressure. Reduction of mean pressure induced both by reduced venous return and by pharmacological means caused a significant decrease in aortic PWV. The effect of SNP on mean pressure and aortic PWV was not affected by a changing venous volume and venous return, as demonstrated by the infusion of saline at the same rate resulting in no change in any of the haemodynamic variables measured. There was no detectable difference in arterial stiffness whether pressure was reduced by a reduction in venous return, or by the pharmacological means of infusing SNP. This result supports the extension of the methodology developed by Fitch et al. (2001), where PWV was measured over a pressure range inflated by phenylephrine infusion. Thus PWV can be measured across pressures above and below the resting blood pressure in the anaesthetised rat and comparison of arterial stiffness made across the entire range of pressures.

The expected trend toward increased arterial stiffness from thoracic to abdominal aortic position, independent of arterial pressure, was evident (Figure 5.6). PWV measurement with the dual pressure sensing catheter showed a statistical difference in arterial stiffness between the thoracic and abdominal region, independent of arterial pressure.

Figure 5.5 gives insight into the absence of significant effects of the catheter in the aortic lumen upon aortic haemodynamics. Through measurement and comparison of the pulse waveform at the same location with the first and second pressure transducers, any effect of the catheter itself would be evident through significant changes in measured pressure or waveform shape. If significant changes were present it would indicate the catheter itself im-

parts haemodynamic changes. However, comparison of waveforms measured at 60 to 90 mm distal of the aortic arch measured with the first and second pressure transducers shows minimal alteration in waveform shape. No detailed analysis of this aspect is presented here and such assumptions are a subject to further investigation.

Inspection of the pressure waves in Figure 5.5 highlights the possibility of measuring PWV for each individual centimetre of the aortic length using the recorded pressure waveform from a single pressure transducer and the ECG waveform. Using the ECG R-wave peak as a reference point, the transit time to the foot could be calculated at each physical location along the length of the aorta and the PWV between two points found by dividing the distance between the two points by the difference of the transit times between those two points and the R-wave, as given in Equation 5.1, where: PWV_{20}^{10} denotes the PWV between the 10 and 20 mm locations; 0.01 is the distance in metres between the two locations; and the transit times (tt) are the transit times between the ECG R-wave peak and the pressure foot at that location. This method has a number of disadvantages over the high fidelity, dual pressure transducer technique used in the current study. Firstly, the distance between the two points of measurement cannot be exactly measured. Whilst all care can be taken in accurately positioning the catheter at the two locations, there is an error associated with the positioning. The dual pressure transducer has two pressure sensors fixed exactly 50 mm apart. The advantage of the use of such a catheter is that no error is associated with the measurement of distance between the two sensors. Secondly, using a single pressure transducer requires gating the signal to the ECG signal, and measuring transit times on separate pulses at two different positions. Small variations in factors such as heart rate, mean pressure, and pulse pressure

will alter both the timing of the pressure wave foot from the ECG R-wave, and also the physical stiffness of the vessel itself.

$$PWV_{20}^{10} = \frac{0.01}{tt_{20} - tt_{10}} \tag{5.1}$$

Both the error introduced by distance measurement and the error introduced by measuring transit time from different pulses are amplified by measurement over short distances where transit time measurements are in the order of milliseconds. Taking a representative PWV in the rat aorta of 3.7 $m{\cdot}s^{-1}$, a 10 mm distance is travelled by the pressure wave in 2.7 milliseconds. An error of just 0.5 milliseconds causes an error of between 0.6 and 0.8 $m{\cdot}s^{-1}$ in PWV, an error of 16 to 22%. A 1 mm error in the positioning of the catheter results in a 0.4 $m{\cdot}s^{-1}$ or 11% error in PWV.

These errors are minimised using the dual pressure transducer technique as the transit time is measured for a single pulse travelling along the artery in a single time period, and the distance between the two pressure transducers is fixed. Whilst the advantage of the dual pressure transducer technique is apparent, the particular catheter used, with a transducer separation of 50 mm, is less suitable for the measurement arterial stiffness in highly localised regions in the rat. According to the aortic dimension taken in the 14 week old Lewis rats in the current study, a 50 mm transducer separation covers the entirety of either the thoracic or abdominal aorta, or alternatively, a proportion of both thoracic and abdominal aorta. Depending on the particular study aim, this may be advantageous, or a disadvantage, and the experimental design should address this accordingly.

The novel approach of high fidelity measurement of rat aortic PWV with a dual pressure sensing catheter has shown a significant difference in rat

aortic PWV both dependent, and independent of mean pressure. For the first time, an active, pharmacological means of lowering blood pressure in the rat has been compared with a passive lowering of blood pressure by reduced venous return. Aortic PWV across a pressure range from 60 to 110 mmHg induced by venous infusion of SNP was indistinguishable from PWV in the same pressure range induced by a reduction in venous return. Additionally, the venous infusion *per se* at a rate of 1 ml/min does not affect mean pressure or PWV in the rat aorta. Using the dual pressure transducer method, arterial stiffness was found to be statistically higher in the abdominal region than in the thoracic region, independent of changes in aortic pressure. This work defines a relationship in the 14 week old Lewis rat, previously unknown, between position in the descending aorta and arterial stiffness. The relationship is defined by Equation 5.2, where PWV is in $m{\cdot}s^{-1}$ and the distance form the aortic arch (x) is in millimetres, such that a 10 mm shift in position in the descending aorta is associated with a 0.04 $m{\cdot}s^{-1}$ change in PWV.

$$PWV = 3.59 + 0.004 \cdot x \tag{5.2}$$

CHAPTER 6

Genetically associated aortic elastic tissue lesions and large artery stiffness in rats

Arterial stiffness, an independent predictor of cardiovascular risk, is regulated by structural and active components. Damage to the structural components (elastin, collagen) could lead to increased vessel stiffness. The effect of elastic lamina lesions on large artery stiffness has not been studied to date. The Brown Norway (BN) rat is predisposed to spontaneous lesion formation in the internal elastic lamina, specifically in the abdominal aortic region and in the iliac arteries (Behmoaras et al., 2005; Capdeville et al., 1989). The aortic lesions found in the BN strain of rat are associated with an autosomal dominant gene (Harris et al., 2001; Jones et al., 2000).

Pulse Wave Velocity (PWV), a measure of arterial stiffness, was measured in the aorta of 9 BN rats, genetically predisposed to aortic elastic lesion defects. The aim of this experiment was to investigate the effect of localised structural defects, predominantly in the intimal region of the arterial wall, on aortic PWV. In the BN strain of rats, elastic lesions have been shown to occur predominantly in the internal elastic lamina (Jones et al., 2000). Results

were compared to 8 Lewis rats, free from aortic elastic lesions. A reduction in aortic PWV would be indicative of the effect of structural changes associated with weakening of the internal elastic lamina, specifically, internal elastic laminar lesions, on large artery stiffness.

6.1 Methods

6.1.1 Experimental animals

Male, BN and Lewis rats (Animal Resource Centre, Perth) of 12 weeks of age were kept in a temperature controlled environment (22 ± 1 ℃), with 12 hours light each day. Rats were fed standard rat chow and water *ad libitum*. The Animal Care and Ethics Committee of the University of New South Wales approved all husbandry and experimental procedures.

6.1.2 Measurement of aortic stiffness

As described previously (Chapter 4), a 2.5F, dual pressure transducing catheter was positioned in the descending aorta of the rat via the femoral artery (Figure 4.1; Figure 4.2). Venous access was easily obtained (Figure 5.1), and arterial pressure altered with 0.2ml venous bolus doses of sodium nitroprusside (SNP) (10μg/ml, David Bull Laboratories) and phenylephrine (50μg/ml, Sovereign Medical).

Data were recorded at a sampling rate of 2kHz using a Biopac MP100 data acquisition system with associated Acquire Knowledge software. The digitally converted signals were then exported for analysis with custom designed software (Chapter 3). Data was analysed over the whole time course of the raising and lowering of blood pressure with phenylephrine and SNP.

The incident and reflected pressure waves were calculated using flow wave triangulation (Chapter 3) and compared at an arbitrarily chosen, mid-range

mean arterial pressure of 95 mmHg.

6.1.3 Lesion quantification

Aortic lesions were quantified by staining and microscopic analysis. The aorta was removed immediately after sacrificing the rat and stored in saline for a maximum of 24 hours before being pinned out on polythene board to *in-vivo* length. Perivascular tissue was removed from around the aorta and the aorta cut longitudinally to expose the endothelium. The aorta was fixed in 10% phosphate buffered formalin for 12 hours. Formalin was removed from the pinned out aorta with water before brief (approximately 2 minutes) submersion in Gills haematoxylin. Gills haematoxylin does not stain elastin and stains elastin-poor regions. Lesions in the internal elastic laminar showed as darkened regions beneath the aortic endothelium. The stain was darkened by washing in Scott's alkaline tap water for approximately 5 minutes. The lesions were quantified under microscopic investigation by an investigator blinded to the strain of rat.

6.1.4 Data analysis

Results across pressure ranges were compared using one way Analysis of Variance (ANOVA) with post-hoc Tukeys Honest Significant Difference (HSD) method with a family-wise confidence level of 95%. Welch two-sided, unpaired t-test were used for within pressure range comparison and for comparing lesion quantity. Results are expressed as mean ± standard deviation.

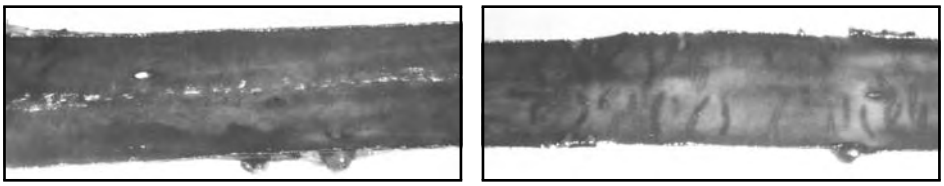

(a) **(b)**

Figure 6.1: Typical stain of the abdominal aortic region of (a) a Lewis rat and (b) a BN rat. Note the darker striations running in the circumferential direction indicating the presence of elastic tissue lesions in the BN rat, but not the Lewis rat.

Table 6.1: Quantified lesions in both the BN and Lewis strain of rat. Lesions differed significantly in the subrenal, suprarenal, and combined total regions between strains. A significant difference was also observed in both strains of rats between the lesion count in the subrenal and suprarenal aortic regions.

Strain	Subrenal lesions	Suprarenal lesions	p-value	Total lesions
BN	25±10	1±1	<0.0001	26±11
Lewis	1±1	0±0	<0.1	1±1
p-value	<0.0001	<0.1		<0.0001

6.2 Results

6.2.1 Lesion quantification

Ex-vivo analysis of the aorta proved a significant difference in the number of lesions between the two strains of rat (BN 26±11 lesions, Lewis 1±1 lesions, $p<0.0001$). Lesions extended 1 to 2mm in length in the circumferential direction, and were concentrated in the abdominal region of the aortic tissue (Figure 6.1). There were significantly greater lesions in the BN strain compared to the Lewis strain of rat (Table 6.1). A count of lesions above and below the renal arteries showed that there were significantly more lesions in the abdominal region compared to the thoracic region in both the BN and Lewis rat. Weight was significantly different between strains, the BN being significantly lighter than the Lewis strain (246±9 g and 296±67g respectively, $p<0.1$).

6.2.2 Haemodynamic measurements

A typical pressure-PWV relationship was observed in both strains of rat (Figure 6.2). PWV was sensitive to changes in Mean Arterial Pressure (MAP), with PWV being significantly different across the measured pressure range in both BN and Lewis rats (Figure C.5–C.6, Appendix C). Pulse pressure was also significantly different across the range of measured pressures (Figure C.7–C.8, Appendix C). Heart rate was consistent across the pressure range (Figure 6.4).

There was no statistical difference across the entire pressure range of 60 to 150mmHg in PWV between rats genetically predisposed to lesion defects and those that were not (Figure 6.2). Pulse pressure varied between rat strains at low pressures (MAP 60 to 70mmHg, $p<0.1$), with no difference observed in the remaining pressure range (Figure 6.3). Heart rate was consistently different between strains across the entire pressure range (Figure 6.4).

Plotting measured aortic PWV against quantified aortic elastic lesions showed little or no relationship between the two parameters (Figure 6.5). Linear regression of PWV and aortic lesions through low (60 to 90mmHg), medium (90 to 120mmHg) and high (120 to 150mmHg) mean pressure ranges showed poor fit and slopes approaching zero. That is, no strong relationship between PWV and aortic lesions was evident. Equation 6.1 gives the linear regression fit across the entire pressure range measured, with a low multiple R^2 value of 0.0004.

$$PWV = -0.002 \times aortic\ lesion\ count + 4.5 \tag{6.1}$$

The incident and reflected pressure waveforms were calculated using an

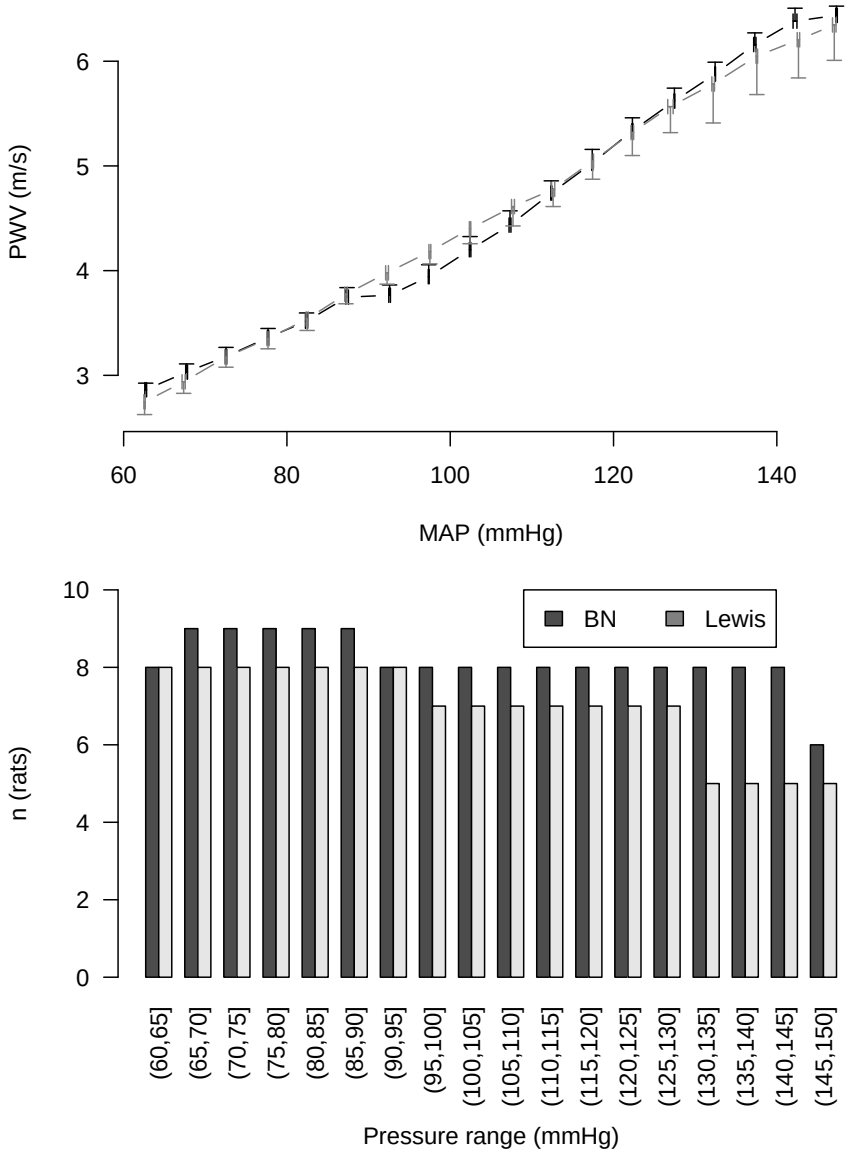

Figure 6.2: The PWV relationship to MAP of the BN (dark line) and Lewis (light line) rats. A typical curvilinear relationship between PWV and MAP was observed in both strains of rat. There was no significant difference in PWV between strains within each pressure range. The histogram shows the number of rats that responded to the SNP and phenylephrine doses to extend into the allotted pressure ranges.

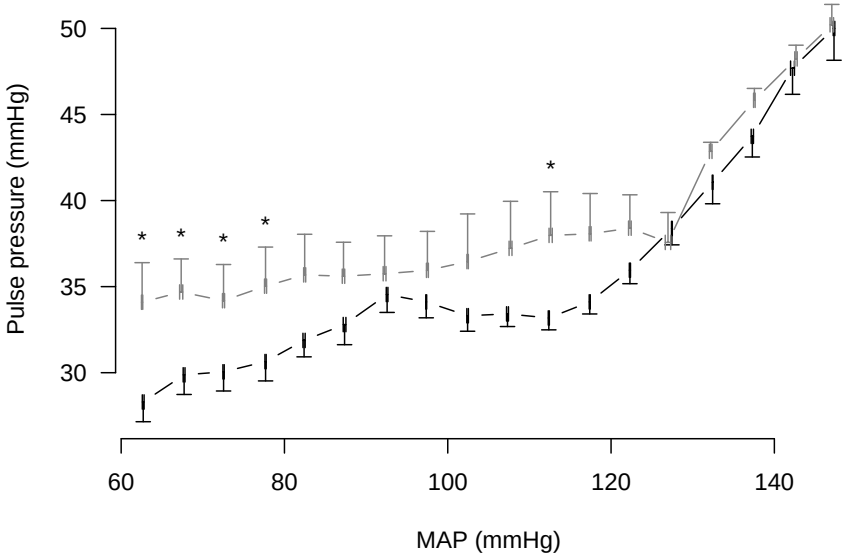

Figure 6.3: The pulse pressure relationship to MAP of the BN (dark line) and Lewis (light line) rats. There was a significant trend towards higher pulse pressure at higher mean pressures. A significant difference between rat strains was only observed at lower pressure ranges. (* $p<0.1$)

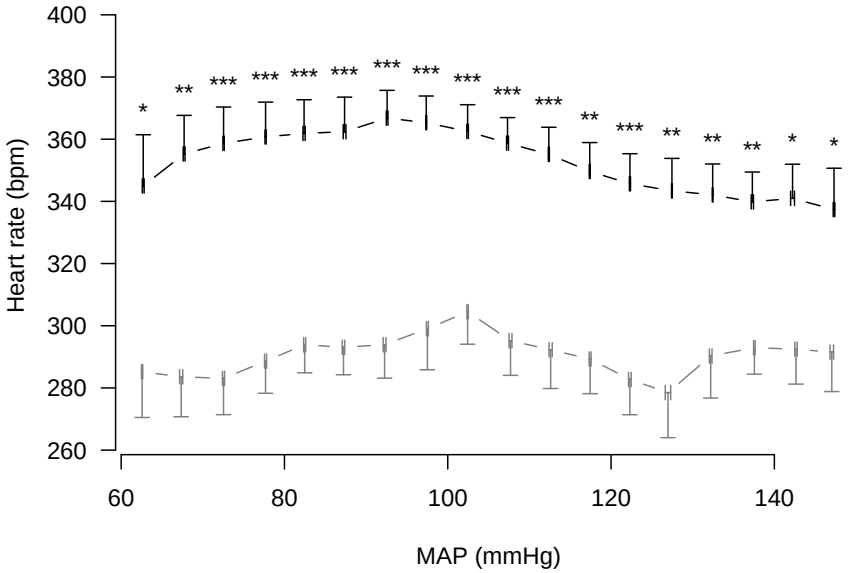

Figure 6.4: The heart rate relationship to MAP of the BN (dark line) and Lewis (light line) rats. There was no significant change in HR relative to MAP. HR was significantly different between rat strains across all pressure ranges. (* $p<0.1$, ** $p<0.01$, *** $p<0.001$)

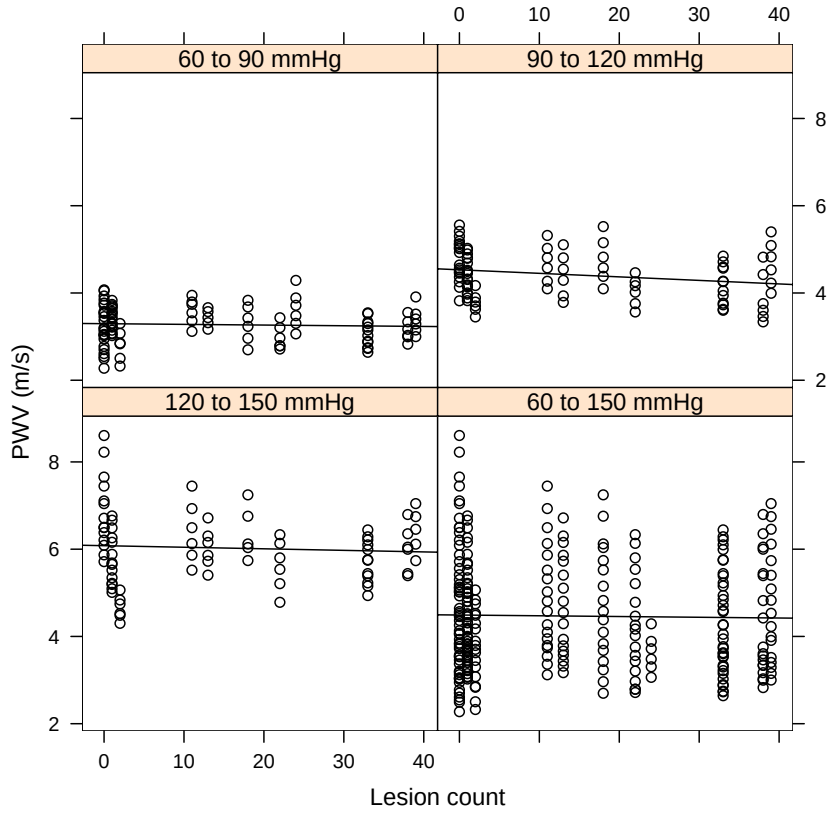

Pressure range	Intercept ($m \cdot s^{-1}$)	Slope ($m \cdot s^{-1} \cdot lesion^{-1}$)	Multiple R^2 value
60 to 90mmHg	3.3	-0.001	0.003
90 to 120mmHg	4.5	-0.008	0.049
120 to 150mmHg	6.1	-0.004	0.004
60 to 150mmHg	4.5	-0.002	0.0004

Figure 6.5: The relationship between aortic elastic lesion defect count and measured aortic PWV in three different mean pressure ranges, 60 to 90 mmHg, 90 to 120 mmHg, and 120 to 150 mmHg. An additional plot provided in the lattice displays data across the entire pressure range of 60 to 150 mmHg. The included table displays values corresponding to the linear regressions fitted to each set of data. Low multiple R^2 values indicate a poor fit of linear regression at all levels of pressure. Slope calculations approximate zero indicating little correlation between aortic PWV and aortic lesion count.

Table 6.2: Measured heart rate and aortic mean pressure for calculated wave reflection parameters of incident (i) and reflected (r) pulse pressures calculated from estimated characteristic impedance (Z_c) for lesion (BN) and control (Lewis) rats.

	Lewis	BN
HR (bpm)	318±15	366±10*
MAP (mmHg)	97.0±1.0	96.9±0.8
PP (mmHg)	33.5±2.6	35.9±1.4
PP_i (mmHg)	21.5±2.0	38.2±3.1†
PP_r (mmHg)	15.1±1.0	25.8±2.0†
Z_c	18.0±2.6	51.5±4.7‡

* $p<0.1$, $^{\dagger}p<0.01$, $^{\ddagger}p<0.001$ by unpaired, Welch two sample t-test.

estimated triangular flow wave (Chapter 2) at a mean pressure of 97±1.0 and 96.9±0.8 mmHg for Lewis and BN strains respectively. Other systemic variables are included in Table 6.2, with no significant difference occurring other than in heart rate (Lewis 318±15 bpm, BN 366±10 bpm, $p<0.1$), as previously observed across the entire pressure range studied. Both incident and reflected pressure waves were found to be of greater amplitude in the BN strain compared to the lesion strain (Table 6.2). However, the ratio of reflected pressure peak to incident pressure peak (RM_{PP} and RI_{PP}) was not not significantly different between rats with lesions and those with out (Figure 6.6). The new indexes of pressure wave inflection intensity proposed in this thesis (RM_{rms} and RI_{rms}), representing ratios of root mean square (RMS) values of pressure, did show a significant difference between the BN strain and Lewis strain, the presence of lesions lowering the RMS ratio of reflected to incident pressure (Figure 6.6). Estimated characteristic impedance was significantly greater in the BN, lesion prone strain compared to the Lewis strain (18.0±2.6 and 51.5±4.7, arbitrary units, $p<0.001$).

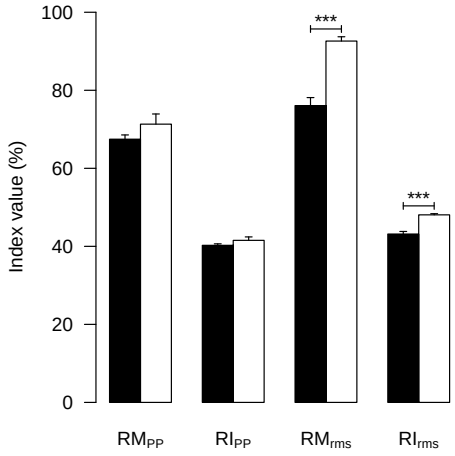

Figure 6.6: Changes in indexes relating to pressure wave reflection intensity in the BN (■) and Lewis (□) strain of rat. (*** $p<0.001$ by unpaired, Welch two sample t-test.)

6.3 Discussion

This the first study investigating the effect of elastic tissue lesions in the rat aorta on large artery stiffness. This study has shown that whilst a significant difference in elastic tissue lesion defects between the BN and Lewis strain of rats was evident, no correlation between PWV and aortic lesions was observed.

Lesion number and lesion severity has been associated with specific chromosomal loci in the BN strain of rat (Harris et al., 2001), the BN strain of rat genetically predisposed to lesions associated with an condition of autosomal dominant, single gene (Jones et al., 2000). The lesions themselves extend to the cerebral arteries and are associated with cerebral aneurysms Coutard et al. (2000). It has previously been shown that the morphology of medial elastin is severely altered in the BN strain of rat with complete failure of abdominal aortic elastic laminae at localised sites (Jones et al., 2000). The BN rat strain is also associated with a reduced aortic elastin content and increased collagen content as compared to the Long Evans strain of

rat (Sauvage et al., 1997). Thoracic aortic elastin content is significantly lower in the BN strain of rat, compared to aortic elastin content of the Lewis strain (Behmoaras et al., 2005) (Figure 6.7). Subsequently, a higher elastin to collagen ratio is observed in the Lewis rat. This structural difference in the segment of aorta measured in this study did not cause a difference in physiological measured PWV in the two strains of rats. That is, in spite of a known difference in elastin content between BN and Lewis rats, there is no difference in arterial stiffness across the range of physiological pressures. Reduced rat aortic elastin and collagen content with age has been shown to increase stiffness measured *in-vitro* (Brel and Oxlund, 1996), however, this was explained by an increase in cross linking of collagenous fibres in the formation of Advanced Glycation Endproducts (AGE). The measurement of PWV *in-vivo* includes contribution to stiffness of both the structural components of elastin and collagen, and the active contribution of smooth muscle tone. The active component of stiffness is absent in *in-vitro* measures. A possible explanation for the observation of no change in aortic stiffness, despite differences in aortic structure, is a compensatory mechanism of smooth muscle activity. That is, smooth muscle in the aortic wall adjusts tone to achieve an optimal physiological stiffness.

Heart rate was significantly higher across all pressures in the BN strain of rat compared to the Lewis strain. This finding is consistent with the work of Behmoaras et al. (2005), who showed a chronic difference in heart rate between BN and Lewis strains of rats. Whilst an acute change in heart rate does not affect PWV (Wilkinson et al., 2002a), increases in heart rate over a chronic scale have been shown to increase atherosclerosis (Bassiouny et al., 1994) and PWV (Avolio and Benetos, 2006; Benetos et al., 2002). The raised heart rate across all pressure ranges in the BN compared to Lewis strain did

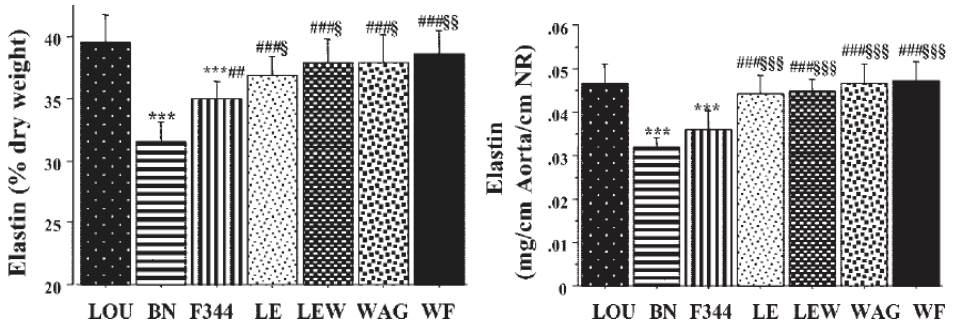

Figure 6.7: Thoracic aortic elastin content, expressed as percent of dry weight and mass per unit nose-to-rump length, in different strains of rat. ## P<0.01 and ### P<0.001 compared to the Brown Norway (BN) strain. The Lewis (LEW) strain has significantly greater aortic elastin content, both as percentage of dry weight, and per unit length. (Reproduced from Behmoaras et al., 2005)

not manifest in a change in aortic PWV. The effect of heart rate on PWV may become evident in rats older than the 12 week age group in the current study.

The presence of localised lesion defects in the elastic laminae did not alter arterial stiffness. This may be due to the minimal interference of such lesions with the aortic structural integrity as a whole. A parallel can be draw to the study by Farrar et al. (1978), where aortic PWV in *Macaca fascicularis* monkeys was only altered following large scale, general atherosclerotic plaques. The changes associated with atherosclerotic plaques did not alter the material properties of the vascular wall, as described by Young's modulus, but altered arterial stiffness. The reverse case is true in the current study, where small scale alterations in the material properties of the wall altered the modulus of elasticity, but the scale of such changes across the aortic length were not such that a change in PWV was observed.

Despite a significant difference in elastic tissue lesion defects between the BN and Lewis strain of rat, no difference in aortic stiffness was observed.

This may be explained by the presence of lesions in only a small proportion of the segment of aorta where PWV was measured. However, this does not account for the known differences in elastin content between the two strains. A compensatory mechanism of smooth muscle tone may be responsible in adjusting aortic stiffness to an optimal working level. The results of this study shows the resilience of the large arterial system. That is, highly localised damage of the aorta and decreased elastin content do not cause changes in arterial stiffness.

CHAPTER 7

Time dependent effects of arterial calcification on aortic pulse wave velocity across pressure ranges in rats

The accumulation of calcium deposits in the arterial wall plays an important role in the stiffening of large arteries (Dao et al., 2005). The mechanisms of calcification are not fully understood. Study of an animal model of calcification may lead to a better understanding of the mechanisms of calcification of the arteries. A variety of animal models of vessel calcification have been developed with varying combinations and doses of vitamin D, nicotine, warfarin, and hypercholesterolemia (Price et al., 2000; Wallin et al., 2001). A regime of hypervitaminosis D_3 and nicotine (VDN) treatment causing arterial calcification in rats was developed by Henrion et al. (1991), though the use of vitamin D and nicotine to induce calcification dates back to 1966 (Hass et al., 1966). The VDN model of calcification was subsequently used in studies by Gaillard et al. (2005); Jegger et al. (2006); Kieffer et al. (2000) and Niederhoffer et al. (1997a,b). The investigation of aortic stiffness with VDN calcification has only been studied at a single time point (2 months) following VDN treatment in the Wistar strain of rat (Gaillard et al., 2005;

Jegger et al., 2006; Niederhoffer et al., 1997b). In contrast to a single time point as in previous studies, an experiment was devised to test the effect of the established VDN calcification model on aortic stiffness across a range of mean arterial pressures at several time points in the Lewis strain of rat. Haemodynamic measurements were made in rats of 12, 13, and 14 weeks of age to study the developmental stages of aortic calcification. In addition to measurement in the intact animal, *ex-vivo* testing of aortic segments was carried out to assess the effect of VDN calcification on aortic structural stiffness.

7.1 Methods

7.1.1 Experimental animals

Seven week old male Lewis rats (Animal Resource Centre, Western Australia) were housed in groups of two to three in a temperature controlled environment (22±1℃), with 12 hours light each day. Rats were fed standard rat chow and water *ad libitum*. The Animal Care and Ethics Committee of the University of New South Wales approved all husbandry and experiments. Animals were handled for one week prior to commencement of calcification treatment regimes.

7.1.2 Induction of calcification

VDN treatment was conducted as previously described (Niederhoffer et al., 1997a). Rats to receive the VDN treatment (n=24) received a single dose of vitamin D_3 (300,000 IU/kg, equivalent to 7.5 mg/kg, intramuscular injection, Sigma-Aldrich) and nicotine (25 mg/kg orally, twice, 9 hours apart, Sigma-Aldrich) at 8 weeks of age. Control rats (n=10) received a single intramuscular injection of saline and two oral introductions of saline 9 hours

	Age (weeks)						
	8	9	10	11	12	13	14
VDN_{12} (n=8)	*				#		
VDN_{13} (n=8)	*					#	
VDN_{14} (n=8)	*						#
Control (n=10)	*						#

Figure 7.1: Treatment and measurement protocol for VDN model of calcification in the rat. * hypervitaminosis D_3 and nicotine (VDN) treatment, or saline dose in controls. # Haemodynamic measurements taken and tensile testing of aortic sections.

apart at 8 weeks of age.

7.1.3 Haemodynamic measurements

Aortic Pulse Wave Velocity (PWV) was measured using a 2.5F catheter containing two high fidelity pressure sensors set 5 cm apart (Millar SPC-721). The catheter was introduced into the descending aorta via the femoral artery (Figure 4.1). Central blood pressure was measured using the pressure sensor at the tip of the catheter. PWV and haemodynamic parameters were calculated using custom designed software, as previously described (Chapter 3). Mean pressure was raised with a single 30 second infusion of phenylephrine (50 μg/ml, Sovereign Medical, UK), and lowered with a single 30 second infusion of sodium nitroprusside (SNP) (10 μg/ml, David Bull Laboratories, Australia) via the femoral vein at a rate of 1 ml/min. PWV was measured in eight VDN rats at each of 12, 13 and 14 weeks of age with the rats being sacrificed at the end of the procedure. PWV in ten control rats was measured at 14 weeks of age (Figure 7.1).

7.1.4 *Ex-vivo* testing of aortic tissue

The aorta from arch to iliac bifurcation was extracted after animal sacrifice and stored in saline. Within 24 hours of animal sacrifice, the aorta was

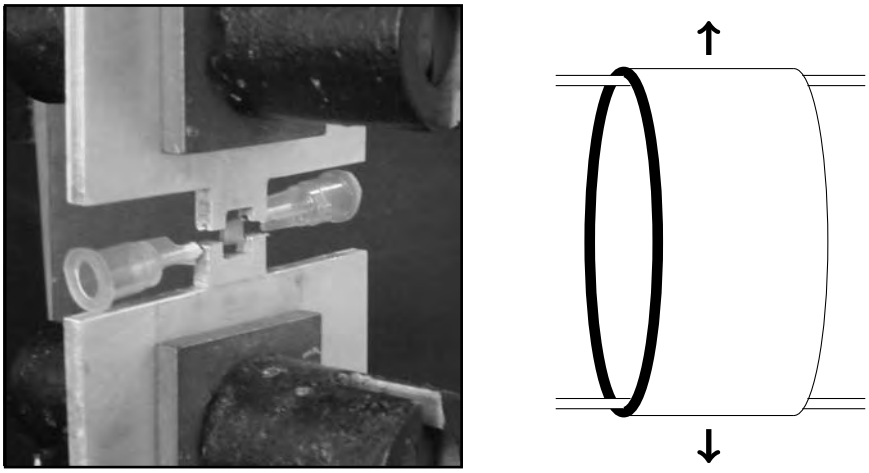

Figure 7.2: The custom made jig for tensile testing of rat aortic rings shown in photographic and exploded schematic form. Two 26 gauge (0.457 mm diameter) needles thread through the lumen of the ring to apply the force to the luminal surface and to the aortic ring.

cleaned of perivascular tissue and two rings of approximately 3 mm length cut from the thoracic and abdominal section of the aorta, immediately distal to the aortic arch and renal branches respectively. Wet mass and external radius of the aortic rings were recorded. The aortic rings were mounted directly for tensile testing (Instron 5543) using a custom made jig comprising two 26 gauge (0.457 mm diameter) metal supports placed through the vessel lumen (Figure 7.2). Samples were subjected to pre-cycling at 6 mm/min between an equivalent load of 80 and 160 mmHg until steady state hysteresis was achieved to eliminate any effect of active smooth muscle tension (Figure 7.3). The samples were then stretched at a constant strain rate of 2 mm/min and applied load recorded until vessel fracture .

Stress was calculated as applied load per longitudinal length of sample, per wet weight of sample (N/mm/mg). Breaking stress and breaking strain were noted for each sample. The incremental modulus of elasticity (E_{inc}) was calculated for a strain of 50%, a strain of 50% being nominally chosen

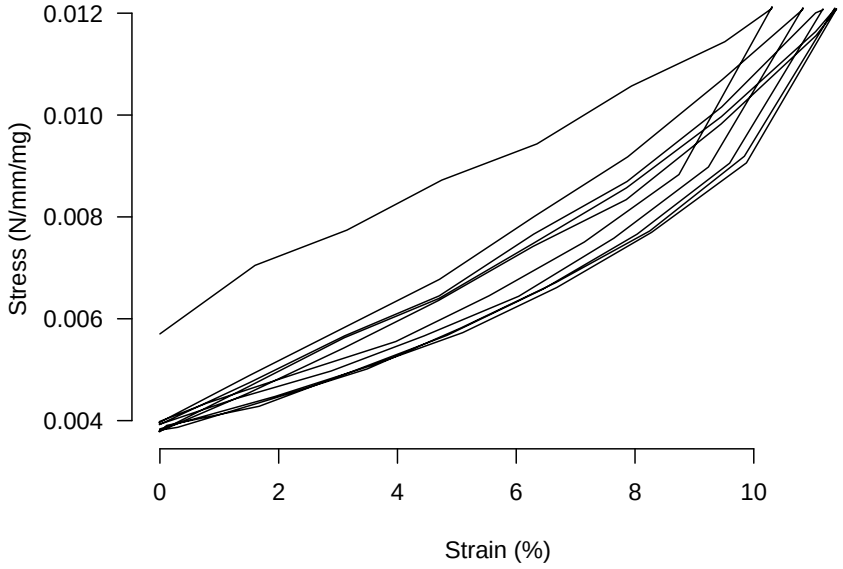

Figure 7.3: The stress–strain relationship for pre-cycling tensile load of *ex-vivo* testing of an aortic ring. Pre-cycling continued until steady state hysteresis was achieved, indicating a loss of smooth muscle activity, the subsequent stress–strain curve (Figure 7.11) being indicative of vessel structural stiffness alone.

for purposes of standardised comparison across all measurements.

7.1.5 Data analysis

PWV and associated haemodynamic parameters were calculated, pulse by pulse, across the entire achieved pressure range as previously described (Chapter 3). For the calculation of pressure wave reflection, 30 pulses were analysed at a mean pressure of 90 mmHg in each rat using an estimated triangular flow wave as outlined in Chapter 3.

All results are expressed as means and standard error of means, unless specified otherwise. Haemodynamic parameters were compared across pressure ranges by one-way Analysis of Variance (ANOVA) with post-hoc Tukey Honest Significant Difference (HSD) tests with a family-wise confidence interval of 95%. Statistical differences across age groups in the VDN treated rats was found by one-way ANOVA with post-hoc Bonferroni correction. Within

pressure range comparison of haemodynamic variables between control and VDN treated rats was made by Welch two sample unpaired t-tests.

The tensile testing parameters of breaking stress, breaking strain, and incremental modulus of elasticity at 50% strain were compared between thoracic and abdominal section by Student's paired t-tests. Comparison across age groups in the VDN treated rats was made by one-way ANOVA with post-hoc Bonferroni correction, comparison between VDN treated and control rats by Welch two sample t-test.

7.2 Results

7.2.1 PWV measurement

There was a significant difference between age groups in the VDN treated rats in pulse pressure at mean pressures less than 80 mmHg (Figure 7.4) and in heart rate at mean pressures greater than 115 mmHg (Figure 7.5). PWV across all age groups showed a typical curvilinear relationship with increasing Mean Arterial Pressure (MAP) and did not differ significantly between age groups at any mean pressure range (Figure 7.6). Results of statistical comparison across pressure ranges are included in Appendix C (Figure C.9-C.16). There were significant differences across pressure ranges in all age groups in pulse pressure and PWV, but not in heart rate.

There was no difference in heart rate and pulse pressure between the 14 week old VDN treated rats and the 14 week old controls across most mean arterial pressures (Figure 7.7–7.8), though a trend toward higher heart rate in the VDN treated rats became significant at mean pressures above 140 mmHg. PWV in VDN treated and control rats showed an expected curvilinear relationship with pressure. There was no difference between treated and

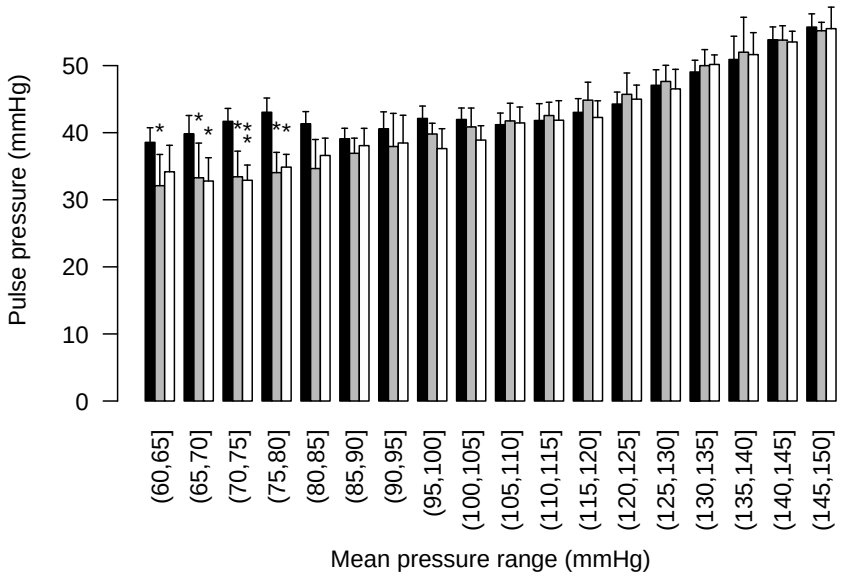

Figure 7.4: Pulse pressure in the VDN treated rats with increasing age (black = 12 weeks; grey = 13 weeks; white = 14 weeks). Pulse pressure increased with mean pressure. A significant difference between age groups in pulse pressure developed in pressure ranges less than 80 mmHg (* $p<0.1$, ** $p<0.01$ compared to 12 weeks of age).

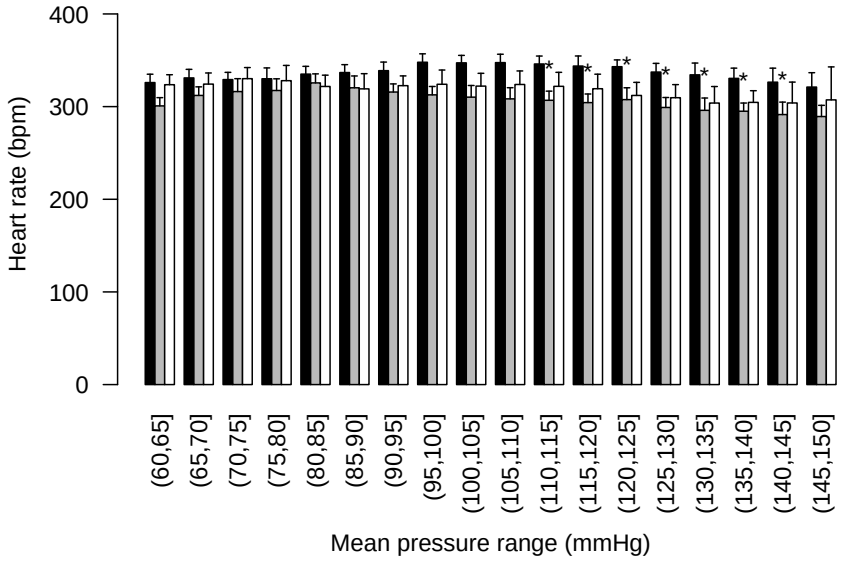

Figure 7.5: Heart rate in the VDN treated rats with increasing age (black = 12 weeks; grey = 13 weeks; white = 14 weeks). Heart rate was consistently lower in the 13 and 14 week old rats, becoming significant for mean pressures greater than 110 mmHg (* $p<0.1$ compared to 12 weeks of age).

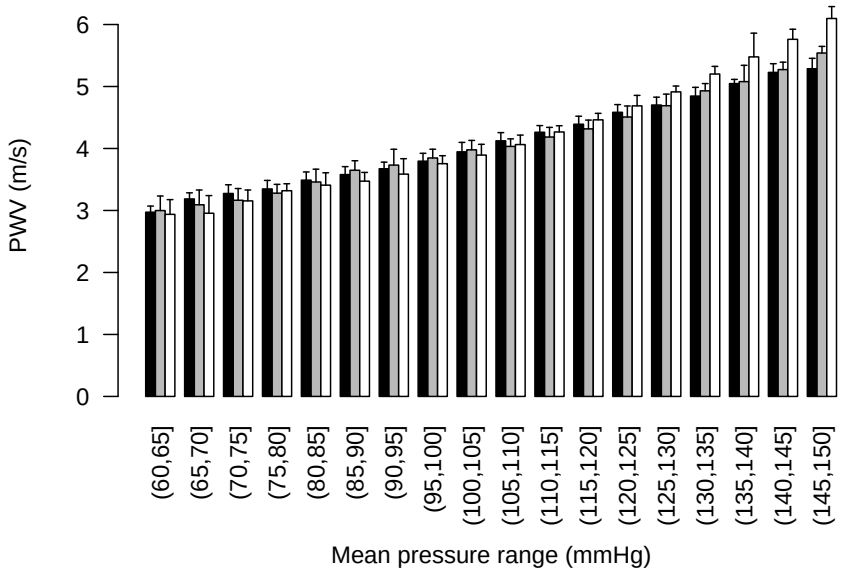

Figure 7.6: Aortic PWV in the VDN treated rats with increasing age (black = 12 weeks; grey = 13 weeks; white = 14 weeks). There was no significant difference in arterial stiffness at any pressure range, though a trend toward higher PWV in the 14 week old rat existed at pressures above 130 mmHg.

control rats at any pressure range (Figure 7.9).

7.2.2 Pressure wave reflection

Calculation of wave reflection parameters, as described in Chapter 2, was made on collected data segments with a mean pressure of approximately 90 mmHg, with no change in heart rate or pulse pressures across the segments analysed in either the VDN treated rats or controls (Table 7.1). Estimated characteristic impedance was higher in VDN treated rats across all age ranges compared to controls, but the trend was insignificant (Figure 7.10). There was a slight, but insignificant trend toward lower reflection magnitude of the pulse pressures (RM_{PP}) with increasing age in the VDN treated rats. All other measured indexes of wave reflection showed no significant difference either with age, or treatment (Figure 7.10).

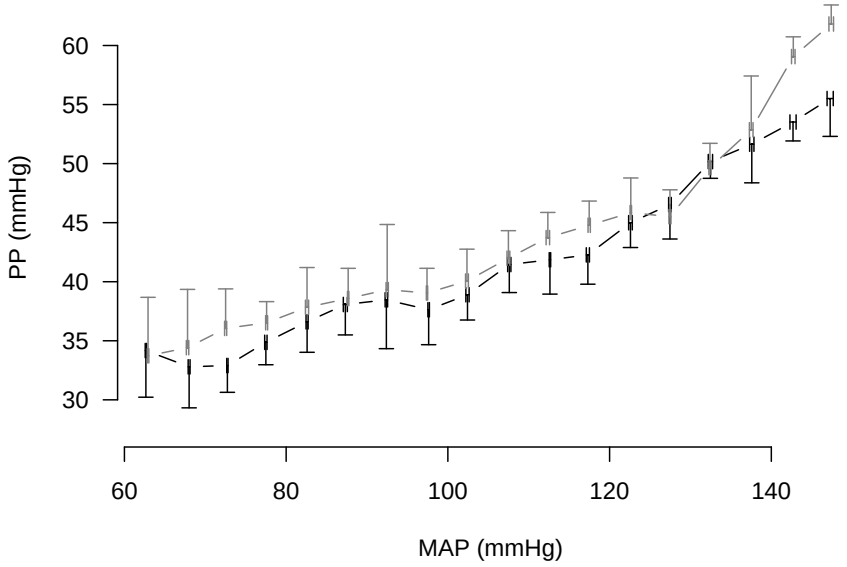

Figure 7.7: Pulse pressure in 14 week old VDN treated (dark line) and control (light line) rats. Pulse pressure increased with mean arterial pressure. There was no significant difference between VDN treated and control rats.

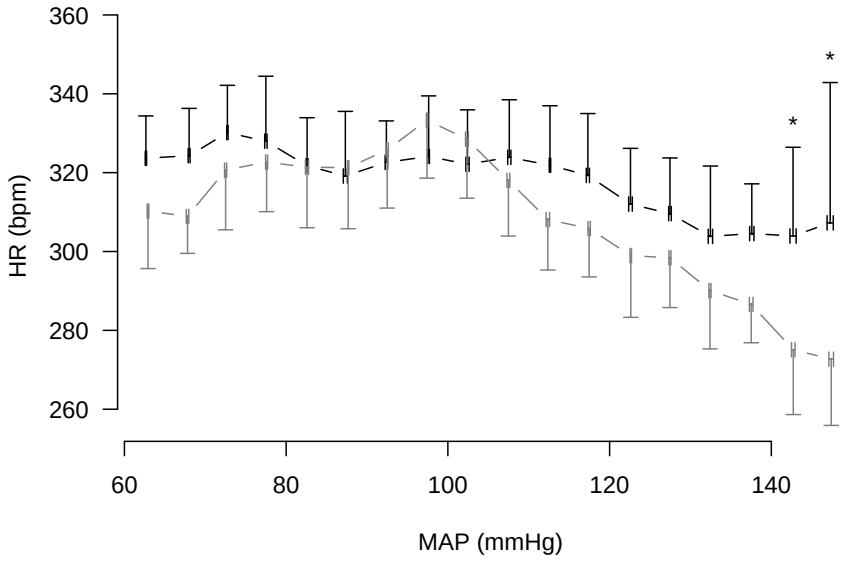

Figure 7.8: Heart rate in 14 week old VDN treated (dark line) and control (light line) rats. There was a divergence in heart rate at higher pressures, becoming significant for pressures greater than 140 mmHg (* $p<0.1$ between VDN and control at that pressure range).

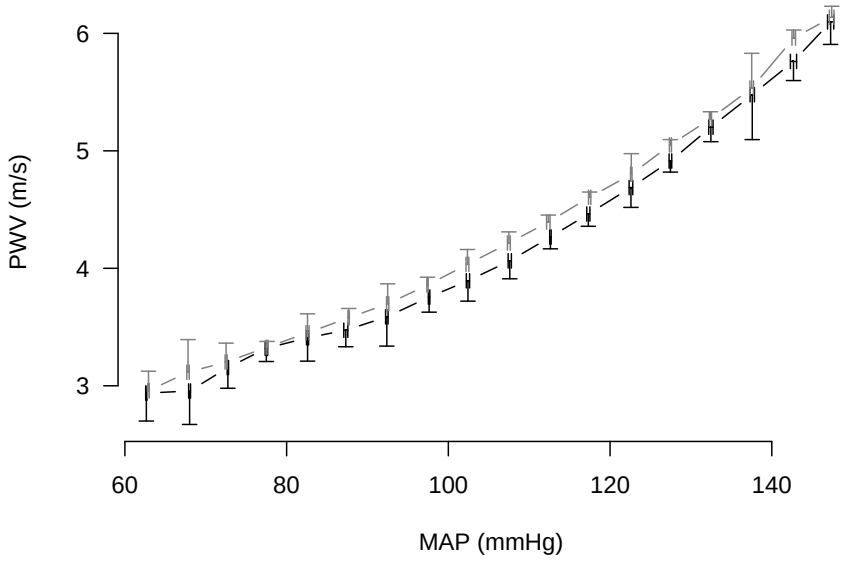

Figure 7.9: Aortic PWV in 14 week old VDN treated (dark line) and control (light line) rats. The expected curvilinear relationship between MAP and PWV was evident. No statistical difference existed between control and VDN treated rats at any pressure range.

Table 7.1: Mean haemodynamic parameters of segments analysed for pressure wave reflection in VDN rats of 12, 13, and 14 weeks of age, and controls. Measurements were made at a mean pressure of approximately 90 mmHg (difference between VDN 14 weeks and control of 1.3 mmHg, $p<0.1$). All other parameters were constant throughout, including the pulse pressures of the calculated incident (PP_i) and reflected (PP_r) waves.

	VDN			Control
	12 weeks	13 weeks	14 weeks	14 weeks
HR (bpm)	333±13	313±10	342±17	349±11
MAP (mmHg)	90.6±0.2	91.3±1.0	89.3±0.4*	90.6±0.4
PP (mmHg)	41.5±2.4	36.4±2.3	35.3±2.5	34.0±2.1
PP_i (mmHg)	29.8±1.8	29.0±3.7	28.4±2.6	24.8±1.6
PP_r (mmHg)	18.6±1.1	16.6±1.1	16.1±1.1	15.1±0.9

* $p<0.1$ compared to control by unpaired, Welch two-sample t-test.

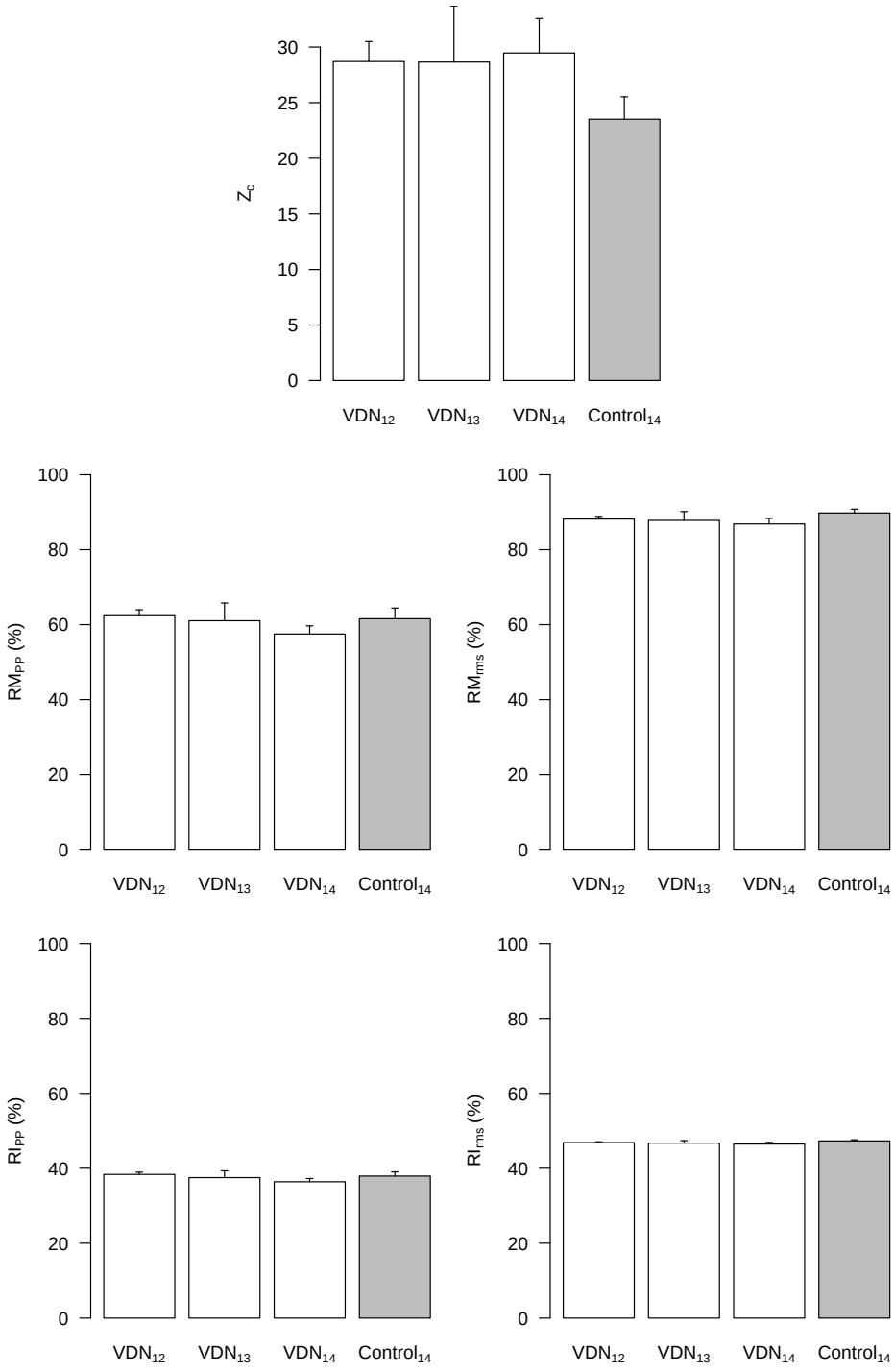

Figure 7.10: Calculated wave reflection parameters (Chapter 3) in VDN treated rats of 12, 13, and 14 weeks of age, and in the 14 week old controls. All changes were not significant. Characteristic impedance (Z_c) was consistently higher in the VDN treated rats compared to controls.

7.2.3 *Ex-vivo* analysis of aortic tissue

A representative stress–strain curve for the tensile testing of the thoracic and abdominal aortic rings is presented in Figure 7.11. *Ex-vivo* tensile testing of aortic segments showed that the breaking stress in the abdominal aorta was consistently higher than that of the thoracic aorta and did not change with increasing age in the VDN treated rats. The breaking strain in the abdominal aorta showed a significant reduction with age to be significantly less than the thoracic breaking strain at 14 weeks of age (52±2% and 63±4% respectively, $p<0.1$). The incremental modulus of elasticity (E_{inc}) at 50% strain was greater in the thoracic than abdominal section at 12 weeks of age (0.082±0.032 N/mm/mg and 0.018±0.005 N/mm/mg respectively, $p<0.1$) and was lower in the thoracic than abdominal section at 14 weeks of age (0.011±0.004 N/mm/mg and 0.064±0.019 N/mm/mg respectively, $p<0.1$). This was caused by a significant reduction in incremental modulus of elasticity with age in the thoracic aorta, mirrored by a non-significant increase in abdominal incremental modulus of elasticity with age (Figure 7.12).

Comparison of 14 week old VDN treated rats and 14 week old control rats showed that breaking strain decreased significantly in the abdominal aorta (control 64±5%, VDN 53±2%, $p<0.1$). The inverse was true in the thoracic aorta where breaking strain increased with VDN treatment (control 46±2%, VDN 63±4%, $p<0.01$). The abdominal aorta showed a non-significant increase in incremental modulus of elasticity at 50% strain with VDN treatment (control 0.042±0.011 N/mm/mg, VDN 0.064±0.019, $p=0.3$) and the thoracic aorta a significant reduction in incremental modulus of elasticity at 50% strain with VDN treatment (control 0.036±0.006 N/mm/mg, VDN 0.011±0.003, $p<0.01$). Results for breaking stress, breaking strain, and the incremental modulus of elasticity at 50% strain for VDN and control rats of

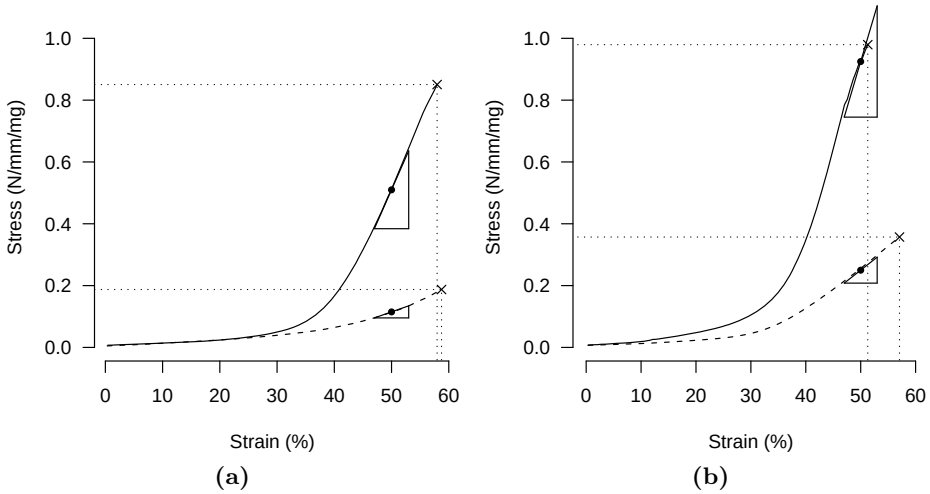

Figure 7.11: An example of the recorded stress–strain curve for an abdominal (solid line) and thoracic (dashed line) aortic ring from (a) a 14 week old VDN treated rat and (b) a 14 week old control rat. The breaking stress and breaking strain (×) are indicated by the dotted lines. The incremental elastic modulus at 50% strain is given by the slope of the stress-strain curve at the point of 50% strain (●). The individual example shows abdominal and thoracic breaking strain is approximately equal and abdominal breaking strain and incremental elastic modulus at 50% strain much greater in the abdominal compared to the thoracic region.

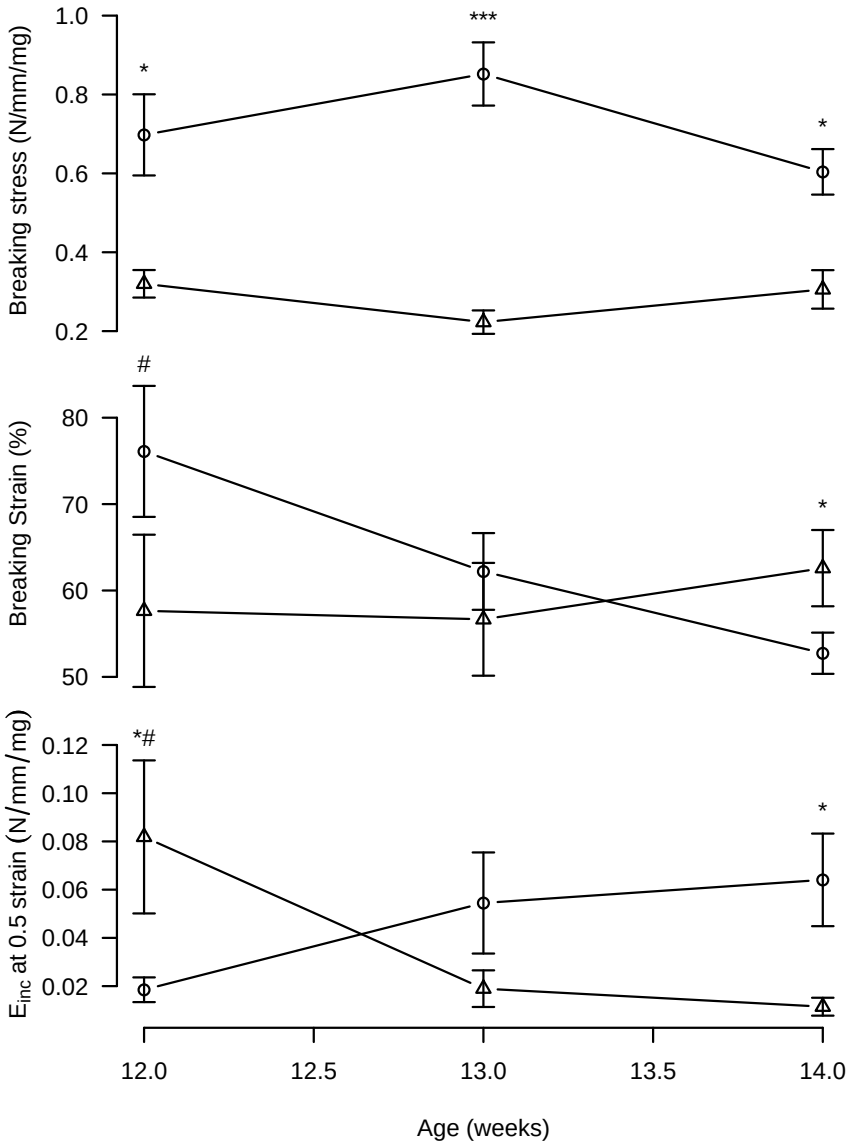

Figure 7.12: Changes in mean breaking stress and breaking strain of the abdominal (○) and thoracic (△) aorta with increasing age and VDN treatment. There was a consistent significant difference between abdominal and thoracic section breaking stress. Breaking stress was constant with age, as was breaking strain in the thoracic aorta. Breaking strain in the abdominal aorta decreased with age, as did E_{inc} at 50% strain in the thoracic aorta. * $p<0.1$ compared to abdominal aorta at the same age; ** $p<0.001$ compared to abdominal aorta at the same age; # $p<0.1$ compared to the same aortic section at 14 weeks of age.

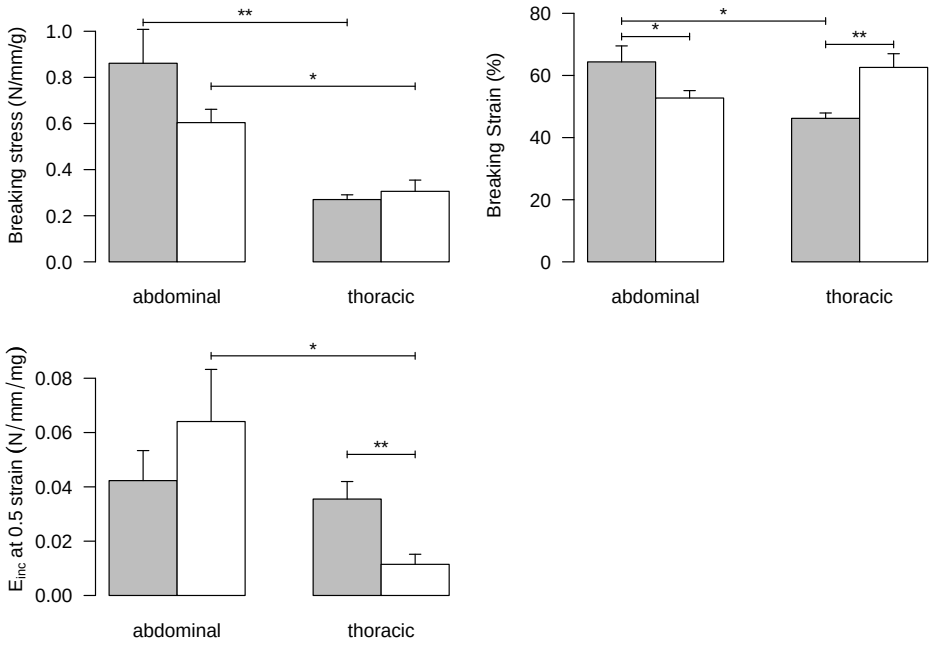

Figure 7.13: Breaking stress, breaking strain, and the incremental modulus of elasticity (E_{inc}) in the 14 week old control rat (grey) and the 14 week old VDN treated rat (white). VDN treatment induced significant changes in abdominal and thoracic breaking strain, and in thoracic incremental modulus of elasticity (* $p<0.1$; ** $p<0.01$).

14 weeks of age are presented in Figure 7.13.

7.3 Discussion

Tensile testing of abdominal aortic rings showed a decrease in breaking strain and a non-significant increase in the incremental modulus of elasticity at 50% strain with calcification treatment at 14 weeks of age compared to controls. Fourier decomposition of the measured pressure and estimated flow waves showed a non-significant but consistent increase in characteristic impedance with VDN across all age ranges measured. However, this indication of increased stiffness in the arterial system did not manifest in an alteration of PWV measured *in-vivo* six weeks following VDN treatment in the Lewis strain

of rat. The results differ from those of Niederhoffer et al. (1997b), Gaillard et al. (2005), and Jegger et al. (2006), though direct comparison cannot be made as these studies used a longer time point of 2 months.

Niederhoffer et al. (1997b) showed in the Wistar strain of rat, 2 months after VDN treatment, an increase in aortic PWV using two separate pressure cannulae introduced into the aorta via the common carotid and femoral arteries. These results were confirmed in a study of similar methodology by the same group (Gaillard et al., 2005), investigating the effect of pioglitazone treatment on aortic calcification, where VDN treated rats were shown to have a higher aortic PWV than that of the controls. Jegger et al. (2006), using an estimated value of PWV calculated from characteristic impedance, showed increased aortic stiffness in Wistar rats also 2 months after VDN treatment. The current study is the first to investigate the effect of VDN treatment on aortic stiffness at time periods other than 2 months, and is the first to investigate the effect of VDN treatment on aortic stiffness in a strain of rat other than the Wistar strain.

Kieffer et al. (2000) demonstrated that calcification by VDN treatment was an effective mechanism of aortic calcification in Wistar, Wistar Kyoto, and spontaneously hypertensive strains of rats, as measured by total calcium levels found in the aortic tissue. Calcium levels in the thoracic aorta increased 25 to 30 times over 16 days following VDN treatment. Abdominal aortic calcium levels were not measured. These results indicate that calcium deposition in arterial tissue by VDN treatment occurs in a variety of rat strains and is not particular to the Wistar strain of rat.

The tensile tests conducted in the current study indicated that VDN treatment caused an increase in vessel structural stiffness in the abdominal aorta. Abdominal aortic sections became stiffer (an increase in the incre-

mental modulus of elasticity), and weaker (a decrease in breaking strain). Thoracic aortic sections, however, became less stiff (a decrease in the incremental modulus of elasticity), and stronger (an increase in breaking strain). The mechanisms behind the inverse relationship between thoracic and abdominal structural stiffness and breaking strain is not understood and subject to further research. A theory that may explain the relationship is that thoracic aortic remodelling is initiated by changes in vascular impedance caused by calcification and increased stiffness in the more distal arteries, including the abdominal aorta. Further studies involving histological investigation of changes in vessel wall structure with age and VDN treatment may confirm or deny the presence of structural remodelling. Histological analysis may also provide a quantitative measure of vessel wall calcium content and the progression of calcium deposition with treatment duration, a parameter absent in the current study.

Changes in structural stiffness were evident 6 weeks after treatment with VDN treated rats compared to controls. However, this did not manifest in a change in measured arterial stiffness *in-vivo*. This may be due to a compensatory mechanism of the functional components of the vessel wall for increased structural stiffness. A change in *in-vivo* stiffness may be evident in longer time periods, such as those studied by Niederhoffer et al. (1997b), Gaillard et al. (2005), and Jegger et al. (2006). Tensile testing in the current study also exposed differing responses in the thoracic and abdominal aortic sections to VDN treatment. The position of the dual pressure sensing catheter was such that PWV was measured across both the thoracic and abdominal sections, the resulting measure of PWV an average of the thoracic and abdominal arterial stiffness. The incremental modulus of elasticity and breaking strain between abdominal and thoracic aortic sections had an in-

verse relationship. The averaging of these measures of structural stiffness and strength may result in a net zero change in arterial stiffness across the length of the descending aorta, as measured by the dual pressure sensing catheter across the length of the descending aorta. Future studies should consider changes in PWV as a measure of *in-vivo* arterial stiffness in the abdominal and thoracic aorta independently, as changes in structural arterial stiffness is not uniform across the length of the aorta with VDN treatment.

In conclusion, the current study is the first to investigate the effects of VDN treatment with age, and the first to measure arterial stiffness in a strain of rat other than the Wistar strain. Using the method of high fidelity measurement of PWV with a dual pressure sensing catheter, it was shown that *in-vivo* aortic stiffness does not increase at a period of 6 weeks following VDN administration in spite of decreased abdominal breaking strain and a trend toward increased abdominal structural stiffness shown by *ex-vivo* testing. This may be due to compensatory remodelling of the thoracic aorta, suggested by inverse changes in structural stiffness in abdominal and thoracic segments with age and VDN treatment. This result is important in the design of future studies investigating calcification in that abdominal and thoracic arterial stiffness should be assessed independently as the mechanisms of calcification may not be consistent across the aortic length.

CHAPTER 8

A comparison of vasoconstrictor agents with different modes of action on pulse wave velocity in large arteries: a study of angiotensin-II, noradrenaline, and endothelin-1 in the sheep iliac artery

Angiotensin-II, noradrenaline, and Endothelin-1 (ET-1) are known to have vasoconstrictive properties. Basic information and pharmacological mechanisms of angiotensin-II, noradrenaline and ET-1 are described in Chapter 2. Briefly, angiotensin-II, synthesised from angiotensin-I in the presence of renin and Angiotensin-Converting Enzyme (ACE), increases arterial smooth muscle tension by increasing noradrenaline concentration at sympathetic nerve synapses, stimulating sympathetic vasoconstriction (Brunton, 2006; Zimmerman et al., 1984). Noradrenaline is an α_1- and α_2-adrenoreceptor antagonist that causes smooth muscle contraction and incites sympathetic vasoconstriction (Bevan et al., 1988). ET-1 is a potent vasoconstrictor with prolonged action associated with activation of the Endothelin-A (ET_A) and Endothelin-B (ET_B) receptors, although predominantly with the ET_A receptor (Halcox et al., 2007; Spieker et al., 2003; Spratt et al., 2001). The current study aims to investigate the effect of angiotensin-II,

noradrenaline, and ET-1 on both large artery stiffness, as measured by Pulse Wave Velocity (PWV), and blood flow in the large arteries. The *in-vivo* action of the vasoconstrictors was studied in the iliac artery of anaesthetised sheep, an established technique of large artery stiffness assessment (McEniery et al., 2003; Schmitt et al., 2004; Wilkinson et al., 2002c).

8.1 Methods

8.1.1 Experimental animals

Crossbred Suffolk sheep of 12 to 18 months of age were used in all experiments. The Animal Care and Ethics Committee of the University of New South Wales approved all husbandry and experimental procedures.

8.1.2 Haemodynamic measurements

Animals were anaesthetised by intravenous injection of 600 to 900 mg of sodium phenobarbitone (Rhone Merrieux), maintained by 2 to 3% isofluorane, administered with oxygen at 2 L/min through a Boyle rebreathing apparatus. Animals were spontaneously breathing, in the supine position, throughout the duration of the experiment.

Arterial pressure was measured with a 6F, high fidelity, dual pressure sensing catheter with 0.46 mm lumen (Gaeltec, Skye, United Kingdom). The two pressure sensors, 10 and 60 mm from the distal tip, were calibrated before the experiment with a mercury sphygmomanometer. The catheter was introduced via a 7F sheath, inserted in the femoral artery (Figure 8.1). The two pressure sensors were positioned in the common iliac artery, slightly distal of the iliac bifurcation. The catheter position was confirmed directly upon completion of the experiment. Blood flow was measured with an electromagnetic flow sensor (MDL1401, Skalar) of appropriate diameter, fitted

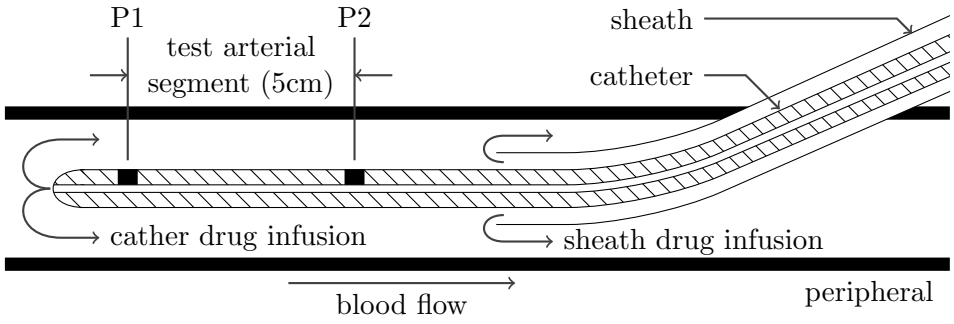

Figure 8.1: Schematic diagram showing the infusion of drug via the catheter (proximal) and the sheath (distal) into an arterial segment. P1 indicates pressure sensor one, and P2 indicates pressure sensor two, separated by a distance of 5cm. (Adapted from McEniery et al., 2003).

around the exposed segment of the femoral artery, slightly distal to the sheath insertion point. Heart Rate (HR) was calculated from a three lead, type II electrocardiogram (ECG) signal. The experimental setup, with exception of the use of electromagnetic flow sensing, has been previously utilised and described (McEniery et al., 2003, 2004; Wilkinson et al., 2002c).

All data was sampled at 1kHz using a PowerLab 800 data acquisition unit with Chart software (ADInstruments). Blood pressure, HR, PWV and blood flow was analysed in custom software written in Octave (Eaton, 2002), as detailed in Chapter 3, over 20 second intervals to allow averaging of variations in the respiratory cycle.

8.1.3 Vasoactive substances

Drugs were delivered in 0.9% saline as the vehicle, infused at 1 ml/min through the catheter and sheath individually, and compared to baseline (vehicle only) results. Infusion through the catheter exposed both the test arterial segment and peripheral vasculature to the drug. Infusion through the sheath, distal to the test segment, exposed only the peripheral vasculature to the drug. Comparison of results given by catheter and sheath

infusions allows indirect drug effects to be differentiated from local effects on smooth muscle activity.

Both angiotensin-II and noradrenaline were infused at doses of 10, 30 and 100 pmol/min through the catheter route. A single sheath infusion of 100 pmol/min was made for both angiotensin-II and noradrenaline. ET-1 was infused at a rate of 10 pmol/min for a period of 45 minutes, with measurements taken following 15, 30 and 45 minutes of infusion. ET-1 (10 pmol/min) was then co-infused with BQ-788 (1 nmol/min), an ET_A and ET_B receptor antagonist, for a period of 45 minutes, readings also taken at 15, 30 and 45 minutes. By blocking endothelin receptors, it was believed that BQ-788 would attenuate the effect of ET-1.

Two baseline recordings of 20 seconds in length were taken during infusion of saline at 1 ml/min before infusion of the drug. Recordings of 20 second length were then taken for each dose of each drug and compared to baseline recordings.

8.1.4 Data analysis

All results are expressed as means±standard error of means. Comparison between baseline (saline infusion) and drug infusion was made by Student's paired t-test on measured values. Significance between doses was by one-way Analysis of Variance (ANOVA) on the percent change from baseline results, with post-hoc Bonferroni correction,

8.2 Results

8.2.1 Angiotensin-II

Angiotensin-II showed a significant increase in both PWV and pressure corrected PWV for doses of 30 and 100 pmol/min with no change in Mean Arterial Pressure (MAP), pulse pressure or heart rate (Table 8.1; Figure 8.2). There was no statistical difference between 10, 30 and 100 pmol/min doses in any measured parameter, though a trend toward increasing pressure corrected PWV with increasing dose concentration was evident. Infusion of angiotensin-II at 100 pmol/min through the sheath did not cause a change in PWV, nor any of the other measured haemodynamic parameters(Table 8.1; Figure 8.2). There was a small but significant decrease in flow with infusion of 100 pmol/min angiotensin-II, all other catheter and sheath infusions showing insignificant changes in mean flow (Figure 8.2).

8.2.2 Noradrenaline

There was no significant change from baseline, nor trend with increasing dose concentration, in pressure corrected PWV with infusion of noradrenaline (Figure 8.2). A significant change from baseline values in MAP occurred only following infusion at 10 pmol/min (1.5±0.7% decrease from baseline, $p<0.1$) and pulse pressure increased for all dose infusions of noradrenaline (Table 8.1). There was a small but significant decrease in heart rate during infusion of noradrenaline at a rate of 100 pmol/min (-0.8±1.6 %, $p<0.1$). There was no significant change in mean flow, and no apparent trend with respect to dose concentration (Figure 8.2).

Table 8.1: Change from baseline in PWV, MAP, PP, and HR during infusion of angiotensin-II, noradrenaline, ET-1, and co-infusion of ET-1 and BQ-788. All changes expressed as percent change from baseline.

	ΔPWV (%)	ΔMAP (%)	ΔPP (%)	ΔHR (%)
Angiotensin-II 10 pmol/min	4.2±2.5	1.3±1.2	0.4±0.6	-0.4±0.5
Angiotensin-II 30 pmol/min	12.3±5.0*	2.2±2.1	1.2±1.4	-1.0±1.1
Angiotensin-II 100 pmol/min	17.3±6.2*	4.9±2.9	-0.3±2.2	-1.1±1.1
Angiotensin-II 100 pmol/min, Sheath	1.8±1.2	1.5±1.2	2.0±0.6	1.0±0.7
Noradrenaline 10 pmol/min	-3.0±3.6	-1.5±0.7*	2.1±0.8*	-1.7±1.3
Noradrenaline 30 pmol/min	9.9±9.6	3.3±2.8	5.5±2.1*	-0.9±1.3
Noradrenaline 100 pmol/min	1.3±3.9	-3.0±2.2	7.2±2.4*	-0.8±1.6*
Noradrenaline 100 pmol/min, Sheath	-1.7±2.7	-0.5±2.0	1.3±1.8*	-1.0±1.0
ET-1 15 minutes	4.2±4.1	-1.2±1.3	2.1±1.1	-1.3±0.6*
ET-1 30 minutes	1.7±2.5	-3.6±1.8*	2.8±1.1*	-2.0±0.6*
ET-1 45 minutes	4.2±4.5	0.3±2.7	5.2±1.2†	-2.2±1.2*
ET-1+BQ-788 15 minutes	-3.1±4.8	-2.0±0.8	-2.0±1.2	1.5±2.4
ET-1+BQ-788 30 minutes	-3.0±8.2	-13.8±12.7	3.0±6.5	2.9±5.1
ET-1+BQ-788 45 minutes	-7.8±4.5	-3.8±2.2	-1.1±3.9	2.3±2.4

* $p<0.1$, $^{\dagger}p<0.01$ compared to baseline by Student's paired t-test on measured values.

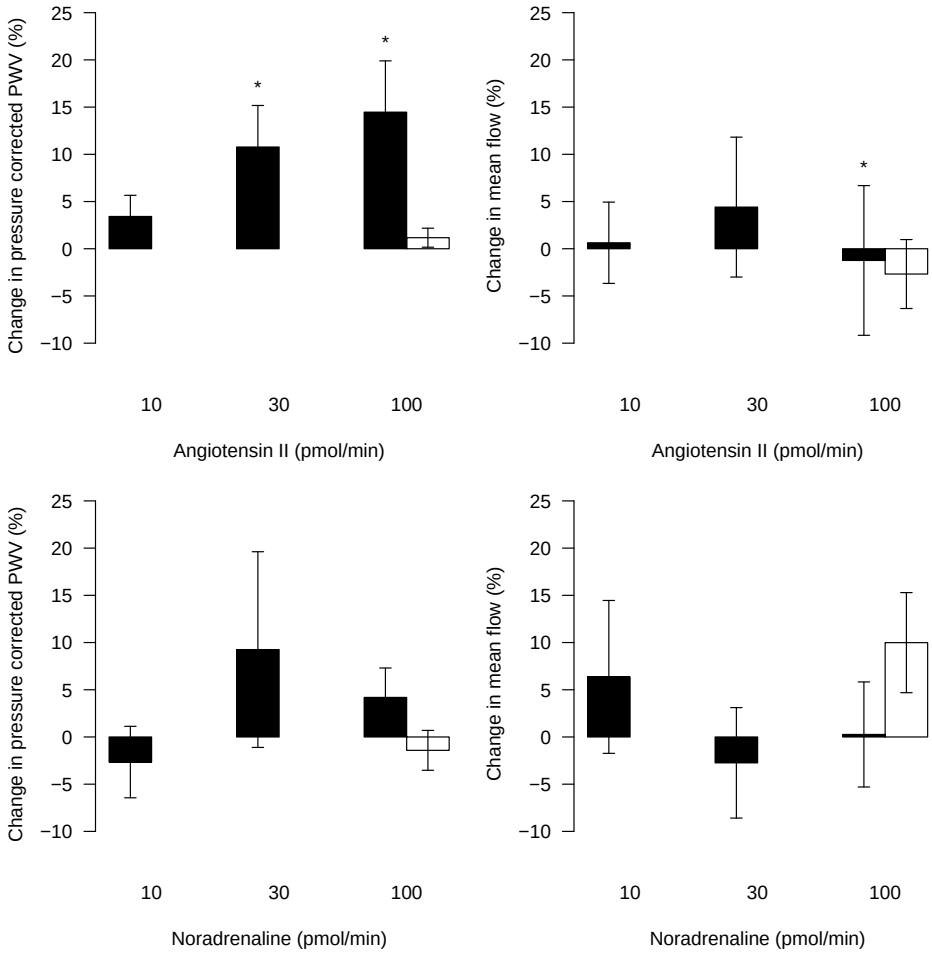

Figure 8.2: Mean pressure independent PWV and flow changes from baseline values with graded doses of angiotensin-II and noradrenaline infused through the catheter (■) and the sheath (□). Whilst the results for noradrenaline infusion were variable and non-significant, angiotensin-II infusion caused a dose dependent increase in arterial stiffness in the local vessel, the localised effect of the infusion confirmed by a near zero change in PWV with sheath infusion of angiotensin-II. (* $p<0.1$ compared to baseline by Student's paired t-test on measured values.)

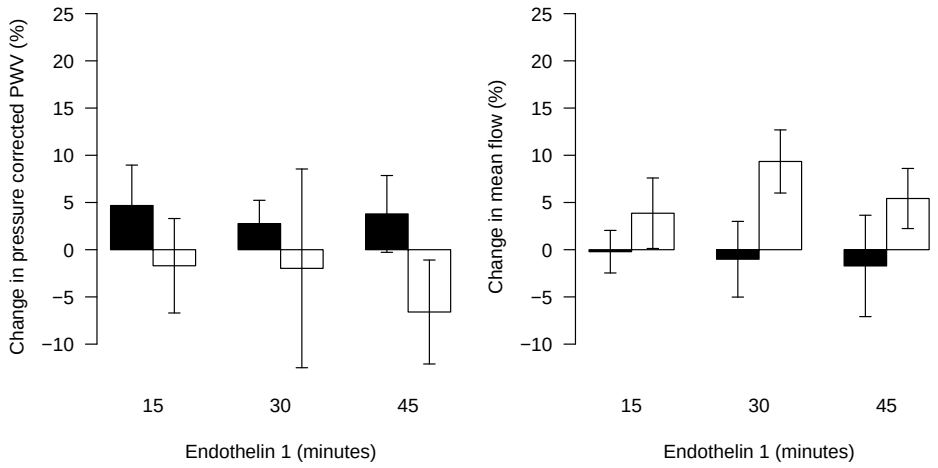

Figure 8.3: Changes in pressure independent PWV and in mean flow with infusion of ET-1 (■), and co-infusion of ET-1 and BQ-788 (□). There was a non-significant trend toward increased arterial stiffness and a decrease in arterial flow with infusion of ET-1. Co-infusion of BQ-788 with ET-1 caused a non-significant decrease in arterial stiffness and an increase in arterial flow.

8.2.3 Endothelin-1

Infusion of ET-1 was associated with a significant decrease in heart rate across the 45 minute period of infusion (Table 8.1). Mean and pulse pressure changed significantly only during measurement following 30 minutes of infusion (-3.6±1.8 % and 2.8±1.1 % respectively, $p<0.1$). There was no significant change from baseline values in MAP, pulse pressure, or heart rate during co-infusion of ET-1 and BQ-788. There was a consistent but non-significant increase in both PWV and pressure corrected PWV with infusion of ET-1 and a consistent but non-significant decrease in PWV and pressure corrected PWV with co-infusion of BQ-788 (Table 8.1; Figure 8.3). ET-1 infusion caused a consistent non-significant decrease in mean flow. Co-infusion with BQ-788 caused a non-significant increase in mean flow (Figure 8.3).

8.3 Discussion

Vascular tone is modified by endogenous circulating factors, and by endothelium derived factors (Chapter 2; Brunton, 2006; Ferro, 2003; Zimmerman et al., 1984). The current study investigates for the first time the effect of three known endogenous vasoactive substances, exogenously introduced, on simultaneously measured large artery stiffness and blood flow.

Infusion of angiotensin-II caused a significant increase in large artery stiffness. A non-significant trend indicated that the increase in PWV was dose dependent. The effect was confirmed as a local vascular effect, with infusion of angiotensin-II through the sheath at maximal concentration causing a near zero change in PWV. There was no significant change in blood flow for any dose of angiotensin-II infused. The results for noradrenalin infusions were highly varied, and no trend, significant or otherwise, existed with increasing dose for either PWV or blood flow measurement. A significant change in pulse pressure and a non-significant but apparent increase in flow with noradrenaline infusion through the sheath imply a systemic effect at a 100 pmol/min dose, however this did not present in any change in MAP. Additionally, the 100 pmol/min dose administered through the catheter lumen failed to induce a similar increase in arterial blood flow. ET-1 infusion at a concentration of 10 pmol/min caused a non-significant increase in large artery stiffness. In a similar experiment, McEniery et al. (2003) were able to show a significant increase in PWV with ET-1 infusion at 10 pmol/min. In the current study there was also a non-significant trend of a decrease in arterial blood flow with increasing time of infusion of ET-1. Similar findings were recently published by Van Guilder et al. (2007) in the study of ET-1 in the human forearm with the effect of age. Blocking of the ET_A and ET_B receptors with co-infusion of BQ-788 caused a non-significant decrease in

PWV, the decrease increasing in magnitude with increasing time of infusion. The non-selective endothelin receptor blocker also caused a non-significant increase in blood flow when co-infused with ET-1.

In conclusion, this is the first study to simultaneously measure both changes in flow and arterial stiffness in large arteries in response to selected vasoconstrictor agents. A trend toward increased arterial stiffness and decreased flow was evident with ET-1 infusion, the effect of which was reversed by blockade of the ET_A and ET_B receptors. Noradrenaline infusion caused a highly variable result in arterial stiffness and blood flow changes. Angiotensin-II increased large artery stiffness with little effect on local blood flow.

CHAPTER 9

The effect of endothelium dependent nitric oxide release induced by the adrenergic β-antagonist, nebivolol, on regional pulse wave velocity in the human iliac artery

Nebivolol is an adrenergic β-antagonist, with high specificity for the β_1 receptor (Bristow et al., 2005). It is an approved anti-hypertensive medication in 65 countries outside of the United States, and is pending approval by the United States Food and Drug Administration (Forest Laboratories, Inc., 2006, 2007). The Study of the Effects of Nebivolol Intervention on Outcomes and Rehospitalisation in Seniors with Heart Failure (SENIORS) trial of nebivolol showed reduced all-cause mortality and cardiovasular hospitalisation in 815 elderly heart failure patients on daily nebivolol medication compared to 1030 placebo treated subjects (Dobre et al., 2007). It has been shown to have a blood pressure lowering effect (DeCrée et al., 1992), but with no greater efficacy than atenolol (Fogari et al., 1997; Nueten et al., 1997).

Nebivolol is a racemic mixture of an L-isomer and a D-isomer in equal proportions (Mangrella et al., 1998). The D-isomer is a β_1 adrenoreceptor blocker, similar, but much more highly specific to the β_1 receptor than

the β_2 receptor than all other β-blockers currently in clinical use (Bristow et al., 2005). The affinity of nebivolol to the β_1 receptor is 321 times higher than the affinity to the β_2 receptor (Bristow et al., 2005). Cardiac cells have three adrenergic receptors, α_1, β_1, and β_2 (Bristow, 2000), with β_1 receptors more dominant in cardiac tissue than β_2 receptors, that are more dominant in the bronchi (Bristow et al., 2005). High selectivity for the β_1 adrenergic receptor is therefore preferable, the preference also accentuated by the higher affinity of noradrenaline for the β_1 over the β_2 receptor (Weber, 2005). Nebivolol differs from other β-blockers in the theorised potential to cause vasorelaxation through the L-arginine – nitric oxide (NO) pathway. The vasoactive property of nebivolol is attributed to both the D- and L-isomer, with the L-isomer being more strongly associated with vasorelaxation (Gao et al., 1991; Maffei et al., 2006; Nueten and Crée, 1998).

The vasoactivity of nebivolol has previously been shown in specific vascular settings, mostly in the smaller arteries. Van Merode et al. (1989) showed that a 4 week period of oral dosing of nebivolol (5mg, daily) reduced carotid arteries distensibility. The association between nebivolol and endogenous NO driven vasodilation was observed in the hand venous system by Bowman et al. (1994), local infusion of nebivolol causing vasodilation, which was blunted by co-infusion of N^G-monomethyl-L-arginine (L-NMMA). In this study, the same vasodilatory effect was not induced by infusion of an alternate β-blocker, atenolol. The potential for nebivolol derived vasodilation in arteries was shown with local infusion of nebivolol in the brachial artery of healthy subjects (Cockcroft et al., 1995). In this study, co-infusion of L-NMMA eliminated the vasodilatory effect of nebivolol, indicating that the mechanism of vasodilation was associated with endogenous NO. A similar experiment by Dawes et al. (1999) with local brachial artery infusion of

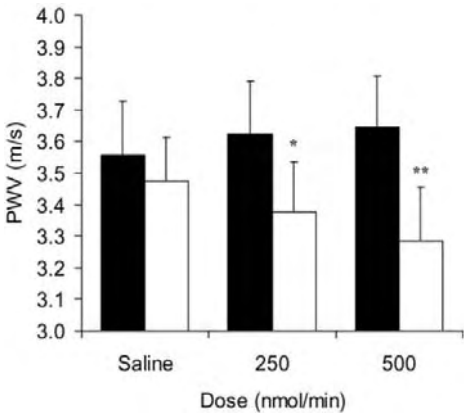

Figure 9.1: PWV in the intact ovine iliac artery (n=6, mean ± standard error of mean) during infusion of atenolol (■) and nebivolol (□). There was a significant decrease in PWV with increasing dose of nebivolol, but not atenolol (* $p<0.05$, ** $p<0.01$). (Reproduced from McEniery et al., 2004)

nebivolol and co-infusion of L-NMMA in hypertensive subjects showed that the vasodilatory effect was consistent in that sub-population.

In experiments concerning large artery stiffness, McEniery et al. (2004) showed that in the ovine iliac artery, nebivolol, but not atenolol, decreased arterial stiffness (Figure 9.1). With the infusion of L-NMMA, they confirmed that the vasorelaxation was associated with endothelium derived NO. The pilot study presented here was designed to observe if the potential for the same vasorelaxation was evident also in human large arteries. Nebivolol was locally infused in the human iliac artery to determine the effect on Pulse Wave Velocity (PWV), a measure of arterial stiffness.

9.1 Methods

9.1.1 Subjects

Subjects were recruited from the patient base submitted for angiographic study at the Eastern Heart Clinic, Sydney, Australia. Patients with coronary artery grafts or stents, a history of asthma (due to contraindications of

nebivolol with asthma), or evidence of significant coronary artery disease were excluded from the study. A total of 26 subjects were recruited, with 20 excluded on angiographic analysis due to significant coronary artery disease. Demography, cardiovascular risk factors, and the medication profile of the remaining 6 subjects is summarised in Table 9.1. Subjects were studied in the supine position following diagnostic angiography, in a temperature controlled environment. All work was approved by the South East Health Human Research Ethics Committee, Eastern Section.

9.1.2 Haemodynamic measurements

Measurements were taken as previously described by Schmitt et al. (2005). Arterial pressure was measured with a 6F, high fidelity, dual pressure sensing catheter with 0.46 mm lumen (Millar). The two pressure sensors, 10 and 60 mm from the distal tip, were calibrated before the experiment using a mercury sphygmomanometer. The catheter was introduced via a sheath inserted in the femoral artery (Figure 8.1), a method previously used in the ovine model and described in Chapter 8. The two pressure sensors were positioned in a straight segment of the common iliac artery, slightly distal of the iliac bifurcation. Positioning in the iliac artery was confirmed by angiography (Figure 9.2). Heart Rate (HR) was calculated from a three lead, type II electrocardiogram (ECG) signal. Recordings were made at a sampling rate of 2kHz with a Biopac MP100 data acquisition unit with associated Acquire Knowledge software. Haemodynamic parameters were calculated from this data using custom designed software (Chapter 3). Segments of data 20 seconds in length were analysed at each dose level of drug.

Table 9.1: Summary of demographic data, cardiovascular risk factors, and medication profile of subjects in the study of nebivolol. Continuous demographic data expressed as mean±standard error of mean, unless otherwise specified.

Demography	
Age (years)	65±3
Sex (male/female, no.)	(2/4)
Height (m)	1.62±0.03
Weight (kg)	80±2
Body mass index (kg/m^2)	30.7±1.0
Smoking history (no.)	
Non-smoker	4
Ex-smoker	1
Current smoker	1
Cardiovascular risk factors (no.)	
Hypertension	5
Hyperlipidaemia	2
Type II diabetes	2
Ischaemic heart disease	1
Medication (no.)	
ACE inhibitor	3
Aspirin	2
β-blocker	
Atenolol	2
Metoprolol	1
Sotalol	1
Calcium channel blocker	1
Diuretic	1
Nitrate	0
NSAID	1
Statin	4

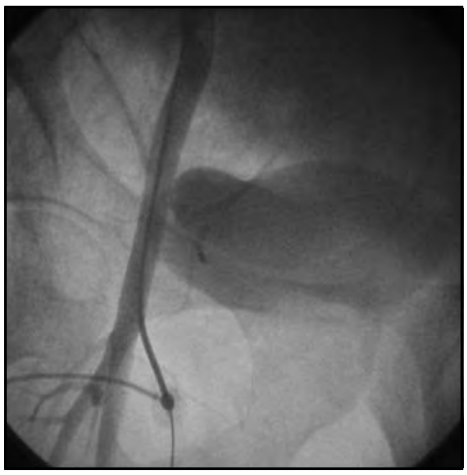

Figure 9.2: Angiography of the iliac artery showing, under fluoroscopy, the placement of the catheter in a straight segment of artery. (Reproduced from Schmitt et al., 2005)

Supine rest (>1hr)	Baseline (saline) (5 minutes)	200μg/min nebivolol (5 minutes)	400μg/min nebivolol (5 minutes)

Figure 9.3: Protocol for drug delivery in the study of the vasoactive effects of nebivolol. Recordings were taken during the last 20 seconds of each 5 minute infusion.

9.1.3 Drugs

Nebivolol (A.Menarini Pharmaceuticals, UK) was diluted with 0.9% saline to concentrations of 200 and 400 μg/ml. Both doses were infused through the catheter lumen at 1 ml/min for 5 minutes, with data being recorded during the final 20 seconds of infusion. Baseline data was collected during the final 20 seconds of a 5 minute infusion of saline at 1ml/min. Figure 9.3 displays a diagrammatic representation of the protocol of drug delivery.

9.1.4 Data analysis

Results were compared by one way Analysis of Variance (ANOVA) with post-hoc Bonferroni test. Results are expressed as means and standard error of mean.

9.2 Results

The results for the six individual subjects in the pilot study are presented in Table 9.2. Systemic haemodynamic variables were steady throughout all doses of nebivolol, with no change from baseline values (Figure 9.4). Mean Arterial Pressure (MAP) changed less than 1% from baseline values with infusion of nebivolol (-0.4±1.7% and 0.4±2.0% for 200 and 400 μg/min nebivolol infusion respectively). Subsequently, any change in PWV was due to local effects on the segment of artery and not correlated to systemic parameters. A non-significant trend towards decreased PWV with increasing dose of nebivolol was evident (Figure 9.4), with a shift from baseline values of -1.0±1.2 $m \cdot s^{-1}$ and -1.2±2.0 $m \cdot s^{-1}$ for 200 and 400 μg/min infusions of nebivolol respectively.

9.3 Discussion

A non-significant, dose dependent decrease in PWV was observed. The trend towards lower arterial stiffness with increasing dose of nebivolol was non-significant due to the limited sample size of the pilot study. The trend towards lower stiffness in human large arteries may be a contributory mechanism behind the improvement in haemodynamic parameters seen with the administration of nebivolol, but not other β-blockers such as atenolol (Nodari et al., 2003).

Four of the six subjects were on β-blockers other than nebivolol, however, this would not have confounded the results as the other β-blockers are not known to affect the endothelium dependent L-arginine and NO pathway that is of particular interest in the administration of nebivolol. If any vasoactive effect of medication were present, it was constant throughout the experiment

Table 9.2: Heart rate and iliac MAP and PWV for individual subjects (n=6) with infusion of nebivolol, expressed as mean ± standard deviation.

	Nebivolol dose (μg/min)		
Subject	0	200	400
Heart rate (bpm)			
A	53±0.5	52±0.9	52±0.3
B	58±1.6	61±2.0	61±1.9
C	63±0.4	63±0.5	63±0.4
D	70±0.4	68±0.4	68±0.4
E	55±0.9	57±2.1	54±1.6
F	59±1.0	59±0.8	58±0.6
MAP (mmHg)			
A	85±0.7	85±0.7	86±0.5
B	103±1.6	108±2.7	111±2.0
C	78±1.2	76±1.3	80±1.0
D	118±1.5	111±1.1	111±1.2
E	102±0.9	99±1.8	98±0.6
F	97±1.0	101±1.8	98±1.2
PWV ($m \cdot s^{-1}$)			
A	12.6±1.4	12.8±1.5	12.8±1.5
B	11.9±1.0	7.6±0.9	6.9±0.8
C	11.9±0.3	12.1±0.2	12.8±0.2
D	16.0±1.0	12.0±0.9	7.3±0.6
E	8.6±1.3	7.2±1.4	14.1±1.3
F	15.5±1.1	18.6±0.6	15.2±0.5

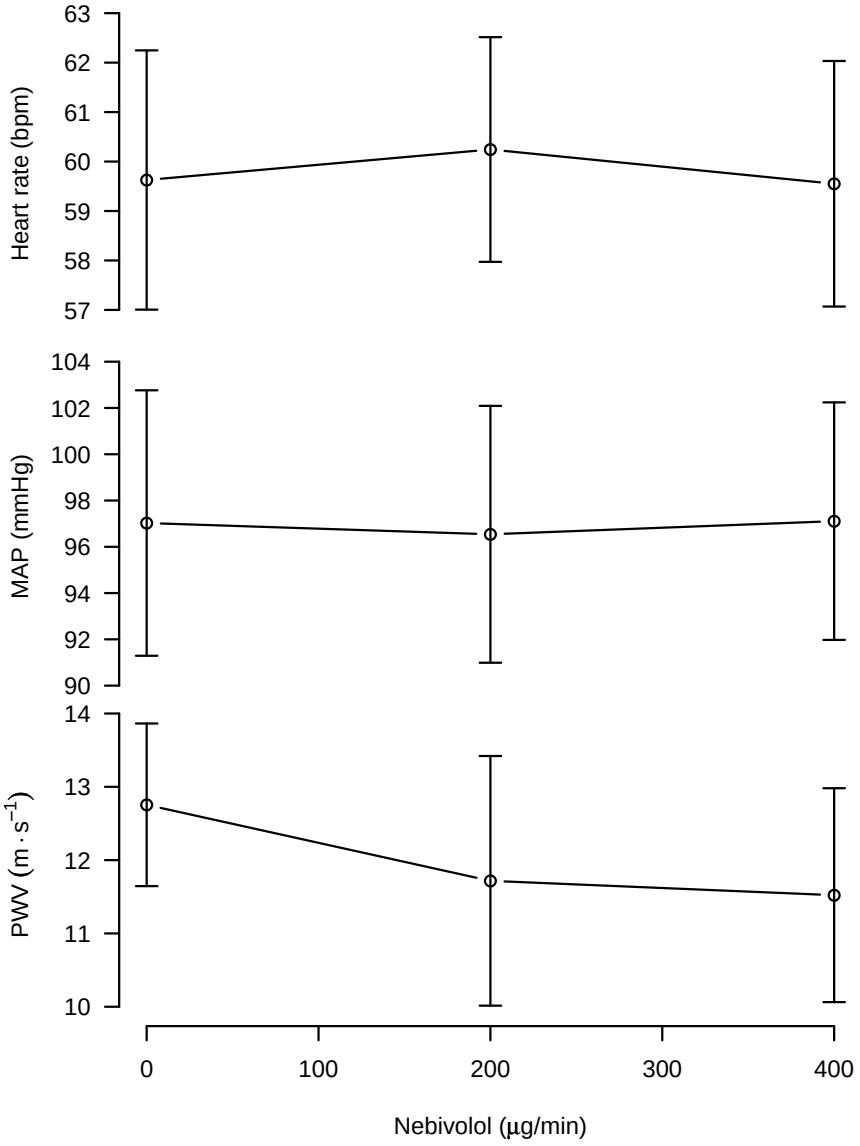

Figure 9.4: Mean heart rate, and iliac MAP, and PWV values for doses of 0, 200 and 400 μg/min of nebivolol. Heart rate and MAP values remained constant. There is a non-significant trend towards decreased PWV with increasing nebivolol dose.

as the study was based on an acute dose of nebivolol, with changes from baseline in the same subject the parameter of interest.

The response of local iliac PWV of individual patients varied with administration of nebivolol. Though there was no noticeable difference in the clinical presentation of any individual patient, the environment itself (recovery after angiographic examination) may be somewhat stressful to the patient and could present in haemodynamic effects. Systemic changes were not evident however, MAP and heart rate remaining relatively constant for all patients throughout the experimental protocol.

The vasoactive effect of nebivolol may well be attenuated due to the condition of the large arteries of the patient group being studied. Previous regional measurements of arterial stiffness recorded iliac artery PWV values of 5.7 $m{\cdot}s^{-1}$ in normotensive, and 7.8 $m{\cdot}s^{-1}$ in hypertensive subjects (Ting et al., 1990). The subjects in the present study of local administration of nebivolol had a mean baseline iliac artery PWV of $12.8{\pm}1.1$ $m{\cdot}s^{-1}$. The higher iliac artery stiffness than that reported in both normotensive and hypertensive subjects by Ting et al. indicates the presence of arterial degenerative conditions, potential calcification, poor endothelial function, or vascular remodelling. Such disease conditions in the arterial segment where nebivolol was locally infused may attenuate the vasodilatory potential of nebivolol in that arterial segment.

To ascertain whether the PWV lowering effect of nebivolol is due to the local effect on the arterial wall of the segment being studied, or due to blood flow related changes induced by an an action of nebivolol on the peripheral vasculature, the effect of nebivolol infusion through the sheath should be studied. An absence of change in measured PWV with sheath infusion of nebivolol would indicate that reduced arterial stiffness is a direct local ef-

fect of nebivolol, and not an effect derived from increased blood flow to the peripheral arterial bed induced by nebivolol. For completeness, L-NMMA should be co-infused with nebivolol to confirm that PWV reduction is due to the L-arginine/NO pathway, as shown in the forearm vasculature (Cockcroft et al., 1995; Dawes et al., 1999), and in animal models (McEniery et al., 2004). These experiments are part of ongoing work following the results of this pilot study.

This pilot study has produced novel findings that indicate for the first time that the conclusions drawn by McEniery et al. (2004) in the ovine model, that nebivolol decreases large artery stiffness by a NO dependent mechanism, have the potential to be translated to the large arteries of humans. Further work is required to increase the sample size of the study in humans to statistically confirm these pilot results.

CHAPTER 10

Assessment of arterial structural stiffness through ischaemia-induced reactive hyperaemia in the human brachial artery

Arterial stiffness, an independent predictor of cardiovascular risk, is regulated by a structural component, associated with mechanical properties of wall elastin and collagen, and an active component, associated with smooth muscle tension. Wall stiffness measured during maximal smooth muscle relaxation is equivalent to a measure predominantly of the structural stiffness. The aim of this study was to investigate whether a maximal decrease in stiffness of the brachial artery during reactive hyperaemia could be observed by non-invasive measurement of Pulse Wave Velocity (PWV) following forearm ischaemia. PWV measured at such a point would be indicative of the structural stiffness.

Giannattasio et al. (2001), in the study of the effects of exercise training on large arteries, specifically the radial artery, assumed that a 12 minute period of ischaemia in the brachial artery elucidated a "maximal or near maximal vessel distension", a stiffness measurement at this point being solely

attributed to that of the structural components of the vessel. That is, following 12 minutes ischaemia, functional components are in a fully relaxed state. The evidence cited for the methodology was a measure of compliance following 13 minutes of forearm ischaemia resulting in a non-significant, non-maximal decrease in arterial compliance (Trazzi et al., 1992). The experiment did not conclusively show a maximal vessel distension. Consequently, on current evidence, a measure of vessel stiffness following a period of 13 minutes ischaemia cannot be attributed to arterial structural stiffness alone.

An experiment was designed to confirm whether a 13 minute period of ischaemia elucidated a maximal decrease in radial artery stiffness. Post-ischaemic values of PWV in the forearm were compared following periods of 2, 5, 13, 20 and 30 minutes ischaemia. A maximum decrease in PWV would indicate that a measure of stiffness at this point would be equivalent to a measure of vessel structural stiffness.

10.1 Methods

10.1.1 Subjects

Thirteen healthy, non-smoking subjects (5 female) with no history of heart disease or stroke, were recruited for the study under the guidelines of the University of New South Wales Human Research Ethics Committee and the Cambridge Research Ethics Committee. The mean age of subjects was 34±11 years (range of 22 to 57 years), with a Body Mass Index (BMI) of 22.4±0.94 kg/m^2.

10.1.2 Haemodynamic measurements

Subjects were rested in the supine position and fitted with a continuous blood pressure monitor (Colin CBM-7000) on the dominant arm. The sub-

jects were fitted with electrocardiogram (ECG) leads in the type II configuration. An adult brachial pressure cuff was placed on the non-dominant arm, positioned in the standard location used to measure brachial blood pressure, for imposition of ischaemia. Two hand-held tonometers (Millar SPT-301) were used to transduce the arterial pulse at the brachial and radial sites below the cuff on the non-dominant arm. Figure 10.1 and Figure 10.2 show the experimental setup in diagrammatic and photographic form respectively. Data was acquired at a sampling rate of 2kHz (Powerlab 8/30, Chart 5 software) and analysed offline with custom designed software (Chapter 3). Heart rate was calculated from the ECG recording. Mean Arterial Pressure (MAP) was monitored from the pulse waveform output of the continuous blood pressure monitor, calibrated to systolic and diastolic values measured with a brachial pressure cuff by the oscillometric method immediately preceding baseline and post-ischaemic measurement. PWV was calculated in the non-dominant arm from the signals acquired from the two hand-held tonometers. A pseudo-PWV was calculated in the dominant arm as an indicative measure of arterial stiffness in the contralateral, non-ischaemic arterial bed. Transit time for the estimate of PWV was measured from the ECG R-wave peak to the radial pressure waveform foot. Distance was measured superficially from the suprasternal notch to the site of the radial pulse following the path of the subclavian, brachial and radial arteries. Due to the time being measured from R-wave peak to pressure wave foot, and not between two pressure wave feet, the PWV estimate was higher than physiological values, but still indicative of changes in arterial stiffness. The estimated PWV measure has been denoted as $\text{PWV}^{\times}$.

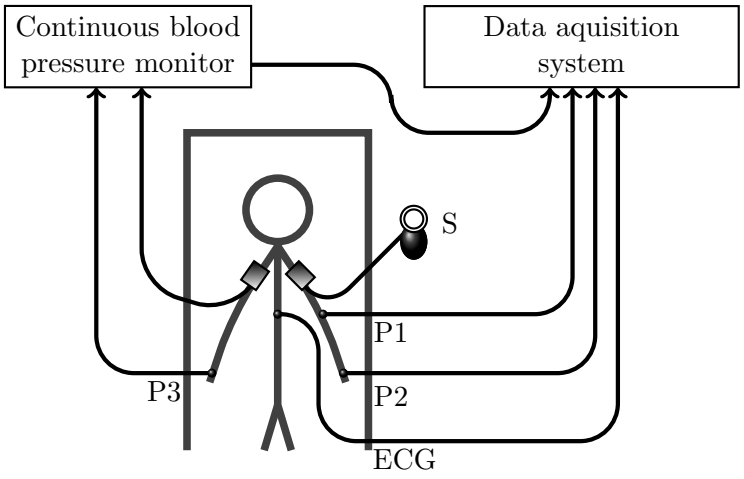

Figure 10.1: A schematic diagram of the experimental setup for the measurement of PWV before and following forearm ischaemia. P1 and P2 indicate the hand-held tonometers at the brachial and radial pulse respectively. P3 indicates the continuous blood pressure measurement derived from the radial pulse and standard brachial oscillometric cuff technique. The cuff on the left arm (S) was used to induce ischaemia.

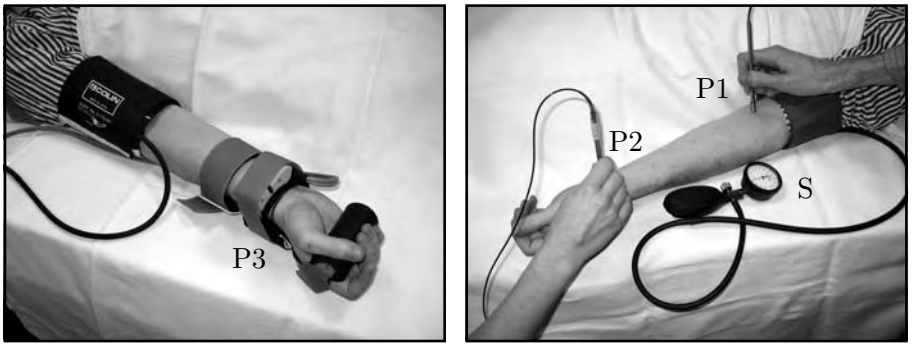

(a) **(b)**

Figure 10.2: Photographs of the (a) dominant, and (b) non-dominant arms with the various devices required for haemodynamic measurements. P1 and P2 label the hand-held tonometers, S the cuff used to induce ischaemia, and P3 the continuous blood pressure monitor.

Supine rest (5 minutes)	2 × baseline recording (5 minutes)	Ischaemia (x minutes)	Post-ischaemia recording (5 minutes)

Figure 10.3: Protocol for the study of the effect of reactive hyperaemia on PWV. x is the period of ischaemia-induced, either 2, 5, 13, or 20 minutes.

10.1.3 Induction of ischaemia

Subjects were rested for five minutes, and two baseline recordings taken over the subsequent five minutes. Hyperaemia was then induced for either 2, 5, 13, 20 or 30 minutes in the non-dominant arm with a brachial pressure cuff inflated to supra-systolic pressure (200 mmHg). A continuous recording of ECG and arterial pressure waveforms was made during the reactive hyperaemic response in the 5 minutes following ischaemia (Figure 10.3). Periods of 2, 5, 13 and 20 minutes of forearm ischaemia were induced in each subject, in randomised order, with only one period of ischaemia on each day of four separate visits. Separating periods of ischaemia by 24 hours avoided accumulative hypoxic effects of repeated ischaemic periods in the arterial bed. Four subjects consented to an additional visit where measurements were taken before, and following, a period of 30 minutes of forearm ischaemia.

10.1.4 Data analysis

Central mean pressures and central pulse pressures were calculated from the calibrated radial pulse in the dominant, non-ischaemic arm using a generalised peripheral to central transfer function (Karamanoglu et al., 1993) that has been validated at rest (Chen et al., 1997; Pauca et al., 2001) and during exercise (Sharman et al., 2006). Ten second samples were taken from the recorded signal during baseline, and in the period immediately following ischaemia, and resampled at 128Hz. These were then processed by the

SphygmoCor software (Atcor Medical, 2007) and the central parameters, as calculated by the transfer function, extracted.

Statistical analysis was conducted using the statistical package, R. Comparison between ischaemic periods was conducted by one way Analysis of Variance (ANOVA) with post-hoc Bonferroni correction. Significant change from baseline within each ischaemic period was analysed with Student's paired t-tests. Results are expressed as mean ± standard error of mean unless specified otherwise.

10.2 Results

10.2.1 Haemodynamic measurements

Haemodynamic parameters were measured and analysed continuously for a period before and following ischaemia. PWV changed maximally in the period immediately following the restoration of blood flow following ischaemia, with a trend back to baseline values within the following 5 minute recording time (Figure 10.4).

Baseline results before 2, 5, 13, 20 and 30 minutes ischaemia was induced did not differ for brachial to radial PWV, brachial MAP, brachial pulse pressure, heart rate, central MAP, nor central pulse pressure on the different days of study (Table 10.1).

Changes in systemic haemodynamic variables are displayed in Table 10.2. There was no significant change in brachial MAP following either 2, 5, 13, 20 or 30 minutes ischaemia. Central MAP showed a significant decrease following 13 minutes of ischaemia only (-5.5±4.1%, $p<0.1$). Brachial pulse pressure showed a significant drop of 9.1±1.1% ($p<0.1$) following 2 minutes of ischaemia only. Central pulse pressure changed significantly following

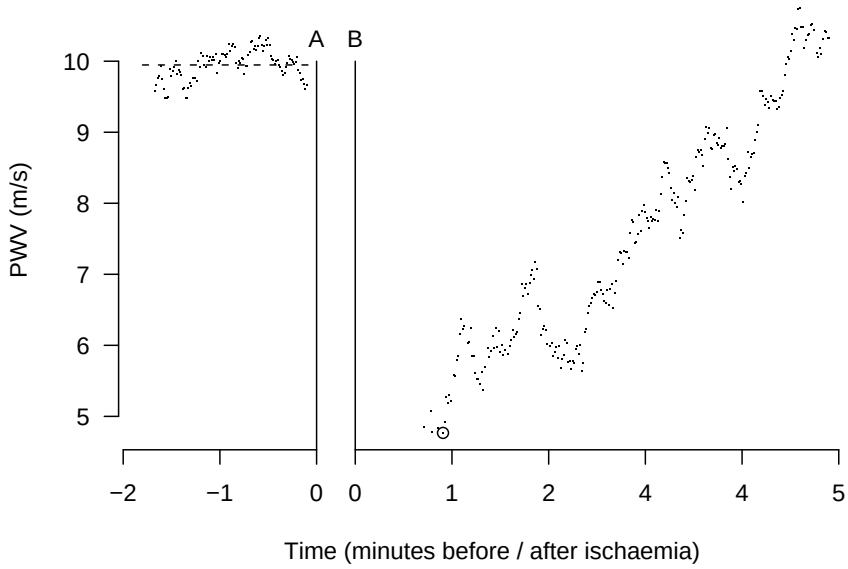

Figure 10.4: An example of the dynamic PWV response to ischaemia. The horizontal axis gives time before (negative) and after (positive) a period of 30 minutes of ischaemia (AB) for an individual subject. Mean baseline PWV is given by the dashed line. The maximum change in PWV (○) occurred in the first minute of reactive hyperaemia. In this subject, the maximum change in PWV from baseline following 30 minutes of ischaemia was -52%.

Table 10.1: Baseline means preceding ischaemia for non-dominant arm PWV, central and brachial MAP and PP, HR, and dominant arm pseudo-PWV ($PWV^{\times}$). Statistic p-value from one-way ANOVA between ischaemic periods. There were no statistical difference between baseline values.

	Baseline values for ischaemic period (minutes)					
Parameter	2	5	13	20	30	p-value
Non-dominant arm $PWV^{\times}$ ($m \cdot s^{-1}$)	11.8±0.1	11.2±0.2	11.9±0.2	12.4±0.1	12.3±0.3	0.77
Brachial MAP (mmHg)	85±1	76±2	83±1	81±2	87±1	0.72
Brachial PP (mmHg)	57±1	50±1	56±1	50±1	57±1	0.54
HR (bpm)	63±0.5	64±0.6	60±0.7	63±0.5	65±0.5	0.63
Dominant arm PWV ($m \cdot s^{-1}$)	4.7±0.08	5.0±0.07	4.7±0.09	5.0±0.07	5.1±0.04	0.84
Central MAP (mmHg)	83±3	82±4	88±2	85±3	82±4	0.62
Central PP (mmHg)	43±1	42±2	40±2	43±3	42±2	0.90

Table 10.2: Values for changes from baseline of systemic haemodynamic parameters MAP, PP, and HR, following graded periods of forearm ischaemia.

	Ischaemic period (minutes)				
	2	5	13	20	30
Brachial measurements					
ΔMAP (%)	-0.9±1.0	-1.6±0.9	0.6±0.8	-5.8±1.5	6.2±0.8
ΔPP (%)	-9.1±1.1*	0.0±0.7	-1.2±1.0	2.9±1.1	17.3±1.9
Central parameters					
ΔHR (%)	-0.9±0.4	-2.4±0.2†	0.8±0.7	1.8±0.7	3.4±1.1
ΔMAP (%)	-5.1±2.8	0.0±4.1	-5.5±4.1*	0.0±3.2	-1.1±4.3
ΔPP (%)	-6.9±3.6*	-9.1±3.0	-4.3±2.7*	11.9±8.7	-1.5±3.0

* $p<0.1$, † $p<0.01$, paired Student's t-test compared with baseline values.

periods of 2 and 13 minutes of ischaemia (-6.9±3.6% and -4.3±2.7% respectively, $p<0.1$). Heart rate showed a significant change following 5 minutes of ischaemia only (-2.4±0.2%, $p<0.01$). PWV$^{\times}$ in the non-ischaemic arterial bed consistently increased from baseline values, and changed significantly following 2 and 5 minutes ischaemia (-20.7±1.5%, $p<0.1$, and -25.4±1.3%, $p<0.01$, respectively), but did not show significant change for ischaemic periods greater than 5 minutes (Figure 10.5a). PWV in the arm subjected to ischaemia consistently decreased from baseline values following forearm ischaemia, changes following all periods of ischaemia being significant (Figure 10.5b).

Changes in systemic haemodynamic parameters did not significantly differ in response between different periods of ischaemia, with the exception of changes in pulse pressure following 2 and 30 minutes of ischaemia (-9.1±1.1% and 17.3±1.9% respectively, $p<0.01$). Change in PWV in the ischaemic arterial bed between graded periods of ischaemia significantly differed, namely between: 2 and 20; 2 and 30; 5 and 20; 5 and 30; and, 13 and 30 minutes of ischaemia (Figure 10.5b).

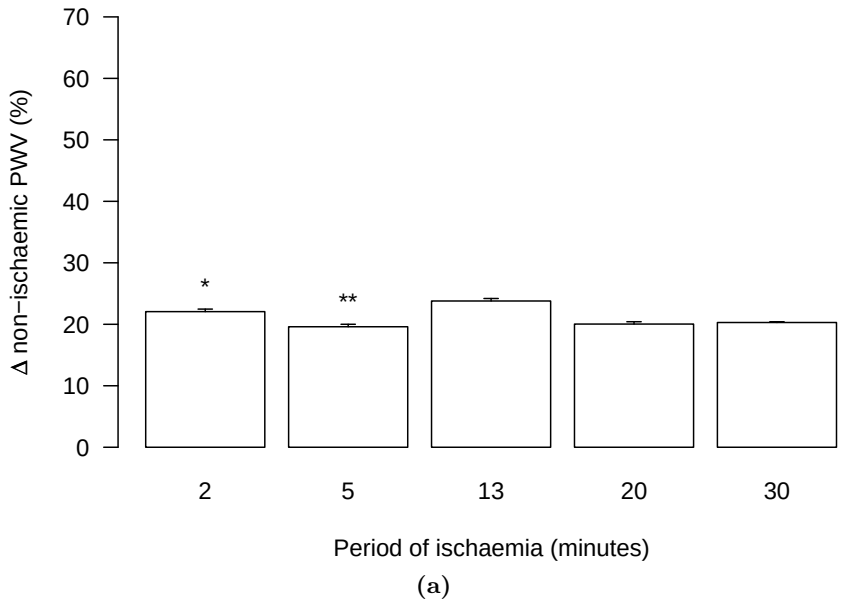

(a)

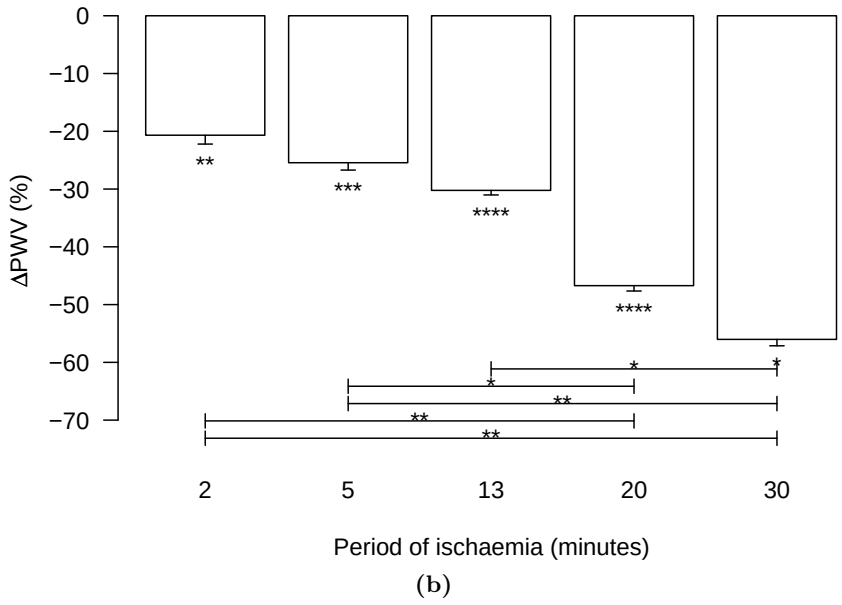

(b)

Figure 10.5: Maximal change in PWV measured (a) in the non-ischaemic arm ($PWV^{\times}$), and (b) in the ischaemic arterial bed, expressed as percentage of baseline values, during reactive hyperaemia. There was a consistent, significant decrease in arterial stiffness in the ischaemic bed in spite of a consistent trend toward an increase in arterial stiffness in the control, non-ischaemic arm. This increase was likely to be due to systemic reflex responses to sensations felt in the ischaemic arterial bed upon restoration of blood flow. (* $p<0.1$, ** $p<0.01$, *** $p<0.001$, **** $p<0.0001$)

10.2.2 Regression analysis

To ascertain what period of ischaemia would be required to invoke a hyperaemic response causing maximal change in arterial stiffness, various regression models were fitted to the data. Pure linear regression analysis provided poor fit and did not explain physiological expectations, including an ordinate intercept of 18% decrease in PWV from baseline values with a period of zero minutes ischaemia, and infinitely decreasing PWV with increasing period of ischaemia-induced (Figure 10.6). A logarithmic fit across the data provided a reasonable physiological explanation, approaching zero change in PWV with zero minutes of ischaemia, and with asymptote independent of ischaemia for long periods of ischaemia. However, the logarithmic fit poorly described the mean values observed in the current study, especially for values of 13 and 30 minutes of ischaemia.

An alternate model was developed by dividing the data set into two regions separated by, and sharing, the values for 13 minutes of forearm ischaemia. That is, a region of ischaemic periods less than, or equal to, 13 minutes of ischaemia, and a region of ischaemic periods greater than, or equal to, 13 minutes of ischaemia. A logarithmic curve was fitted to each of the two regions (Figure 10.7) and is described by Equation 10.1-10.2, where ip is the ischaemic period. The fit was found to accurately describe the data set, and correlated well with mean values across the range of ischaemic periods in the data. In terms of physiological expectations, the regression trended towards zero with decreasing ischaemic period, and the asymptote for extended periods of ischaemia was independent of ischaemic period.

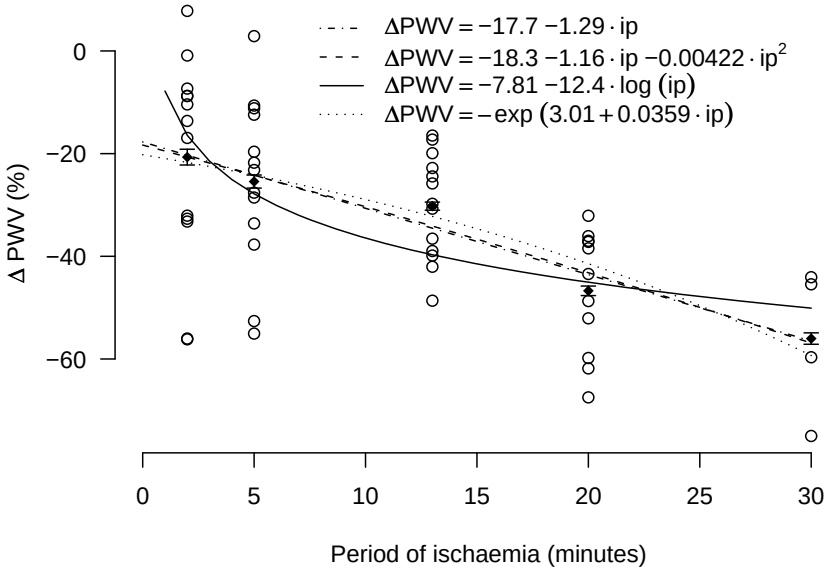

Figure 10.6: Rejected regression models of the change in arterial stiffness following varied periods of forearm ischaemia (*ip*). Individual results (○), mean values (◆), and standard errors are plotted. The physiological expectation of zero change in PWV with zero minutes of ischaemia is not explained by linear and exponential fits, nor do such regressions reach asymptotes independent of ischaemic period. However, a logarithmic fit across the data range does not predict the mean values, especially for 13 and 30 minutes of ischaemia.

$$\Delta PWV(\%) = -17.2 - 5.1 \cdot ln(ip) \qquad 0 < ip \leq 13\ minutes \quad (10.1)$$

$$\Delta PWV(\%) = 53.3 - 32.8 \cdot ln(ip) \qquad ip \geq 13\ minutes \quad (10.2)$$

10.3 Discussion

There was a consistent decrease in brachial artery PWV during the reactive hyperaemic response following all periods of ischaemia. This was independent of systemic MAP, as systemic MAP did not change significantly from baseline values. PWV as measured from ECG R-wave peak to radial pulse pressure foot in the non-ischaemic, dominant arm ($PWV^{\times}$) did significantly change across all graded periods of forearm ischaemia. However, the change was a consistent increase in $PWV^{\times}$, opposite to the vasorelaxation indicated by the decrease in PWV in the ischaemic bed. The increase in $PWV^{\times}$ in the non-ischaemic arterial bed was likely to be a systemic reflex response to sensations felt in the ischaemic arm upon restoration of blood flow. The fact that $PWV^{\times}$ increased in the non-ischaemic arm indicates that the reduction in PWV in the non-dominant arm following forearm ischaemia was not amplified by systemic changes in haemodynamic parameters.

A limitation of the method of measuring arterial stiffness following ischaemia was the inability to record the pressure pulse signal in the first 30 seconds immediately following restoration of blood flow, an example of which is shown in Figure 10.4. This is in part due to the absence of a strong pulse during this period, replaced by a less pulsatile flow in the initial stages. Once the pulse is present, operator variability effects the brevity at which the pulse is detected and recorded. The operators in this study

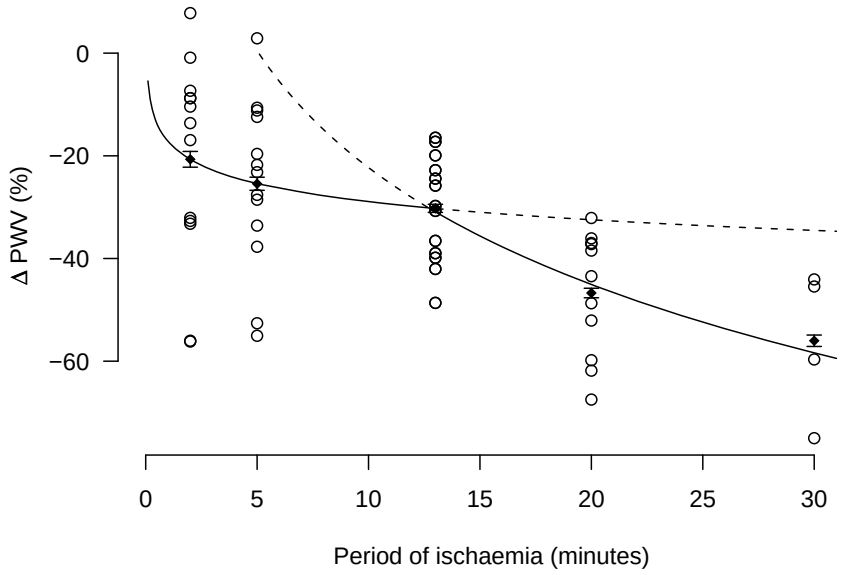

	Ischaemic period range	
	≤13 minutes	≥13 minutes
Fitted curve	$\Delta PWV = -17.2 - 5.1 \cdot ln(ip)$	$\Delta PWV = 53.3 - 32.8 \cdot ln(ip)$
Statistics on individual data		
R^2 value	0.06	0.44
RSE	15.88	11.44
Statistics on mean values		
R^2 value	0.99	0.98
RSE	0.02	1.16

Figure 10.7: Curve fit to change in PWV results as a function of ischaemic period (ip). All individual data (○), means (◆) and standard errors are plotted. Natural log curves were fitted to two regions of the individual data results, $0 < ip \leq 13$ minutes, and $ip \geq 13$ minutes of ischaemia. The resulting two curves are given in the included table, with the intercept of the two curves being an ischaemic period of 12 minutes and 40 seconds. Multiple R^2 and residual standard error (RSE) values are given for both the fit to data for all individuals, and to the overall mean values.

were highly skilled, and this delay was minimised. Trazzi et al. (1992) cited a delay in pulse detection following ischaemia, the delay in that particular study increased further by the automatic calibration of a finger pressure recording device (Finapres, Ohmeda Monitoring Systems) used to detect the pulse. Pressure pulse in the ischaemic arterial bed in the current study was recorded in a direct, uncalibrated form, and processing did not delay the detection of the pulse following restoration of blood flow.

There was a consistent trend of increased change in PWV in the ischaemic bed with increasing period of induced ischaemia across all ranges of ischaemia. The decrease in PWV following 20 minutes of forearm ischaemia was significantly greater than following 2 and 5 minutes of ischaemia. PWV following 30 minutes of ischaemia showed a significantly larger decrease than that following 2, 5 and 13 minutes of ischaemia. Arterial compliance following 13 minutes of forearm ischaemia is non-maximal and a measure of arterial stiffness during reactive hyperaemia following 13 minutes of forearm ischaemia does not represent solely the stiffness of the structural components of the vascular wall.

Anecdotal reports from subjects who participated in the study revealed experience of paraesthesia in the ischaemic arm following restoration of blood flow. The intensity of paraesthesia was minimal following 2 and 5 minutes ischaemia, but increased with increasing ischaemic period. Subjects reported symptoms of paraesthesia especially following periods of 20 and 30 minutes of ischaemia. The discomfort did not represent itself in the form of significant changes in systemic haemodynamic parameters such as heart rate and mean pressure. Paraesthesia generally lasted no longer than 5 minutes following cuff release, extending in isolated cases to no longer than 10 minutes following cuff release after 30 minutes of ischaemia. One

of 14 subjects recruited for the study did not complete the protocol citing discomfort as the reason for their withdrawal following the second visit. There were no reported complaints or complications in the days and months following the study. The level of discomfort due to paraesthesia precludes the use of such a test in routine measurement of structural stiffness, especially where maximal vessel relaxation occurs for some extended period of ischaemia greater than 13 minutes.

A characteristic of the two region regression fit requiring physiological explanation is the bi-phasic nature of the model. At the intercept of the two curves of 12 minutes and 40 seconds, or approximately 13 minutes, there is a rapid increase in the rate of change in the decrease of PWV following ischaemia (Figure 10.8). Decrease in PWV during reactive hyperaemia is driven by vessel smooth muscle relaxation initiated by a series of time dependent mechanisms (Figure 10.9). During the ischaemic period there is a build-up of vasodilatory metabolites in the hypoxic tissue. The metabolites include adenosine, lactic acid, and H^+ and are formed during hyperaemic periods longer than 45 seconds (Tóth et al., 2007). Doshi et al. (2001) proposed that these metabolites contribute to the vasodilatory response following as little as 5 minutes of forearm ischaemia. Adenosine stimulates production of the potent vasodilator, nitric oxide (NO), through the endothelial A_1 receptor, which in turn generates prostaglandin and cyclic adenosine monophosphate (cAMP) and subsequently NO (Ray et al., 2002). Lactic acid build up also acts upon guanylate cyclase directly to induce smooth muscle relaxation in the arterial wall (Chen et al., 1996; Frøbert et al., 2002). Increased H^+ and acidosis is associated with increased K^+ channel permeability (Siegel et al., 1992), and subsequent arterial dilation invoked through the potassium sensitive adenosine triphosphate (ATP) channels (Ishizaka et al.,

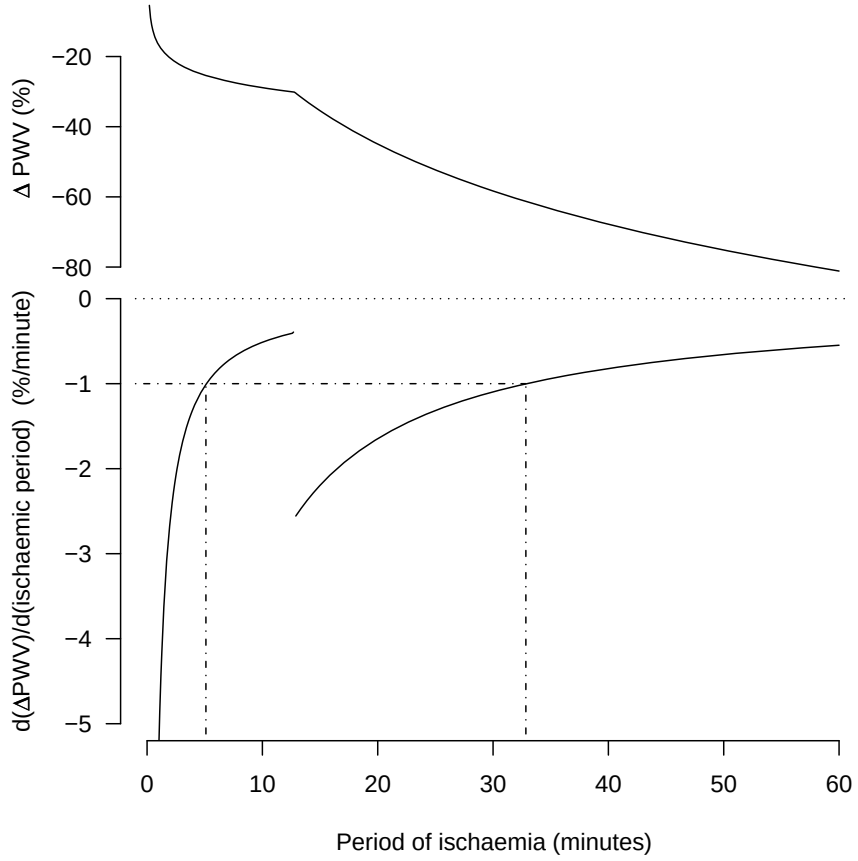

Figure 10.8: The fitted curve relating change in PWV to ischaemic period, extrapolated to a theoretical period of 60 minutes ischaemia with slope of the curve displayed on the same abscissa. The dashed line demonstrates that the same rate of change of ΔPWV is observed following two different periods of ischaemia, corresponding to the first and second region and logarithmic fit.

1999).

An additional vasodilatory phase is invoked upon restoration of blood flow. The inflated rate of blood flow increases endothelial shear stress and leads to smooth muscle relaxation induced by endogenous NO upregulation (Kaiser and Sparks Jr, 1986). This mechanism has been used to gauge endothelial dysfunction by measuring brachial artery Flow-Mediated Dilatation (FMD) following forearm ischaemic periods of between 3 and 5 minutes (Joannides et al., 1995; McEniery et al., 2006; Wallace et al., 2007).

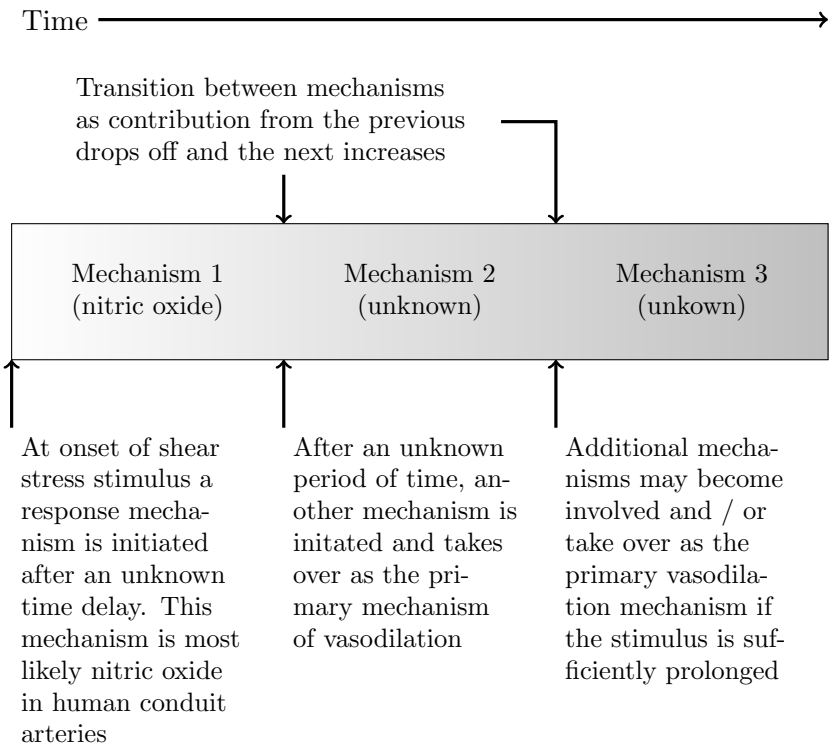

Figure 10.9: Vasodilatory mechanisms of ischaemia-induced reactive hyperaemia as theorised by Pyke and Tschakovsky (2005). Continuation of the reactive hyperaemia stimulus leads to a currently unknown number and type of mechanisms invoking decreased arterial stiffness and vasodilation. The first mechanism is a NO related mechanism stimulated by endothelial shear stress. Not included in the diagram is the vasodilatory effect of metabolites accumulated during the ischaemic period. The vasodilatory effect of metabolites occurs before restoration of blood flow to the ischaemic bed and flow mediated release of NO. The previously undefined period of time at which mechanism 2 is the primary vasodilatory mechanism, above the NO vasodilatory effect of mechanism 1, is approximately 13 minutes of ischaemia, as defined by the bi-phasic logarithmic regression developed in the current study. (Adapted from Pyke and Tschakovsky, 2005)

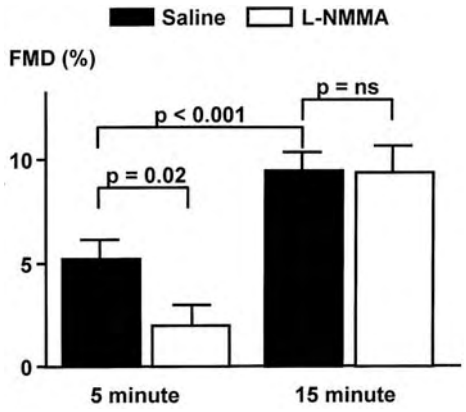

Figure 10.10: Two different vasodilatory mechanisms dependent on the length of the ischaemic period. Mullen et al. (2001) demonstrated that radial artery vasodilation following 5 minutes of hand ischaemia was attenuated by L-NMMA infusion, indicating endogenous NO dependence. L-NMMA infusion following 15 minutes of ischaemia did not attenuate the vasodilatory response, indicating the presence of a secondary vasodilatory mechanism independent of endothelial derived NO.

Pyke and Tschakovsky (2005) hypothesise that there may be additional vasodilatory mechanisms following prolonged periods of ischaemia causing arterial dilatation independent of endothelial derived NO (Figure 10.9). Mullen et al. (2001) provided evidence for two different time dependent vasodilatory mechanisms. In a study measuring radial artery diameter following ischaemia-induced by a wrist cuff occlusion, a period of 5 minutes of ischaemia induced NO dependent vasodilation, but a period of 15 minutes of ischaemia induced vasodilation that was not attenuated by N^G-monomethyl-L-arginine (L-NMMA) infusion (Figure 10.10). This indicates a secondary vasodilatory mechanism with prolonged periods of ischaemia that is independent of endothelial derived NO. The study of Mullen et al. suggests the secondary mechanism is effective following ischaemic periods of 15 minutes, but not following 5 minutes of ischaemia. This complies with the model devised in the current study, with a secondary phase taking effect for periods of ischaemia greater than 13 minutes.

Utilising the fitted model of bi-phasic response of change in PWV follow-

ing forearm ischaemia and extrapolating beyond ischaemic periods greater than 30 minutes, a 1% change in PWV per additional minute of ischaemia is observed for values following both 5 and 33 minutes of ischaemia (Figure 10.8). A less than 0.5% change in PWV per additional minute of ischaemia requires ischaemic periods greater than 10 and 66 minutes for the two phases. Such an observation is important in the consideration of the period of ischaemia used in FMD studies for the measurement of endothelial dysfunction. The parameter of interest in FMD quantification of endothelial dysfunction is the release of endothelial derived NO. Endothelial derived NO is the main mechanisms for vasodilation following 5, but not 15 minutes of ischaemia (Mullen et al., 2001), and is consistent with the logarithmic model for periods of ischaemia less than 13 minutes. Therefore, a near maximal response to endothelial derived NO during the reactive hyperaemic response occurs for periods of ischamia greater than 5 minutes. However, for periods of ischaemia greater than, or equal to, 13 minutes, endothelial dysfunction may be masked by vasodilation due to the secondary mechanism causing reduced arterial stiffness.

In the current study, PWV was measured as an indicator of arterial stiffness during the hyperaemic response in the brachial artery. The Moens-Korteweg equation states proportionality between the fundamental vessel wall stiffness, as denoted by the incremental modulus (E_{inc}), and PWV (Equation 2.35). This relationship holds true for small changes in wall thickness (h) and vessel radius (r), or where the ratio of wall thickness to vessel radius is constant (Chapter 2). During reactive hyperaemia, vessel radius changes significantly from baseline values, though the maximal magnitude of this change is of some dispute (Pyke and Tschakovsky, 2005). Wall thickness is also subject to change with vasodilation, although previous

studies have assumed this change to be insignificant in terms of the Moens-Korteweg equation when compared to the observed change in radius (Safar et al., 1986). Taking into account changes in arterial wall dimensions and lumen diameter, the change in PWV following forearm ischaemia is a function of changes in vessel wall stiffness, vessel wall thickness, and arterial radius (Equation 10.3). Measurement of vessel diameter and wall thickness by B-mode ultrasound throughout the cardiac cycle (Pearson et al., 1996; Selzer et al., 2001) following graded periods of ischaemia, combined with change in PWV measurements as taken in the current study, will enable calculation of the modulus of elasticity of the arterial wall material. Such a parameter may lend additional mechanistic information to the bi-phasic model of arterial stiffness following forearm ischaemia that has been developed in this thesis, and may be the subject of further work.

$$\Delta PWV = \sqrt{\frac{\Delta E_{inc} \cdot \Delta h}{2\rho \Delta r}} \tag{10.3}$$

Acute forearm ischaemia inducing reactive hyperaemia consistently elucidates a decrease in vessel stiffness in the ischaemic arterial bed. This decrease is not maximal following periods of ischaemia less than and up to 13 minutes. Subjects reported paraesthesia and discomfort in the ischaemic arm following restoration of blood flow. Whilst not causing systemic haemodynamic changes, the discomfort limits the use of longer periods of ischaemia to quantify large artery structural stiffness.

The current study is the first to show conclusively that arterial compliance following 13 minutes of ischaemia is non-maximal and does not represent the structural stiffness of the vessel, and that forearm ischaemia may not be a useful technique for quantification of structural stiffness of the

large arteries. A two phase regression model, as defined by Equation 10.1-10.2, describes the observed data. The model complies with the theory of vasodilatory mechanisms additional to, and independent of endothelial derived NO (Pyke and Tschakovsky, 2005) and is consistent with physiological observations that NO is not the main mechanism of vasodilation for a period of ischaemia of 15 minutes (Mullen et al., 2001). The exponential regression model may be useful in devising an effective and standardised method of FMD measurement for the quantification of endothelial dysfunction at maximal vasodilation caused by endothelial derived NO, independent of the secondary mechanism of vasodilation evident following extended periods of ischaemia.

CHAPTER 11

Conclusions

Cardiovascular disease is a wide-reaching and costly adverse health condition in both social and economic terms (Access Economics Pty Limited, 2005b; Mackay and Mensah, 2004; World Health Organisation, 2007). The stiffness of arteries is a strong predictor of cardiovascular events and all-cause mortality both in disease sub-populations (Blacher et al., 1999a,b; Cruickshank et al., 2002; Laurent et al., 2001a; London et al., 2001; Meaume et al., 2001) and in the general community (Avolio et al., 1985; Laurent and Boutouyrie, 2007; Mattace-Raso et al., 2006; Simon et al., 1985). Increased arterial stiffness causes amplification of pressure wave reflection and systolic pressures, which detrimentally impacts on left ventricular load, left ventricular mass, and cardiovascular events (Mitchell and Pfeffer, 1999). Evidence supports the use of arterial stiffness measurement in the clinical setting (Laurent et al., 2006; Nichols, 2005) and such a directive has been adopted by the European Society of Hypertension in the guidelines for the treatment of hypertension (Mancia et al., 2007). In light of this evidence, this thesis presents a series of novel experiments investigating the effect of structural

and functional changes in large arterial properties and the consequent effect upon stiffness in the *in-vivo* setting.

New methods were devised for the measurement of Pulse Wave Velocity (PWV) and for the assessment of wave reflection intensity (Chapter 3). A robust, operator independent, foot-to-foot method of calculating PWV was developed such that end diastolic variation did not alter the calculated pressure foot location. The novel method, utilising a linear regression fit during early systole, permitted PWV calculation in a variety of arterial sites across different animal species, including humans, and was robust in significant variation of the pressure waveform foot.

Two new indexes of wave reflection intensity were proposed, extending the work of Westerhof et al. (2006). The two parameters, reflection magnitude of the root mean square (RMS) values (RM_{rms}) and reflection index of the RMS values (RI_{rms}) are ratios of the RMS values of the incident and reflected waves (Equation 11.1–11.2). These parameters were used in two studies investigating the effect of aortic lesions, and the effect of calcification, on rat aortic stiffness.

$$RM_{rms} = \frac{(P_r)_{rms}}{(P_i)_{rms}} \tag{11.1}$$

$$RI_{rms} = \frac{(P_r)_{rms}}{(P_r)_{rms} + (P_i)_{rms}} \tag{11.2}$$

Three chapters of work (Chapter 4–7) explore results arrived at by a method of measuring rat aortic PWV unique to this thesis. The use of a 2.5F, dual pressure sensing catheter (Millar SPC-721) with two pressure sensors a fixed distance (50 mm) apart permitted high fidelity, highly accurate PWV measurement, eliminating any errors due to measurement of the

distance between pressure sensors. The concept was first applied in the study of experimental inflammation by Adjuvant-Induced Arthritis (AIA) in rats (Chapter 4). The study opens new avenues of research linking functional large artery stiffness with inflammatory phase and suggests the potential for the role of inducible nitric oxide synthase (iNOS) in inflammation and arterial stiffness to be an area of interest.

Changes in functional stiffness in large arteries was examined with respect to active and passive reduction in blood pressure (Chapter 5). Over a range of 110 to 60 mmHg, the blood pressure lowering effect of sodium nitroprusside (SNP) (active) and reduced venous return (passive) on rat aortic PWV was studied for the first time. The active hypotensive effect of SNP was indistinguishable from the passive reduction in blood pressure by reduced venous return in terms of aortic stiffness. In an extended protocol, the stiffness profile along the aortic length of the 14 week old Lewis rat was measured using the high fidelity, dual pressure sensing method outlined. The abdominal region was found to be significantly stiffer than the thoracic region, and PWV found to increase at a rate of 0.04 $m \cdot s^{-1}$ per 10 mm length of aorta, as defined by Equation 11.3, where PWV is in $m \cdot s^{-1}$ and the distance from the aortic arch (x) in millimetres.

$$PWV = 3.59 + 0.004 \cdot x \tag{11.3}$$

The effect of aortic elastic tissue lesion defects upon aortic stiffness in the rat were studied for the first time (Chapter 6). No correlation between the genetically associated lesions and PWV was found, indicating that either localised elastin fragmentation has little effect on the stiffness of the vessel as a whole, or that functional arterial stiffness mechanisms effectively compensate for localised structural damage.

The study of calcification in Lewis rats was the first to address time dependent effects of hypervitaminosis D_3 and nicotine (VDN) calcification on aortic stiffness (Chapter 7). *In-vivo* arterial stiffness did not increase with VDN treatment in spite of observed changes in structural stiffness, as indicated by *ex-vivo* testing. Abdominal aortic sections became stiffer (increased incremental modulus of elasticity) and weaker (decrease in breaking strain) whilst thoracic aortic sections became less stiff (decreased incremental modulus of elasticity) and stronger (increase in breaking strain).

The functional changes imposed by the selected vasoconstrictor agents angiotensin-II, noradrenaline, and Endothelin-1 (ET-1), with known different modes of action, on the ovine iliac artery were observed with blood flow and PWV measured simultaneously (Chapter 8). Whilst the results for noradrenaline infusion were highly variable, ET-1 infusion caused a non-significant trend toward increased blood flow and arterial PWV. The effect of ET-1 was reversed by infusion of the ET_A and ET_B receptor antagonist, BQ-788, confirming previous research associating endothelin with these receptors. The vasoconstrictor angiotensin-II did not effect blood flow in the same manner as ET-1, but did cause a dose dependent response in increased large artery stiffness. The study is the first to compare the effect of these selected vasoconstrictors with simultaneously measurement of blood flow and PWV.

The β-antagonist, nebivolol, was studied in the large arteries of humans with respect to the potential vasodilatory effect associated with stimulated endogenous nitric oxide (NO) release (Chapter 9). The pilot study showed a non-significant trend toward decreased arterial stiffness, independent of systemic changes in pressure, with infusion of nebivolol at rates of 200 and 400 μg/min in the human iliac artery. This novel work approves the expansion of this study in future research to confirm with statistical power

whether the findings of McEniery et al. (2004), that nebivolol releases NO by a β_2 adrenoreceptor-dependent mechanism causing vasorelaxation in the ovine iliac artery, are consistent with observations in the large arteries of humans.

The study of the effect of reactive hyperaemia in the forearm, induced by ischaemia, on vessel stiffness revealed that arterial stiffness following 13 minutes of ischaemia is non-maximal, rejecting previous theory (Giannattasio et al., 2001), and is not a measure of the structural stiffness of that vessel (Chapter 10). Exponential regression curve fitting explained this result in terms of a bi-phasic response to increasing periods of induced ischaemia. The two distinct curves, given by Equation 11.4 and Equation 11.5, suggest two different mechanisms causing vasodilation, the mechanism dependent on the period of ischaemia induced.

$$\Delta PWV(\%) = -17.2 - 5.1 \cdot ln(ip) \qquad 0 < ip \leq 13\ minutes \quad (11.4)$$

$$\Delta PWV(\%) = 53.3 - 32.8 \cdot ln(ip) \qquad ip \geq 13\ minutes \quad (11.5)$$

This finding supports the theory proposed by Pyke and Tschakovsky (2005) that multiple mechanisms are responsible for ischaemia induced vasodilation and decreased arterial stiffness. The model of two exponential regression curves with intersecting points at approximately 13 minutes of ischaemia is supported by finding of Mullen et al. (2001), that vasodilation following a 5 minute period of ischaemia is associated with endogenous NO release, and vasodilation following 15 minutes of ischaemia is not associated with endogenous NO release, but with some other, yet undiscovered mechanism. These new findings and exponential regression model may provide use-

ful information in the standardisation of Flow-Mediated Dilatation (FMD) measurement for the quantification of endothelial dysfunction associated with endothelial derived NO.

The work in this thesis presents a series of *in-vivo* experimental studies into the effects of changes in arterial structure and function upon large artery stiffness. The findings of this work are new quantitative and qualitative contributions to the understanding of the aetiology of large artery stiffness, a risk factor in cardiovascular disease.

The following lists the major findings and conclusions of this thesis.

(i) A more robust method of pressure foot location for PWV measurement was developed, using a fit of linear regression during early systole alone.

(ii) Two new parameters to measure wave reflection intensity were proposed, the reflection magnitude of the RMS values (RM_{rms}) and reflection index of the RMS values (RI_{rms}), accounting for mean wave amplitude in the form of an RMS ratio for quantification of functional correlates of arterial stiffness.

(iii) A novel method of PWV measurement in the rat aorta was used. A dual pressure sensing catheter eliminated error associated with distance measurement, an error of significance when measuring PWV over short distances, as in the rat aorta.

(iv) Acute, experimental inflammation in the form of Adjuvant-Induced Arthritis (AIA) in the rat was shown to have no effect on aortic stiffness, which raises the possibility of a role of iNOS regulation of functional stiffness in certain early phases of inflammation.

(v) Active (SNP infusion) and passive (reduced venous return) hypotensive effects were shown to be indistinguishable in terms of large artery stiffness in rats. This indicates for the first time that pharmacological

means of lowering blood pressure do not confound the possible pressure effects when performing functional measurements of PWV in the rat aorta.

(vi) The *in-vivo* stiffness profile of the aortic length of a 14 week old Lewis rat was characterised with the finding that each 10 mm distal shift along the aorta is associated with a 0.04 $m \cdot s^{-1}$ increase in PWV.

(vii) Lesions in the elastic laminae of the aorta in rats with a genetic predisposition to such were found to have no significant correlation with aortic stiffness, indicating that highly localised structural alterations in the vessel wall do not change the overall vessel stiffness of the aortic trunk.

(viii) Increased regional structural stiffness by *ex-vivo* testing, but not physiological stiffness as measured by PWV *in-vivo* in the whole aortic trunk, was shown to increase with age in rats with induced aortic calcification, suggesting that functional changes counteract structural changes in the aortic wall.

(ix) The comparison of three vasoconstrictors of differing modes of action showed that changes in functional vessel stiffness and blood flow differed between angiotensin-II, noradrenaline, and Endothelin-1.

(x) The β-antagonist, nebivolol, was shown in a pilot study to have potential vasodilatory effects in the human large artery, suggesting that findings in animal studies confirming nebivolol as inducing endogenous NO may be transferred to humans.

(xi) Ischaemia in the forearm was investigated as a possible method for measurement of brachial structural stiffness, with the conventionally accepted 13 minutes of ischaemia inducing a non-maximal decrease in arterial stiffness.

(xii) Increasing periods of ischaemia in the forearm were found to have a bi-phasic relationship with changes in functional stiffness, suggesting two different mechanisms of vasorelaxation, a finding of importance in the clinical investigation of endothelial dysfunction.

Collectively, the findings in basic research on arterial haemodynamics presented in this thesis lead to a greater understanding of the physiological significance of large artery stiffness and potential clinical applications in cardiovascular health.

CHAPTER 12

Future research

Sections of the research presented in this thesis are part of ongoing studies, whilst others present conclusive findings that pose questions of interest that may inspire future research. Ongoing research of note is the study of the effect of the β-antagonist and nitric oxide (NO) donor, nebivolol, on large artery stiffness in humans (Chapter 9). The pilot data gives an indication that the study of nebivolol by (McEniery et al., 2004) in the ovine hindlimb preparation may be translated to humans. That is, nebivolol releases nitric oxide (NO) in a β_2 adrenoreceptor-dependent mechanism that leads to decreased arterial stiffness. Ongoing research endeavours to increase the sample size of the study in humans to statistically confirm these pilot results.

The proof of concept study into acute experimental inflammation in the form of Adjuvant-Induced Arthritis (AIA) in rats (Chapter 4) raised questions of the role of different vasoactive substances associated with different phases of inflammation. In particular, the role of inducible nitric oxide synthase (iNOS) during acute inflammation may be of interest. Further studies may investigate the progression of AIA with time and monitor

changes in large artery stiffness. The progression of inflammation with time could be measured by assay detection of inflammatory markers such as c-reactive protein (CRP), and the role of iNOS investigated by infusion of an iNOS inhibitor such as aminoguanidine.

The study of hypervitaminosis D_3 and nicotine (VDN) calcification with age in the Lewis strain of rat uncovered an inverse relationship between changes in structural stiffness in the thoracic and abdominal aorta (Chapter 7). Whilst incremental elastic modulus increased in the abdominal sections, incremental elastic modulus decreased in thoracic sections with VDN treatment and age. Measurement of breaking strain indicated increased strength in thoracic sections and decreased strength in abdominal sections. Whilst the inverse relationships in structural stiffness parameters in thoracic and abdominal sections may account for the observation that *in-vivo* arterial stiffness did not change when averaged across the length of the aorta, the mechanisms behind the changes are not fully understood. Future research may involve the measurement of more localised *in-vivo* arterial stiffness to gauge thoracic and abdominal aortic stiffness independently. Such a study might take the experiment to longer time points, including the 2 month period used in studies by Gaillard et al. (2005); Niederhoffer et al. (1997b) and Jegger et al. (2006). Histological examination and calcium content quantification compared between thoracic and abdominal aortic sections would also expand the understanding of the mechanisms behind the arterial stiffness changes in the VDN model of calcification that the current study suggests are variable across the length of the aorta.

The study of changes in Pulse Wave Velocity (PWV) in the human forearm during a hyperaemic response induced by ischaemia showed a two phase response in arterial stiffness, as measured by PWV, to increasing time pe-

riods of ischaemia (Chapter 10). In this study, PWV was measured as an indicator of local arterial stiffness. The use of algorithms to calculate the Augmentation Index (AIx) from data collated during this study is possible as simultaneous, continuous pressure waveforms were recorded. Whilst the measurement of regional stiffness as indicated by AIx was not included in the scope of the thesis, such analysis may lead to new insights and could be the subject of future work. It is also important to note that whilst PWV is an accepted measure of arterial stiffness (Nichols, 2005; Wilkinson et al., 1998b), it is proportional to the vessel wall elastic modulus for insignificant changes in wall thickness and vessel radius (Chapter 2). A measure of wall thickness and vessel radius during reactive hyperaemia by B-mode ultrasound, combined with PWV measurements, would permit calculation of the incremental modulus itself, as defined by the Moens-Korteweg equation (Equation 2.35). Further research involving such measurements could lead to additional mechanistic information related to the bi-phasic model of the arterial stiffness response to forearm ischaemia developed in this thesis.

APPENDIX A

Indices of arterial stiffness

Table A.1: Various indexes used as markers of arterial stiffness (Gosling and Budge, 2003; Nichols and O'Rourke, 1998; O'Rourke and Mancia, 1999; O'Rourke et al., 2002).

Term	Definition	Equation
Augmentation Index (AIx)	the % increase in pressure after the peak of blood flow in the vessel. Units: % of pulse pressure	$\frac{P_s - P_i}{P_s - P_d}$
Capacitive compliance; large artery elasticity index	ratio of pressure and volume decrease in the arterial tree during diastolic pressure decay. Units: $m^3 \cdot mmHg^{-1}$	$\frac{\Delta V}{\Delta P}$
Characteristic impedance (Z_c)	ratio of pressure and flow velocity in the absence of wave reflections. Units: mmHg/m/s	$\frac{\Delta P}{\Delta V}$
Characteristic Pulse Wave Velocity (PWV_C)	velocity of the pressure pulse in an infinitely long, thin-walled, isotropic, elastic tube filled with an essentially incompressible fluid. Units: $m \cdot s^{-1}$	$\sqrt{\frac{B}{\rho}}$
Compliance (C)	diameter or area change for a change in pressure with fixed vessel length. Units: m/mmHg or m^2/mmHg	$\frac{\Delta D}{\Delta P}$
Distensibility or compressibility	diameter or area change for a small change in pressure; the inverse of Peterson's elastic modulus. Units: $mmHg^{-1}$	$\frac{\Delta D}{\Delta P.D}$

Table A.1: Various indexes used as markers of arterial stiffness (Continued)

Term	Definition	Equation
Input impedance (Z_{in})	ratio of measured pressure to measured flow	$\frac{P}{Q}$
Oscillatory compliance or small artery elasticity index	ratio of oscillating pressure change and oscillating volume change during the pressure decay of diastole. Units: m^3/mmHg	$\frac{\Delta V}{\Delta P}$
Peterson's modulus (E_p)	pressure step required for a theoretical 100% stretch from resting diameter at a fixed vessel length. Units: mmHg	$\frac{\Delta P \cdot D}{\Delta D}$
Pulse Wave Velocity (PWV)	velocity of the pressure pulse along an arterial segment. Units: $m \cdot s^{-1}$	$\frac{distance}{time}$
Stiffness index (β)	logarithm of the ratio of systolic and diastolic pressures, divided by the relative change in diameter. Units: non-dimensional	$\frac{ln\left(P_s/P_d\right)}{\left(D_s - D_d\right)/D_d}$
Volume elastic modulus or bulk modulus (B)	pressure change required for a theoretical 100% increase in volume at constant arterial length. Units: mmHg	$\frac{\Delta P \cdot V}{\Delta V} = \frac{\Delta P \cdot D}{2\Delta D}$
Young's modulus (E)	pressure change per unit area required for a theoretical 100% stretch from the original length. Units: mmHg/m	$\frac{\Delta P \cdot D}{\Delta D \cdot h}$
Young's modulus, static incremental (E_{inc})	the ratio of a small pressure change over the resulting small change in dimension. Units: mmHg/m	$\frac{\Delta P \cdot D^2}{2h \cdot \Delta D}$

APPENDIX B

Adjusting pulse wave velocity for changes in pressure

As Pulse Wave Velocity (PWV) is dependent on blood pressure (Nichols and O'Rourke, 1998), a statistical comparison of PWV between two samples or populations must be made at the same Mean Arterial Pressure (MAP). Where statistically significant changes in MAP are present, PWV can be corrected for pressure, and a subsequent statistical comparison conducted on the values of pressure corrected PWV.

A scatter plot of PWV and MAP may be fitted with a linear relationship (Equation B.1). The desired linear fit of pressure corrected PWV defines PWV independent of MAP. The linear fit (Equation B.2) has a slope (m) of zero and is thus independent of MAP.

$$PWV = m_1 MAP + b_1 \tag{B.1}$$

$$PWV = b_2 \tag{B.2}$$

Substitution of the desired linear fit (Equation B.2) into the actual linear fit (Equation B.1) results in Equation B.3. This can then be solved for

a chosen value of MAP (MAP_O), for example, the known operating MAP. The pressure corrected value of PWV ($PWV_{corrected}$) can be calculated by substitution of the value of b_2 into Equation B.4.

$$b_2 = m_1 MAP_O + b_1 \tag{B.3}$$

$$PWV_{corrected} = PWV + b_2 - (m_1 MAP + b_1) \tag{B.4}$$

Figure B.1 provides an example application of the method of correcting PWV for changes in MAP in a data set collected in the study of the effect of experimental inflammation on rat aortic PWV (Chapter 4). Using a PWV intercept of 3.44m·s^{-1} that correlates to the mean pressure, 83.8mmHg, of all the results, Equation B.3 and Equation B.4 were solved. $PWV_{corrected}$ is independent of MAP, evident in the very small value of the multiplier of MAP in Figure B.1 ($\varepsilon_1 = -5 \times 10^{-18}$). Statistical comparisons can subsequently be made across pressure ranges for $PWV_{corrected}$.

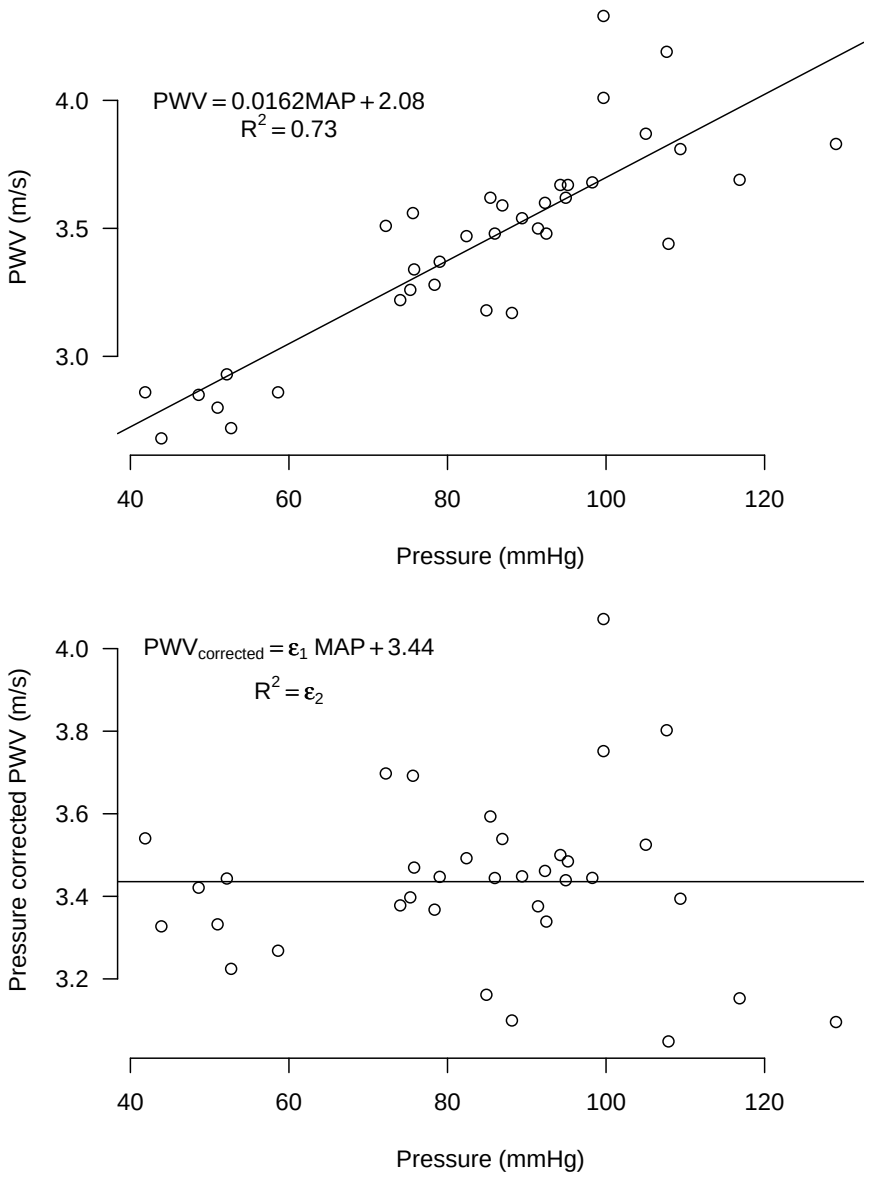

Figure B.1: Correcting PWV for changes in MAP. Raw data of measured PWV and MAP with linear regression fit, and PWV corrected for changes in MAP, where $\varepsilon_1 \approx \varepsilon_2 \approx 0$. The horizontal linear regression fit for PWV corrected for changes in MAP indicates that corrected PWV is independent of MAP.

APPENDIX C

Post-hoc Tukey Honest Significant Difference (HSD) statistical tests across arterial pressure ranges

Statistical comparisons across pressure range changes for variables where a significant difference was suggested by one-way Analysis of Variance (ANOVA) were made by Tukey's HSD with a family-wise confidence interval of 95%. Tukey's HSD method was used due to the large size of the independent variable (pressure range) as Bonferroni correction for comparison across independent variables of large size inflates the probability of a significant difference being found. Differences by Tukey's HSD are significant when the error bars of the plots do not cross the zero difference line.

Ordinate values in all the presented plots are values of Mean Arterial Pressure (MAP) range in mmHg. The statistical plots are of the following:

Figure C.1–C.4 Pressure ranges comparison for the reduction in pressure following a reduction in venous return, or sodium nitroprusside (SNP) venous infusion (Chapter 5).

Figure C.5–C.8 The pressure range comparisons for the Brown Norway (BN) strain of rat, susceptible to aortic elastic lesions, and the control (Lewis strain) rat (Chapter 6).

Figure C.9-C.16 Statistical comparison of variables across pressure ranges in the study of the effect of calcification on rat aortic Pulse Wave Velocity (PWV) (Chapter 7).

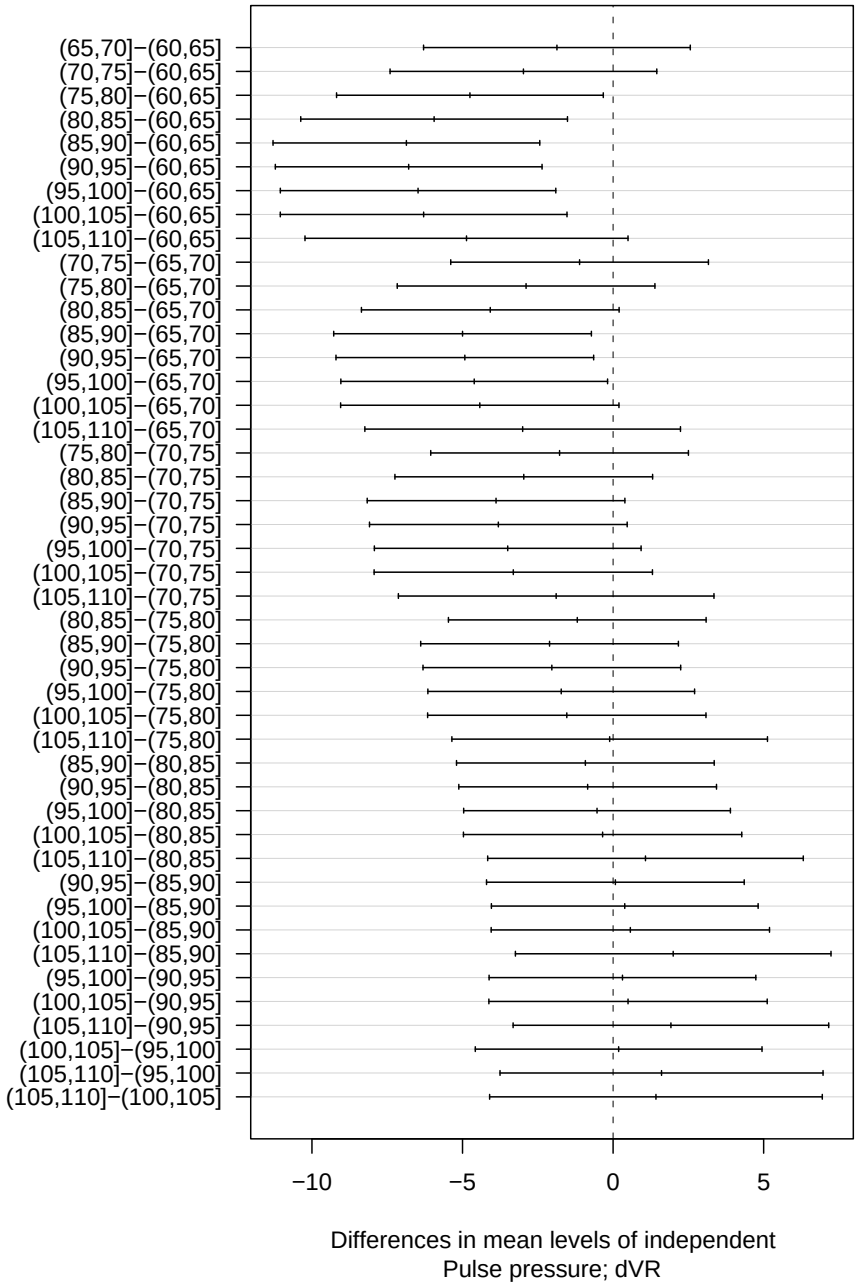

Figure C.1: Differences across pressure ranges in pulse pressure following a reduction in venous return assessed by Tukey's HSD. Relating to results from Chapter 5.

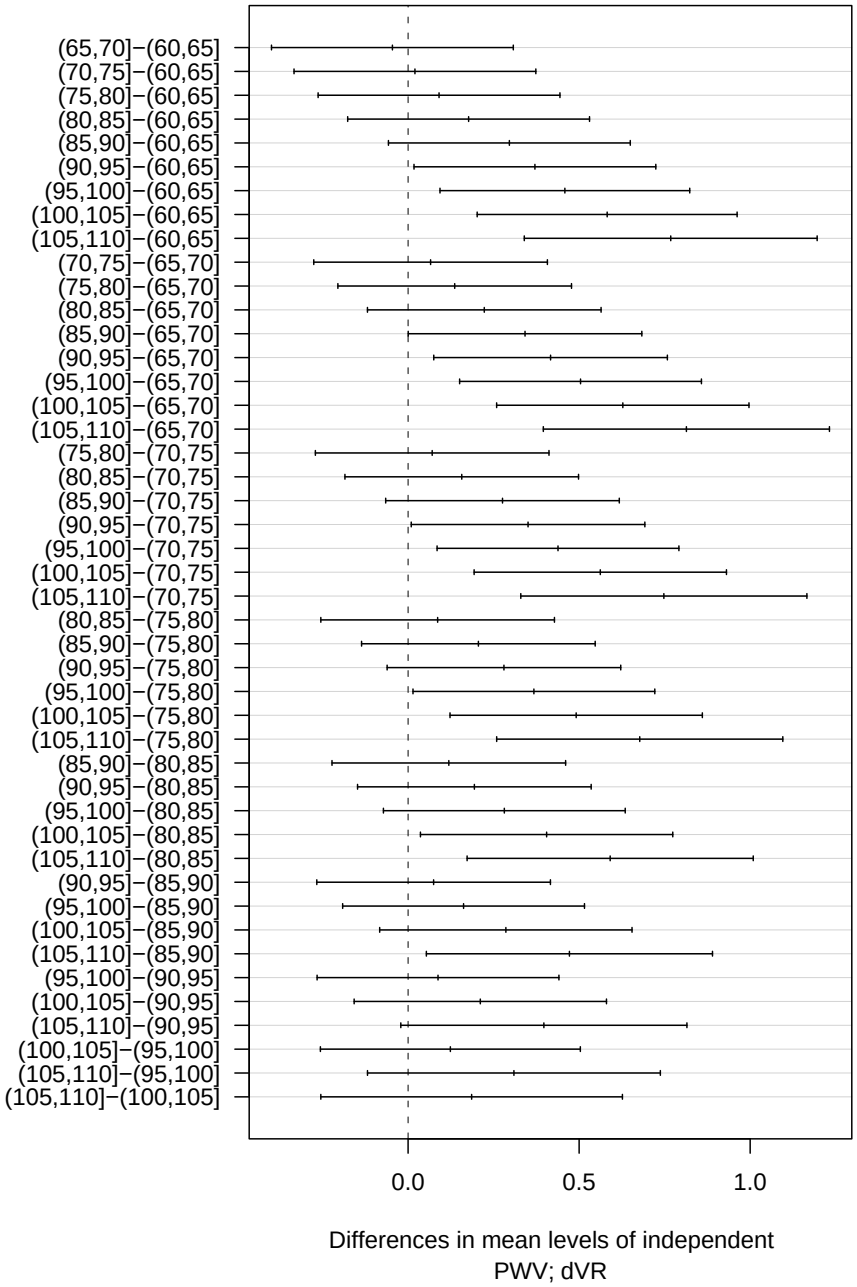

Figure C.2: Differences across pressure ranges in PWV following a reduction in venous return assessed by Tukey's HSD. Relating to results from Chapter 5.

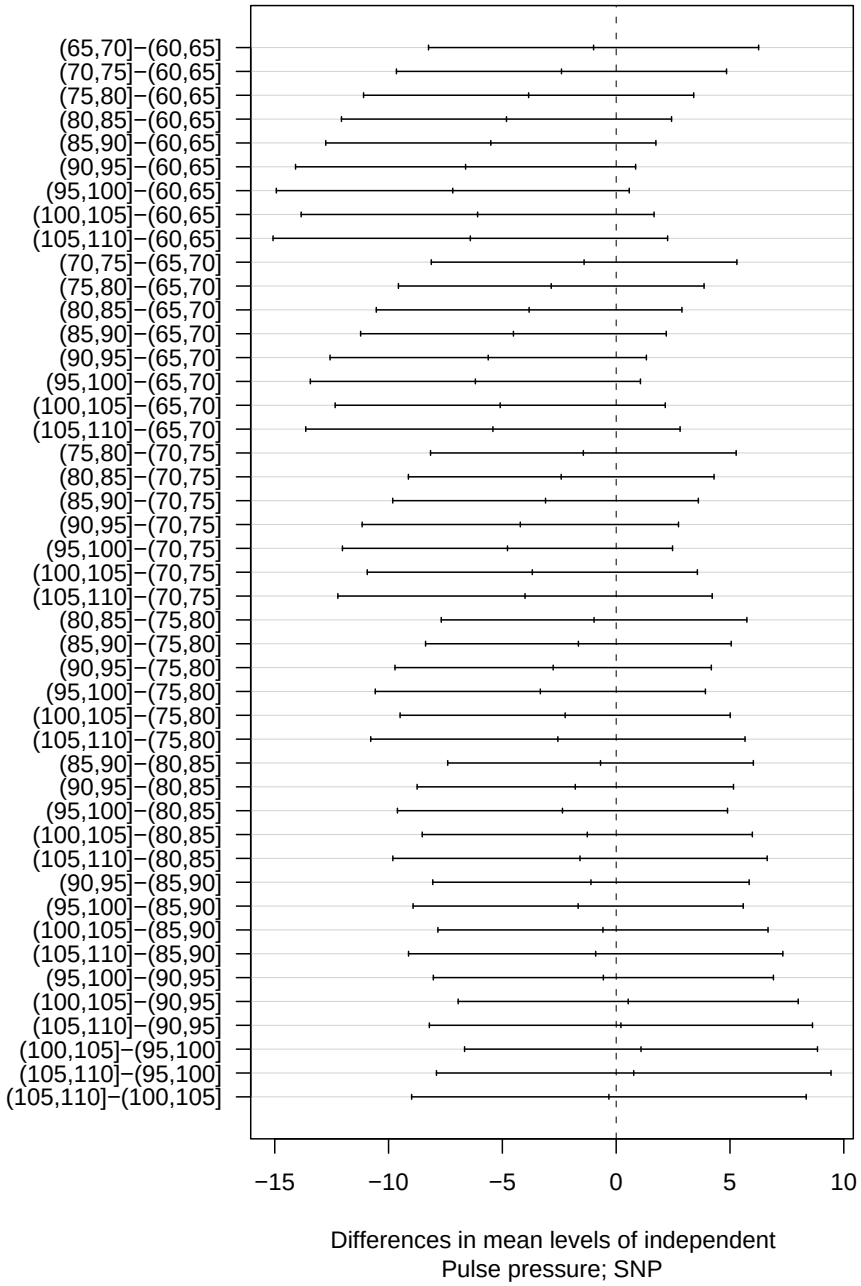

Figure C.3: Differences across pressure ranges in pulse pressure following venous infusion of SNP assessed by Tukey's HSD. Relating to results from Chapter 5.

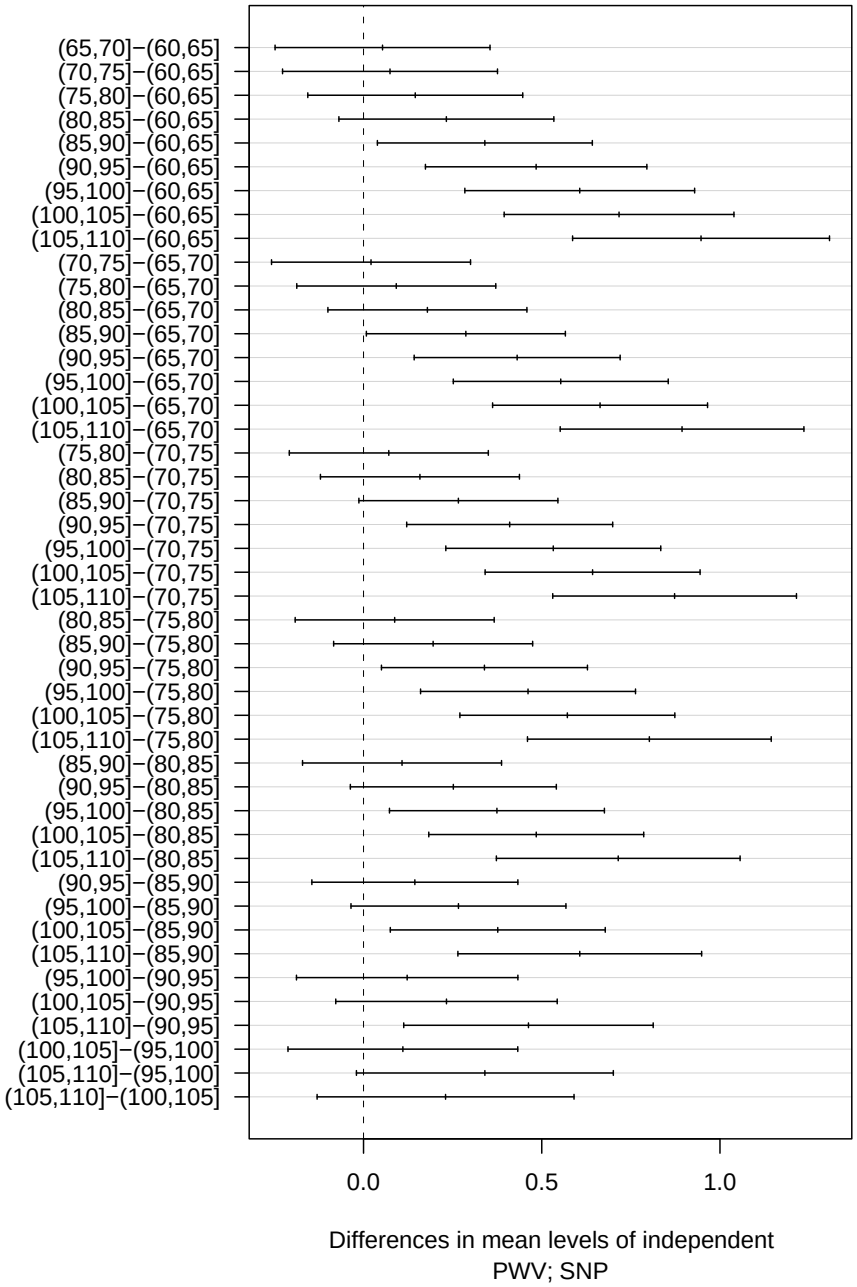

Figure C.4: Differences across pressure ranges in PWV following venous infusion of SNP assessed by Tukey's HSD. Relating to results from Chapter 5.

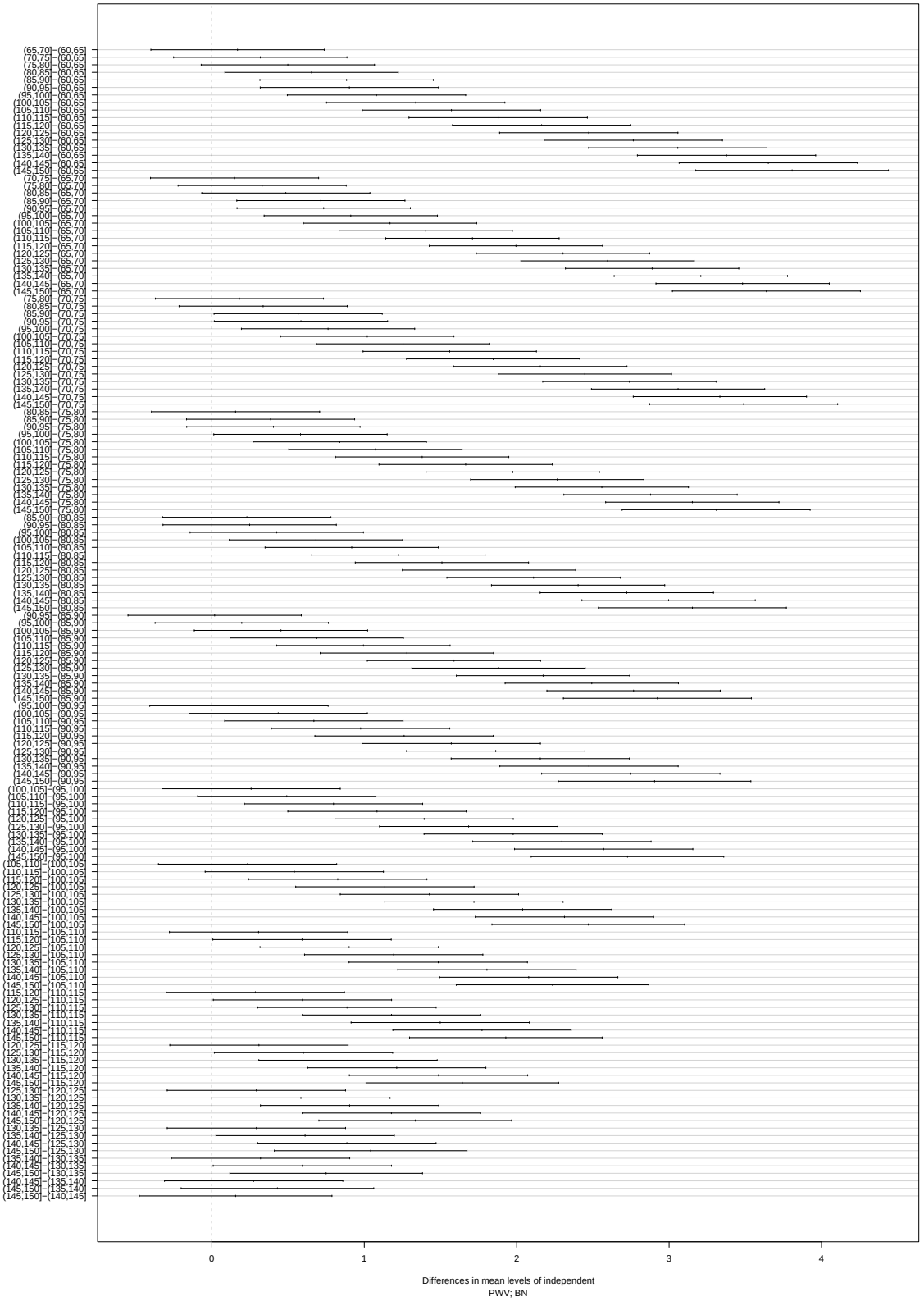

Figure C.5: Differences across pressure ranges in PWV in the BN rat as assessed by Tukey's HSD. Relating to results from Chapter 6.

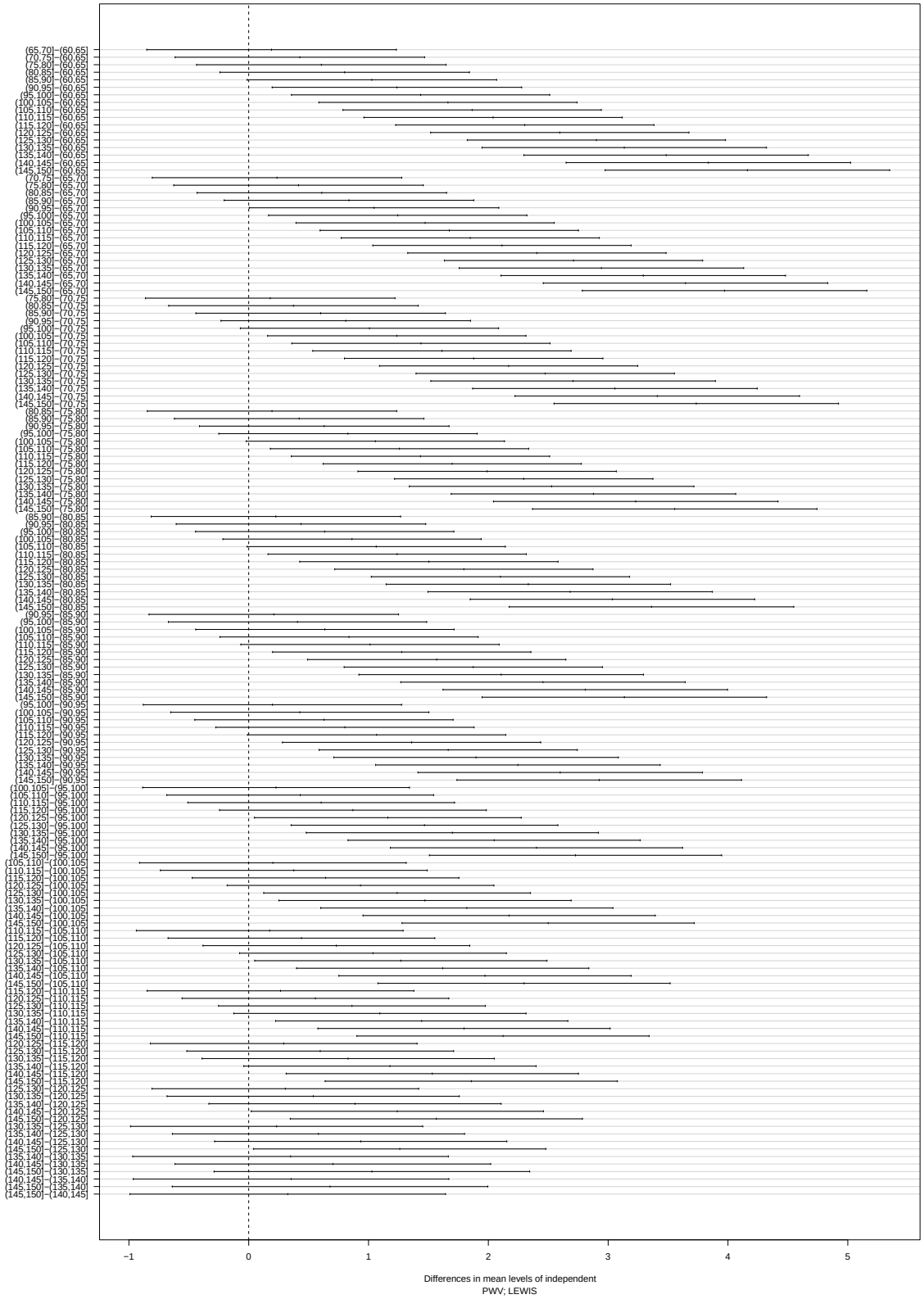

Figure C.6: Differences across pressure ranges in PWV in the Lewis rat as assessed by Tukey's HSD. Relating to results from Chapter 6.

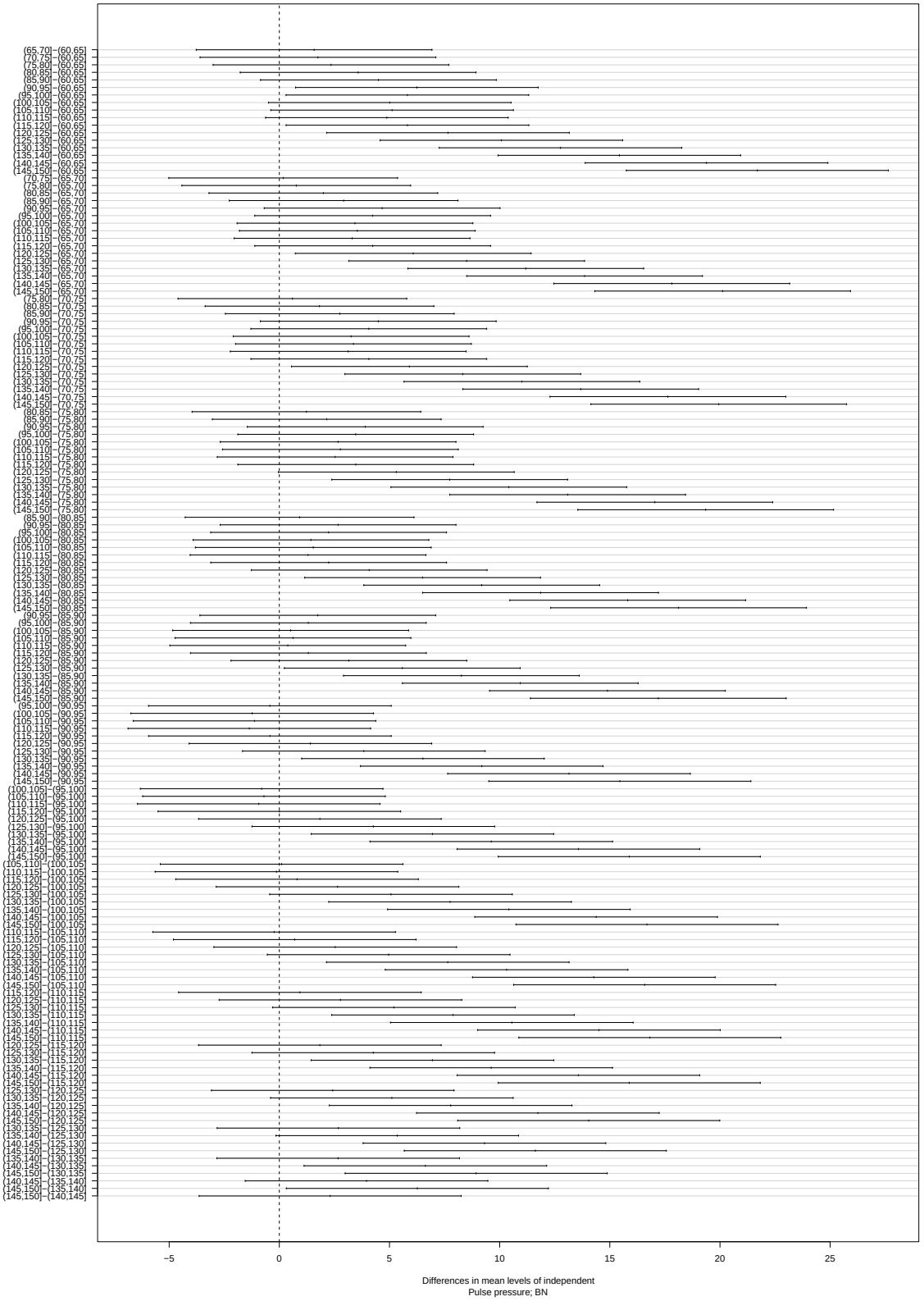

Figure C.7: Differences across pressure ranges in pulse pressure in the BN rat as assessed by Tukey's HSD. Relating to results from Chapter 6.

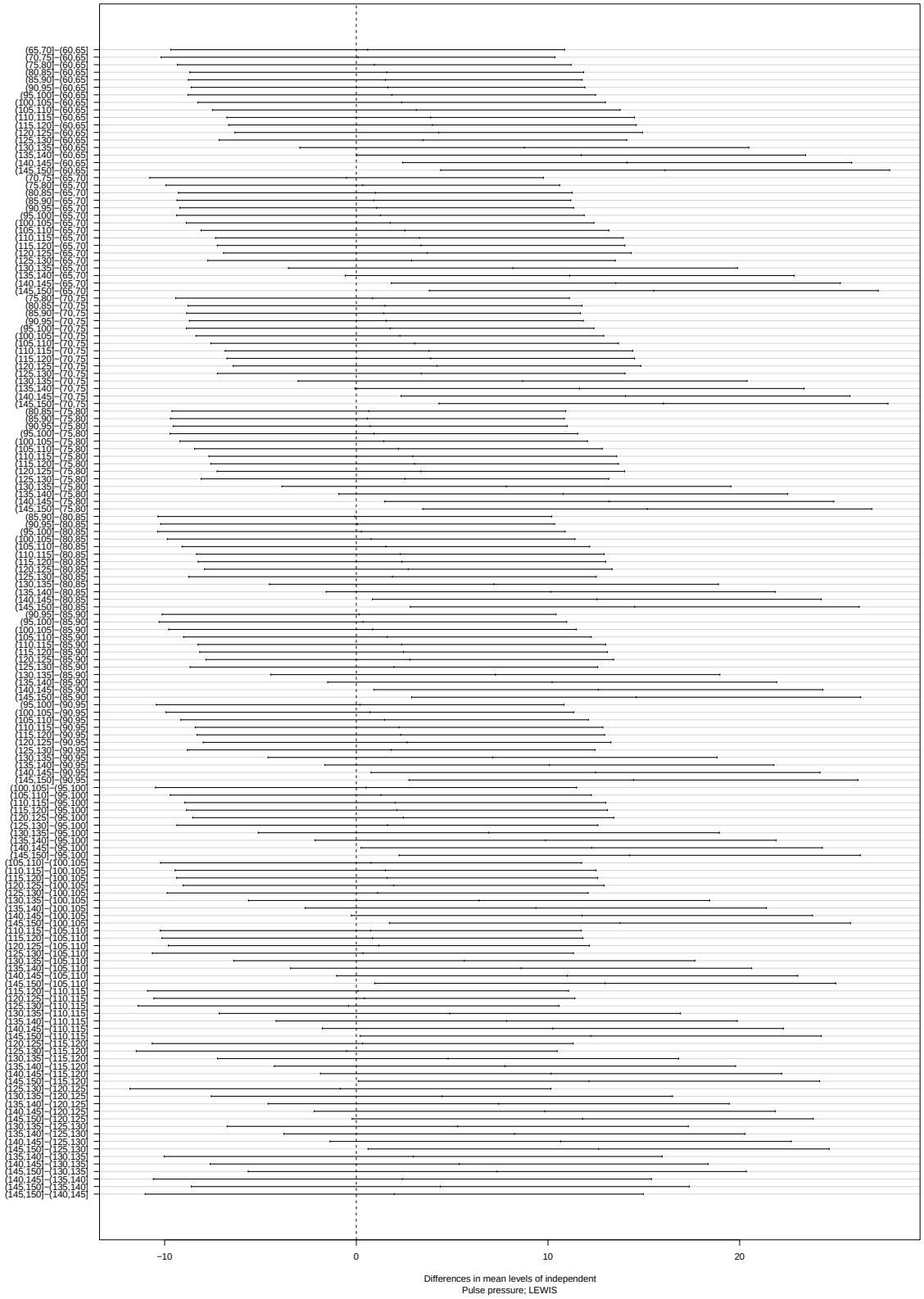

Figure C.8: Differences across pressure ranges in pulse pressure in the Lewis rat as assessed by Tukey's HSD. Relating to results from Chapter 6.

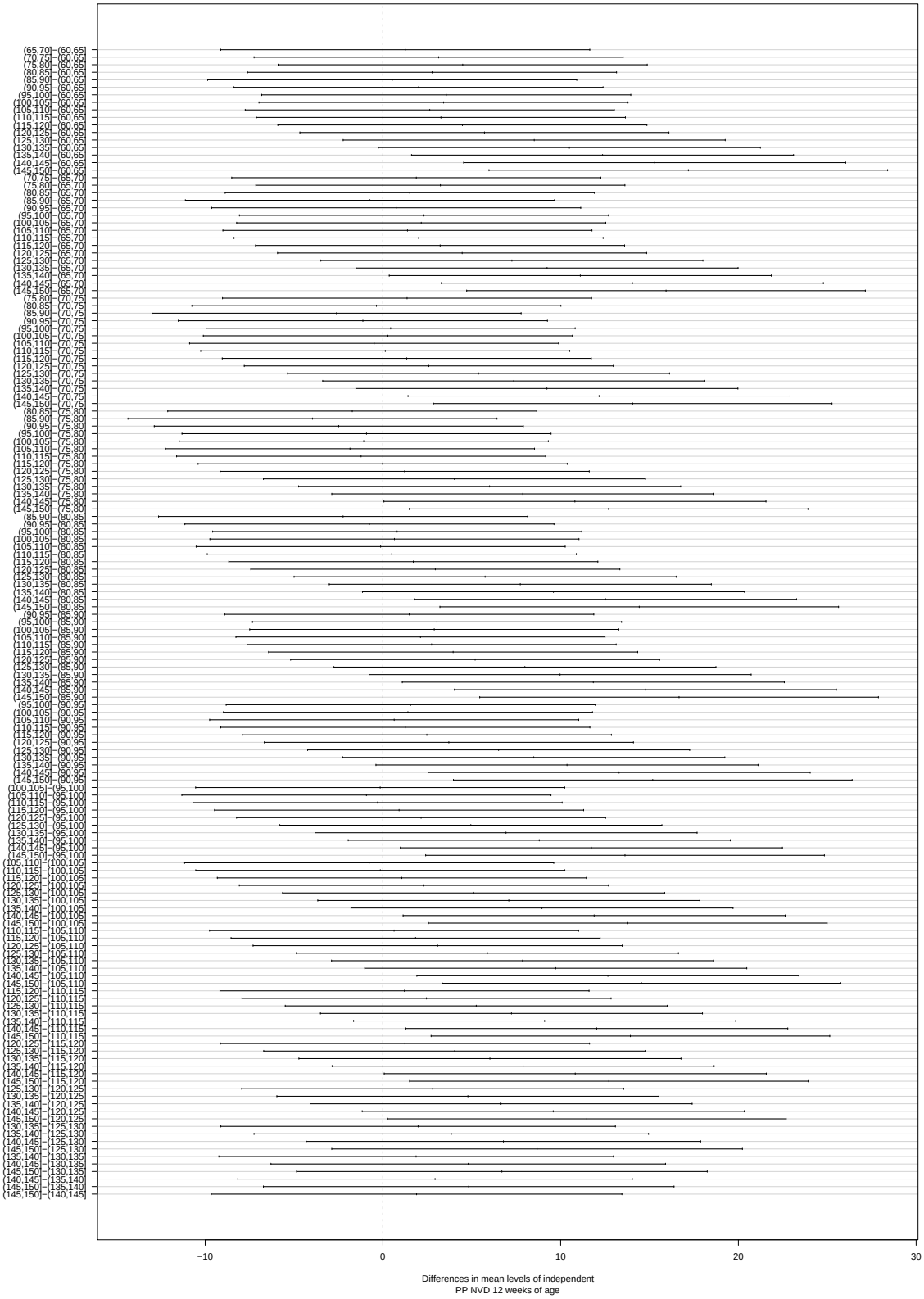

Figure C.9: Differences across pressure ranges in pulse pressure in the 12 week old Lewis rat with VDN calcification treatment by Tukey's HSD. Relating to results from Chapter 7.

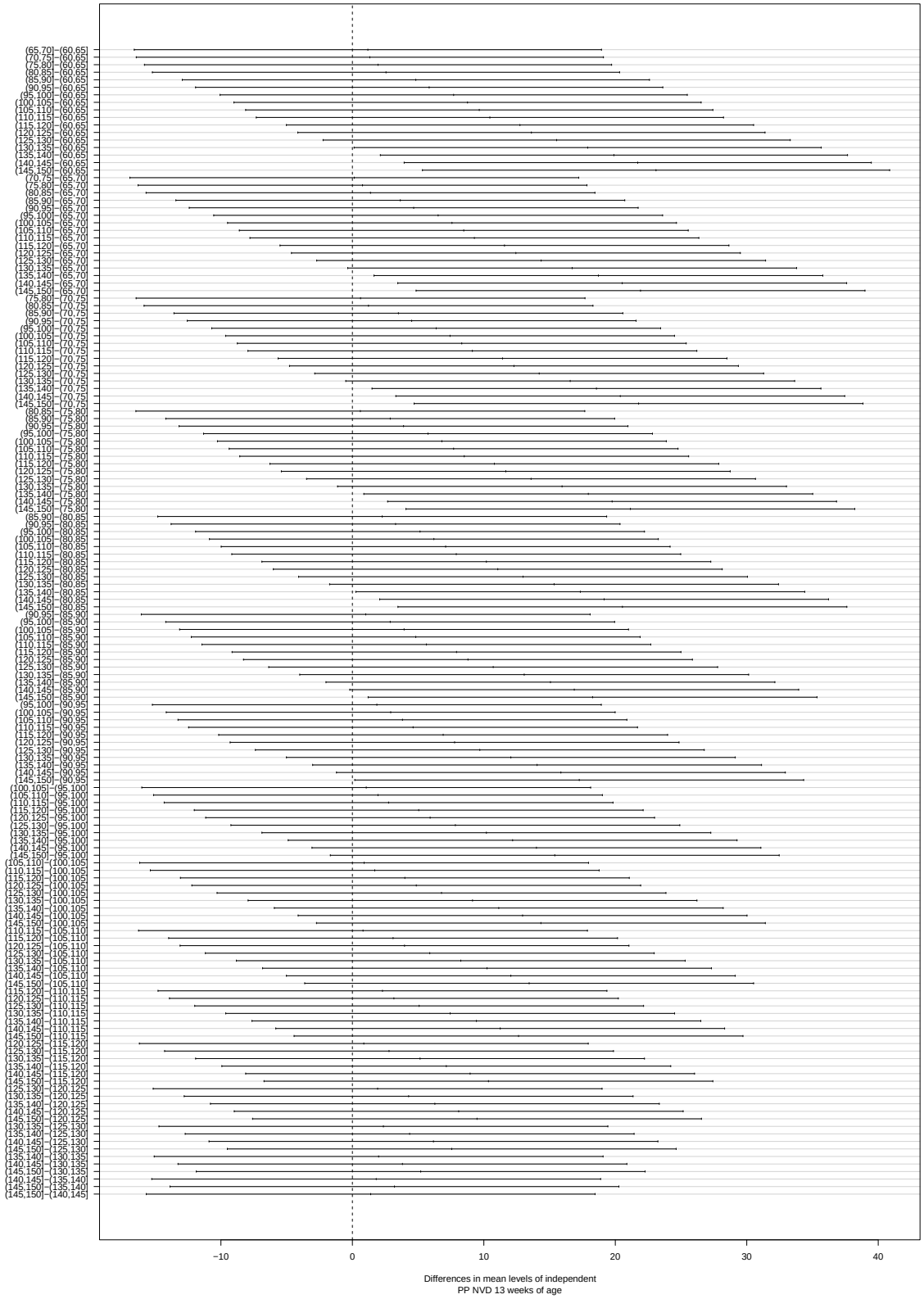

Figure C.10: Differences across pressure ranges in pulse pressure in the 13 week old Lewis rat with VDN calcification treatment by Tukey's HSD. Relating to results from Chapter 7.

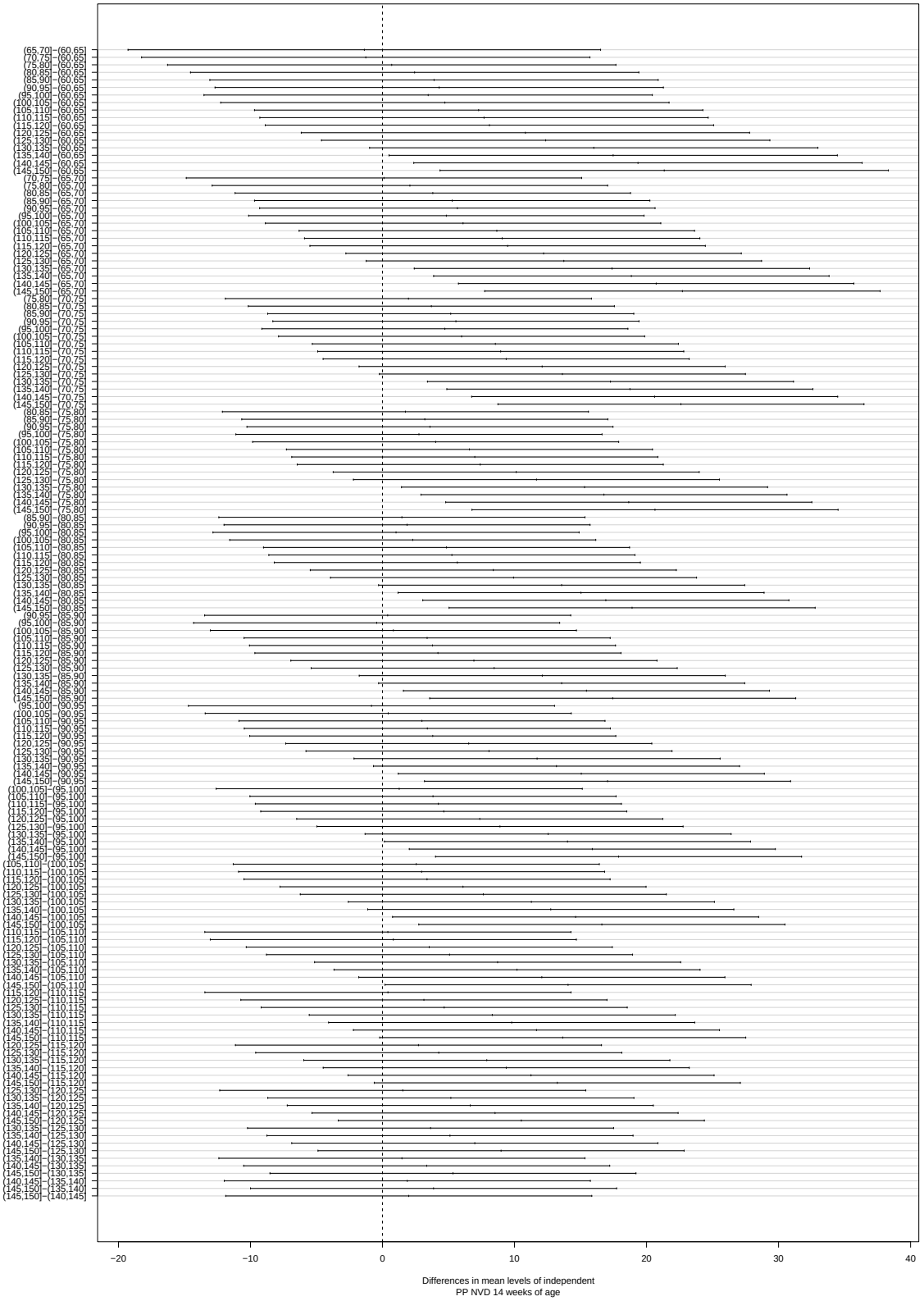

Figure C.11: Differences across pressure ranges in pulse pressure in the 14 week old Lewis rat with VDN calcification treatment by Tukey's HSD. Relating to results from Chapter 7.

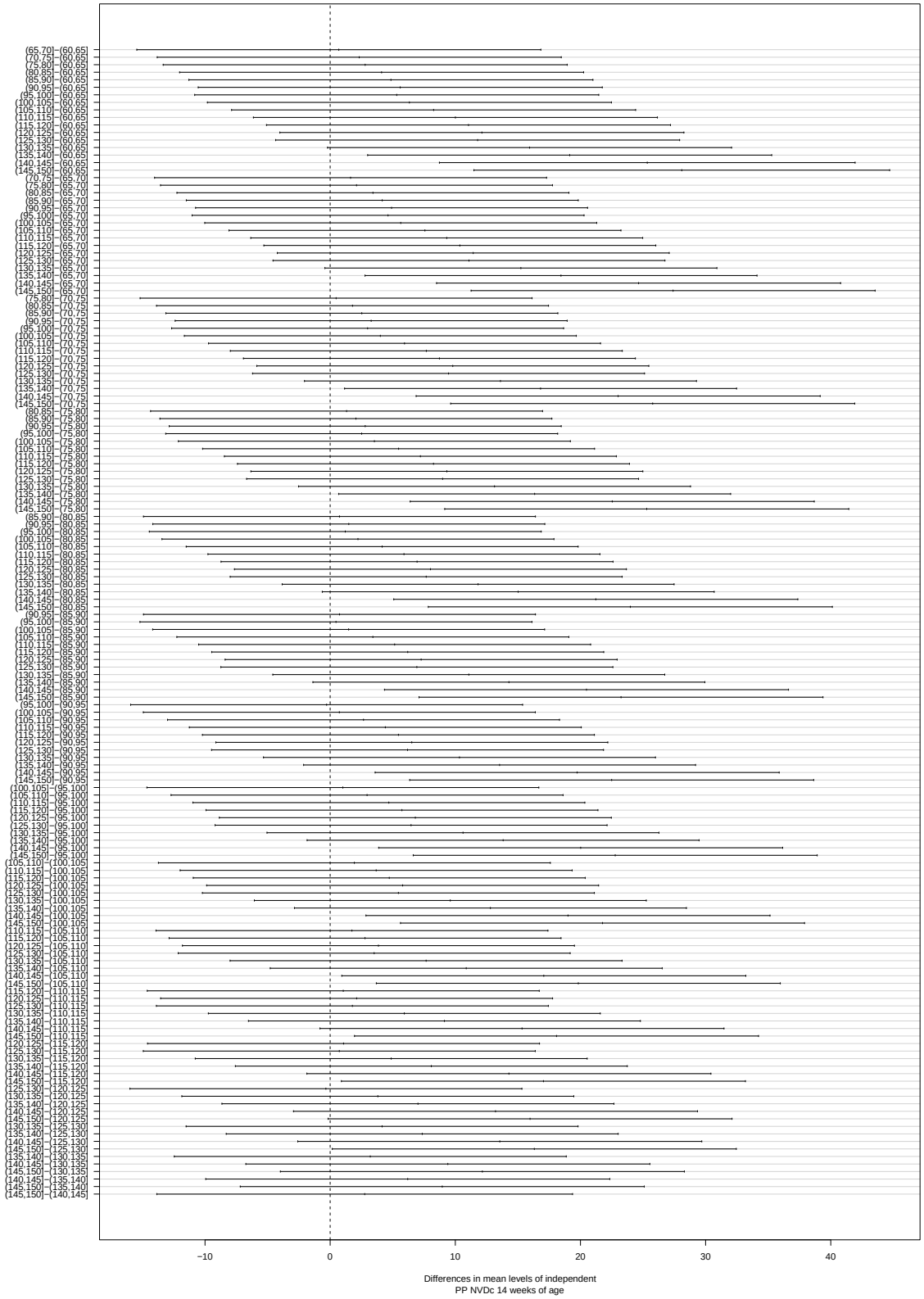

Figure C.12: Differences across pressure ranges in pulse pressure in the 14 week old Lewis rat, control for calcification treatment, by Tukey's HSD. Relating to results from Chapter 7.

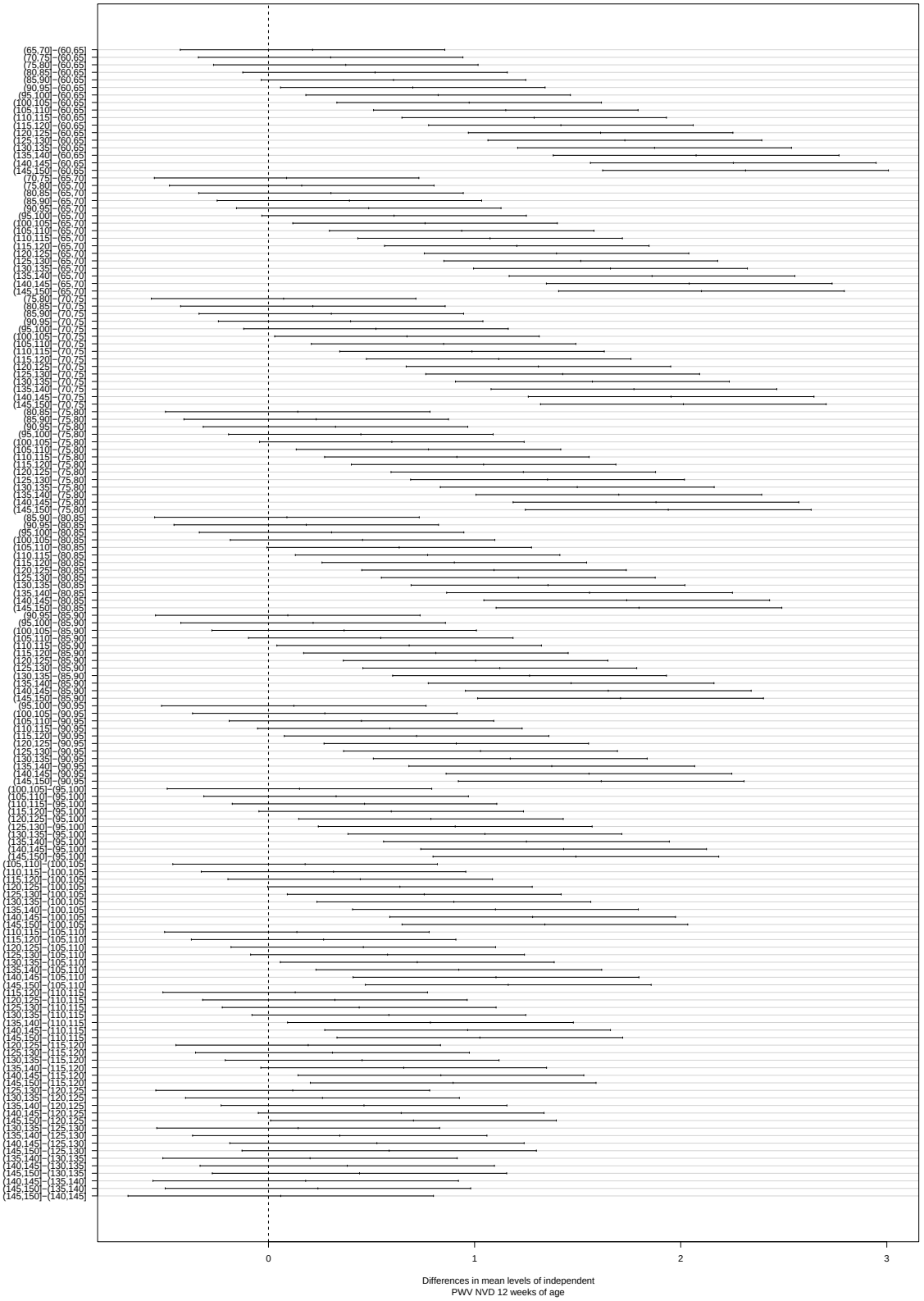

Figure C.13: Differences across pressure ranges in PWV in the 12 week old Lewis rat with VDN calcification treatment by Tukey's HSD. Relating to results from Chapter 7.

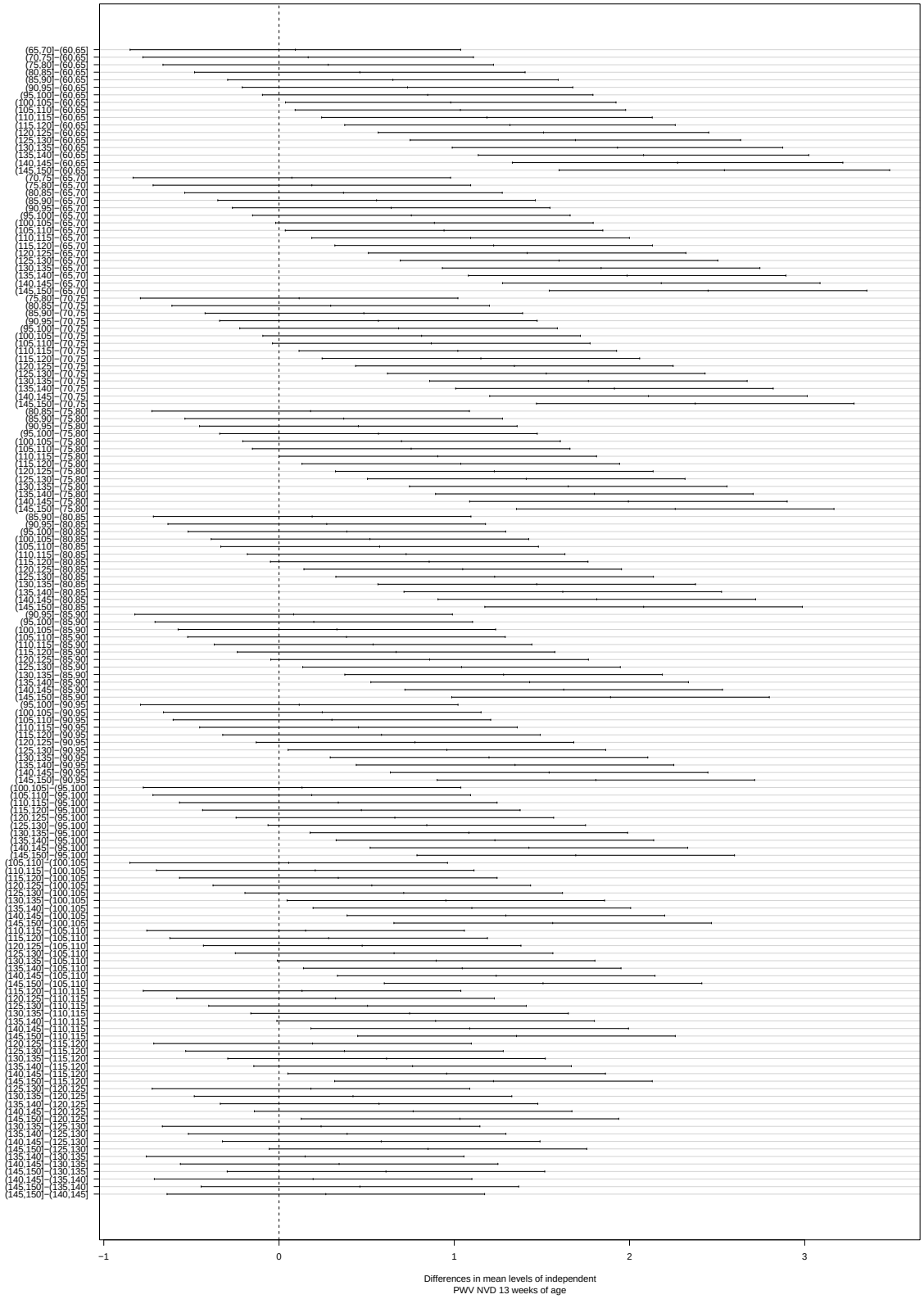

Figure C.14: Differences across pressure ranges in PWV in the 13 week old Lewis rat with VDN calcification treatment by Tukey's HSD. Relating to results from Chapter 7.

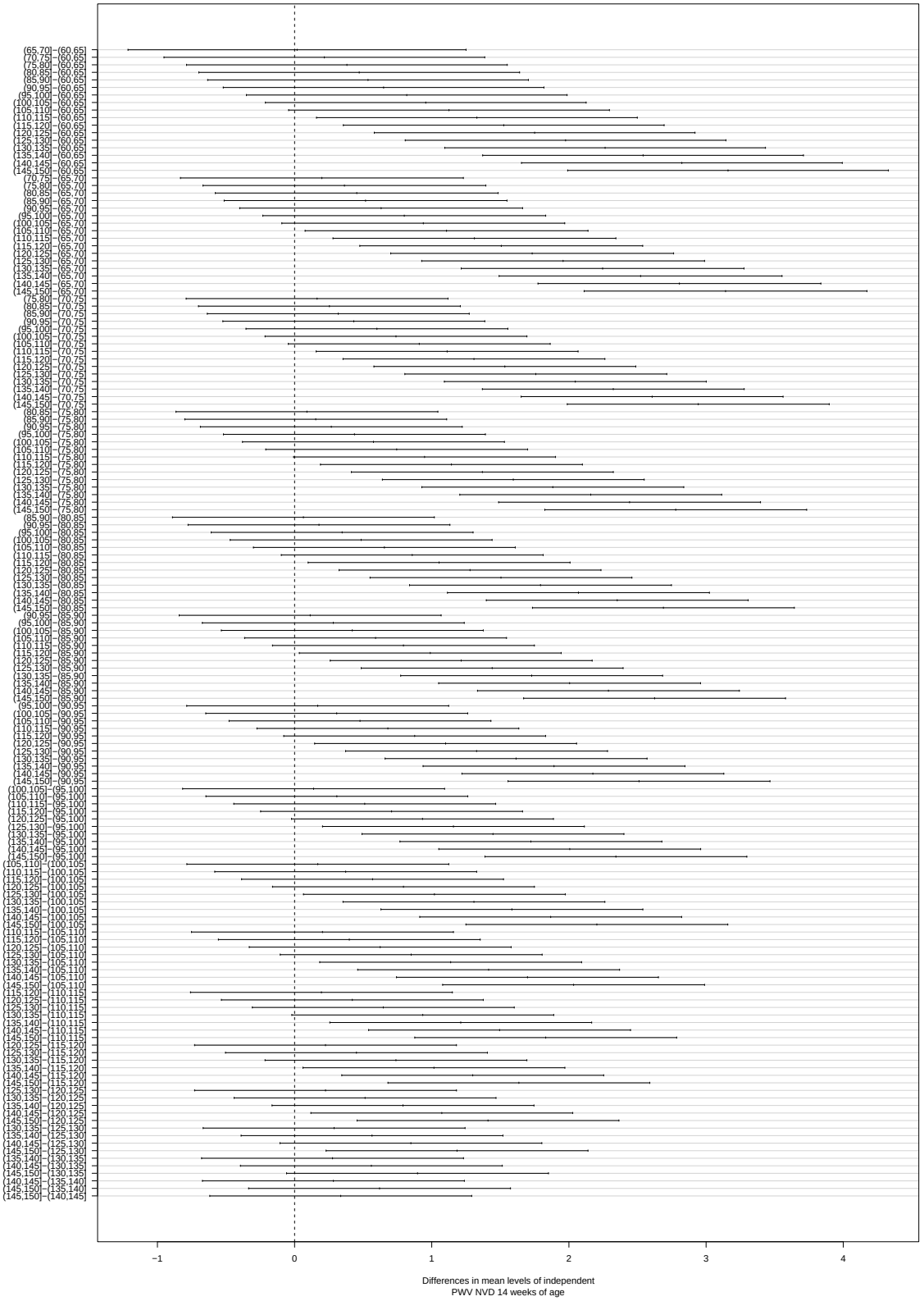

Figure C.15: Differences across pressure ranges in PWV in the 14 week old Lewis rat with VDN calcification treatment by Tukey's HSD. Relating to results from Chapter 7.

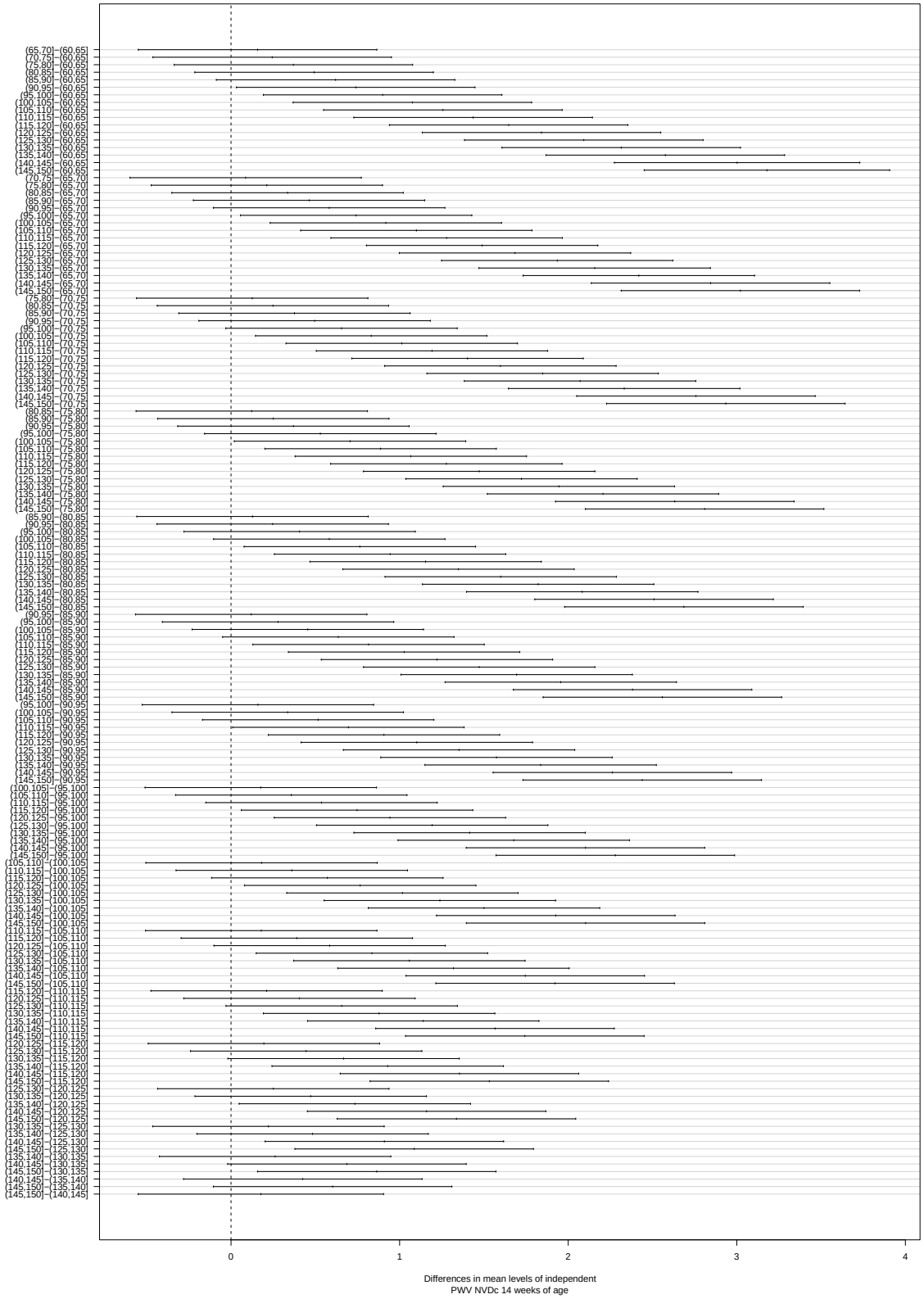

Figure C.16: Differences across pressure ranges in PWV in the 14 week old Lewis rat, control for calcification treatment, by Tukey's HSD. Relating to results from Chapter 7.

List of acronyms

ACCT Anglo-Cardiff Collaborative Trial

ACE Angiotensin-Converting Enzyme

AGE Advanced Glycation Endproducts

AIA Adjuvant-Induced Arthritis

AIx Augmentation Index

ANCA Antineutrophilic Cytoplasmic Antibody

ANOVA Analysis of Variance

ANP Atrial Natriuretic Peptide

ATP adenosine triphosphate

BMI Body Mass Index

BN Brown Norway

cAMP cyclic adenosine monophosphate

cGMP cyclic guanosine monophosphate

CRP c-reactive protein

DA Dark Agouti

ECG electrocardiogram

EDRF endothelial derived relaxing factor

eNOS endothelial derived nitric oxide synthase

ECE endothelin converting enzyme

ET-1 Endothelin-1

ET$_A$ Endothelin-A

ET$_B$ Endothelin-B

FCA Freund's complete adjuvant

FMD Flow-Mediated Dilatation

GTN glyceryl trinitrate

GTP guanosine triphosphate

HR Heart Rate

HSD Honest Significant Difference

IL-1 interleukin-1

IL-6 interleukin-6

iNOS inducible nitric oxide synthase

l-NAME N^{ω}-nitro-L-arginine methyl ester

l-NMMA N^{G}-monomethyl-L-arginine

MAP Mean Arterial Pressure

NO nitric oxide

NOS nitric oxide synthase

NSAID non-steroidal anti-inflammatory drug

PP pulse pressure

PWV Pulse Wave Velocity

PWV$_C$ Characteristic Pulse Wave Velocity

RI$_{PP}$ reflection index of the pulse pressures

RI$_{rms}$ reflection index of the root mean square (RMS) values

RM$_{PP}$ reflection magnitude of the pulse pressures

RM$_{rms}$ reflection magnitude of the RMS values

RMS root mean square

RSD relative standard deviation

RSE residual standard error

SENIORS Study of the Effects of Nebivolol Intervention on Outcomes and Rehospitalisation in Seniors with Heart Failure

SNP sodium nitroprusside

TNF-α tumour necrosis factor-α

VDN hypervitaminosis D_3 and nicotine

Nomenclature

$\boldsymbol{\beta}$	Stiffness index	$\boldsymbol{E_p}$	Peterson's modulus
$\boldsymbol{\Gamma}$	Reflection coefficient	$\boldsymbol{F}$	Force
$\boldsymbol{\varepsilon}$	Strain	$\boldsymbol{h}$	Wall thickness
$\boldsymbol{\eta}$	Viscosity	$\boldsymbol{K}$	Bulk modulus
$\boldsymbol{\lambda}$	Longitudinal loading modulus	$\boldsymbol{l}$	Length
		$\boldsymbol{m}$	Mass
$\boldsymbol{\mu}$	Shear modulus (Modulus of rigidity)	$\boldsymbol{P}$	Transmural pressure
		$\boldsymbol{Q}$	Flow
$\boldsymbol{\nu}$	Poisson's ratio	$\boldsymbol{R}$	Resistance
$\boldsymbol{\rho}$	Density	$\boldsymbol{r}$	Radius
$\boldsymbol{\sigma}$	Stress	$\boldsymbol{t}$	Time
$\boldsymbol{\omega}$	Frequency	$\boldsymbol{V}$	Volume
$\boldsymbol{A}$	Vessel cross sectional area	$\boldsymbol{v}$	Velocity
$\boldsymbol{a}$	Acceleration	$\boldsymbol{x}$	Distance
$\boldsymbol{B}$	Bulk modulus	$\boldsymbol{Z_c}$	Characteristic impedance
$\boldsymbol{C}$	Compliance	$\boldsymbol{Z_{in}}$	Input impedance
$\boldsymbol{c_o}$	Wave velocity	$\boldsymbol{Z_L}$	Longitudinal impedance
$\boldsymbol{E}$	Young's elastic modulus	$\boldsymbol{Z_T}$	Terminal impedance
$\boldsymbol{E_{inc}}$	Incremental modulus		

Bibliography

Abramson JL, Weintraub WS, Vaccarino V, Association between pulse pressure and C-reactive protein among apparently healthy US adults. *Hypertension*. 2002;39(2):197–202.

Access Economics Pty Limited, Arthritis - the bottom line, the economic impact of arthritis in Australia. Published report. 2005a, URL `http://www.accesseconomics.com.au/publicationsreports/getreport.php?report=21&id=110`.

Access Economics Pty Limited, The shifting burden of cardiovascular disease in Australia. Published report. 2005b, URL `http://www.accesseconomics.com.au/publicationsreports/getreport.php?report=15&id=18`.

ADInstruments, Powerlab data aquisition systems, Chart recorder software, LabTutor. Web site. 2007, URL `www.adinstruments.com`.

Ambrosini A, Louin G, Croci N, Plotkine M, Jafarian-Tehrani M, Characterization of a rat model to study acute neuroinflammation on histopathological, biochemical and functional outcomes. *J Neurosci Methods*. 2005;144(2):183–191.

Apter JT, Rabinowitz M, Cummings DH, Correlation of visco-elastic properties of large arteries with microscopic structure. *Circ Res*. 1966;19(1):104–121.

Armentano RL, Barra JG, Santana DB, Pessana FM, Graf S, Craiem D, Brandani LM, Baglivo HP, Sanchez RA, Smart damping modulation of carotid wall energetics in human hypertension: effects of angiotensin-converting enzyme inhibition. *Hypertension*. 2006;47(3):384–390.

Arnett DK, Evans GW, Riley WA, Arterial stiffness: a new cardiovascular risk factor? *Am J Epidemiol*. 1994;140(8):669–82.

Arroyo-Espliguero R, Mollichelli N, Avanzas P, Zouridakis E, Newey V, Nassiri D, Kaski J, Chronic inflammation and increased arterial stiffness in patients with cardiac syndrome X. *European Heart Journal*. 2003;24(22):2006.

Atcor Medical, SphygmoCor technology. Web site. 2007, URL `www.atcormedical.com`.

Avolio A, Genetic and environmental factors in the function and structure of the arterial wall. *Hypertension*. 1995;26(1):34–7.

Avolio A, Benetos A, *Handbook of Hypertension*, Volume 23 Arterial stiffness in hypertension, Chapter 18 Heart Rate, pulse pressure and arterial stiffness, pp. 279–294. Elsevier. 2006;.

Avolio A, Deng F, Li W, Luo Y, Huang Z, Xing L, O'Rourke M, Effects of aging on arterial distensibility in populations with high and low prevalence of hypertension: comparison between urban and rural communities in China. *Circulation*. 1985;71(2):202.

Avolio A, Jones D, Tafazzoli-Shadpour M, Quantification of alterations in structure and function of elastin in the arterial media. *Hypertension*. 1998;32(1):170–5.

Avolio AP, Chen S, Wang R, Zhang C, Li M, O'Rourke M, Effects of aging on changing arterial compliance and left ventricular load in a northern Chinese urban community. *Circulation*. 1983;68(1):50.

Bassiouny HS, Zarins CK, Kadowaki MH, Glagov S, Hemodynamic stress and experimental aortoiliac atherosclerosis. *J Vasc Surg*. 1994;19(3):426–434, abstract.

Behmoaras J, Osborne-Pellegrin M, Gauguier D, Jacob MP, Characteristics of the aortic elastic network and related phenotypes in seven inbred rat strains. *Am J Physiol Heart Circ Physiol*. 2005;288(2):H769–77.

Belz GG, Elastic properties and windkessel function of the human aorta. *Cardiovasc Drugs Ther*. 1995;9(1):73–83.

Benetos A, Adamopoulos C, Bureau JM, Temmar M, Labat C, Bean K, Thomas F, Pannier B, Asmar R, Zureik M, Safar M, Guize L, Determinants of accelerated progression of arterial stiffness in normotensive subjects and in treated hypertensive subjects over a 6-year period. *Circulation*. 2002;105(10):1202–1207.

Benetos A, Bouaziz H, Albaladejo P, Lvy BI, Safar ME, Physiological and pharmacological changes in the carotid artery pressure-volume curve in situ in rats. *J Hypertens Suppl*. 1992;10(6):S127–S131.

Bergel DH, The dynamic elastic properties of the arterial wall. *The Journal of Physiology*. 1961a;156(3):458–469.

Bergel DH, The static elastic properties of the arterial wall. *Circ Res*. 1961b;156(3):445–457.

Bevan JA, Bevan RD, Kite K, Oriowo MA, Species differences in sensitivity of aortae to norepinephrine are related to alpha-adrenoceptor affinity. *Trends Pharmacol Sci*. 1988; 9(3):87–89.

Billiau A, Matthys P, Modes of action of freund's adjuvants in experimental models of autoimmune diseases. *J Leukoc Biol*. 2001;70(6):849–860.

Binder W, Carmody J, Walker J, Effect of gender on anti-inflammatory and analgesic actions of two kappa-opioids. *J Pharmacol Exp Ther*. 2000;292(1):303–9.

Blacher J, Asmar R, Djane S, London G, Safar M, Aortic pulse wave velocity as a marker of cardiovascular risk in hypertensive patients. *Hypertension*. 1999a;33(5):1111.

Blacher J, Guerin A, Pannier B, Marchais S, Safar M, London G, Impact of aortic stiffness on survival in end-stage renal disease. *Circulation*. 1999b;99(18):2434.

Booth AD, Wallace S, McEniery CM, Yasmin, Brown J, Jayne DR, Wilkinson IB, Inflammation and arterial stiffness in systemic vasculitis: a model of vascular inflammation. *Arthritis Rheum.* 2004;50(2):581–8.

Boutouyrie P, Tropeano AI, Asmar R, Gautier I, Benetos A, Lacolley P, Laurent S, Aortic stiffness is an independent predictor of primary coronary events in hypertensive patients: a longitudinal study. *Hypertension.* 2002;39(1):10–15.

Bowman AJ, Chen CP, Ford GA, Nitric oxide mediated venodilator effects of nebivolol. *Br J Clin Pharmacol.* 1994;38(3):199–204.

Bramwell JC, Hill AV, The velocity of the pulse wave in man. *Proceedings of the Royal Society of London Series B.* 1922a;93(652):298–306.

Bramwell JC, Hill AV, Velocity transmission of the pulse wave and elasticity of arteries. *Lancet.* 1922b;199(5149):891–892.

Bristow MR, beta-adrenergic receptor blockade in chronic heart failure. *Circulation.* 2000; 101(5):558–569.

Bristow MR, Nelson P, Minobe W, Johnson C, Characterization of [beta]1-adrenergic receptor selectivity of nebivolol and various other beta-blockers in human myocardium. *American Journal of Hypertension.* 2005;18(5, Supplement 1):A51–A52.

Brunton LL (editor), *Goodman & Gilman's The Pharmacological Basis of Therapeutics.* McGraw Hill, 11th edition. 2006.

Brel A, Oxlund H, Changes in biomechanical properties, composition of collagen and elastin, and advanced glycation endproducts of the rat aorta in relation to age. *Atherosclerosis.* 1996;127(2):155–165.

Capdeville M, Coutard M, Osborne-Pellegrin MJ, Spontaneous rupture of the internal elastic lamina in the rat: the manifestation of a genetically determined factor which may be linked to vascular fragility. *Blood Vessels.* 1989;26(4):197–212.

Chen CH, Nevo E, Fetics B, Pak PH, Yin FC, Maughan WL, Kass DA, Estimation of central aortic pressure waveform by mathematical transformation of radial tonometry pressure. validation of generalized transfer function. *Circulation.* 1997;95(7):1827–1836.

Chen YL, Wolin MS, Messina EJ, Evidence for cgmp mediation of skeletal muscle arteriolar dilation to lactate. *J Appl Physiol.* 1996;81(1):349–354.

Cockcroft J, Chowienczyk P, Brett S, Chen C, Dupont A, Van Nueten L, Wooding S, Ritter J, Nebivolol vasodilates human forearm vasculature: evidence for an L-arginine/NO-dependent mechanism. *J Pharmacol Exp Ther.* 1995;274(3):1067–71.

Coutard M, Huang W, Osborne-Pellegrin M, Heritability of intracerebral hemorrhagic lesions and cerebral aneurysms in the rat. *Stroke.* 2000;31(11):2678–2684.

Cox RH, Comparison of carotid artery mechanics in the rat, rabbit, and dog. *Am J Physiol.* 1978;(3).

Cruickshank K, Riste L, Anderson SG, Wright JS, Dunn G, Gosling RG, Aortic pulse-wave velocity and its relationship to mortality in diabetes and glucose intolerance: an integrated index of vascular function? *Circulation.* 2002;106(16):2085–90.

Dao HH, Essalihi R, Bouvet C, Moreau P, Evolution and modulation of age-related medial elastocalcinosis: impact on large artery stiffness and isolated systolic hypertension. *Cardiovasc Res.* 2005;66(2):307–17.

Davies JE, Hadjiloizou N, Leibovich D, Malaweera A, Alastruey-Arimon J, Whinnett ZI, Manisty CH, Francis DP, Aguado-Sierra J, Foale RA, Malik IS, Parker KH, Mayet J, Hughes AD, Importance of the aortic reservoir in determining the shape of the arterial pressure waveform - the forgotten lessons of frank. *Artery Research.* 2007;1(2):40–45, abstract.

Dawes M, Brett SE, Chowienczyk PJ, Mant TG, Ritter JM, The vasodilator action of nebivolol in forearm vasculature of subjects with essential hypertension. *Br J Clin Pharmacol.* 1999;48(3):460–463.

de Groot E, Hovingh GK, Wiegman A, Duriez P, Smit AJ, Fruchart JC, Kastelein JJP, Measurement of arterial wall thickness as a surrogate marker for atherosclerosis. *Circulation.* 2004;109(23 Suppl 1):III33–III38.

de Groot E, Hovingh GK, Zwinderman AH, Wiegman A, Smit AJ, Kastelein JJP, Data density curves of b-mode ultrasound arterial wall thickness measurements in unaffected control and at-risk populations. *Int Angiol.* 2005;24(4):359–365.

DeCrée J, Rooy PV, Geukens H, Haeverans K, Verhaegen H, The antihypertensive and cardiac hemodynamic effects of nebivolol. *Angiology.* 1992;43(5):369–377.

Dobre D, van Veldhuisen DJ, Mordenti G, Vintila M, Haaijer-Ruskamp FM, Coats AJS, Poole-Wilson PA, Flather MD, Investigators SENIORS, Tolerability and dose-related effects of nebivolol in elderly patients with heart failure: data from the Study of the Effects of Nebivolol Intervention on Outcomes and Rehospitalisation in Seniors with Heart Failure (SENIORS) trial. *Am Heart J.* 2007;154(1):109–115.

Dobrin PB, Mechanical properties of arterises. *Physiol Rev.* 1978;58(2):397–460.

Dörger M, Allmeling AM, Kiefmann R, Mnzing S, Messmer K, Krombach F, Early inflammatory response to asbestos exposure in rat and hamster lungs: role of inducible nitric oxide synthase. *Toxicol Appl Pharmacol.* 2002;181(2):93–105.

Doshi SN, Naka KK, Payne N, Jones CJ, Ashton M, Lewis MJ, Goodfellow J, Flow-mediated dilatation following wrist and upper arm occlusion in humans: the contribution of nitric oxide. *Clin Sci (Lond).* 2001;101(6):629–635.

Dujardin J, Stone D, Forcino C, Effects of blood volume changes on characteristic impedance of the pulmonary artery. *Am J Physiol.* 1982;.

Eaton JW, *GNU Octave Manual.* Network Theory Limited. 2002, URL `http://www.octave.org`.

Farrar DJ, Green HD, Bond MG, Wagner WD, Gobbe RA, Aortic pulse wave velocity, elasticity, and composition in a nonhuman primate model of atherosclerosis. *Circ Res.* 1978;43(1):52–62.

Ferro A, *The Endothelium Made Easy, From basic science to clinical applications.* Excerpta Medica Publications, Elsevier Limited. 2003.

Fitch RM, Vergona R, Sullivan ME, Wang YX, Nitric oxide synthase inhibition increases aortic stiffness measured by pulse wave velocity in rats. *Cardiovasc Res.* 2001;51(2):351–8.

Fogari R, Zoppi A, Lazzari P, Mugellini A, Lusardi P, Preti P, Nueten LV, Vertommen C, Comparative effects of nebivolol and atenolol on blood pressure and insulin sensitivity in hypertensive subjects with type ii diabetes. *J Hum Hypertens*. 1997;11(11):753–757.

Food and Drug Administration, Oncology Tools Product Label Details in Conventional Order for zoledronate. Website. 2003, URL `http://www.accessdata.fda.gov/scripts/cder/onctools/labels.cfm?GN=zoledronate`.

Forest Laboratories, Inc, Mylan laboratories and forest laboratories announce nebivolol licensing agreement. Press Release. 2006, URL `http://www.frx.com/news/PressRelease.aspx?ID=803356`.

Forest Laboratories, Inc, Response submitted to FDA approvable letter for hypertension compound nebivolol. Press release. 2007, URL `http://www.frx.com/news/PressRelease.aspx?ID=993641`.

Frøbert O, Mikkelsen EO, Bagger JP, Gravholt CH, Measurement of interstitial lactate during hypoxia-induced dilatation in isolated pressurised porcine coronary arteries. *J Physiol*. 2002;539(Pt 1):277–284.

Furchgott RF, Cherry PD, Zawadzki JV, Jothianandan D, Endothelial cells as mediators of vasodilation of arteries. *J Cardiovasc Pharmacol*. 1984;6 Suppl 2:S336–43.

Furchgott RF, Zawadzki JV, The obligatory role of endothelial cells in the relaxation of arterial smooth muscle by acetylcholine. *Nature*. 1980;288(5789):373–6.

Gaillard V, Casellas D, Seguin-Devaux C, Schohn H, Daua M, Atkinson J, Lartaud I, Pioglitazone improves aortic wall elasticity in a rat model of elastocalcinotic arteriosclerosis. *Hypertension*. 2005;46(2):372–9.

Gambillara V, Montorzi G, Haziza-Pigeon C, Stergiopulos N, Silacci P, Arterial wall response to ex vivo exposure to oscillatory shear stress. *J Vasc Res*. 2005;42(6):535–544.

Gamboa A, Shibao C, Diedrich A, Choi L, Pohar B, Jordan J, Paranjape S, Farley G, Biaggioni I, Contribution of endothelial nitric oxide to blood pressure in humans. *Hypertension*. 2007;49(1):170–7.

Gao YS, Nagao T, Bond RA, Janssens WJ, Vanhoutte PM, Nebivolol induces endothelium-dependent relaxations of canine coronary arteries. *J Cardiovasc Pharmacol*. 1991; 17(6):964–969.

Giannattasio C, Failla M, Grappiolo A, Calchera I, Grieco N, Carugo S, Bigoni M, Randelli P, Peretti G, Mancia G, Effects of physical training of the dominant arm on ipsilateral radial artery distensibility and structure. *J Hypertens*. 2001;19(1):71–7.

Gosling RG, Budge MM, Terminology for describing the elastic behavior of arteries. *Hypertension*. 2003;41(6):1180–2.

Gow B, *Cardiovascular Fluid Dynamics*, Volume 2, Chapter 12: The influence of vascular smooth muscle on the viscoelastic properties of blood vessels, pp. 65–110. Acadaemic Press. 1972;.

Gow BS, An electrical caliper for measurement of pulsatile arterial diameter changes in vivo. *J Appl Physiol*. 1966;21(3):1122–1126.

Gow BS, Taylor MG, Measurement of viscoelastic properties of arteries in the living dog. *Circ Res*. 1968;23(1):111–122.

Greenwald SE, Pulse pressure and arterial elasticity. *QJM*. 2002;95(2):107–112.

Greenwald SE, Ageing of the conduit arteries. *J Pathol*. 2007;211(2):157–172.

Grimm N, Arthritis could cripple economy: report. Radio report, AM, ABC Radio National. 2005, URL `http://www.abc.net.au/am/content/2005/s1303797.htm`.

Halcox JP, Nour KR, Zalos G, Quyyumi AA, Endogenous Endothelin in Human Coronary Vascular Function: Differential Contribution of Endothelin Receptor Types A and B. *Hypertension*. 2007;49(5):1134–1141.

Harris EL, Stoll M, Jones GT, Granados MA, Porteous WK, Rij AMV, Jacob HJ, Identification of two susceptibility loci for vascular fragility in the brown norway rat. *Physiol Genomics*. 2001;6(3):183–189.

Hass GM, Landerholm W, Hemmens A, Production of calcific athero-arteriosclerosis and thromboarteritis with nicotine, vitamin d and dietary cholesterol. *Am J Pathol*. 1966; 49(4):739–771.

Haynes WG, Noon JP, Walker BR, Webb DJ, Inhibition of nitric oxide synthesis increases blood pressure in healthy humans. *J Hypertens*. 1993;11(12):1375–1380.

Haynes WG, Webb DJ, Contribution of endogenous generation of endothelin-1 to basal vascular tone. *Lancet*. 1994;344(8926):852–854.

Henrion D, Chillon JM, Godeau G, Muller F, Capdeville-Atkinson C, Hoffman M, Atkinson J, The consequences of aortic calcium overload following vitamin D3 plus nicotine treatment in young rats. *J Hypertens*. 1991;9(10):919–26.

Herrington DM, Brown WV, Mosca L, Davis W, Eggleston B, Hundley WG, Raines J, Relationship between arterial stiffness and subclinical aortic atherosclerosis. *Circulation*. 2004;110(4):432–437.

Hurlimann D, Forster A, Noll G, Enseleit F, Chenevard R, Distler O, Bechir M, Spieker LE, Neidhart M, Michel BA, Gay RE, Luscher TF, Gay S, Ruschitzka F, Anti-tumor necrosis factor-alpha treatment improves endothelial function in patients with rheumatoid arthritis. *Circulation*. 2002;106(17):2184–7.

Ishizaka H, Gudi SR, Frangos JA, Kuo L, Coronary arteriolar dilation to acidosis: role of atp-sensitive potassium channels and pertussis toxin-sensitive g proteins. *Circulation*. 1999;99(4):558–563.

Jacobson PB, Morgan SJ, Wilcox DM, Nguyen P, Ratajczak CA, Carlson RP, Harris RR, Nuss M, A new spin on an old model: in vivo evaluation of disease progression by magnetic resonance imaging with respect to standard inflammatory parameters and histopathology in the adjuvant arthritic rat. *Arthritis Rheum*. 1999;42(10):2060–2073.

Jegger D, da Silva R, Jeanrenaud X, Nasratullah M, Tevaearai H, von Segesser LK, Segers P, Gaillard V, Atkinson J, Lartaud I, Stergiopulo N, Ventricular-arterial coupling in a rat model of reduced arterial compliance provoked by hypervitaminosis D and nicotine. *Am J Physiol Heart Circ Physiol*. 2006;291(4):H1942–H1951.

Joannides R, Haefeli WE, Linder L, Richard V, Bakkali EH, Thuillez C, Lscher TF, Nitric oxide is responsible for flow-dependent dilatation of human peripheral conduit arteries in vivo. *Circulation*. 1995;91(5):1314–9.

Joe B, Wilder RL, Animal models of rheumatoid arthritis. *Mol Med Today*. 1999;5(8):367–369.

Jones GT, Harris EL, Jacob HJ, van Rij AM, Spontaneous elastic tissue lesions in the rat abdominal aorta, a genetically determined phenotype. *J Vasc Res*. 2000;37(2):73–81.

Kaiser L, Sparks Jr H, Mediation of flow-dependent arterial dilation by endothelial cells. *Circulatory Shock*. 1986;18(2):109.

Kampus P, Kals J, Ristime T, Fischer K, Zilmer M, Teesalu R, High-sensitivity c-reactive protein affects central haemodynamics and augmentation index in apparently healthy persons. *J Hypertens*. 2004;22(6):1133–1139.

Kampus P, Kals J, Ristime T, Muda P, Ulst K, Zilmer K, Salonen RM, Tuomainen TP, Teesalu R, Zilmer M, Augmentation index and carotid intima-media thickness are differently related to age, c-reactive protein and oxidized low-density lipoprotein. *J Hypertens*. 2007;25(4):819–825.

Kampus P, Muda P, Kals J, Ristime T, Fischer K, Teesalu R, Zilmer M, The relationship between inflammation and arterial stiffness in patients with essential hypertension. *Int J Cardiol*. 2006;112(1):46–51.

Karamanoglu M, O'Rourke MF, Avolio AP, Kelly RP, An analysis of the relationship between central aortic and peripheral upper limb pressure waves in man. *Eur Heart J*. 1993;14(2):160–167.

Kieffer P, Robert A, Capdeville-Atkinson C, Atkinson J, Lartaud-Idjouadiene I, Age-related arterial calcification in rats. *Life Sci*. 2000;66(24):2371–81.

Kinlay S, Creager M, Fukumoto M, Hikita H, Fang J, Selwyn A, Ganz P, Endothelium-derived nitric oxide regulates arterial elasticity in human arteries in vivo. *Hypertension*. 2001;38(5):1049.

Klocke R, Cockcroft J, Taylor G, Hall I, Blake D, Arterial stiffness and central blood pressure, as determined by pulse wave analysis, in rheumatoid arthritis. *Ann Rheum Dis*. 2003;62(5):414.

Krafka Jr J, Comparative study of the histo-physics of the aorta. *Am J Physiol*. 1938; 125(1):1–14.

Lacolley P, Osborne-Pellegrin M, Labat C, Challande P, *Handbook of Hypertension*, Volume 23 Arterial stiffness in hypertension, Chapter 11 Animal models for studies of arterial stiffness, pp. 175–190. Elsevier. 2006;.

Langewouters GJ, Wesseling KH, Goedhard WJ, The static elastic properties of 45 human thoracic and 20 abdominal aortas in vitro and the parameters of a new model. *J Biomech*. 1984;17(6):425–435.

Langewouters GJ, Wesseling KH, Goedhard WJ, The pressure dependent dynamic elasticity of 35 thoracic and 16 abdominal human aortas in vitro described by a five component model. *J Biomech*. 1985;18(8):613–620.

Latham RD, Westerhof N, Sipkema P, Rubal BJ, Reuderink P, Murgo JP, Regional wave travel and reflections along the human aorta: a study with six simultaneous micromanometric pressures. *Circulation*. 1985;72(6):1257–69.

Laurent S, Boutouyrie P, Recent advances in arterial stiffness and wave reflection in human hypertension. *Hypertension*. 2007;49(6):1202–1206.

Laurent S, Boutouyrie P, Asmar R, Gautier I, Laloux B, Guize L, Ducimetiere P, Benetos A, Aortic stiffness is an independent predictor of all-cause and cardiovascular mortality in hypertensive patients. *Hypertension*. 2001a;37(5):1236–41.

Laurent S, Cockcroft J, Bortel LV, Boutouyrie P, Giannattasio C, Hayoz D, Pannier B, Vlachopoulos C, Wilkinson I, Struijker-Boudier H, Expert consensus document on arterial stiffness: methodological issues and clinical applications. *Eur Heart J*. 2006; 27:2588–2605.

Laurent S, Katsahian S, Fassot C, Tropeano AI, Gautier I, Laloux B, Boutouyrie P, Aortic stiffness is an independent predictor of fatal stroke in essential hypertension. *Stroke*. 2003;34(5):1203–1206.

Laurent S, Tropeano AI, Lillo-Lelouet A, Jondeau G, Laloux B, Boutouyrie P, Local pulse pressure is a major determinant of large artery remodelling. *Clin Exp Pharmacol Physiol*. 2001b;28(12):1011–1014.

Levy BI, Curmi P, Poitevin P, Safar ME, Modifications of the arterial mechanical properties of normotensive and hypertensive rats without arterial pressure changes. *J Cardiovasc Pharmacol*. 1989;14(2):253–259.

Libby P, Inflammation in atherosclerosis. *Nature*. 2002;420(6917):868.

Libby P, Ridker P, Maseri A, Inflammation and atherosclerosis. *Circulation*. 2002; 105(9):1135.

Lillie MA, Gosline JM, Mechanical properties of elastin along the thoracic aorta in the pig. *J Biomech*. 2006;.

London GM, Blacher J, Pannier B, Guerin AP, Marchais SJ, Safar ME, Arterial wave reflections and survival in end-stage renal failure. *Hypertension*. 2001;38(3):434–8.

Mackay J, Mensah GA, *The atlas of heart disease and stroke*. Myriad Editions Limited. 2004, produced for the World Health Organization.

Mackenzie IS, Wilkinson IB, Cockcroft JR, Assessment of arterial stiffness in clinical practice. *QJM*. 2002;95(2):67–74.

Mackenzie IS, Wilkinson IB, Cockcroft JR, *Hypertension*. Elsevier Churchill Livingstone. 2005.

Maffei A, Vecchione C, Aretini A, Poulet R, Bettarini U, Gentile MT, Cifelli G, Lembo G, Characterization of nitric oxide release by nebivolol and its metabolites. *Am J Hypertens*. 2006;19(6):579–586.

Mahomed F, The physiology and clinical use of the sphygmograph. *Medical Time Gazette*. 1872;1:62.

Mäki-Petäjä KM, Hall FC, Booth AD, Wallace SML, Yasmin, Bearcroft PWP, Harish S, Furlong A, McEniery CM, Brown J, Wilkinson IB, Rheumatoid arthritis is associated with increased aortic pulse-wave velocity, which is reduced by anti-tumor necrosis factor-alpha therapy. *Circulation*. 2006;114(11):1185–1192.

Mancia G, Backer GD, Dominiczak A, Cifkova R, Fagard R, Germano G, Grassi G, Heagerty AM, Kjeldsen SE, Laurent S, Narkiewicz K, Ruilope L, Rynkiewicz A, Schmieder RE, Boudier HAJS, Zanchetti A, Vahanian A, Camm J, Caterina RD, Dean V, Dickstein K, Filippatos G, Funck-Brentano C, Hellemans I, Kristensen SD, McGregor K, Sechtem U, Silber S, Tendera M, Widimsky P, Zamorano JL, Erdine S, Kiowski W, Agabiti-Rosei E, Ambrosioni E, Lindholm LH, Viigimaa M, Adamopoulos S, Agabiti-Rosei E, Ambrosioni E, Bertomeu V, Clement D, Erdine S, Farsang C, Gaita D, Lip G, Mallion JM, Manolis AJ, Nilsson PM, O'Brien E, Ponikowski P, Redon J, Ruschitzka F, Tamargo J, van Zwieten P, Waeber B, Williams B, of Arterial Hypertension of the European Society of Hypertension M, of Cardiology ES, 2007 guidelines for the management of arterial hypertension: The task force for the management of arterial hypertension of the European Society of Hypertension (ESH) and of the European Society of Cardiology (ESC). *J Hypertens*. 2007;25(6):1105–1187.

Mangrella M, Rossi F, Fici F, Rossi F, Pharmacology of nebivolol. *Pharmacol Res*. 1998; 38(6):419–431.

Mattace-Raso F, van der Cammen T, Hofman A, van Popele N, Bos M, Schalekamp M, Asmar R, Reneman R, Hoeks A, Breteler M, Witteman J, Arterial stiffness and risk of coronary heart disease and stroke: the Rotterdam Study. *Circulation*. 2006;113(5):657–63.

Mattace-Raso FU, van der Cammen TJ, van der Meer IM, Schalekamp MA, Asmar R, Hofman A, Witteman JC, C-reactive protein and arterial stiffness in older adults: the Rotterdam Study. *Atherosclerosis*. 2004;176(1):111–6.

McDonald D, Regional pulse-wave velocity in the arterial tree. *J Appl Physiol*. 1968;.

McEniery CM, Qasem A, Schmitt M, Avolio AP, Cockcroft JR, Wilkinson IB, Endothelin-1 regulates arterial pulse wave velocity in vivo. *J Am Coll Cardiol*. 2003;42(11):1975–1981.

McEniery CM, Schmitt M, Qasem A, Webb DJ, Avolio AP, Wilkinson IB, Cockcroft JR, Nebivolol increases arterial distensibility in vivo. *Hypertension*. 2004;44(3):305–10.

McEniery CM, Wallace S, Mackenzie IS, McDonnell B, Yasmin, Newby DE, Cockcroft JR, Wilkinson IB, Endothelial function is associated with pulse pressure, pulse wave velocity, and augmentation index in healthy humans. *Hypertension*. 2006;48(4):602–608.

McEniery CM, Yasmin, Hall IR, Qasem A, Wilkinson IB, Cockcroft JR, ACCT Investigators, Normal vascular aging: differential effects on wave reflection and aortic pulse wave velocity: the Anglo-Cardiff Collaborative Trial (ACCT). *J Am Coll Cardiol*. 2005; 46(9):1753–1760.

Meaume S, Benetos A, Henry OF, Rudnichi A, Safar ME, Aortic pulse wave velocity predicts cardiovascular mortality in subjects >70 years of age. *Arterioscler Thromb Vasc Biol*. 2001;21(12):2046–50.

Middleton PM, Henry JA, Pulse oximetry: evolution and directions. *Int J Clin Pract*. 2000;54(7):438–444.

Milnor WR, *Hemodynamics*. Williams & Wilkins, Baltimore. 1982.

Mitchell G, Pfeffer M, Finn P, Pfeffer J, Comparison of techniques for measuring pulse-wave velocity in the rat. *Journal of Applied Physiology*. 1997;82(1):203.

Mitchell GF, Pfeffer MA, Pulsatile hemodynamics in hypertension. *Curr Opin Cardiol.* 1999;14(5):361–9.

Moncada S, Palmer RM, Higgs EA, Nitric oxide: physiology, pathophysiology, and pharmacology. *Pharmacol Rev.* 1991;43(2):109–42.

Mullen MJ, Kharbanda RK, Cross J, Donald AE, Taylor M, Vallance P, Deanfield JE, MacAllister RJ, Heterogenous nature of flow-mediated dilatation in human conduit arteries in vivo: relevance to endothelial dysfunction in hypercholesterolemia. *Circ Res.* 2001;88(2):145–151.

Mulvany MJ, Vascular remodelling in hypertension. *Eur Heart J.* 1993;14 Suppl C:2–4.

Murgo JP, Westerhof N, Giolma J, Aortic input impedance in normal man:. *Circ.* 1980;.

Nichols WW, Clinical measurement of arterial stiffness obtained from noninvasive pressure waveforms. *Am J Hypertens.* 2005;18(1 Pt 2):3S–10S.

Nichols WW, Re: Defining the dichrotic notch. 2006, e-mail correspondence.

Nichols WW, O'Rourke MF, *McDonald's Blood Flow in Arteries, Theoretical, experimental and clinical principles.* Arnold, London, fourth edition. 1998.

Niederhoffer N, Bobryshev YV, Lartaud-Idjouadiene I, Giummelly P, Atkinson J, Aortic calcification produced by vitamin D3 plus nicotine. *J Vasc Res.* 1997a;34(5):386–398.

Niederhoffer N, Lartaud-Idjouadiene I, Giummelly P, Duvivier C, Peslin R, Atkinson J, Calcification of medial elastic fibers and aortic elasticity. *Hypertension.* 1997b; 29(4):999–1006.

Nitta K, Akiba T, Uchida K, Otsubo S, Otsubo Y, Takei T, Ogawa T, Yumura W, Kabaya T, Nihei H, Left ventricular hypertrophy is associated with arterial stiffness and vascular calcification in hemodialysis patients. *Hypertens Res.* 2004;27(1):47–52.

Nodari S, Metra M, Cas LD, Beta-blocker treatment of patients with diastolic heart failure and arterial hypertension. a prospective, randomized, comparison of the long-term effects of atenolol vs. nebivolol. *Eur J Heart Fail.* 2003;5(5):621–627.

Nueten LV, Crée JD, Nebivolol: comparison of the effects of dl-nebivolol, d-nebivolol, l-nebivolol, atenolol, and placebo on exercise-induced increases in heart rate and systolic blood pressure. *Cardiovasc Drugs Ther.* 1998;12(4):339–344.

Nueten LV, Dupont AG, Vertommen C, Goyvaerts H, Robertson JI, A dose-response trial of nebivolol in essential hypertension. *J Hum Hypertens.* 1997;11(2):139–144.

O'Rourke M, *Handbook of Hypertension*, Volume 23 Arterial stiffness in hypertension, Chapter 1 Principles and definitions of arterial stiffness, wave refelections, and pulse pressure amplification, pp. 3–20. Elsevier. 2006;.

O'Rourke M, Taylor M, Vascular impedance of the femoral bed. *Circ Res.* 1966;.

O'Rourke MF, Vascular impedance in studies of arterial and cardiac function. *Physiol Rev.* 1982;62(2):570–623.

O'Rourke MF, Mancia G, Arterial stiffness. *J Hypertens.* 1999;17(1):1–4.

O'Rourke MF, Staessen JA, Vlachopoulos C, Duprez D, Plante GE, Clinical applications of arterial stiffness; definitions and reference values. *Am J Hypertens.* 2002;15(5):426–44.

Palmer RM, Ashton DS, Moncada S, Vascular endothelial cells synthesize nitric oxide from L-arginine. *Nature.* 1988a;333(6174):664–666.

Palmer RM, Ferrige AG, Moncada S, Nitric oxide release accounts for the biological activity of endothelium-derived relaxing factor. *Nature.* 1987;327(6122):524–6.

Palmer RM, Rees DD, Ashton DS, Moncada S, L-Arginine is the physiological precursor for the formation of nitric oxide in endothelium-dependent relaxation. *Biochem Biophys Res Commun.* 1988b;153(3):1251–1256.

Patel DJ, Janicki JS, Carew TE, Static anisotropic elastic properties of the aorta in living dogs. *Circ Res.* 1969;25(6):765–779.

Pauca AL, O'Rourke MF, Kon ND, Prospective evaluation of a method for estimating ascending aortic pressure from the radial artery pressure waveform. *Hypertension.* 2001; 38(4):932–937.

Pearson A, Peterson J, Orsinelli D, Guo R, Boudoulas H, Gray P, Comparison of thickness and distensibility in the carotid artery and descending thoracic aorta: in vivo ultrasound assessment. *Am Heart J.* 1996;131(4):655.

Peterson L, Jensen R, Parnell J, Mechanical properties of arteries in vivo. *Circ Res.* 1960; 8(3):622–639.

Price PA, Faus SA, Williamson MK, Warfarin-induced artery calcification is accelerated by growth and vitamin D. *Arterioscler Thromb Vasc Biol.* 2000;20(2):317–327.

Pyke KE, Tschakovsky ME, The relationship between shear stress and flow-mediated dilatation: implications for the assessment of endothelial function. *J Physiol.* 2005; 568(Pt 2):357–369.

Qasem A, Avolio A, Determination of aortic pulse wave velocity from waveform decomposition of the central aortic pressure pulse. *Hypertension.* 2007;Pre-press.

Ray CJ, Abbas MR, Coney AM, Marshall JM, Interactions of adenosine, prostaglandins and nitric oxide in hypoxia-induced vasodilatation: in vivo and in vitro studies. *J Physiol.* 2002;544(Pt 1):195–209.

Ridker P, Cushman M, Stampfer M, Tracy R, Hennekens C, Inflammation, aspirin, and the risk of cardiovascular disease in apparently healthy men. *N Engl J Med.* 1997; 336(14):973.

Ridker P, Hennekens C, Buring J, Rifai N, C-reactive protein and other markers of inflammation in the prediction of cardiovascular disease in women. *N Engl J Med.* 2000; 342(12):836.

Riva-Rocci S, Un nuovo sfigmomanometro. *Gazzetta Medica di Torino.* 1896;50:981–1017.

Safar ME, London GM, Asmar RG, Hugues CJ, Laurent SA, An indirect approach for the study of the elastic modulus of the brachial artery in patients with essential hypertension. *Cardiovasc Res.* 1986;20(8):563–567.

Satriano J, Arginine pathways and the inflammatory response: interregulation of nitric oxide and polyamines: review article. *Amino Acids.* 2004;26(4):321–9.

Sauvage M, Jacob MP, Osborne-Pellegrin M, Aortic elastin and collagen content and synthesis in two strains of rats with different susceptibilities to rupture of the internal elastic lamina. *J Vasc Res.* 1997;34(2):126–136.

Schmitt M, Avolio A, Qasem A, McEniery CM, Butlin M, Wilkinson IB, Cockcroft JR, Basal NO locally modulates human iliac artery function in vivo. *Hypertension.* 2005; 46(1):227–31.

Schmitt M, Qasem A, McEniery C, Wilkinson IB, Tatarinoff V, Noble K, Klemes J, Payne N, Frenneaux MP, Cockcroft J, Avolio A, Role of natriuretic peptides in regulation of conduit artery distensibility. *Am J Physiol Heart Circ Physiol.* 2004;287(3):H1167–71.

Selzer R, Mack W, Lee P, Kwong-Fu H, Hodis H, Improved common carotid elasticity and intima-media thickness measurements from computer analysis of sequential ultrasound frames. *Atherosclerosis.* 2001;154(1):185.

Sharman JE, Lim R, Qasem AM, Coombes JS, Burgess MI, Franco J, Garrahy P, Wilkinson IB, Marwick TH, Validation of a generalized transfer function to noninvasively derive central blood pressure during exercise. *Hypertension.* 2006;47(6):1203–1208.

Siegel G, Emden J, Wenzel K, Mironneau J, Stock G, Potassium channel activation in vascular smooth muscle. *Adv Exp Med Biol.* 1992;311:53–72.

Simon AC, Levenson J, Bouthier J, Safar ME, Avolio AP, Evidence of early degenerative changes in large arteries in human essential hypertension. *Hypertension.* 1985;7(5):675–680.

Sims NA, Green JR, Glatt M, Schlict S, Martin TJ, Gillespie MT, Romas E, Targeting osteoclasts with zoledronic acid prevents bone destruction in collagen-induced arthritis. *Arthritis Rheum.* 2004;50(7):2338–46.

Spieker L, Luscher T, Noll G, ETA receptors mediate vasoconstriction of large conduit arteries during reduced flow in humans. *J Cardiovasc Pharmacol.* 2003;42:315–318.

Spratt JC, Goddard J, Patel N, Strachan FE, Rankin AJ, Webb DJ, Systemic ETA receptor antagonism with BQ-123 blocks ET-1 induced forearm vasoconstriction and decreases peripheral vascular resistance in healthy men. *Br J Pharmacol.* 2001;134(3):648–654.

Stefanadis C, Dernellis J, Tsiamis E, Diamantopoulos L, Michaelides A, Toutouzas P, Assessment of aortic line of elasticity using polynomial regression analysis. *Circulation.* 2000;101(15):1819–1825.

Stoerk H, Bielinski T, Budzilovich T, Chronic polyarthritis in rats injected with spleen in adjuvants. *Am J Pathol.* 1954;30:616.

Stone PH, Coskun AU, Kinlay S, Popma JJ, Sonka M, Wahle A, Yeghiazarians Y, Maynard C, Kuntz RE, Feldman CL, Regions of low endothelial shear stress are the sites where coronary plaque progresses and vascular remodelling occurs in humans: an in vivo serial study. *Eur Heart J.* 2007;28(6):705–710.

Tahiliani AG, Verma SC, McNeill JH, Cyclic amp-dependent and independent positive inotropic effects of phenylephrine. *Gen Pharmacol.* 1982;13(5):369–374.

Tan JH, Abed AA, Brock JA, Inhibition of K_{ATP} channels in the rat tail artery by neurally released noradrenaline acting on postjunctional α_2-adrenoceptors. *J Physiol.* 2007;581(2):757–765.

Ting CT, Chang MS, Wang SP, Chiang BN, Yin FC, Regional pulse wave velocities in hypertensive and normotensive humans. *Cardiovasc Res.* 1990;24(11):865–872.

Tomiyama H, Arai T, Koji Y, Yambe M, Hirayama Y, Yamamoto Y, Yamashina A, The relationship between high-sensitive C-reactive protein and pulse wave velocity in healthy Japanese men. *Atherosclerosis.* 2004;174(2):373–7.

Tóth A, Pal M, Intaglietta M, Johnson PC, Contribution of anaerobic metabolism to reactive hyperemia in skeletal muscle. *Am J Physiol Heart Circ Physiol.* 2007;292(6):H2643–H2653.

Trazzi S, Omboni S, Santucciu C, Parati G, Mancia G, Variability in arterial diameter and compliance: compliance modulation reserve. *J Hypertens Suppl.* 1992;10(6):S41–3.

Vallance P, Collier J, Moncada S, Effects of endothelium-derived nitric oxide on peripheral arteriolar tone in man. *Lancet.* 1989;2(8670):997–1000.

Van Guilder GP, Westby CM, Greiner JJ, Stauffer BL, DeSouza CA, Endothelin-1 vasoconstrictor tone increases with age in healthy men but can be reduced by regular aerobic exercise. *Hypertension.* 2007;50(2):403–409.

van Merode T, van Bortel LM, Smeets FA, Mooij JM, Bohm RO, Rahn KH, Reneman RS, Verapamil and nebivolol improve carotid artery distensibility in hypertensive patients. *J Hypertens Suppl.* 1989;7(6):S262–S263.

van Popele NM, Grobbee DE, Bots ML, Asmar R, Topouchian J, Reneman RS, Hoeks AP, van der Kuip DA, Hofman A, Witteman JC, Association between arterial stiffness and atherosclerosis: the Rotterdam Study. *Stroke.* 2001;32(2):454–460.

Vane JR, Anggård EE, Botting RM, Regulatory functions of the vascular endothelium. *N Engl J Med.* 1990;323(1):27–36.

Wallace SML, Yasmin, McEniery CM, Mäki-Petäjä KM, Booth AD, Cockcroft JR, Wilkinson IB, Isolated systolic hypertension is characterized by increased aortic stiffness and endothelial dysfunction. *Hypertension.* 2007;.

Wallin R, Wajih N, Greenwood GT, Sane DC, Arterial calcification: a review of mechanisms, animal models, and the prospects for therapy. *Med Res Rev.* 2001;21(4):274–301.

Wang JJ, O'Brien AB, Shrive NG, Parker KH, Tyberg JV, Time-domain representation of ventricular-arterial coupling as a windkessel and wave system. *Am J Physiol Heart Circ Physiol.* 2003;284(4):H1358–H1368.

Weber MA, The role of the new beta-blockers in treating cardiovascular disease. *Am J Hypertens.* 2005;18(12 Pt 2):169S–176S.

Westerhof BE, Guelen I, Westerhof N, Karemaker JM, Avolio A, Quantification of wave reflection in the human aorta from pressure alone: a proof of principle. *Hypertension.* 2006;48(4):595–601.

Westerhof N, Sipkema P, van den Bos G, Elzinga G, Forward and backward waves in the arterial system. *Cardiovasc Res.* 1972;6(6):648–56.

Wilkinson I, Fuchs S, Jansen I, Spratt J, Murray G, Cockcroft J, Webb D, Reproducibility of pulse wave velocity and augmentation index measured by pulse wave analysis. *Journal of Hypertension.* 1998a;16(12 II):2079.

Wilkinson I, Hall I, MacCallum H, Mackenzie I, McEniery C, van der Arend B, Shu Y, MacKay L, Webb D, Cockcroft J, Pulse-wave analysis: clinical evaluation of a non-invasive, widely applicable method for assessing endothelial function. *Arteriosclerosis, Thrombosis & Vascular Biology*. 2002a;22(1):147.

Wilkinson I, MacCallum H, Cockcroft J, Webb D, Inhibition of basal nitric oxide synthesis increases aortic augmentation index and pulse wave velocity in vivo. *Br J Clin Pharmacol*. 2002b;53(2):189.

Wilkinson I, Qasem A, McEniery C, Webb D, Avolio A, Cockcroft J, Nitric oxide regulates local arterial distensibility in vivo. *Circulation*. 2002c;105(2):213.

Wilkinson IB, Cockcroft JR, Webb DJ, Pulse wave analysis and arterial stiffness. *J Cardiovasc Pharmacol*. 1998b;32 Suppl 3:S33–7.

Willerson JT, Ridker PM, Inflammation as a cardiovascular risk factor. *Circulation*. 2004; 109(21 Suppl 1):II2–10.

World Health Organisation, Cardiovascular diseases. Online fact sheet. 2007, URL `http://www.who.int/mediacentre/factsheets/fs317/en/index.html`.

Xie J, Zhou J, Fung YC, Bending of blood vessel wall: stress-strain laws of the intima-media and adventitial layers. *J Biomech Eng*. 1995;117(1):136–45.

Yanagisawa M, Kurihara H, Kimura S, Tomobe Y, Kobayashi M, Mitsui Y, Yazaki Y, Goto K, Masaki T, A novel potent vasoconstrictor peptide produced by vascular endothelial cells. *Nature*. 1988;332(6163):411–5.

Yasmin, McEniery CM, Wallace S, Mackenzie IS, Cockcroft JR, Wilkinson IB, C-reactive protein is associated with arterial stiffness in apparently healthy individuals. *Arterioscler Thromb Vasc Biol*. 2004;24(5):969–74.

Yki-Jarvinen H, Bergholm R, Leirisalo-Repo M, Increased inflammatory activity parallels increased basal nitric oxide production and blunted response to nitric oxide in vivo in rheumatoid arthritis. *Ann Rheum Dis*. 2003;62(7):630–4.

Young T, The Croonian Lecture: On the functions of the heart and arteries. *Philosophical Transactions of the Royal Society of London*. 1809;99:1–31.

Zimmerman BG, Sybertz EJ, Wong PC, Interaction between sympathetic and renin-angiotensin system. *J Hypertens*. 1984;2(6):581–587.